



SAPIENZA
UNIVERSITÀ DI ROMA

PhD Thesis

**SOFT NANOCARRIER DEVELOPMENT
AS A VERSATILE APPROACH TO BRAIN
DELIVERY AND TARGETING**

Patrizia Nadia Hanieh

Pharmaceutical Sciences (XXX Cycle)

Supervisor: Professor Maria Carafa

Department of Drug Chemistry and Technologies

Sapienza - University of Rome (Italy)

18th December 2017

To my parents and my sister

Abstract

The blood–brain barrier (BBB) is a selective system of endothelial cells, joined through the tight junctions, that protect and maintain the homeostasis of the Central Nervous System (CNS). Only small molecule or drugs, with high lipid solubility and a lower molecular mass under 400–500 Da, can cross the BBB in pharmacologically significant amounts, limiting the uptake of most therapeutic agents into the brain.

Currently, the management of neurological with aggressive and invasive techniques (surgery, see **Appendix 3**), achieves higher therapeutic effect compared to conventional delivery methods, such as systemic administration via intravenous injection or oral administration. However invasive techniques achieve less compliance.

This has led to the development of vogue treatments such as nose-to-brain technologies (see **Appendix 2**), FUS-induced BBB opening, fusion protein chaperones, stem cells, gene therapy, use of natural compounds and neuroprotectants, in order to increase the neuroavailability of various advanced drug delivery systems. These strategies provide promising alternatives that are able to ameliorate the treatment of brain disease.

At this purpose, several nanocarriers ranging from the more established systems, e.g. polymeric nanoparticles, liposomes, niosomes and micelles to the newer systems, e.g. nanoemulsions, micro- and nano-bubbles, nanosuspensions and nanogels, have been studied for the delivery of therapeutics to CNS. Many of the proposed nanomedicines can be effectively transported across various *in vitro* and *in vivo* BBB models by endocytosis and/or transcytosis, and demonstrated early preclinical success for the management of CNS conditions such as brain tumours, HIV encephalopathy, neurodegenerative disease and acute ischemic stroke. Future development of CNS nanomedicines need to focus on increasing their drug-trafficking performance and specificity for brain tissue using novel targeting moieties, improving their BBB permeability and reducing their neurotoxicity. Targeted drug delivery is a means of concentrating drugs at a specific site relative to other parts of the body. It spares the rest of the body from toxic effects of the drug and it is also a potential means of improving therapeutic index.

This Ph.D. thesis focused on the study of the formulation of different nanocarriers for brain delivery by two different administration route:

- ❖ **Focused Ultrasound-mediated drug delivery**, a technique that offer a unique non-invasive avenue to deliver drugs to the brain through transient opening of the BBB by using of ultrasound in combination with gas-filled bubbles. Our laboratory developed new carriers, the “Bubblesomes”[®], able to combine the characteristics of a drug carrier and a contrast agent

(theranostic system). When focused ultrasound is applied in presence of drug loaded nanobubbles intravenously administered, inertial cavitation is induced, due to the rapid expansion and violent collapsing of bubbles. This can cause the temporal and fully reversible opening of BBB due to the enhanced endothelial porosity and vascular permeability phenomenon called sonoporation, resulting in an increased drug uptake.

- ❖ **Intranasal drug delivery**, a non-invasive route to reach directly the brain, circumvent the BBB, from the nose along the olfactory and trigeminal nerve pathways. These nerve pathways initiate in the nasal cavity at olfactory neuroepithelium and terminate in the brain.

CONTENTS

ABSTRACT	5
CONTENTS	7
INTRODUCTION	11
1. BRAIN DELIVERY	12
2. NANOTECHNOLOGY FOR BRAIN DELIVERY	14
REFERENCES	18
FOCUSED ULTRASOUND-MEDIATED DRUG DELIVERY	21
1. INTRODUCTION	22
1.1. FOCUSED ULTRASOUND-MEDIATED DRUG DELIVERY	22
1.2. ULTRASOUND CONTRAST AGENTS (UCAS): FROM MICROBUBBLES TO NANOBUBBLES	23
1.3. GENERAL PROPERTIES OF NANOBUBBLES	24
REFERENCES	26
BUBBLESOMES[®]	27
AIM	28
OVERVIEW OF EXPERIMENTAL SETUP	29
FORMULATION AND CHARACTERIZATION OF BUBBLESOMES[®]	31
1. EXPERIMENTAL SECTION	32
1.1.MATERIALS	32
1.2.PREPARATION OF NBS[®]	32
1.3.SIZE, SIZE DISTRIBUTION AND Z-POTENTIAL	33
1.4.ACOUSTIC ANALYSES	34
1.5.MORPHOLOGY STUDIES	37
1.6.NBS[®] STABILITY STUDIES	38
1.7. BILAYER ANALYSES	38
1.8.PROBES LOADED NBS[®]	40
2. RESULTS	41
2.1. SIZE, SIZE DISTRIBUTION AND Z-POTENTIAL	41
2.2.NBS[®] ACOUSTIC EFFICIENCY	41
2.3.NBS[®] MORPHOLOGY	43
2.4.NBS[®] STABILITY STUDIES	46
2.5.BILAYER CHARACTERIZATION	51
2.6.FLUORESCENT PROBES LOADED NBS[®]	52
2.7.COMPARISON BETWEEN NBS[®] AND MBS[®]	53
3. CONCLUSIONS	54
REFERENCES	55
REVERSIBLE BBB OPENING BY FOCUSED ULTRASOUND	57
1. INTRODUCTION	58
1.1. AIM	59
2. MATERIALS AND METHODS	59
2.1. SONOVUE[®]	59
2.2. BUBBLESOMES[®]	59
2.3. NANOSIGHT MEASUREMENTS	60

2.4. MICE	60
2.5. BBB OPENING PROTOCOL	60
2.6. EVANS BLUE DYE EXTRAVASATION	61
2.7. FLUORESCENCE ANALYSIS	62
2.8. HISTOLOGICAL ANALYSIS	62
2.9. STATISTICS	62
3. RESULTS	63
3.1. NBS [®] CONCENTRATIONS	63
3.2. <i>IN VIVO</i> OPENING OF THE BBB USING NBS [®]	63
3.3. HISTOLOGICAL ASSESSMENT	64
3.4. VOLUE OF EVAN'S BLUE INTO THE BRAIN FOLLOWING FUS DISRUPTION	63
3.5. BBB CLOSING AFTER FUS APPLICATION	67
3.6. VOLUME OF CALCEIN DELIVERED INTO THE BRAIN	69
4. DISCUSSION	72
5. CONCLUSIONS	73
REFERENCES	74
<u>FORMULATION AND CHARACTERIZATION OF DRUG LOADED-BUBBLESOMES[®]</u>	<u>75</u>
1. BUBBLESOMES [®] AS THERANOSTIC AGENT	76
2. EXPERIMENTAL SECTION	77
3. RESULTS	77
REFERENCES	80
<u>NOSE TO BRAIN DELIVERY</u>	<u>81</u>
1. INTRODUCTION	82
2. NASAL ANATOMY AND PHYSIOLOGY	83
3. BIOFATE, NASAL PATHWAYS AND MECHANISMS INVOLVED IN THE NOSE TO BRAIN DELIVERY	84
4. STRATEGY TO ENHANCE NOSE TO BRAIN DELIVERY	85
4.1. CHITOSAN	86
REFERENCES	88
<u>HYBRID NIOSOMES</u>	<u>91</u>
AIMS	92
1. NIOSOMES	93
2. FORMULATION AND PHYSICO-CHEMICAL CHARACTERIZATION OF HYBRID NIOSOMES	95
REFERENCES	97
<u>PAPER: DLS CHARACTERIZATION OF NON-IONIC SURFACTANT VESICLES FOR POTENTIAL NOSE TO BRAIN APPLICATION</u>	<u>99</u>
<u>PAPER: PENTASOMES FOR DELIVERY OF PENTAMIDINE TO CNS BY INTRANASAL ROUTE (SUBMITTED)</u>	<u>109</u>
<u>NANOEMULSIONS</u>	<u>125</u>
1. NANOEMULSIONS	126
2. NANOEMULSIONS FOR BRAIN DELIVERY	128
3. AIM	128

REFERENCES	129
<u>PAPER: NEEM OIL NANOEMULSIONS: CHARACTERISATION AND ANTIOXIDANT ACTIVITY</u>	131
<u>CONCLUSIONS</u>	143
<u>APPENDIX 1: PATENT NUMBER WO 2017/178954 A1</u>	145
<u>APPENDIX 2: NOSE TO BRAIN DELIVERY: NEW TRENDS IN AMPHIPHILE-BASED “SOFT” NANOCARRIERS</u>	187
<u>APPENDIX 3: DRUG DELIVERY IN OVERCOMING THE BLOOD–BRAIN BARRIER: ROLE OF NASAL MUCOSAL GRAFTING</u>	197
<u>ACKNOWLEDGEMENTS</u>	211
<u>LIST OF PUBLICATIONS</u>	213

Introduction

1. Brain delivery

Conventional drug delivery systems fail to deliver numerous neuropharmaceutical agents to the CNS for treatment of brain diseases such as cancer therapy, schizophrenia, epilepsy, insulin-dependent diabetes, Parkinson's disease and Alzheimer's disease. [1]

The primary cause of the limited access of many drugs is the presence of three barriers: (1) the blood-brain barrier (BBB), that regulates the exchanges between the blood and the brain, (2) the arachnoid epithelium and (3) the choroid plexus epithelium, which separate the blood from the cerebrospinal fluid (CSF).

In particular, the BBB plays a key role for the protection of the brain from several pathogens and toxic substances, including drugs, and for maintaining its homeostasis.

The BBB surrounds the cerebral microvessels and it is composed by the endothelial cells strongly joined by the tight junctions.

The tight junctions are composed by transmembrane proteins: claudins, occluding and junctional adhesion molecules. Their membranes are localized in two different cellular sites: luminal, in the blood side, and abluminal, in the brain side.

Functionally, this barrier is regulated by several cell types: the astrocytic end-feets, pericytes and neurons. [2]

Molecules may cross the BBB following two fluxes, from the blood to the brain parenchyma, or vice versa, by efflux transporters, controlling the brain concentration of exogenous substances in the brain. Several pathways are involved in the transport through the BBB, as shown in the figure 1. [3]

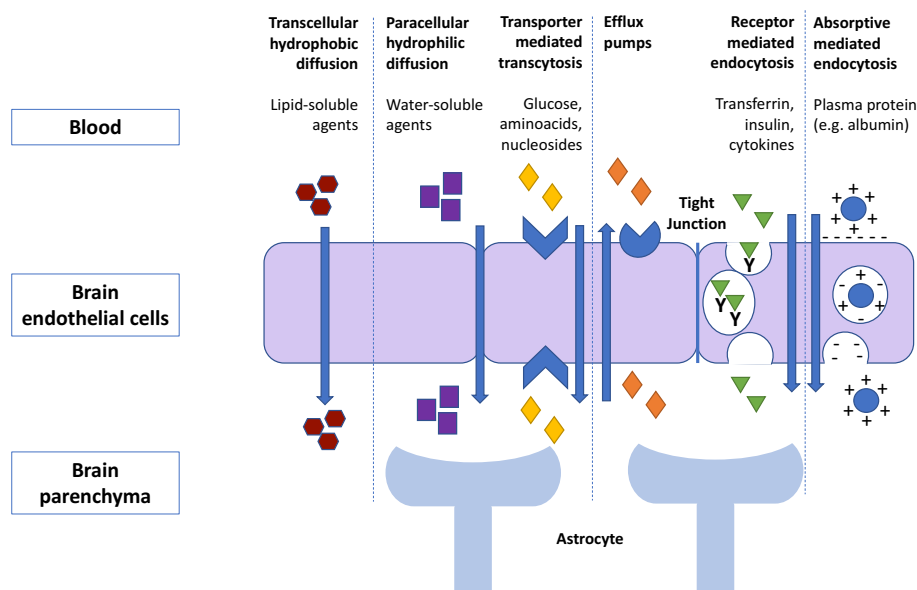


Figure. 1 Transport pathways across blood brain barrier.

- **Transcellular passive diffusion:** this mechanism involves the transport of endogenous molecules (e.g. drugs) and it mainly depends by the drug properties and the concentration gradient. Generally, only the small molecules, with a molecular weight less than 400 Da and a high lipid solubility, are able to cross BBB by this way in a significant amount. Furthermore, this way is favored for unionized substance with have a log P value near to 2 and a cumulative number of hydrogen bonds not beyond 8-10 and. [4]
- **Carrier-mediated transcytosis:** the essential nutrients, metabolites and neurotransmitters, such as glucose, iron or amino acids, are transported into the CNS through specific carriers, e.g. the glucose transporter 1, large neutral amino acids transporter 1, etc.
- **Receptor-mediated endocytosis:** concern the internalization in the brain of insulin, transferrin, lactoferrin, immunoglobulin, epidermal growth factor and low density lipoproteins. These molecules are internalized from the abluminal side of the brain and transported to the side pole of cells through a lysosome. This process is receptor-mediated and the receptor is specific for each molecule.
- **Absorption-mediated endocytosis:** starts with the interaction between the negative charges on the cellular membrane and a cationic substance, followed by endocytosis of the molecules in the brain.

- **Efflux transporter:** concern a large number of endogenous and exogenous substances are pumped out of the brain by the efflux transporters, such as P-glycoproteins or the multi-drug resistance-related proteins). [5]

Therefore, many polar drugs are unable to reach the brain because of the absence of paracellular pathways on the BBB.

Consequently, a significant number of CNS diseases seem to have no efficient therapy and many promising therapeutic agents are not further investigated because of their inability to achieve sufficient levels in brain through systemic administration.

Since various active drugs for the CNS diseases do not reach the brain in therapeutic concentrations, many drug are administrated in excessive doses with the associated risk of systemic side effects. [6] Currently strategies to increase drug delivery to the brain provide the use of invasive or non-invasive approaches.

Invasive approach requires: the intraventricular or intracerebral infusion of the neurotherapeutic agent, the intrathecal implantation of formulation or the transitory permeability increase of BBB, for example by using mannitol. [7]

Unfortunately, these techniques shown a high risk of complications for the patients, like infections or oedema. Moreover, they are expensive, require hospitalization with a long recovery period and a high surgical expertise. [8]

Non-invasive approach includes various types of drug modifications: chemical, by using prodrugs or drug conjugates, biological, through the conjugation of drug with antibodies or by peptides as carrier and the use of colloidal drug delivery.

Despite many researchers having developed several methods to overcome the BBB, obtaining very promising *in vitro* results, only a few number of strategies have shown good results when applied *in vivo*.

Therefore, new strategies are necessary to go through CNS barriers to fulfill efficient treatment of neurological diseases.

2. Nanotechnology for brain delivery

In the last years, the design and development of nanocarriers as drug delivery systems involved many research team, in particular, to enhance the drug delivery to the CNS.

In 1980, Paul Ehrlich referred to a drug delivery systems (DDS), as a ‘magic bullet’, designed to achieve a selective target avoiding the healthy tissue and organs. Afterwards many researchers have

formulated several carriers to enhance the brain delivery including liposomes, niosomes, ethosomes and colloidosomes. [9, 10]

Despite promising researches, only few nanocarriers have actually shown significant clinical potential and practical application. Among commercially available nanocarriers, vesicular carriers, such as the liposomes, are present in quite a large number. (Table. 1)

Product	Drug	Type of system
Abraxane [®]	Paclitaxel	Nanoparticles
Caelyx [®] /Doxil [®]	Doxorubicin	Liposomes
Emend [®]	Aprepitant	Nanoparticles
Mepact [®]	Mifamurtide	Liposomes
Myocet [®]	Doxorubicin	Liposomes
Pegasy [®]	Interferon 2a	Polymer-protein conjugate
Rapamune [®]	Sirolimus	Nanoparticles
Zevalin [®]	Ibritumomab tiuxetan	Antibody-conjugate

Table. 1 Clinically approved nanocarriers.

The use of liposomes as drug delivery is encouraging, but still it presents some problems such as their physico-chemical instability and leakage of entrapped drug. Synthetic phospholipids are expensive and the natural phospholipid show a variable degree of purity. [11]

In addition to these vesicular systems, other carriers are able to encapsulate drug to be delivered to the brain: cyclodextrins, dendrimers, nanoemulsions and nanoparticles. [12, 13] (Figure. 2)

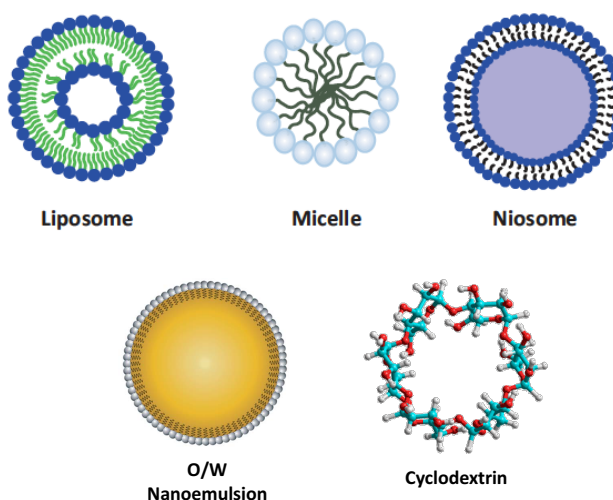


Figure. 2 Drug delivery systems.

Ideally, a drug delivery system for the brain should be:

- nontoxic, biodegradable and biocompatible;
- nanometric;
- stable *in vivo* and *in vitro*;
- able to void the RES (reticulo-endothelial system) to prolong the blood circulation time;
- prepared by scalable and cost-effective manufacturing process;
- able to avoid drug alteration (chemical degradation/alteration or protein denaturation);
- able to control the drug release.

The nanocarriers exhibit numerous advantage for drug delivery, including cargo protection from enzymatic degradation and an increase of drug dosage delivered to target sites, so limiting the systemic side effects.

Vesicular nanocarriers show a hydrophilic core, able to entrap water-soluble drugs and a hydrophobic shell that stabilize the system and entrap lipophilic drugs.

Furthermore, the use of nanocarriers do not require any chemical modification of the therapeutically molecule for the brain delivery, since the system can mask the drug properties by entrapping it.

The nanometric size range (10-1000 nm) potentially allows carriers to pass through several biological barriers, such as nasal mucosa or BBB [14, 15], and to reach to hitherto inaccessible disease sites.

Several researchers show that the primary immune system is less active for the molecules with lower dimensions than hundred nanometers, allowing for longer blood circulation of these carriers.

The surface of nanocarrier may be functionalized to improve their pharmacokinetic and biodistribution. For example, the surface PEGylation induces steric repulsion from blood opsonins (molecules which improve phagocytosis) enabling enhancement of the *in vivo* longevity of nanocarrier and the capability of extravasation through the endothelium of inflammatory tissues (the enhanced permeability and retention effect).

Alternatively, the functionalization of DDS by using biologically active ligands eases the targeting of specific cells.

Among the several features that the nanocarriers can acquire, one of the most attractive is the stimuli-responsive property. The application of a specific stimulus may cause structural or conformational changes in the DDS and consequently inducing capture and release of drugs, chemical reactions, and morphology transitions.

These formulations may be sensitive to: (Figure. 3)

- endogenous stimuli: including pH variations, redox gradients, the concentration of a specific enzymes, etc. For example, at the cellular level, pH sensitivity can trigger the release of the drug in the endosomes or lysosomes. Moreover, the nanocarrier can take advantage of the

microenvironmental changes associated to the inflammatory diseases, neoplastic diseases, infections or other pathological situations such as ischemia.

- exogenous stimuli: for systems which are able to release the drug in response to externally applied stimuli, such as temperature changes, ultrasound, magnetic and electric fields. In particular, thermos-responsive drug delivery is governed by the change in the properties of at least one component of the nanocarrier material with the temperature. Ideally, these systems should retain their drug load at the physiological temperature and release the drug in correspondence of heated body area, such as tumor area ($\approx 40\text{-}42^\circ\text{C}$). Also, ultrasound waves in combination with drug-loaded micro- or nano-bubbles can trigger the release of drug through the thermal/mechanical effects generated by cavitation mechanisms or radiation force. [16]

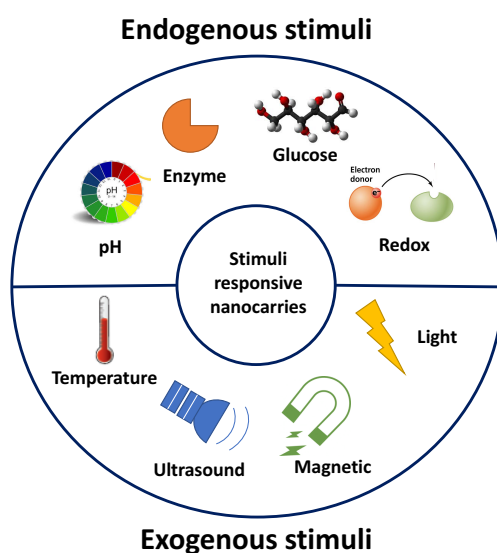


Figure. 3 Examples of stimuli triggers for nanocarriers.

A further advantage of these systems is the possibility to use them as imaging/contrast agents for several imaging techniques, such as ultrasonography, gamma-scintigraphy, magnetic resonance imaging, computed tomography.

These systems are namely theranostic agents and combine both the diagnostic properties and the therapy in a single system.

After injection, the theranostic agent containing drug can be tracked by an imaging techniques and, reaching the target site, release their contents, after exposure to specific stimuli.

References

- [1]. Bahadur S, Pathak K. Physicochemical and physiological considerations for efficient nose-to-brain targeting. *Expert Opin Drug Deliv*, 9 (1), 19-31, 2012.
- [2]. Abbott NJ, Patabendige AA, Dolman DE, Yusof SR, Begley DJ. Structure and function of the blood-brain barrier. *Neurobiol Dis*, 37 (1), 13-25, 2010.
- [3]. Abbott NJ, Rönnbäck L, Hansson E. Astrocyte–endothelial interactions at the blood–brain barrier. *Nat Rev Neurosci*, 7(1), 41-53, 2006.
- [4]. Pardridge WM. Blood-brain barrier delivery. *Drug Discov Today*, 12(1-2), 54-61, 2007.
- [5]. Hawkins BT, Sykes DB, Miller DS. Rapid, reversible modulation of blood-brain barrier P-glycoprotein transport activity by vascular endothelial growth factor. *J Neurosci*, 30 (4), 1417–1425, 2010.
- [6]. Reimold I, Domke D, Bender J, Seyfried CA, Radunz HE, Fricker G. Delivery of nanoparticles to the brain detected by fluorescence microscopy. *Eur J Pharm Biopharm*, 70 (2), 627-632, 2008.
- [7]. Marianecci C, Rinaldi F, Hanieh PN, Di Marzio L, Paolino D, Carafa M. Drug delivery in overcoming the blood–brain barrier: role of nasal mucosal grafting. *Drug Des Devel Ther*, 27 (11), 325-335, 2017.
- [8]. Yi X, Manickam DS, Brynskikh A, Kabanov AV. Agile delivery of protein therapeutics to CNS. *J Control Release*, 190, 637-63, 2014.
- [9]. Lai F, Fadda AM, Sinico C. Liposomes for brain delivery. *Expert Opin Drug Deliv*, 10, 1003–1022, 2013.
- [10]. Marianecci C, Rinaldi F, Hanieh PN, Paolino D, Marzio LD, Carafa M. Nose to Brain Delivery: New Trends in Amphiphile-Based "Soft" Nanocarriers. *Curr Pharm Des*, 21 (36), 5225-32, 2015.
- [11]. Desai TR, Finlay WH. Nebulization of niosomal all-trans-retinoic acid: an inexpensive alternative to conventional liposomes. *Int J Pharm*, 241 (2), 311-7, 2002.
- [12]. Kreuter J. Drug delivery to the central nervous system by polymeric nanoparticles: What do we know?. *Adv Drug Deliv Rev*, 71, 2–14, 2014.
- [13]. Rajshree LS, Anil BJ, Padma VD. Microemulsions and Nanoemulsions for Targeted Drug Delivery to the Brain. *Curr Nanoscience*, 7 (1), 119-133, 2011.
- [14]. Florence AT. The oral absorption of micro- and nanoparticulates: neither exceptional nor unusual. *Pharm Res*, 14, 259–66, 1997.

- [15]. Lockman PR, Mumper RJ, Khan MA, Allen DD. Nanoparticle technology for drug delivery across the blood-brain barrier. *Drug Dev Ind Pharm*, 28 (1), 1–13, 2002.
- [16]. Mura S, Nicolas J, Couvreur P. Stimuli-responsive nanocarriers for drug delivery. *Nat Mater*, 12 (11), 991-1003, 2013.

Focused Ultrasound-mediated Drug delivery

1. Introduction

1.1. Focused Ultrasound-mediated drug delivery

Ultrasound (US) waves are mechanical pressure waves that propagate through a medium, with a frequency > 20 kHz.

In the last 50 years, ultrasonography has been widely used as a non-invasive diagnostic technique that show a real-time imaging in clinical diagnosis.

Since the blood shows a low back-scatter of US waves at clinical diagnostic frequencies (between 1-40 MHz) ultrasound contrast agents (UCAs), have been developed to improve the visualization of the microvascularization.

Recently, the deep research on ultrasound for diagnostic imaging has helped to expand and define its role in other fields, including therapy, such as the thermal ablation of a pathological tissue by using high intensity focused US (HIFU) [1], the break-down of calculi by lithotripsy [2], the stimulation of the tissue and bone repair by low-intensity US [3].

In particular, US have been established as a versatile tool to increase cellular permeability and enhance the drug uptake.

Based on the used exposure condition, in terms of frequency, intensity, pressure and duration, US has shown to improve the drug delivery by different mechanisms:

- **Thermal effect**: the absorption of waves by a tissue can cause a localized temperature increase the, allowing drug release from a thermosensitive carrier, without tissue damage. [4]
- **Acoustic radiation force**: when the US propagate through tissue, the energy can be absorbed by microbubbles (MBs) intravenously injected. This phenomenon generates a net force that pushes particles away from the ultrasound transducer promoting their extravasation and diffusion through a tumor matrix. [5]
- **Cavitation**: during the alternating cycles of rarefaction and compression generated by US waves, MBs are able to expand and contract. [6] (Figure. 1)

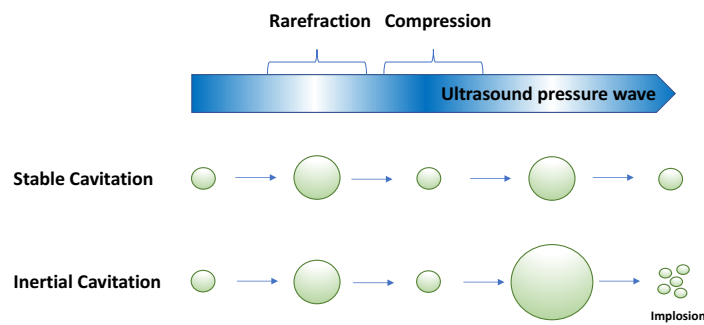


Figure. 1 Several cavitation mechanisms due to US pressure wave.

At low acoustic power, with a mechanical index (MI) of 0.1-0.5, MBs show a **stable cavitation**, resulting in nonlinear volumetric oscillation, the bubbles will oscillate but will not collapse. At high acoustic power, with MI greater than 0.5, the **inertial cavitation** is induced, because of the rapid expansion and violent collapse of MBs. This mechanism is often accompanied by the generation of shock waves and microstreaming, which can cause shear stresses on the adjacent cells, with a consequently increased endothelial porosity and vascular permeability, called **sonoporation**. Inertial cavitation can be useful in drug delivery to enhance the uptake of the drug intravenously injected into the cells through the temporarily permeabilized membranes due to the MBs implosion. [7]

1.2. Ultrasound Contrast Agents (UCAs): from microbubbles to nanobubbles

UCAs are generally gas-filled microsized bubbles with a biodegradable shell composed by phospholipid, polymer or protein, commercially available as contrast agent for ultrasound imaging. (Table. 1)

<i>UCA</i>	<i>Shell</i>	<i>Gas</i>	<i>Mean diameter (μm)</i>	<i>Half-life (minutes)</i>	<i>Stability after reconstitution (hours)</i>
Albunex [®]	Albumin	Air	4.3	1 – 1	4
Optison [®]	Albumin	Octafluoropropane	2.0 - 4.5	2 – 4	0.5
Definity [®]	Lipid	Octafluoropropane	1.1 - 3.3	2 – 10	12
Imagent [®]	Lipid	N ₂ /perfluorohexane	6.0	60 – 180	NA
Sonovue [®]	Lipid	Sulphurhexafluoride	2.0 - 3.0	2 – 6	6
Sonazoid [®]	Lipid	Air	2.0	60 – 120	NA
Levovist [®]	Lipid/ galactose	Air	2.0 - 4.0	2 – 5	NA

Table. 1 Characteristics of commercially available microbubbles.

NA=data not available.

The gas core usually is composed by air or a bioinert gas such as sulfur hexafluoride, nitrogen or a perfluorocarbon (PFC).

Typically, UCAs show size between 1 – 10μm, approximately equal to red blood cell, and, after the intravenous administration, they remain trapped in the blood pool, limiting the UCAs clinical application only in the cardiovascular target, such as inflammation, thrombus and arteriosclerosis.

Furthermore, they are cleared rapidly from the bloodstream due to their poor stability, captured by the reticuloendothelial system (RES) and then eliminated by the spleen. [8]

Nevertheless, commercially available MBs show a short half-life during body circulation and they are unstable over time, in fact they must be reconstituted just before administration.

Recently, to overcome these problems, nanoscale bubbles (nanobubbles, NBs) have been developed, but the research is still at the initial stage.

1.3. General properties of nanobubbles

The main advantage of these systems is their potential use as therapeutic drug carriers together with their diagnostic application as contrast agent.

In particular, by using ultrasound, the drug loaded NBs can release drugs to target cells or tissues, after implosion. Furthermore, the uptake of the released drug into the cells is enhanced due to the temporarily permeabilization of the membranes, by sonoporation.

Moreover, these NBs can provide the protection of the drugs from degradation phenomena and the drug targeting to specific site of action, limiting toxicity and adverse effects.

The NBs must be sufficiently stable circulating in the blood stream in order to reach the target site.

Several factors affect the stability of NBs in the biological fluids:

- **Pressure:** LAPLACE pressure is an important parameter which governs the in vivo dissolution rate of NBs.

The gas pressure within a bubble is:

$$\Delta P = P_i - P_o = (2\sigma / r)$$

where P_i and P_o are the pressure inside and outside the bubble respectively in the bloodstream, σ is the interfacial tension and r is the bubble radius.

LAPLACE pressure is inversely proportional to the bubble size, so smaller bubble will have a higher-pressure value than larger bubbles. When the inner gas leaves the core, the bubbles shrink and LAPLACE pressure increases, thereby increasing the gas dissipation rate and the system collapse. [9]

- **Gas entrapped:** the air-filled bubbles dissolve very rapidly in the blood due to arterial pressure. NBs formulations can be stabilized by using gas with poor aqueous solubility, such as perfluorocarbons, reducing the dissolution of the gas in the bloodstream.

- **Shell composition:** The thickness and the elasticity of the shell can determine micro/nanobubble stability, since they affect the gas exchange from the core to the external medium.

Soft shells are characterized by a thin flexible shell of surfactant material that causes their high sensitiveness to the US waves, in fact they are able to oscillate and cause stable and instable cavitation. Phospholipid shells are the most elastic due to the hydrocarbon tails, so NBs covered by lipid with longer acylchains exhibit a longer shelf-life.

Instead, hard shells (e.g. polymers) are less responsive to US compared to soft shells due to the fact they are cannot oscillate caused from acoustic waves application at low pressure. Only with high acoustic pressure, hard sells are able to produce cavitation phenomena. [10]

References

- [1]. Haar GT, Coussios C. High intensity focused ultrasound: physical principles and devices. *Int J Hyperthermia*, 23 (2), 89-104, 2007.
- [2]. Sokolov DL, Bailey MR, Crum LA. Dual-pulse lithotripter accelerates stone fragmentation and reduces cell lysis in vitro. *Ultrasound Med Biol*, 29 (7), 1045-52, 2003.
- [3]. Yang M, Lim K, Choung P, Cho C, Chung JH. Application of Ultrasound Stimulation in Bone Tissue Engineering. *Int J Stem Cells*, 3 (2), 74-79, 2010.
- [4]. Dromi S, Frenkel V, Luk A, Traugher B, Angstadt M, Bur M, Poff J, Xie J, Libutti SK, Li KC, Wood BJ. Pulsed-High Intensity Focused Ultrasound and Low Temperature--Sensitive Liposomes for Enhanced Targeted Drug Delivery and Antitumor Effect. *Clin Cancer Res*, 13 (9), 2722-7, 2007.
- [5]. Dalecki D. Mechanical bioeffects of ultrasound. *Annu Rev Biomed Eng*, 6, 229-48, 2004.
- [6]. Fan Z, Kumon RE, Deng CX. Mechanisms of microbubble-facilitated sonoporation for drug and gene delivery. *Ther Deliv*, 5 (4), 467-86, 2014.
- [7]. Qiu, Y, Luo Y, Zhang Y, Cui W, Zhang D, Wu J, Zhang, J, Tu J. The correlation between acoustic cavitation and sonoporation involved in ultrasound-mediated DNA transfection with polyethylenimine (PEI) in vitro. *J Control Release*, 145 (1), 40–48, 2010.
- [8]. Willmann JK, Cheng Z, Davis C, Lutz AM, Schipper ML, Nielsen CH, Gambhir SS. Targeted Microbubbles for Imaging Tumor Angiogenesis: assessment of Whole-Body Biodistribution with Dynamic Micro-PET in Mice. *Radiology*, 249 (1), 212-19, 2008.
- [9]. Schutt EG, Klein DH, Mattrey RM, Riess JG. Injectable microbubbles as contrast agents for diagnostic ultrasound imaging: the key role of perfluorochemicals. *Angew Chem Int Ed*, 42, 3218–3235, 2003.
- [10]. Borden MM, Kruse DE, Caskey CE, Zhao SK, Dayton PA, Ferrara KW. Influence of lipid shell: physic-chemical properties on ultrasound induced microbubble destruction. *IEEE Trans Ultrason Ferroelectr Freq Control*, 52 (11), 1992–2002, 2005.

Bubblesomes[®]

Aim

The aim of a part of this PhD project has been mainly focused on the formulation and characterization of a new theranostic carrier, the Bubblesomes[®] (NBs[®]), potentially able to act both as drug delivery system (therapy) and as contrast agent (diagnostic).

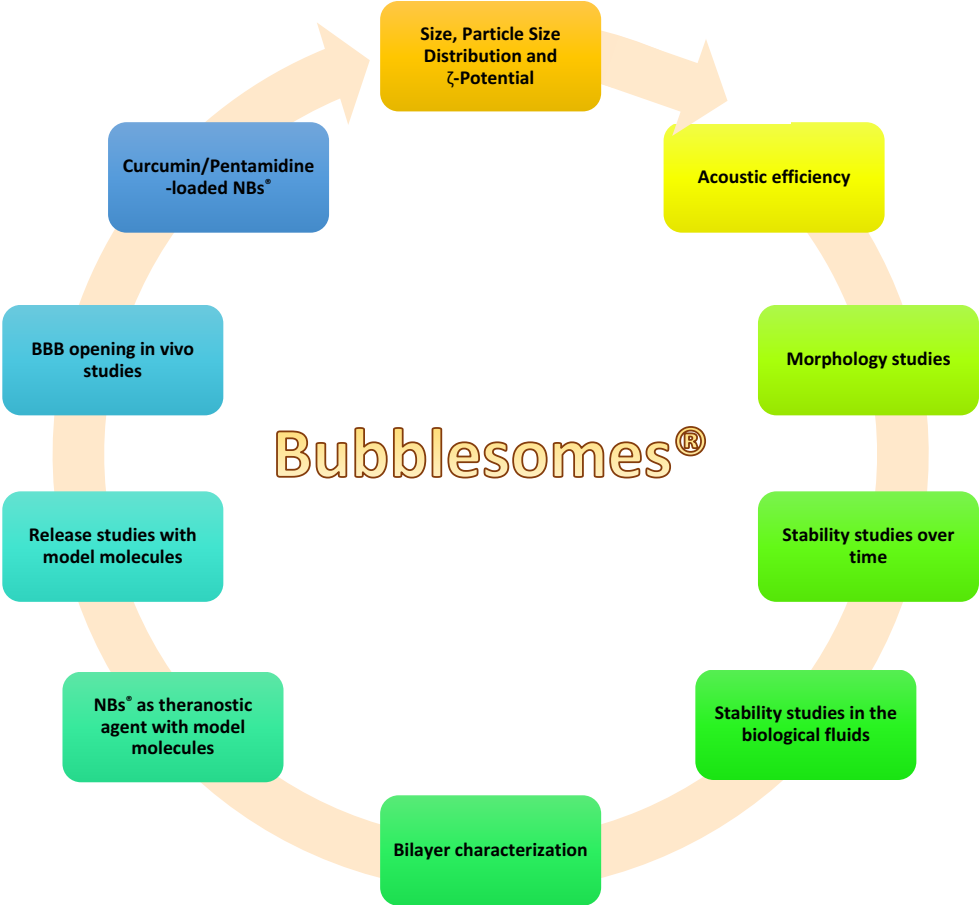
In particular, the goals of this thesis can be summarized in the following points:

- ✓ Formulation and physico-chemical characterization of NBs[®] in order to obtain a theranostic agent.
- ✓ *In vivo* studies to investigate the non-invasive localized opening of BBB by using focused ultrasound (FUS) exposure, after NBs[®] systemic administration.
- ✓ Formulation and physico-chemical characterization of drug-loaded NBs[®].

All formulations of NBs[®] present in this PhD thesis have been patented:

Appendix 1: Patent number WO 2017/178954 A1.

Overview of experimental setup



**Formulation and characterization
of Bubblesomes[®]**

1. Experimental section

1.1. Materials

1,2-dimyristoyl-sn-glycero-3-phosphocholine (DMPC) and dipalmitoylphosphatidylcholine (DPPC) were purchased from Avanti Polar Lipids.

Dicetyl phosphate (DCP), Span[®] 20, cholesterol (Chol), Hepes salt {N-(2-idroxyethyl) piperazine-N'-(2-ethanesulfonicacid)}, calcein, nile red, tetradecafluorohexane (PFC) were Sigma–Aldrich products (Sigma–Aldrich SRL, Milan, Italy).

All other chemicals used throughout this investigation were of analytical grade and no additional purification was carried out.

1.2. Preparation of NBs[®]

The formulations selected in this project are:

- 1) DMPC NBs[®]
- 2) DMPC-DCP NBs[®]
- 3) DPPC NBs[®]
- 4) Span20 NBs[®]

The NBs[®] have been prepared by using different phospholipids and surfactants, with cholesterol (Chol), in different molar ratio. (Table. 1)

Components	Ratio %
DMPC-Chol	40-60 : 20-40
DMPC-DCP-Chol	50-70 : 50-30
DPPC-Chol	60-90 : 40-10
Span20+Chol	30-50 : 70-50

Table. 1

All samples were obtained using the “film” technique according to the procedure described in the patent (Appendix 1) and summarize in figure 1.

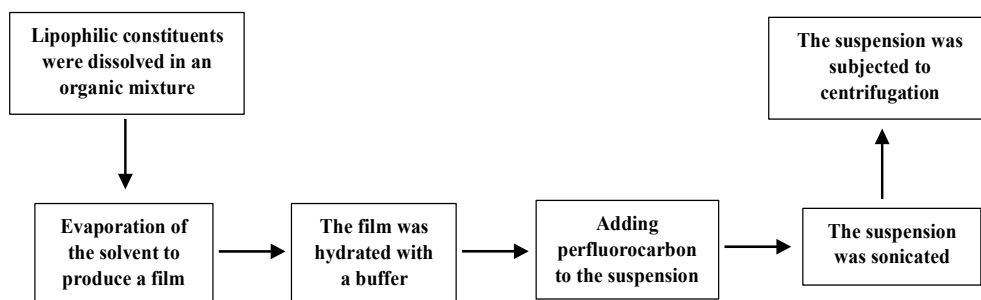


Figure. 1 Schematic representation of the NBs[®] preparation.

The hydrophobic components, such as Nile red, phospholipids/surfactants and cholesterol, in the reported ratios (Table 1), were dissolved in a mixture of organic solvents (3/1 v/v chloroform/methanol), evaporated in a rotavapor to obtain a “film”. [1]

The dried film was hydrated by the addition of an aqueous phase (10 mM of HEPES buffer pH 7.4 or a solution of Calcein 0.01 M in HEPES buffer) in order to obtain the NBs[®] dispersion.

Liquid PFC in equilibrium with its gas was added to the dispersion in order to obtain nanobubble formulations.

The dispersion was then sonicated for 15 minutes at 25°C using an ultrasound sonicator provided with a microprobe operating at a frequency of 20 kHz and an amplitude of 16% (Vibracell-VCX 400-Sonics, USA)

Finally, the NBs[®] were purified by centrifuge MPW-260R (MPW Med. Instruments) at 600 rpm for 20 minutes at 25°C.

1.3. Size, size distribution and ζ -potential

Dynamic light scattering (DLS) was used to determine mean size and size distribution of NBs[®].

The sample was diluted 100 times with the HEPES buffer in order to avoid multiscattering phenomena. NLBs mean size and size distribution (polydispersity index, PDI) were measured at 25

°C using a Malvern Nano ZS90 light scattering apparatus (Malvern Instruments Ltd., Worcestershire, UK) at a scattering angle of 90.0°.

The same apparatus was used for the evaluation of ζ -potential of NBS[®].

The Laser Doppler Anemometry was used and hence the electrophoretic mobility of the vesicles was measured. The ζ -potential value was calculated from the electrophoretic mobility using a Smoluchowsky constant F (Ka) of 1.5. [2]

Measurement of the ζ -potential provides information on the physical-chemical characteristics of the particles in suspension and is extensively used to predict the stability of systems in relation to aggregation phenomena. A suspension is generally considered stable when the ζ -potential values are less than -30 mV or greater than +30 mV.

The distribution curve for NBS[®] dimensions is characterized by a polydispersity index (PDI), which should not be greater than 0.25 for monodispersed populations.

The analyses were performed at 25°C and each value reported relates the average of three measurements of all samples.

1.4. Acoustic analyses

[Acoustic measurements were performed by Dr. Andrea Bettucci and Dr. Angelo Biagioni, Department of Basic and Applied Sciences for Engineering, Sapienza, University of Rome (Italy)]

- Pulse-echo technique

In order to determinate the acoustic behavior of the NBS[®] at different concentrations and at different time intervals to evaluate their shelf stability, the pulse-echo technique was used.

This technique uses of the same physical principle (measurement of the intensity of the reflected echo) used for the formation of US images. So, it can be used to evaluate the efficiency of the NBS as a contrast medium in medical US imaging. The increase of attenuation of the US signal transmitted caused by the solution containing NBS is associated to an increase of the efficiency with which the incident elastic energy is scattered into space.

In clinic, during a medical investigation, the increase of US reflection capacity (echogenicity) will registered by a sensor connected to the ultrasound unit.

In this study, the pulse technique is used to measure the frequency spectrum of the NBs[®] scattering efficiency or to determine the US frequency at which the elastic energy is most diffused by the NBs[®] into space.

The experimental apparatus is composed of an immersion transducer, that generates ultrasound bursts in the frequency band 11-17 MHz and centered at 14 MHz, a cylindrical test tube, which contains the bubble suspension, and a digital oscilloscope for data capture. The transducer is driven by an ultrasonic pulser-receiver (Panametrics 500PR) that generates and receives electrical signals. (Figure. 2)

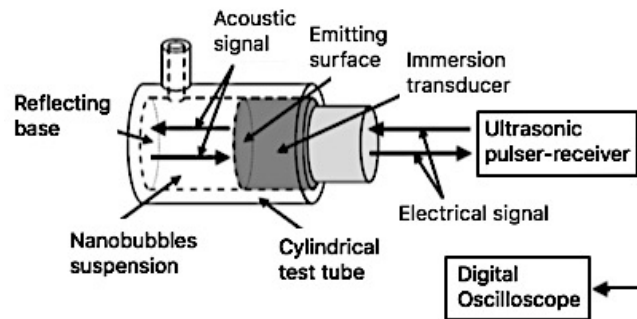


Figure. 2 Pulse-echo apparatus

The test tube is a Plexiglas hollow cylinder, with an inner total volume $V=1.7 \text{ cm}^3$, which is closed at one base by the emitting surface of the immersion transducer (it is not a focused transducer); the sample suspension can be placed into the test tube through a pipe on the lateral surface. The transducer can be used both in transmitting and receiving modes, hence, the ultrasound pulses emitted by the transducer are reflected by the opposite base and return back to the transducer, crossing twice the test tube containing the sample solution, and afterwards they go to the oscilloscope through the ultrasonic pulser-receiver.

The spectrum of the detected signal gives the acoustic behavior of the NBs[®].

Firstly, the test tube was filled with hepes buffer to obtain the decrease of the ultrasound emitted by the transducer only by the hepes acoustic attenuation and it represents the reference signal. Successively, NBs[®] is added to the hepes in the test tube and the acoustic burst attenuation due to NBs[®] suspended in hepes is measured.

Results are expressed as the mean of three experiments \pm SD.

Statistical data analysis was performed using the t-test. To evaluate if obtained differences in experimental results were statistically significant, $P \leq 0.05$ was used as the significance criterion.

- Photoacoustic technique

The photoacoustic technique measuring the decreasing amplitude of the resonance peaks corresponding to the intrinsic frequencies of an acoustic resonator used as a photoacoustic cell as the concentration of NBs[®] in the cell was varied.

The photoacoustic cell, of brass, is an acoustically resonant structure of cylindrical shape having an internal volume of $V = 7.68 \text{ cm}^3$, within which was located the liquid solution which has to be characterized photoacoustically. (Figure. 3)

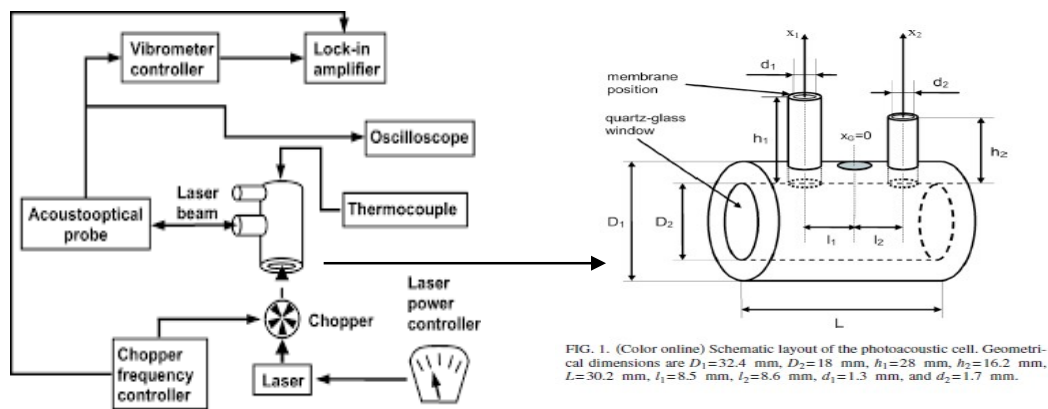


Figure. 3

An argon ion laser (wavelength 4880 \AA units), periodically modulated in amplitude at a variable frequency between 50 and 2000 Hz, struck the liquid through a transparent window of the cell. The periodic heating of the liquid caused periodic variations in its volume which is reflected in displacements of a small polyvinyl membrane in contact with the liquid; these displacements were measured with a laser vibration meter. The measurement relating to gas content within the NBs[®] is based on the fact that the more gas is present in the micro/nanobubbles dispersed in the liquid, the greater will be the decrease in amplitude of the oscillation of the polyvinyl membrane at the resonant frequencies of the photoacoustic cell. [3]

1.5. Morphology studies

- Small Angle X-Ray Scattering (SAXS)

[SAXS measurements were performed by Professor Elena Del Favero, Department of Medical Biotechnology and Translational Medicine, University of Milan, Milan (Italy)]

SAXS measurements were performed in order to investigate the structural and morphological characteristics of the NBS[®].

The ERSF (European Synchrotron Radiation Facility, Grenoble, France) ID02 facility was used.

SAXS measurements were obtained by keeping the position of the sample fixed and automatically moving the detector in a vacuum tube from 0.75 m and 10 m from the sample, so as to be able to gain access to a wide range of scattering wave vectors: $0.1 \text{ nm}^{-1} < q < 3 \text{ nm}^{-1}$, where $q = (4\pi/\lambda) \sin(\theta/2)$, with λ being wavelength ($\sim 0.1 \text{ nm}$) and θ the scattering angle.

The samples were placed in plastics capillaries (KI sheet, ENKI srl, Concesio, Italy) of internal diameter of 2 mm, thickness 0.05 mm and with 98% X-ray transmission, sealed with polyethylene caps. The capillaries were then mounted horizontally in a 6-station sample holder and were filled after they had been installed. In this configuration, it is possible to guarantee almost simultaneous measurements of empty and solvent samples under the same conditions; this is very important in order to be able to subtract backgrounds in an optimum way and compare the results obtained.

In order to be able to carry out precise temperature measurements an ad hoc built thermostat suitable for fitting to the ID02 line was used; the temperature stabilization error within the capillaries was less than 0.05°C.

The measurements were performed at 25°C and the exposure time of each measurement was very short, 0.1 s, in order to minimize any eventual radiation damage.

The measured SAXS profiles report the diffracted radiation intensity as a function of momentum transfer, q . Some spectra for empty and solvent cells were also obtained, carefully compared and subtracted from the spectra of each sample.

The analyses were performed to obtain information on size and morphology of the gas-loaded samples.

- Cryogenic Transmission Electron Microscopy (Cryo-TEM) analyses

[Cryo-TEM images were performed by Dr. Roberto Marotta, Research Technologist at the Electron Microscopy Laboratory, Nanochemistry Department of the Italian Institute of Technology (IIT), Genova (Italy)]

Morphological characterization was performed on the NBS[®] formulations at cryogenic temperatures by (Cryo-TEM).

This technique allows a study of the morphology and size of the vesicles, using as an electron beam radiation to produce the image of the observed sample.

A sample drop (5 μ L) was spread on a Lacey formar/carbon electron microscopy grid and preserved in a frozen state by using liquid ethane.

The vitrification process was carried out by means of FEI Vitrobot System (settings: single blot of 3 sec, offset of 1 sec, drying time and wait of 1 sec).

The sample is observed at JEOL 2100 TEM (accelerating voltage: 200 kV, magnifications: 20,000x and 40000x) at low temperatures.

1.6. NBS[®] stability studies

The stability of NBS[®] stored at 25°C and 4°C was evaluated over time up to 90 days by determining size and ζ -potential at different time intervals (1, 30, 60 and 90 days).

Simultaneously, the acoustic attenuation was measured in order to confirm the presence of inner gas in the NBS[®] stored at 4°C after 90 days.

In addition, SAXS measurements were carried out on NBS[®] stored at 4°C after 30 days.

In order to study the stability of NBS[®] in the biological fluids, human serum or bovine serum was added to the sample until reached at 45% and the changes in dimensions and ζ -potential were measured for 3 hours at a temperature of 37°C.

1.7. Bilayer analyses

- Fluidity

The fluidity of NBS[®] membranes was evaluated by using 1,6-diphenyl-1,3,5-hexatriene (DPH), as “fluidity probe”. [4]

DPH is a nonpolar fluorescent probe localized in the hydrophobic region of the bilayer membrane. The evaluation of fluorescence anisotropy (A) is a generally used method to determine the degree of molecular packing order in the hydrophobic bilayer region.

Anisotropy value is inversely proportional to membrane fluidity, so a high value of A will correspond to a high structural order and low membrane fluidity. [5]

DPH (2×10^{-4}) was added in the first step of NBS[®] preparation (as reported previously). Fluorescence anisotropy measurements were carried out at room temperature with a Perkin-Elmer LS50B spectrofluorimeter at an excitation and emission wavelengths of 400 nm and 425 nm, respectively. The A value of the all formulations was calculated according to the following equation:

$$A = [(I_{VV} - I_{VH}) \times G] / [I_{VV} + (2I_{VH} \times G)]$$

where I_{VV} and I_{VH} are the parallel and perpendicular intensities, respectively, of the emitted fluorescence, compared to the direction of the vertically polarized excitation light. G is the grating correction factor representing the ratio between the vertically (I_{HV}) and the horizontally (I_{HH}) polarized emission when the excitation light is polarized in the horizontal direction. [6] (Figure.4)

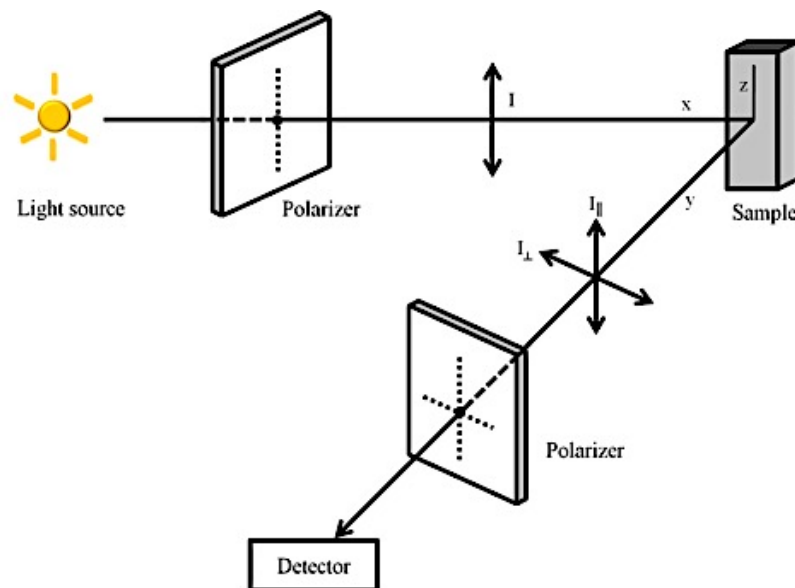


Figure. 4

- Polarity and microviscosity

The fluorescence experiments on NBS[®] loaded with Pyrene probe were carried out to evaluate the polarity and microviscosity of the bilayer in the vesicles. By fluorescence measurements is possible to investigate about the lateral distribution and the mobility of membrane compounds.

Pyrene is a fluorescence probe, with a spectrum characterized by five emission peaks as monomer (from I₁ to I₅) and one as excimer (I_E). (Figure. 5)

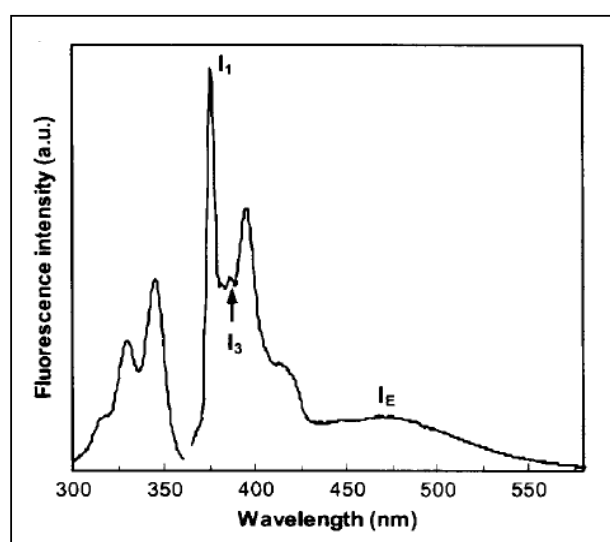


Figure. 5

The monomer and the excimer have different fluorescence signals and the ratio between the several fluorescence intensities is directly related to the probe distribution in the bilayer. In particular, the ratio I_1/I_3 , corresponding to first and third vibration bands of pyrene spectrum, is related to the polarity of the probe environment. At low value of this ratio correspond to a non-polar environment, so the information obtained from this study refers to the bilayer of the vesicles pigeon-hole. [7]

Pyrene can form intramolecular excimer based on the viscosity of the probe microenvironment [8], and it is estimated with the ratio I_E/I_3 , where I_E is the excimer intensity.

1.8. Probes loaded NBS[®]

In order to demonstrate the ability of NBS[®] to entrap drugs and gas, simultaneously, calcein (hydrophilic probe) and Nile red (hydrophobic probe) were included within the NBS[®].

NBs[®] charged with the fluorescent probes were characterized in terms of acoustic efficiency, comparing it with that of the NBs[®] as such.

2. Results

2.1. Size, size distribution and ζ -potential

The dimensions of NBs[®], according to DLS measurements, are around 130-260 nm and the surface charge, expressed as the ζ -potential value, is from weakly to markedly negative (-4 / -71 mV). (Table. 2)

Sample	Dimensions (nm) \pm SD	ζ -potential (mV) \pm SD	PDI
DMPC NBs [®]	151.90 \pm 3.55	-4.35 \pm 0.15	0.20
DMPC-DCP NBs [®]	130.10 \pm 2.20	-70.90 \pm 1.60	0.20
DPPC NBs [®]	166.00 \pm 1.88	-15.70 \pm 0.57	0.10
Span20 NBs [®]	243.30 \pm 3.70	-41.90 \pm 1.82	0.12

Table. 2

The PDI of all samples is always below 0.25, generally 0.2 or less. In particular, a vesicular suspension with a monodisperse population probably will behave uniformly both during storage and after administration *in vivo* in the distribution and cell internalization stages.

2.2. NBs[®] acoustic efficiency

Since NBs[®] are systems full of gas dispersed in a liquid, they act as diffusion (scattering) centers for an elastic wave propagating in the liquid and incident upon them.

The acoustic efficiency of gas trapping within the NBs[®] was evaluated using pulse-echo technique. Figure 6 shows the change in attenuation, expressed as dB/cm at the frequency of 14 MHz, with the variation of DMPC NBs[®] and Span20 NBs[®] concentration.

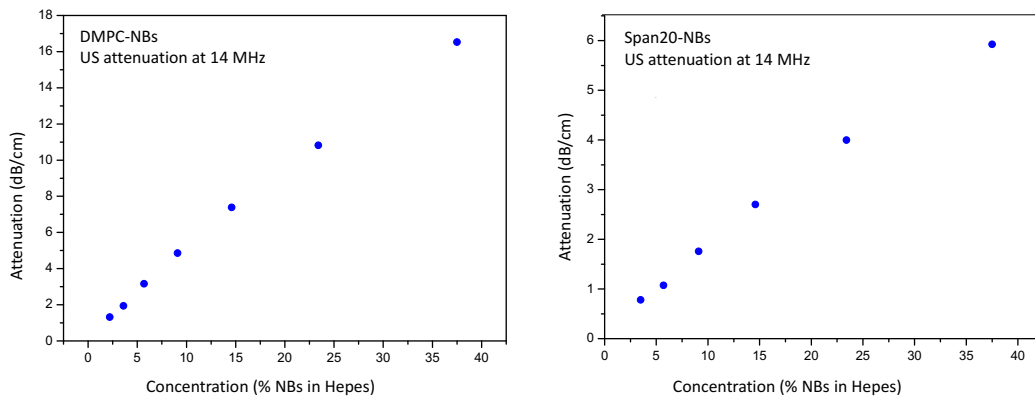


Figure. 6

There is a linear variation of the attenuation with the increase of NBs[®] concentration.

Phospholipid NBs[®] (DMPC, DPPC and DMPC-DCP) show the maximum attenuation values (at a NBs[®] concentration in hepes of a little less than 40%) around of 18 dB/cm and surfactant NBs[®] (Span20) of 6-8 dB/cm.

The obtained results show that the diagnostic power of NBs[®] is comparable or higher compared to micrometer-sized contrast agents SonoVue[®] (around 5-6 dB/cm) measured for the same quantity of micro- and nanobubbles in suspension. (Figure. 7)

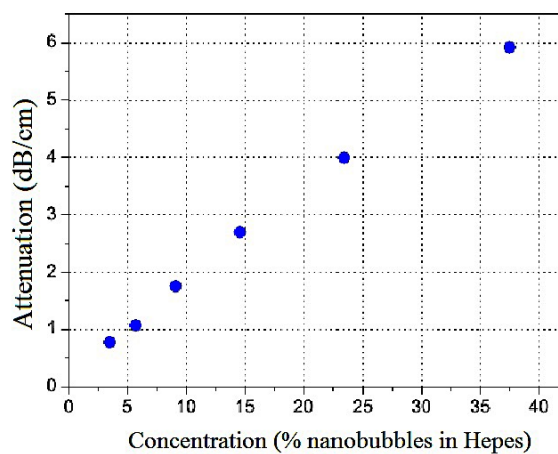


Figure. 7

In addition, the frequency spectrum of the US signal attenuation shows that the US frequencies increases with the increase of Span20 NBs[®] concentration in hepes, reaching maximum values at the frequency range between 22 and 24 MHz. (Figure. 8)

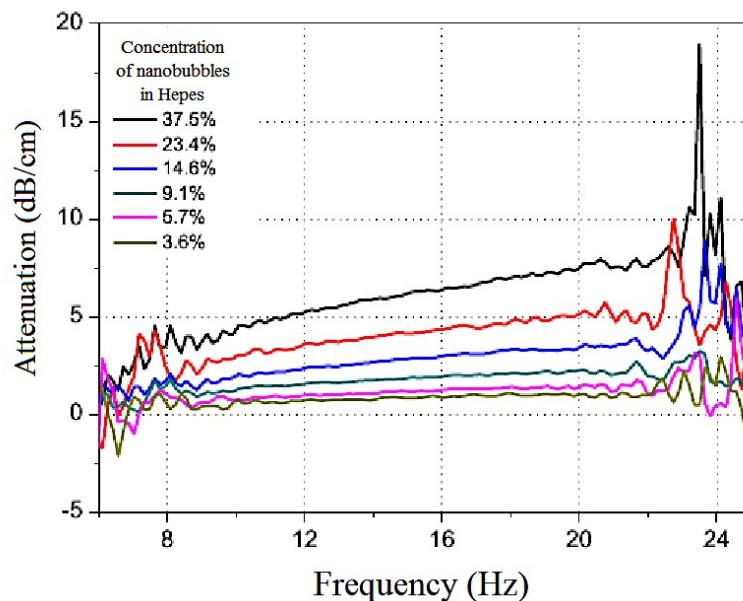


Figure. 8

2.3. NBs[®] morphology

- By SAXS analyses

SAXS measurements show spectra having characteristic peaks corresponding to the internal distance within the particles, providing information about their local structure.

As shown in the figure 9, the intensity profile of DMPC NBs[®] (line red) is quite different compared to a typical DMPC bilayer (line blue), mainly in the low q region.

It is possible to recognize the form factor of the DMPC bilayer, superimposed to the form factor of a nanobubble, with hard interface between air and lipids (characterized by the q^{-4} intensity decay).

In addition, the system results quite unilamellar, as no multilamellar structure peaks appear in the region $q = 1 \text{ nm}^{-1}$, and the size range of the NBs obtained by DLS measurements is confirmed.

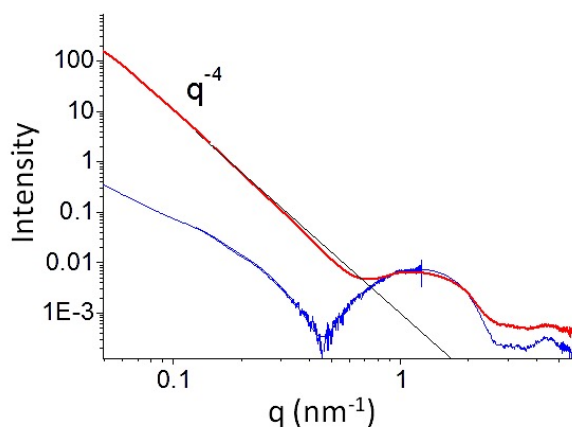


Figure. 9

In figure 10 is represented the hypothetical structure of the NBs[®], according with SAXS measurements.

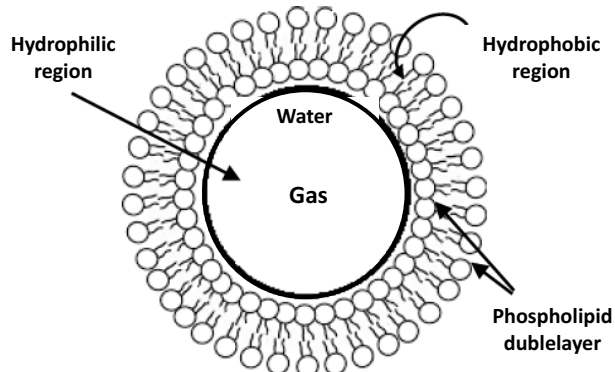


Figure. 10

The NBs[®] are characterized by an apolar double layer or bilayer membrane, containing an internal compartment in which an aqueous layer and the gas coexist.

The presence of a lipophilic double layer stabilizes the structure of the NBs[®] preventing the escape of the gas contained within them, as after confirmed by stability studies.

In addition, the lipophilic double layer may contain compounds of a lipophilic nature and the aqueous layer located between the lipophilic double layer and the central gaseous portion may contain compounds of a hydrophilic nature.

- **By Cryo-TEM analyses**

The morphology of NBs[®] was evaluated by Cryo-TEM analyses (Figure 11 and 12), in addition to SAXS studies.

The images allow to evaluate the shape and dimension of different NBs[®].

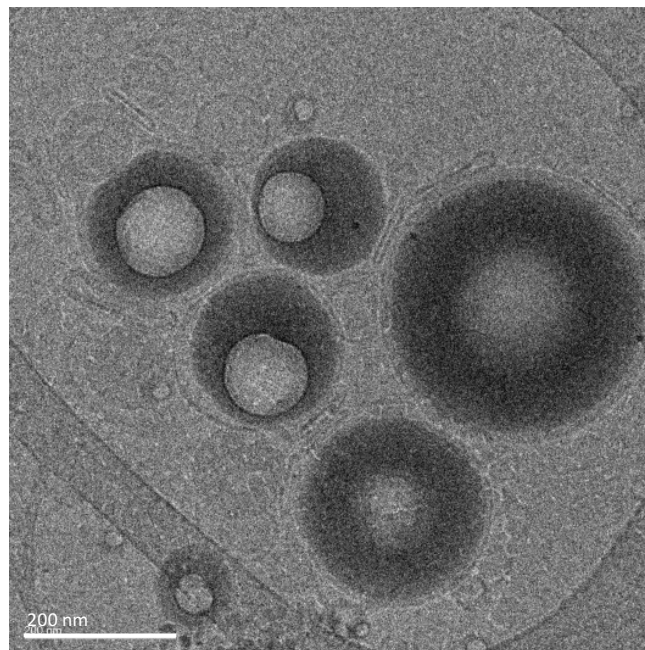


Figure. 11 The image show the average of 5 tomographic slices of the DMPC NBs[®]. Scale bar 200nm.

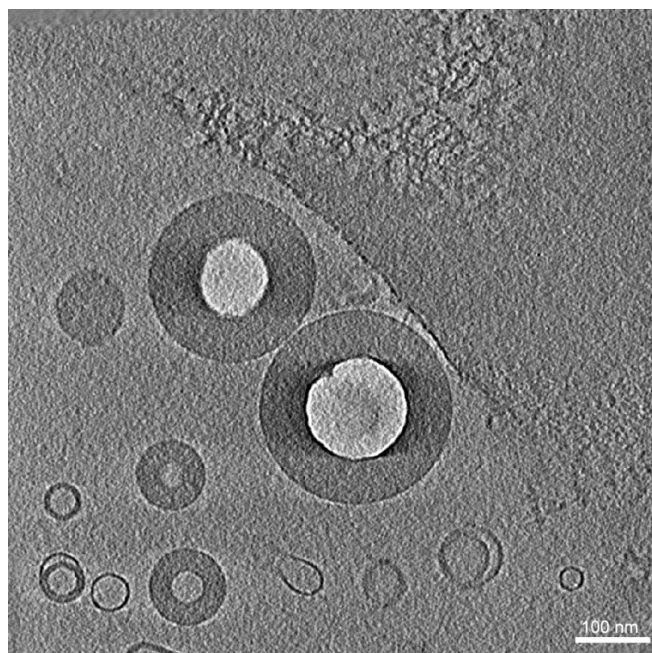


Figure. 12 The image show the average of 5 tomographic slices of Span20 NBs[®].
Scale bar 100nm.

The dimensions obtained for all samples confirm the results acquired by DLS and SAXS measurements. In addition, all prepared NB[®] seemed to have a spherical shape.

2.4. NBs[®] stability studies

- Stability studies over time

Stability tests surprisingly have proved that the NB[®] are extremely stables, as established by the DLS analysis, SAXS analysis and pulse echo analysis.

Stability analyses of NBs[®] were assessed in terms of changes in dimensions and surface charge over a time interval of approximately 3 months at two different storage temperatures. (Figure. 13)

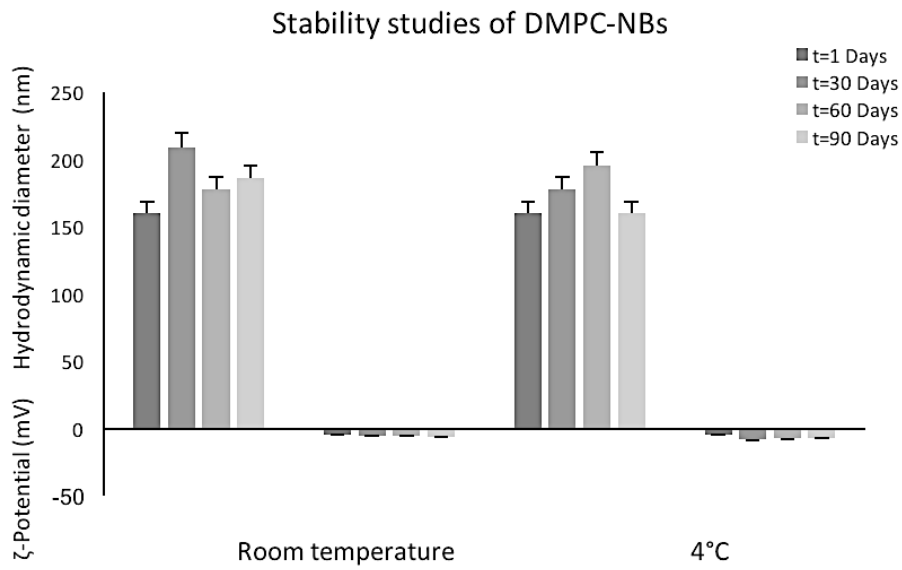


Figure. 13

This study shows that the samples are stable up to 90 days at both storage temperatures because no significant changes are assessed in the parameters investigated.

SAXS measurements show that the morphology of NBs[®] containing gas are still stable after 30 days. (Figure. 14 and 15)

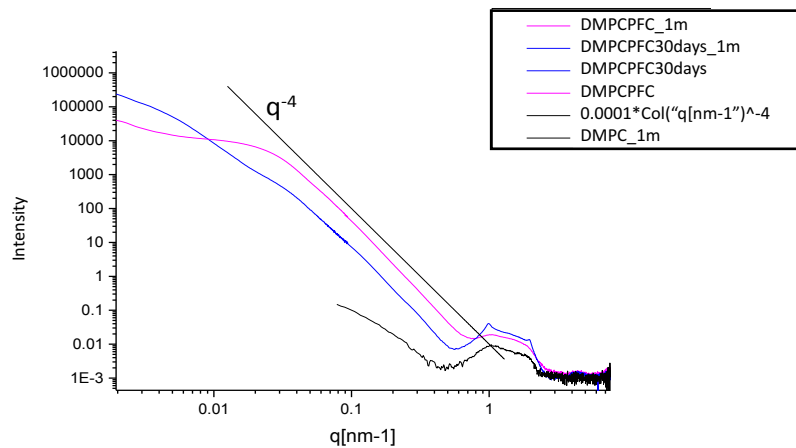


Figure. 14

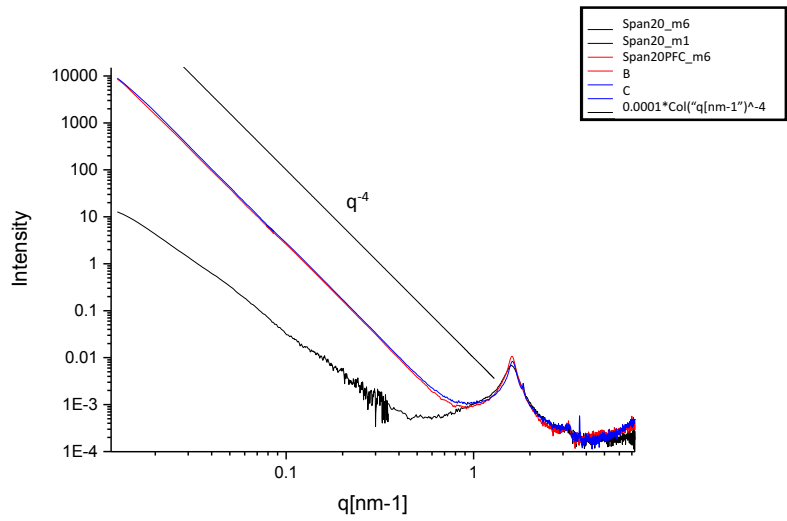


Figure. 15

Also, the acoustic efficiency of the NB[®] are measured as a function of time and it was found that they are capable of maintaining their acoustic properties unchanged after storage for three months, as established comparing the attenuation measured at the first day and after 90 days. (Figure. 16)

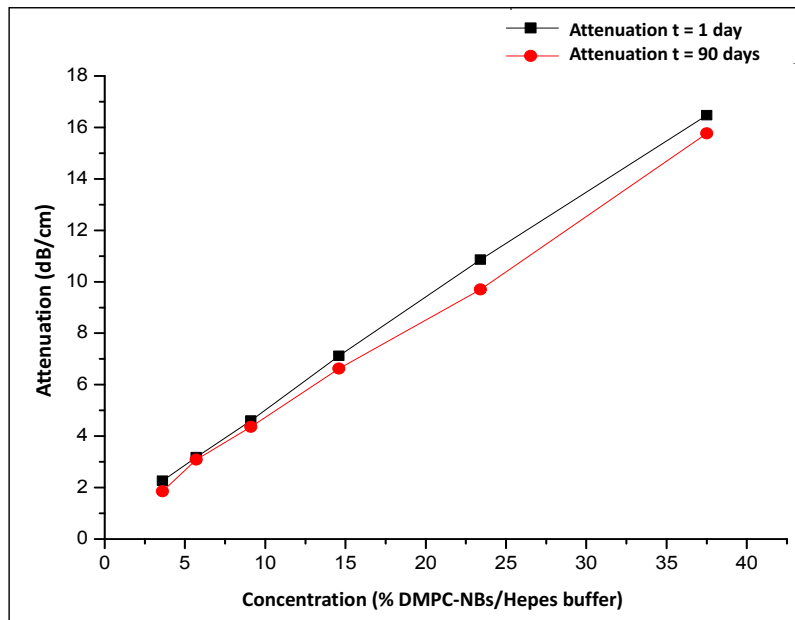


Figure. 16

The NBs[®] tested are stable in terms of maintaining dimensions and ζ -potential, persistence of acoustic signal and gas retention very much better than that of commercial products.

For example, SonoVue[®] diluted according to the manufacturer's specifications and measured using the same technique, it is found that the latter's stability is reduced after approximately 100 hours, as evaluated by pulse-echo (Figure. 17) and photoacoustic (Figure. 18) measurements.

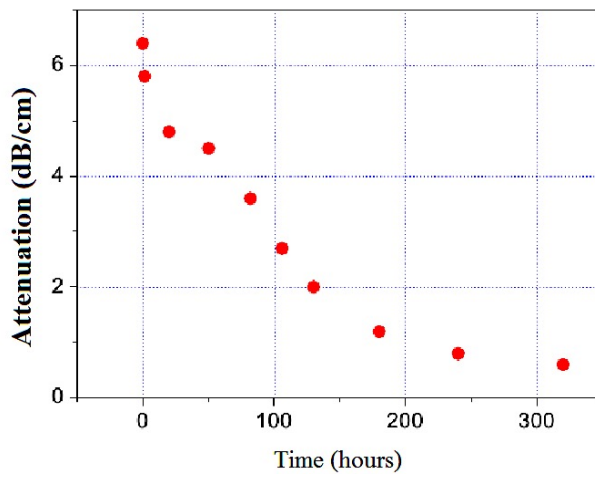


Figure. 17

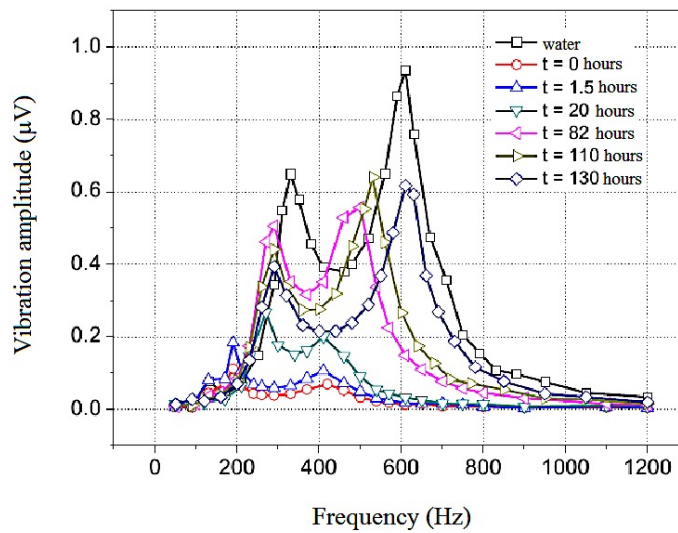


Figure. 18

- **Stability studies in the biological fluids**

NB[®] are also stable for at least 180 minutes at temperatures simulating *in vivo* conditions (37°C and 40°C) and for 180 min in the presence of 45% (v/v) of human and bovine serum.

From the data shown in figure 19, it is clearly evident that the NB[®] are stable if placed in contact with human and bovine serum over the investigated time interval.

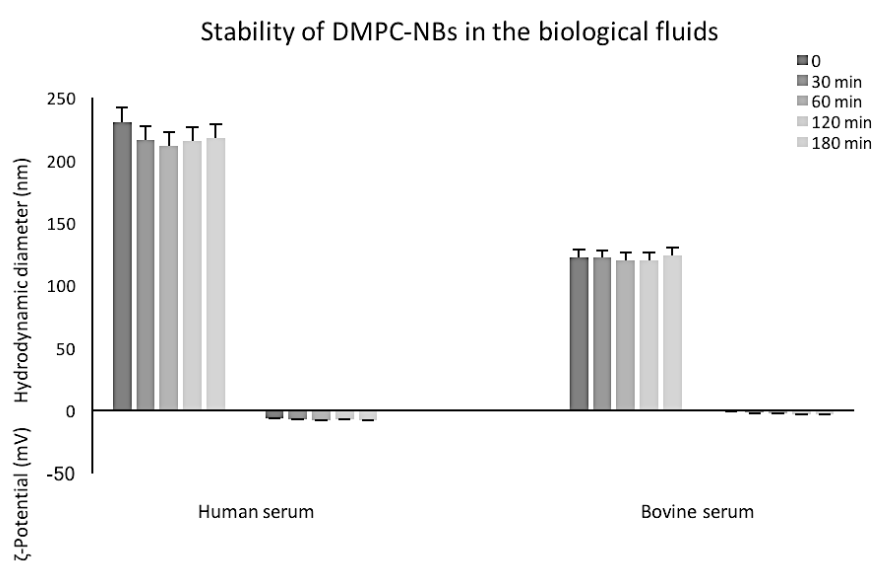


Figure. 19

Furthermore, the NB[®] are stable in terms of acoustic efficiency at temperatures simulating *in vivo* conditions (37°C and 40°C) up to 180 min., as shown in the figure 20.

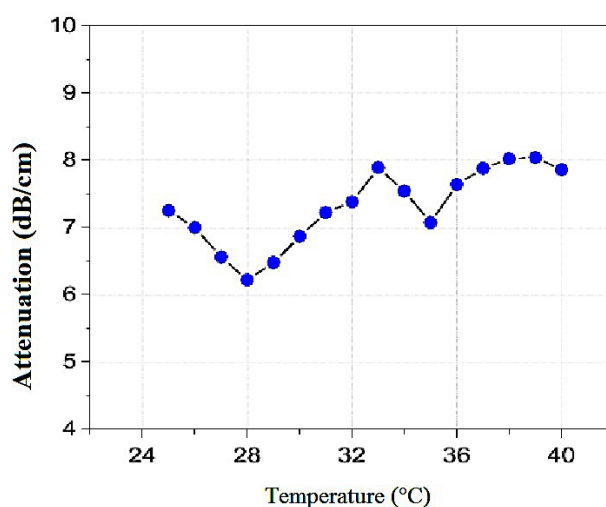


Figure. 20

2.5. Bilayer characterization

In order to deep characterize the nature of the NBs[®] bilayer, fluidity, polarity and microviscosity have been evaluated.

Fluorescence anisotropy data indicated that the vesicular bilayer is quite rigid and the values obtained are similar comparing vesicle with and without gas. (Table. 3)

Furthermore, the data obtained in terms of polarity and microviscosity showed no significant change on the bilayer features in presence of gas inside the vesicles.

Sample	Fluidity	Polarity (I_1/I_3)	Microviscosity (I_E/I_3)
DMPC vesicles without gas	0.27	1.09	0.58
DMPC NBs [®]	0.25	1.05	0.44
DMPC+DCP vesicles without gas	0.26	1.06	0.47
DMPC+DCP NBs [®]	0.24	1.07	0.43
Span20 vesicles without gas	0.23	0.93	0.24
Span20 NBs [®]	0.24	0.95	0.32

Table. 3

These results point out that the gas in the all samples remains trapped in the inner core without conditioning the membrane properties, confirming the results obtained by morphology studies.

2.6. Fluorescent probes loaded NBs[®]

NBs[®] are capable to load both hydrophobic drugs in the double layer and hydrophilic drugs in the aqueous layer, along with gaseous compound, and are therefore potentially capable of being used in the therapeutic, diagnostic and theranostic fields.

A hydrophilic fluorescent probe (calcein) and a hydrophobic one (nile red) have been loaded in the NBs[®], in addition to the gas, to evaluate if physical chemical properties and/or stability remained unchanged.

The Span 20 NBs[®] charged with the fluorescent probes were characterized in terms of acoustic efficiency, compared to Span20 NBs[®], as shown in figure 21.

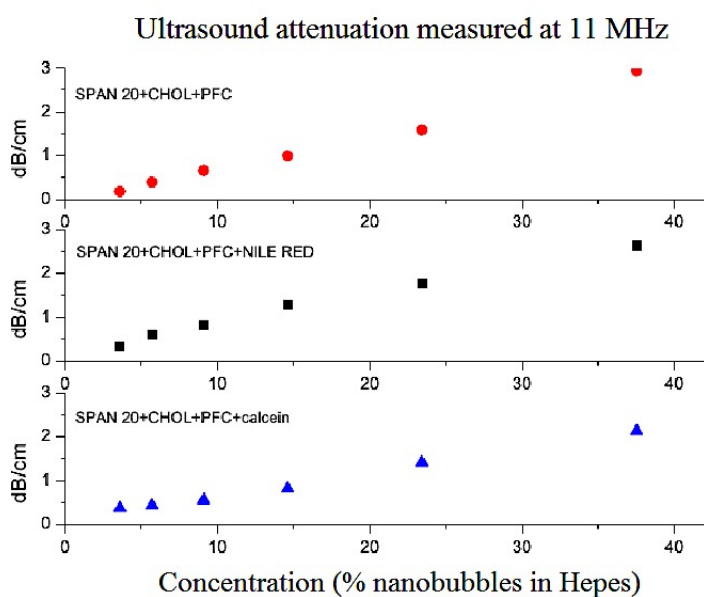


Figure. 21

Therefore, the co-loading of probes does not have affect the acoustic efficiency of the NBs[®].

2.7. Comparison between NBs[®] and MBs[®]

The efficiency of trapping gas within the NBs[®] is also evaluated using a photoacoustic technique and the obtained results are compared with those obtained by SonoVue[®] evaluation. (Figure. 22)

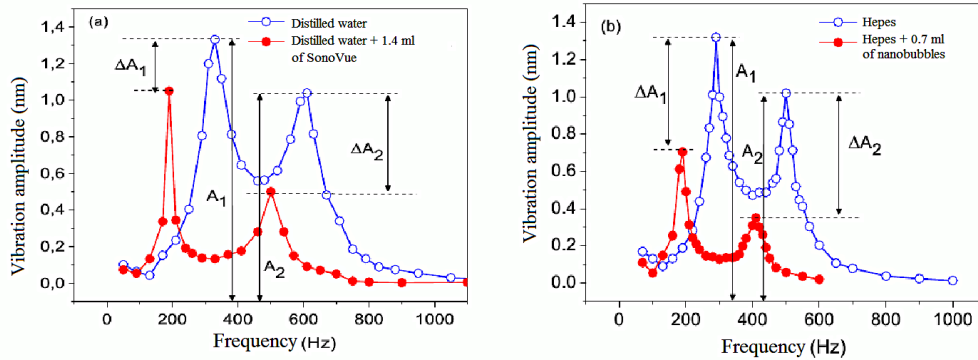


Figure. 22

1.4 ml of SonoVue[®] solution were diluted in 7.68 ml of distilled water causing relative variations in vibration amplitude for the first and second resonance frequencies of the photoacoustic cell equal to $(\Delta A_1/A_1)_{SV} \approx 0.77$ and $(\Delta A_2/A_2)_{SV} \approx 0.48$, respectively. (Figure. 22 panel a)

Instead, 0.7 ml of NBs[®] in 7.68 ml of hepes buffer generated a relative variation in vibration amplitudes at the two resonance frequencies of $(\Delta A_1/A_1)_{NBs} \approx 0.54$ and $(\Delta A_2/A_2)_{NBs} \approx 0.33$, respectively. (Figure. 22 panel b)

Because the measured values for the NBs[®] were approximately 30% lower than those obtained with SonoVue[®], the greater capacity for trapping gas within the NBs[®] must therefore be estimated to be 30% greater than SonoVue[®], for the same volume of micro/nanobubbles dispersed in the liquid.

3. Conclusions

The NBs[®] prepared are able to overcome the limitation of existing UCAs in that they are more stable over time and extremely homogenous in shape and dimensions.

NBs[®] have the following advantages:

- nanometric-sized dimensions;
- a double layer of a lipophilic nature made up of amphiphilic molecules;
- the materials used for their preparation and the gas are not toxic;
- stability in terms of acoustic efficiency, in aqueous solution at a storage temperature of 25 and 4°C (at least 3 months), at temperatures simulating *in vivo* conditions (37 and 40°C) up to 180 min and also in the presence of human and bovine serum for 180 minutes at a temperature of 37°C;
- not need to make use of preservative and reconstitution techniques such as lyophilisation and subsequent dehydration and the addition of gas.

The possibility of adding both water-soluble and fat-soluble therapeutic and/or diagnostic agents to the NBs[®] according to the invention makes it possible to produce vectors for use in diagnostic, therapeutic and theranostic applications.

In particular, these characteristics allow them also to be used when applied to pediatric and veterinary diagnostics, in particular small animals, avoiding the risk of the formation of microembolisms which might occur following the use of micro- or nano-sized bubbles which do not have uniform dimensions.

References

- [1]. Carafa M, Santucci E, Alhaique F, Coviello T, Murtas E, Ricciardi FM, Lucania G, Torrisi MR. Preparation and properties of new unilamellar non-ionic/ionic surfactant vesicles. *Int J Pharm*, 160, 51–59, 1998.
- [2]. Sze A, Erickson D, Ren L, Li D. Zeta-potential measurement using the Smoluchowski equation and the slope of the current-time relationship in electroosmotic flow. *J Colloid Interface Sci*, 261, 402-410, 2003.
- [3]. Alippi A, Bettucci A, Biagioni A, D’Orazio A, Germano M, Passeri D. Photoacoustic cell for ultrasound contrast agent characterization. *Rev Sci Instrum*, 81, 1-7, 2010.
- [4]. Lentz BR. Membrane “fluidity” as detected by diphenylhexatriene probes. *Chem Phys Lipids*, 50 (3–4), 171-190, 1989.
- [5]. Shinitzky M, Barenholz Y. Fluidity parameters of lipid regions determined by fluorescence polarization. *Biochim Biophys Acta*, 515 (4), 367-94, 1978.
- [6]. Marianecchi M, Rinaldi F, Di Marzio L, Mastriota, M, Pieretti S, Celia C, Paolino D, Iannone M, Fresta M, Carafa M. Ammonium glycyrrhizinate-loaded niosomes as a potential nanotherapeutic system for anti-inflammatory activity in murine models. *Int J Nanomedicine*, 9, 635–651, 2014.
- [7]. Vanderkooi J, Fischkoff S, Chance B, Cooper RA. Fluorescent probe analysis of the lipid architecture of natural and experimental cholesterol-rich membranes. *Biochemistry*, 13 (8), 1589-95, 1974.
- [8]. Zachariasse KA. Microviscosity measurements in micelles and phospholipids. *Phys Chem*, 82, 950, 1978.

**Reversible BBB opening
by Focused Ultrasound**

This part of thesis was carried out in collaboration with Julie McNairn, PhD student at the Queen Medical Research Institute, College of Medicine and Veterinary Medicine, University of Edinburgh, under the supervision of Dr. Carmel Moran.

1. Introduction

As previously reported, brain delivery of drugs in the treatment of neurological diseases is mainly restricted due to the blood-brain barrier.

Recently, the possibility of the non-invasive localized opening of BBB by using focused ultrasound (FUS) exposure, in conjunction with systemically administered microbubbles (MBs) have attracted great attention as a new method to deliver active compounds to the brain. [1]

Several researchers have established that the administration of MBs can effectively reversibly open the BBB, without damaging the brain tissue. [2, 3]

Moreover, the use of FUS allows to target specific brain regions through the employment of stereotaxic coordinates and image guidance. [4]

When an appropriate US pressure is applied in presence of injected MBs, the signal intensity of Magnetic Resonant Imaging (MRI) increase in the focal volume, due to the BBB disruption. The intensity is maximal immediately after the FUS applied and proportional to the applied pressure amplitude. Instead, only a small increase of the MRI intensity is observed without the injection of MBs. [5]

The cellular mechanism that causes BBB opening is still unknown, but probably it is thought that when FUS is applied in presence of MBs systemically administrated, inertial cavitation is induced, due to the rapid expansion and violent collapse of bubbles. This can cause the temporal distension of tight junctions with a consequent increase of endothelial porosity and vascular permeability (sonoporation) and an increase of drug intracellular uptake. [6]

Commercially available microbubbles (MBs) show inert gaseous cores coated by a lipid or albumin monolayer shell. These systems are used only as contrast agent in ultrasound imaging. However, clinical application is limited mainly due to their size (1-10 μm), preventing the extravasation out of the blood pool into brain, and short half-life in the systemic circulation. [7]

The new formulated nanobubbles[®] (NBs[®]) combine the characteristic of drug delivery systems and of contrast agents (theranostic system).

In fact, these vesicles are able to entrap drugs not bioavailable to target site of action, limiting their toxicity and adverse effects, to protect the drugs from degradation phenomena and finally to improve

UCAs stability in the systemic circulation.

1.1. Aim

The aim of this work is the evaluation of the effect on the BBB opening by using different UCAs in terms of size and shell composition.

In particular, the commercially available MBs, SonoVue[®], phospholipid (DMPC) and surfactant (Span20) NBs[®] were employed.

The BBB permeability induced by FUS in conjunction with SonoVue[®]/NBs[®] injection was confirmed by the presence of Evans blue (EB) dye in the brain parenchyma.

FUS-induced BBB opening was studied in two different experiments in order to (1) determine the spread of dye into the brain after DMPC/Span20 NBs injection, (2) the time period of BBB opening after sonication using different sized UCAs and finally (3) analyse the spread of fluorescent dye calcein (as hydrophilic model drug molecules) deposition through BBB openings to confirm the ability of these carrier as drugs delivery systems.

2. Materials and methods

2.1. SonoVue[®]

Commercially available microbubbles, SonoVue[®] (Bracco Diagnostics Inc., Milan, Italy), is composed of a phospholipid monolayer membrane composed by distearoyl-phosphatidylcholine (DSPC), dipalmitoylphosphatidylglycerol sodium (DPPG·Na), and palmitic acid. The gas encapsulated within the lipid shell is a sulphur hexafluoride gas. SonoVue[®] have a mean diameter of 3.0-4.5 μm and a concentration of approximately $5.0\text{-}8.0 \times 10^8$ bubbles/ml (as per manufacturer's guidelines).

Toxicology studies performed by manufacturer indicated that a single dose administered up to 20ml/kg in humans, rats and monkeys does not show adverse side-effect.

2.2. Bubblesomes[®]

For these experiments, DMPC and Span20 NBs[®] are used. The preparation and characterization of both samples has been previously reported.

NBs[®] containing the fluorescent probe calcein have been prepared in order to investigate the passage of a hydrophilic model drug across the BBB.

2.3. NanoSight measurements

In order to establish the volume of NBs[®] to inject in the mouse, the concentration of NBs[®] was calculated by using a NanoSight device.

The NanoSight works using laser diffraction by scattering off particles within the solution, to determine their size distribution and concentration. The scan works at a frequency of 16 MHz using a dynamic image probe.

2.4. Mice

HSD2.BKO mice were generated by crossing 11-HSD2^{flx/flx} mice (Artemis Pharmaceuticals, Cologne, Germany) with a Cre mouse line driven by the Nestin promoter [8], (Nestin is expressed in proliferating CNS cells).

Studies were carried out in strict accordance with the UK Home Office Animals (Scientific Procedures) Act, 1986 and the European Communities Council Directive of 24 November 1986 (86/609/EEC) and were assessed by the University of Edinburgh Ethical Review Committee.

All experiments were performed blind to genotype on male mice using littermate controls.

Only nestin.cre-HSD2^{fl/fl} - cre negative mice were used in this study.

2.5. BBB opening protocol

All animal procedures were performed in accordance with the guidelines of our institutional animal committee.

Each mouse was anesthetized with Isoflurane (Isoflo[®], Abbott) and placed prone with its head immobilized by a stereotaxic apparatus (Figure. 1).

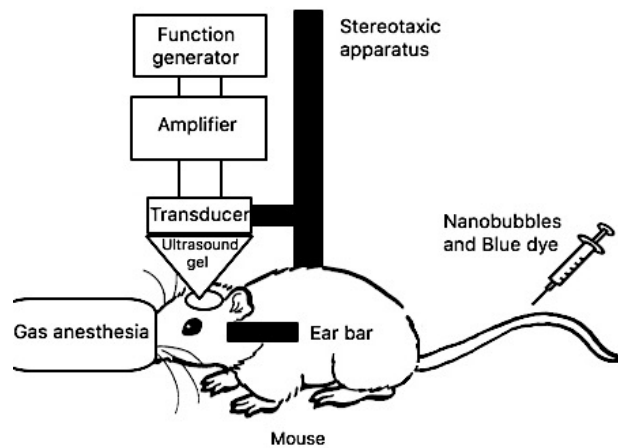


Figure. 1

The fur on top of the head was removed using a depilatory cream and an ointment was applied on the eye to protect it during the surgery.

The FUS transducer was placed on the intact scalp and skull of the mouse and the ultrasound coupling gel was used to eliminate any remaining impedance mismatch between the two surface.

A single-element FUS transducer (central frequency: 3.5 MHz; focal depth: 5.5 mm) was driven by a function generator through a 50dB power amplifier to generate the FUS beam. The focus of the ultrasonic field was positioned to the desired region with its beam axis perpendicular to the surface of the skull.

SonoVue[®] or DMPC/Span20 NBs[®] and Evans Blue (3 μ l/mg) were injected via the tail vein of the mouse. Immediately after, pulsed FUS (peak-rarefactional pressure: 2.1 MPa; pulse length 35.000 cycles at 10Hz; voltage 1 Vpp) was applied, once in each mouse brain, for 3 shots. Each shot consisted of 55 second of sonication with an interval of 5 second between each shot to allow the heat to dissipate.

After 48 hours, animals were sacrificed and the brain was extracted. The brain specimens were placed in 10% buffered formalin to allow the fixation time. A cryostat was employ to obtain several sections of the brain intended to histological and fluorescence analysis.

2.6. Evans blue dye extravasation

To evaluate the integrity of the BBB, after FUS application in conjunction with SonoVue[®] or DMPC/Span20 NBs[®], Evans Blue (EB) extravasation was examined.

EB dye has binding affinity to serum albumin that, in the normal condition, it cannot across the BBB.

However, when BBB was opened, EB-tagged albumin extravasated from vasculature into the brain tissue. Consequently, the accumulation of EB dye could be quantified after extraction from the brain tissue using fluorescence imaging method.

2.7. Fluorescence analysis

Coverslips with anti-fade reagent DAPI (4',6'-diamidino-2-phenylindole – a nuclear marker) were applied on the slide with the brain slide treated with calcein loaded DMPC/Span20 NBS[®] and EB dye. Glass slides were examined with a Zeiss confocal scanning laser microscope. Green fluorescence (calcein) was observed with a filter set at excitation and emission wavelengths of 492 and 520 nm, respectively.

2.8. Histological analysis

The brain matrix slices were paraffin processed, embedded and sectioned, according to standard procedures. Resulting sections were stained by haematoxylin and eosin (H&E). H&E-stained sections were analysed for histopathologic hallmarks of brain injury (haemorrhage, edema, inflammatory cell infiltrate).

2.9. Statistics

All data has the mean plotted \pm SEM. The significance is calculated using an unpaired T-test unless otherwise stated.

3. Results

3.1. NBS[®] concentrations

All sample concentrations are shown in the Table 1, the concentration of SonoVue[®] is provided from the manufacturer. Each NBS[®] have been diluted (1×10^5) in order to inject a number of bubbles to that of SonoVue[®].

The final column shows the volume of each UCAs injected into the animal.

Sample	Dilution	Concentration (bubbles/ml)	Volume injected (μ l/mg)
SonoVue [®]	-	$5.0-8.0 \times 10^8$	0.3
DMPC NBS [®]	-	$2.0-3.0 \times 10^{13}$	0.5
	1×10^5	$2.0-3.0 \times 10^8$	
Span20 NBS [®]	-	$2.0-4.0 \times 10^{13}$	0.4
	1×10^5	$2.0-4.0 \times 10^8$	
DMPC NBS [®] +calcein	-	2.14×10^{13}	0.7
	1×10^5	2.14×10^8	
Span20 NBS [®] +calcein	-	1.26×10^{13}	1.2
	1×10^5	1.26×10^8	

Table. 1

3.2. *In vivo* opening of the BBB using NBS[®]

Figure 2 illustrates the total inspection profiles of the brain tissues, 48 hours after the sonication. The extravasation of EB dye bound to albumin - blue coloration spot - was observed in the brain to the unaided eye and it indicated that BBB was successfully opened by the combination of FUS and Span20 NBS[®] (A) and with DMPC NBS[®] undiluted (B) and diluted (D). For the mouse brain tissue treated with Span20 NBS[®] diluted (C), blue coloration spot was not visible, probably due to no BBB destruction.

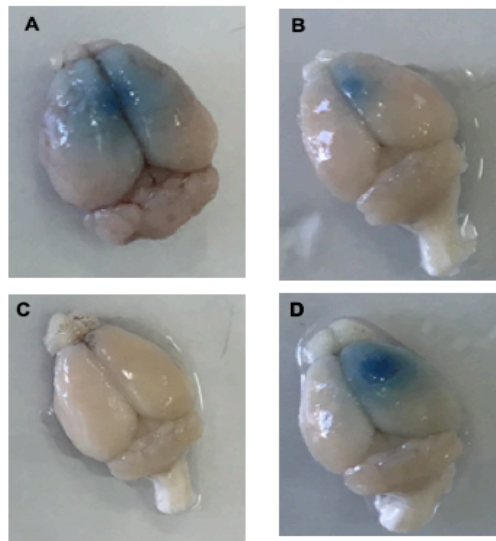


Figure. 2 EB dye extravasation in the brain tissues after FUS exposure of mouse treated with Span20 NBs[®], undiluted (A) and diluted (C), and with DMPC NBs[®], undiluted (B) and diluted (D).

The mouse brain tissue treated with Span20 NBs[®] (A) shows an EB dye extravasation more significant compare to DMPC NBs[®] (B and D).

In particular, for the mouse brains treated with DMPC NBs[®], the blue spot in the picture D (NBs[®] diluted) seemed to be more intensive compared to picture B (NBs[®] undiluted).

3.3. Histological assessment

The histological analysis (Figure 3, 4 and 5) - to detect the tissue injury in the brain – shows that no erythrocyte or haemorrhages were observed in the brain treated with Span20 NBs[®] (a) (n=4).

Moreover, this analysis had confirmed that the surfactant NBs[®] diluted (c) did not open the BBB (no white shadow nearby to the BBB) (n=3).

Instead, following the injection of phospholipids NBs[®] with different concentrations, the effect on the brain tissue was varying. A few erythrocyte extravasations (red spots on the brain parenchyma) were observed in the brain tissue treated with DMPC NBs[®] (b) that it does not appear to cause tissue necrosis (n=4). Whereas the histologic finding for the sample of DMPC NBs[®] diluted (d) suggest a high degree of tissue damage (n=4).

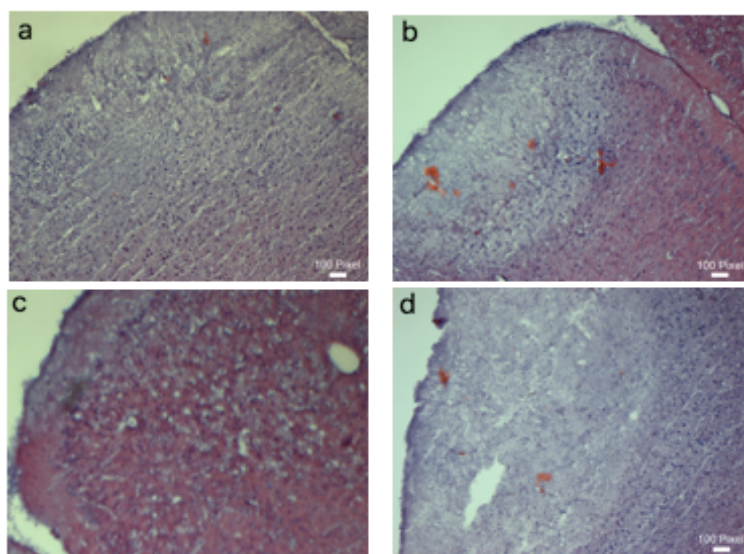


Figure. 3 Histology examination of brain tissues of mice sonicated using FUS with Span20 NBs[®], undiluted (a) and diluted (c), and DMPC NBs[®], undiluted (b) and diluted (d) (x4 magnified region).

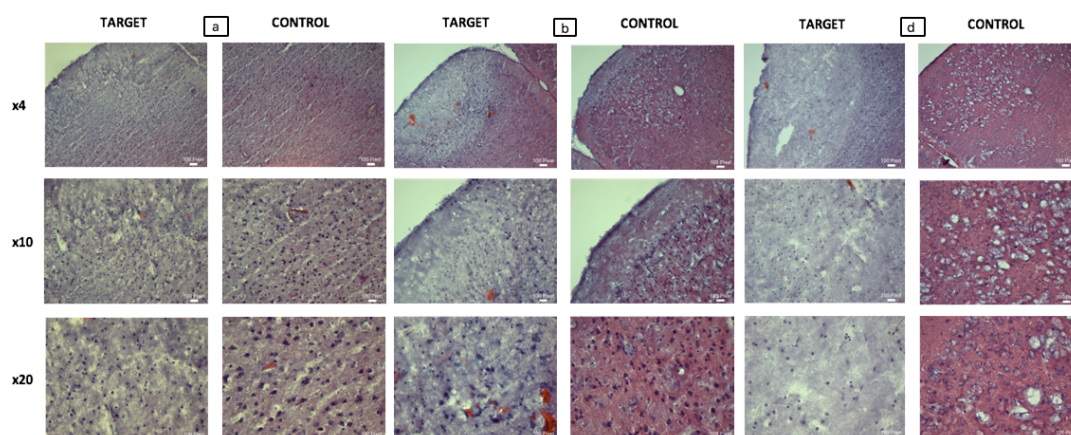


Figure. 4 H&E staining of the brain sections treated with Span20 NBs[®] undiluted (a) and DMPC NBs[®], undiluted (b) and diluted (d) compared with the control (x4, x10 and x20 magnified region).

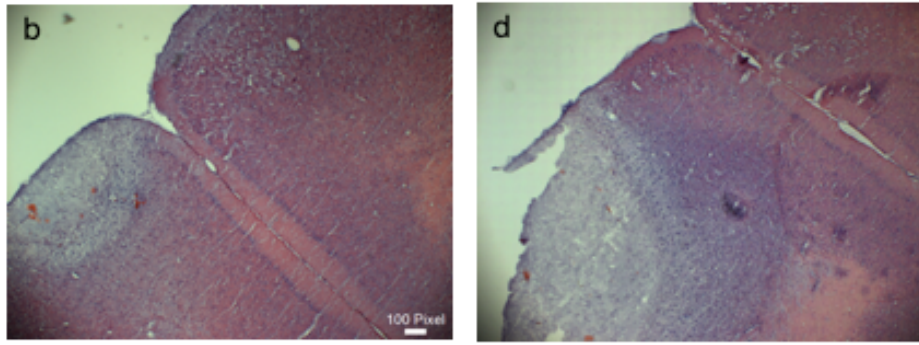


Figure. 5 Histology of the brain sections treated with DMPC NBs[®], undiluted (b) and diluted (d) after H&E staining (x2 magnified region).

3.4. Volume of Evan's Blue into the brain following FUS disruption

In order to evaluate the effect of different UCAs on the BBB opening, the different sized contrast agents have been employed using the same parameters previously mentioned. In particular, SonoVue[®] and Span20 NBs[®] have been injected in the mice and, following the sonication, the EB dye spread were observed into the brain of the mice euthanized after 24hours. (Figure. 6)

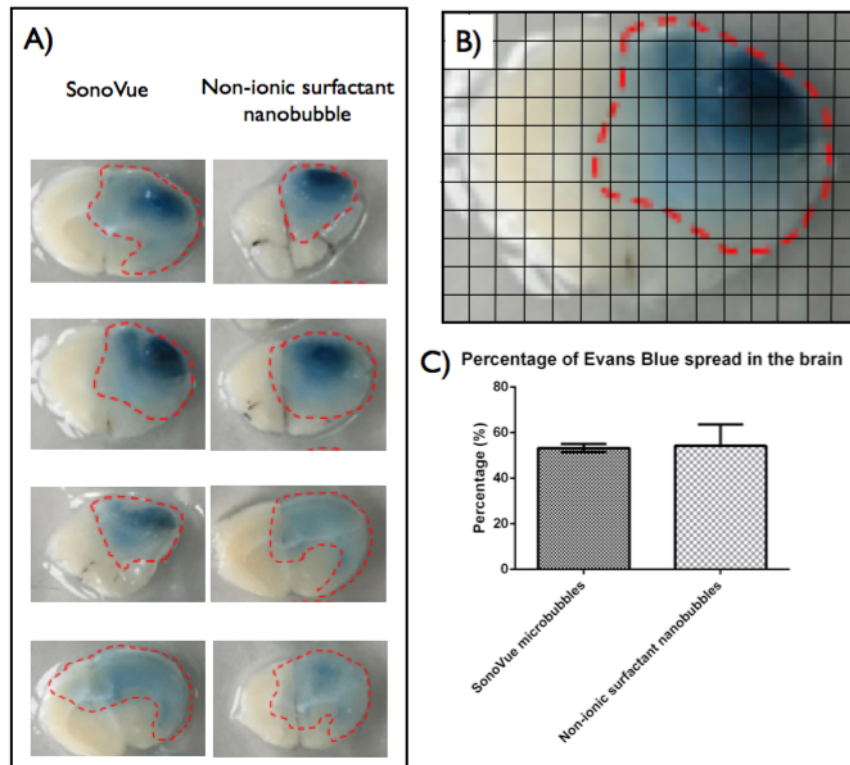


Figure. 6 Spread of EB following BBB disruption: In the panel (A) is shown the spread of Evan's Blue dye on the coronal brain sections (thick=1mm) of 4 mice treated with MBs[®] and NBs[®]. Panel (B): the percentage of area covered in the brain of EB dye was calculated through the overlay of a grid. Panel (C): the graph shows that the spread of dye following BBB disruption using SonoVue[®] or Span20 NBs[®] is no different.

SonoVue[®] mean = 53.25 SEM +/- 1.75 (n=4); Span20 NBs[®] mean =54.25 SEM +/- 9.322 (n=4).

The spread of EB observed appear very similar between the NBs and MBs. Using 4 mice for each UCAs, the spread of dye was calculated by using a grid, whereby the dyed regions were divided by the total brain section in order to calculate the percentage of dye covered regions (outline in figure 6 A by red dashed lines). The percentage of spread of dye was plotted as a percentage (figure 6 C), showing there was no difference between the MBs and NBs on BBB disruptions.

3.5. BBB closing after FUS application

Time needed by BBB closing, after FUS application, was assessed. Initially, 24 hours were the time point chosen to confirm the BBB closing. The BBB was opened using FUS with both SonoVue and Span20 NBs, and the EB dye was administered 24h post sonication. No dye was observed in the brain at the 24h time point indicating that the BBB was completely closed (n=3). (Figure 7)

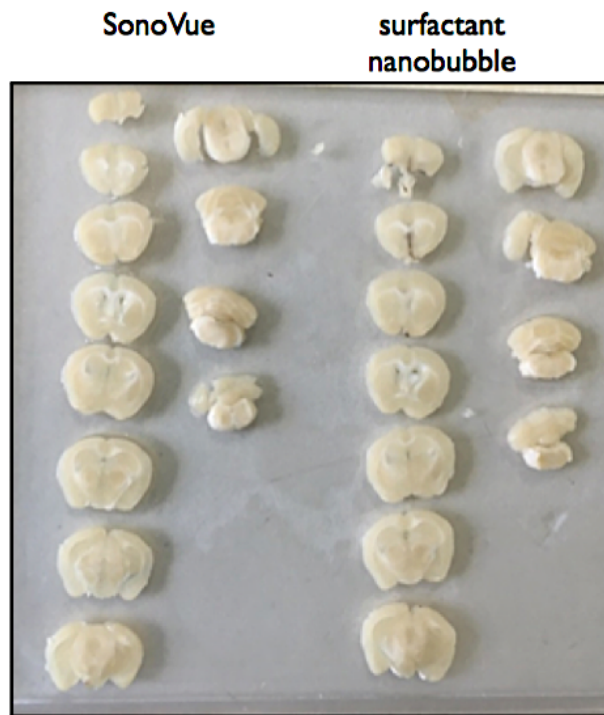


Figure. 7 Brain sections 24h post BBB opening (n=3).

After, shorter time points were then evaluated at 0, 3, 6, 9 and 12 hours to identify how long the BBB is opened following disruption. (Figure. 8)

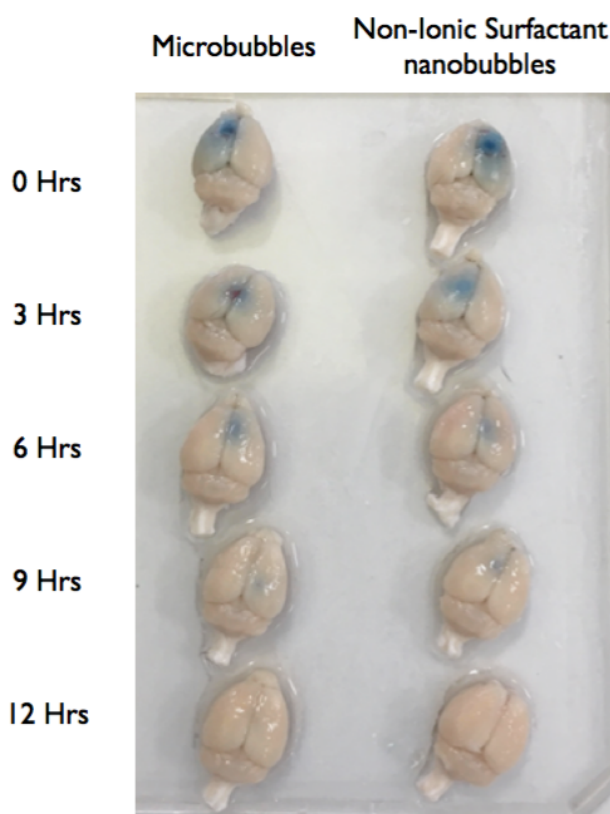


Figure.8 Duration of BBB opening after sonication. The BBB was opened using either SonoVue[®] (n=5) or Span20 NBs[®] (n=5) and at time point 0, 3, 6, 9 and 12-hour time points Evan's Blue dye was injected into the tail vein.

EB dye entering the brain over the 12h but with reducing volumes entering as time progresses due to the barrier closing. At the 12h time point, the BBB is fully closed in the brain treated with the NBs and almost fully closed with MBs.

Therefore, the opening of the BBB is prolonged with the SonoVue[®] compare to Span20 NBs, despite the volume of the EB dye entering over 24 hours not being different between the two UCAs.

3.6. Volume of calcein delivered into the brain

In order to demonstrate the ability of DMPC/Span20 NBs[®] to deliver drugs into the brain, the spread of fluorescent dye calcein (as hydrophilic model drug molecules) deposition was analysed.

In this experiment, the NBs were used as a carrier to deliver calcein into the brain, where it is then released from the bubble into the surrounding brain tissue, after FUS application.

Calcein loaded DMPC/Span20 NBs[®] were injected in the mice, in both concentrations (undiluted and

diluted) with EB dye and after 48 hours, to allow the calcein diffusion, the brain tissues were collected. (Figure. 9)

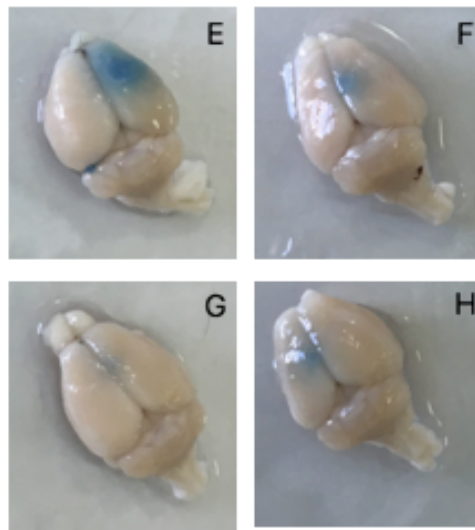


Figure. 9 EB dye extravasation in the brain tissues after FUS exposure treated with Span20 NBs[®], undiluted (E) and diluted (G), and with DMPC NBs[®], undiluted (F) and diluted (H). This was a pilot study (n=1) to confirm the optimum concentration to elicit BBB opening.

The EB extravasation was clearly visible for all brain treated with NBs[®], in particular, it is greater for the undiluted NBs[®] (E and F) compare to diluted (G and H).

Finally, in order to evaluate the volume of calcein delivered into the brain, the mice were treated with both NBs formulations undiluted.

The presence of the calcein (green) in the brain parenchyma was visualized at the 488nm wavelength by using Azioskop microscope. (Figure. 10 A).

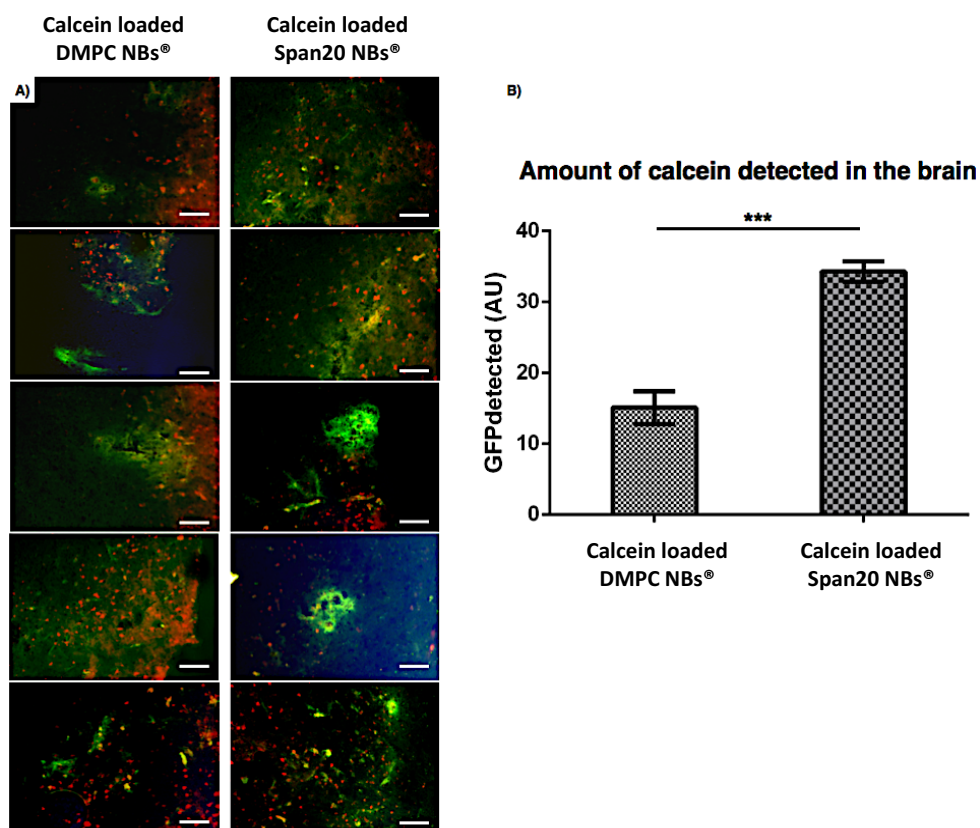


Figure. 10 Panel (A) Calcein release after FUS application in the brain treated with DMPC NBs[®] (n=5) and Span20 NBs[®] (n=5). Green: calcein; Red: EB; Blue: DAPI. Scale bars = 100 μ m. Panel (B) Quantification of calcein across the 5 brains for each brain. DMPC NBs[®] mean = 15.1 SEM \pm 2.304 (n=5). Span20 NBs[®] mean 34.327 SEM \pm 1.44 (n=5). Statistical analysis = Unpaired T-test P=0.0002 *** F=2.562.

The volume of calcein was calculated using ImageJ software quantifying the green fluorescence averaged over five regions for five brains. (Figure. 10 B)

In particular, the brain section treated with Span20 NBs[®] (B) shows a major spread of calcein compare to the brain section treated with DMPC NBs[®] (A).

4. Discussion

The use of focused ultrasound in conjunction with microbubbles has been demonstrated by several groups to successfully induce BBB opening noninvasively, locally and reversibly.

Unfortunately, the *in vivo* studies with drug-loaded microbubbles are mainly restricted to cardiovascular targets and to tumour endothelia due to some their characteristics, e.g. the large size, rather short half-life (in the order of minutes) and after the injection their instability in the systemic circulation.

To solve this problem, two new formulations of NBs are designed, DMPC and Span20 NBs[®], which have smaller size and longer stability over time. These NBs show the advantage to deliver therapeutic agents of different nature (lipophilic and hydrophilic) and to obtain an ultrasound triggered drug release and permeabilization of cell membranes, simultaneously.

In this study, DMPC/Span20 NBs[®] are used to achieve BBB opening after FUS application and calcein-loaded DMPC/Span20 NBs[®] were applied to demonstrate targeted drug delivery into the brain after FUS-induced BBB opening in the mice. Furthermore, the NBs[®] behaviour, after the FUS application, is compared to SonoVue[®], a commercial contrast agent.

It is interesting to note that the DMPC NBs[®], diluted to achieve the same number of bubbles/ml of SonoVue[®], show a greater BBB disruption, while Span poor or no BBB opening.

After FUS application, the two formulations show opposite behaviour based on different concentrations used: in the brain treated with the Span20 NBs[®], a decrease of the EB extravasation is assessed with the increase of sample dilution, whereas, in the mice treated with DMPC NBs[®], the dilution of the sample leads a higher power of BBB disruption compared to undiluted sample. These differences could be caused by the smaller size and higher attenuation of DMPC NBs[®] in comparison to Span20 NBs[®]. Probably when the sample of DMPC NBs[®] was diluted and exposed to FUS, the oscillating bubbles had more space to oscillate with resulted to generate a larger stress on the BBB than the sample undiluted.

The data suggest that EB extravasation of the brain treated with SonoVue[®] and Span20 NBs[®] are comparable in terms of concentration, but there is a difference in the time it takes for the BBB closing. In particular, the BBB is fully closed after 12 hours in brains treated with Span20 NBs[®], instead, at the same time in the brain treated with MBs still is observed EB dye to investigate whether FUS-targeted NBs[®] cavitation could deliver drug into the CNS following BBB disruption, calcein-loaded DMPC/Span20 NBs[®] are injected into the mice intravenously, previous FUS application.

Calcein is a water-soluble polyanionic fluorescein derivative used as a fluorescent indicator in drug release studies.

Fluorescence analyses show that the two formulations are able to spread calcein after FUS application, confirming the capability of these carriers to release therapeutic agents across the BBB. In particular, the formulation Span20 NBs[®] shows a higher calcein release than DMPC NBs[®].

5. Conclusions

The *in vivo* experiments demonstrate that ultrasound-mediated DMPC and Span20 NBs[®] destruction has the potential to open the BBB tight junctions and trigger therapeutic agent deposition in the brain. It can be concluded that the NBs[®] formulated are a promising tool for both ultrasound imaging and drug delivery.

References

- [1]. Timbie FK, Mead BP, Price RJ. Drug and gene delivery across the blood–brain barrier with focused ultrasound. *J Control Release*, 219, 61-75, 2015.
- [2]. Hynynen K, McDannold N, Vykhodtseva N, Raymond S, Weissleder R, Jolesz FA, Sheikov N. Focal disruption of the blood–brain barrier due to 260-kHz ultrasound bursts: a method for molecular imaging and targeted drug delivery. *J Neurosurgery*, 105, 445-454, 2006.
- [3]. McDannold N, Vykhodtseva N, Raymond S, Jolesz FA, Hynynen K. MRI-guided targeted blood-brain barrier disruption with focused ultrasound: Histological findings in rabbits. *Ultrasound Med Biol*, 31, 1527–1537, 2005.
- [4]. Choi JJ, Feshitan JA, Baseri B, Shougang Wang, Yao-Sheng Tung, Borden MA, Konofagu EE. Microbubble-Size Dependence of Focused Ultrasound-Induced Blood-Brain Barrier Opening in Mice In Vivo. *IEEE Trans Biomed Eng*, 57 (1), 145–54, 2010.
- [5]. Yang F, Fu WM, Yang RS, Liou HC, Kang KH, Lin WL. Quantitative evaluation of focused ultrasound with a contrast agent on blood-brain barrier disruption. *Ultrasound Med Biol*, 33 (9), 1421-7, 2007.
- [6]. Van Wamel A, Kooiman K, Harteveld M, Emmer M, Ten Cate FJ, Versluis M, De Jong N. Vibrating microbubbles poking individual cells: drug transfer into cells via sonoporation. *J Control Release*, 112 (2), 149-55, 2006.
- [7]. Zhang X, Hu J, Zhao G, Huang N, Tan Y, Pi L, Huang Q, Wang F, Wang Z, Wang Z, Cheng Y. PEGylated PLGA-based phase shift nanodroplets combined with focused ultrasound for blood brain barrier opening in rats. *Oncotarget*, 8 (24), 38927-38936, 2017.
- [8]. Tronche F, Kellendonk C, Kretz O, Gass P, Anlag K, Orban PC, Bock R, Klein R, Schütz G. Disruption of the glucocorticoid receptor gene in the nervous system results in reduced anxiety. *Nat Genet*, 23 (1), 99-103, 1999.

**Formulation and characterization
of drug loaded-Bubblesomes[®]**

1. Bubblesomes[®] as theranostic agent

Bubblesomes[®] have been formulated in order to obtain a theranostic agent, therefore a system which provides diagnostic support and therapeutic treatment.

Since Bubblesomes[®] can reflect the ultrasound, it should be possible not only to localize the drug release but also providing an image of this process and facilitating access of the drug to its target through cavitation mechanism.

In previous studies, the ability of NBs[®] to entrap the gas and the hydrophilic (calcein) or hydrophobic (nile red) probes at the same time, maintaining unchanged their acoustic efficiency and physico-chemical properties, have been already demonstrated.

Afterwards, different drugs were entrapped in the NBs[®] and their theranostic potential application was evaluated in terms of drug entrapment efficiency, morphology and acoustic attenuation.

NBs[®] have been loaded with two active compounds:

❖ Hydrophobic compound: **Curcumin** is a natural compound extract from the rhizome of *Curcuma longa* Linn., with several biological activities, including antioxidant, anti-inflammatory, anti-infective, anti-cancer and amyloid- β -protein inhibitor (for Alzheimer's treatment). [1] In addition, same reviews have shown the neuroprotective effects of curcumin against brain injury after intracerebral haemorrhage-induced BBB disruption in animal models. [2, 3]

This effect can be helpful for BBB reconstruction after the FUS application after NBs[®] administration.

Despite of the wide range of activities, the pharmaceutical application of curcumin is limited due to its physicochemical characteristics such as poor water solubility, low bioavailability, photodegradation, chemical instability and short half-life.

❖ Hydrophilic drug: **Pentamidine isethionate** (for further details see **paper (submitted): Pentasomes for delivery of pentamidine to CNS by intranasal route**).

2. Experimental section

- Entrapment Efficiency

The concentrations of curcumin and pentamidine in the NBs were determined by UV-Vis spectroscopy (Perkin-Elmer, lambda 3a) by dissolving the curcumin in a hydroalcoholic solution and pentamidine in hepes buffer.

Spectrophotometric analyses were carried out at 425 nm for curcumin and 270 nm for pentamidine.

The % entrapment efficiency (%EE) was calculated by applying the equation:

$$EE\% = [(Concentration\ of\ drug\ determined) / (Total\ concentration\ of\ drug\ loading)] \times 100$$

3. Results

Drug-loaded NBs[®] are prepared as previously reported. Curcumin (2.5 mg/ml) is dissolved with the other hydrophobic components at the first step of NBs[®] preparation, instead Pentamidine (5mg/ml) is solubilized in hepes buffer and added to the formulation during the hydration step.

After the NBs[®] preparation, the EE% is evaluated by UV-Visible spectroscopy.

As shown in the table 1, both NBs[®] formulations show an excellent drug encapsulation efficiency.

Sample	EE%	Concentration (mg/ml)
DMPC-DCP NBs [®] +Curcumin	95	2.3
DMPC-DCP NBs [®] +Pentamidine	70	3.5

Table. 1

Moreover, the efficiency of trapping gas within the NBs[®] in presence of different drugs was evaluated by comparing the NBs[®] without and within drugs (Figure. 1 and 2, respectively), in term of acoustic efficiency.

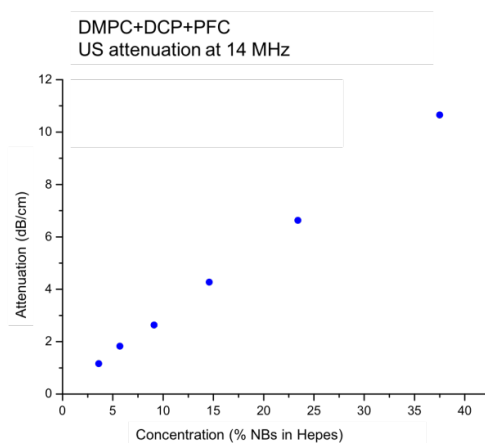


Figure. 1 Acoustic efficiency graph of DMPC-DCP NBs[®].

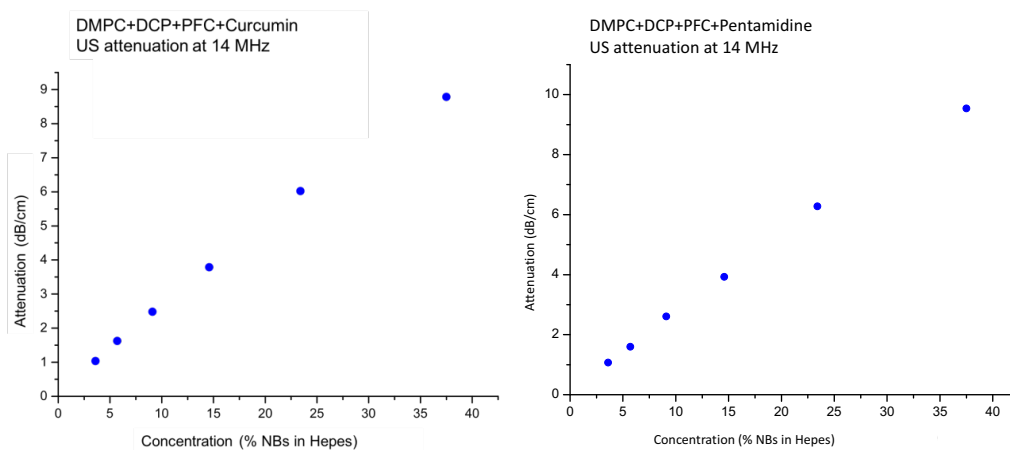


Figure. 2 Acoustic efficiency graphs of different drugs loaded DMPC-DCP NBs[®].

As shown in figures 1 and 2, the attenuation is similar for all examined samples, confirming that the co-entrapment of gas and drug does not affect the acoustic efficiency of NBs[®].

SAXS measurements were employed to examine the morphology of drugs loaded NBs[®]. (Figure. 3)

The intensity profile of DMPC-DCP NBs[®] (the black line) shows the typical characteristics of a single double layer, since there are no peaks indicating a multilamellar structure in the region $q=1 \text{ nm}^{-1}$.

In presence of PFC, the intensity profile changes drastically, in particular in the low q region (the red line). The trend of q^{-4} intensity decay is typical of interface between air and lipids, confirming the presence of nanobubble structures.

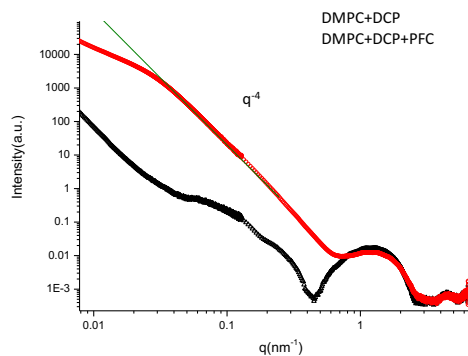


Figure. 3 SAXS analysis of DMPC-DCP NBs[®] compared to the vesicle without gas.

In presence of drugs, the nanobubbles structure is confirmed by the presence of q^{-4} intensity decay. (Figure. 4)

In the case of pentamidine (the green line), the peaks in position of $q = 0.98-1.96-2.94 \text{ nm}^{-1}$ indicate the presence of lipid multilayer with an interlamellar distance of 6.4 nm.

The presence of curcumin change the membrane contrast profile (the violet line), in particular, in the upper q regions, the spectra are different, so it can be assumed that the drug is inserted into the lipid membrane.

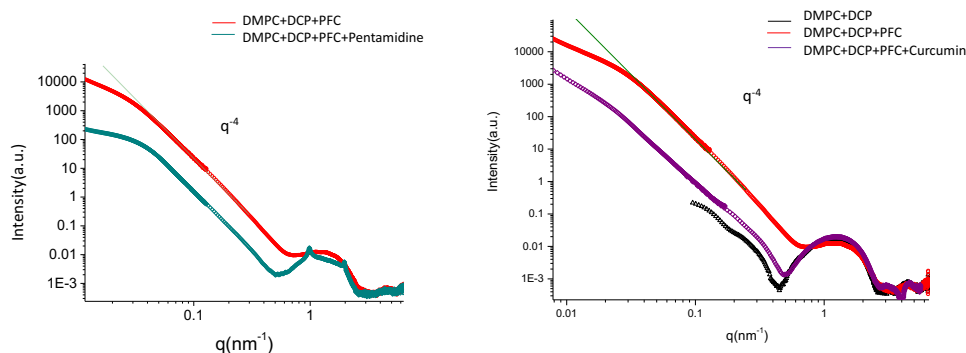


Figure. 4 SAXS measurements of different drugs loaded NBs[®].

All the obtained results confirm the ability of NBs[®] to co-deliver gas and active compounds.

References

- [1]. Naksuriya O, Okonogi S, Schiffelers RM, Hennink WE. Curcumin nanoformulations: a review of pharmaceutical properties and preclinical studies and clinical data related to cancer treatment. *Biomaterials*, 35 (10), 3365-83, 2014.
- [2]. Zhang ZY, Jiang M, Fang J, Yang MF, Zhang S, Yin YX, Li DW, Mao LL, Fu XY, Hou YJ, Fu XT, Fan CD, Sun BL. Enhanced Therapeutic Potential of Nano-Curcumin Against Subarachnoid Hemorrhage-Induced Blood-Brain Barrier Disruption Through Inhibition of Inflammatory Response and Oxidative Stress. *Mol Neurobiol*, 54 (1), 1-14, 2017.
- [3]. Yuan J, Liu W, Zhu H, Zhang X, Feng Y, Chen Y, Feng H, Lin J. Curcumin attenuates blood-brain barrier disruption after subarachnoid hemorrhage in mice. *J Surg Res*, 207, 85-91, 2017.

Nose to brain delivery

1. Introduction

The nasal route has been conventionally restricted for delivery of therapeutic agent to the treatment of local diseases such as the nasal allergy, sinusitis, nasal infections and nasal congestion.

Recently, intranasal drug delivery has attracted the interest of many researchers as an alternative method to circumvent the BBB and directly reach the brain.

The intranasal delivery method for drug delivery in to the brain was discovered by Dr William H. Frey (1991), and now, it has demonstrated in both animals and humans to be an efficient and safe way to deliver exogenous molecules to the CNS. [1, 2, 3 and 4]

The intranasal route offers several advantages but show limitation for the drug delivery showed in the table 1.

Advantages	Weakness
<ul style="list-style-type: none">• Non-invasiveness and safe method for drug delivery• Improving patient compliance compared to other conventional routes• Fast pharmacological activity onset achieved by the rich vascularization and high permeability of the epithelium of nasal mucosa• Large surface area for absorption• Presence of porous endothelial membrane• Avoid hepatic first-pass metabolism, enhanced bioavailability• Low systemic exposure of drugs, reducing side effects	<ul style="list-style-type: none">• Rapid elimination of drug due to mucociliary clearance• Enzymatic degradation by nasal cytochrome P450, proteases and peptides• Irritation of nasal mucosa• Mechanisms of drug transport are unknown• Individual variability

Table. 1 Advantages and weakness of intranasal delivery.

In spite of limitations, the intranasal delivery of therapeutics offers a non-invasive, safe, practical, cost effective and patient agreeable alternative to parenteral or oral route for rapid drug delivery to the brain/CNS. [5, 6]

2. Nasal anatomy and physiology

The nose plays an important role to heat, humidify and remove from the microorganisms and particles the air inhaled, before it reaches the lungs.

The nose is divided by the midline septum in two nasal cavities, each cavity has a volume of 13 ml and a surface area of 152 cm². [7]

It is organized in three regions: the vestibule (anterior and posterior), the respiratory region (separated in inferior, middle and superior turbinate) and the olfactory region composed by a pseudostratified epithelium formed by several types of cells: ciliated, non-ciliated, basal and goblet cells.

The goblet cells produce a secretion, namely mucus, that supports the mucociliary clearance and is structured in two layers on the nasal epithelium is composed by 95% water, 2% mucin, 1% salts, 1% of other proteins, such as albumin, lactoferrin, lysozymes and immunoglobulins, and less than 1% of lipids. [8]

About the 20% of respiratory cells are covered by a layer of mobile cilia and through their coordinated movements drive the mucus across the epithelium towards the esophagus and finally in the gastrointestinal tract.

Therefore, the exogenous materials inhaled with the air are trapped by the mucus layer and moved through the cilia in one direction only from the nasal cavity to the nasopharynx localized to the throat with a speed of 5 mm/min. [9]

The epithelium of the olfactory region is composed by olfactory neural cells, the sustentacular or supporting cells and their progenitors cell, the basal cells. The olfactory neural cells, or axons originate from the olfactory bulb and terminate to the olfactory neuroepithelium. Potentially, the small molecules could be transported from the nasal mucosa along the olfactory bulb to the brain. These neurons terminate to the amygdala, the anterior olfactory nucleus, the entorhinal cortex and the hippocampus, the hypothalamus and thalamus. [10]

Under the olfactory epithelium, the lamina propria contains the blood, the mucus secreted by Bowman's glands, nasal lymphatics and neuronal supply which are composed by the olfactory axon, autonomic nerve fibers and the branch of trigeminal nerve.

3. Biofate, nasal pathways and mechanisms involved in the nose to brain delivery

The specific mechanisms underlying the intranasal drug delivery to the CNS are still unknown, but several studies demonstrate that four pathways are involved: the vasculature, the trigeminal and olfactory nerves and the lymphatic systems. [11] (Figure. 1)

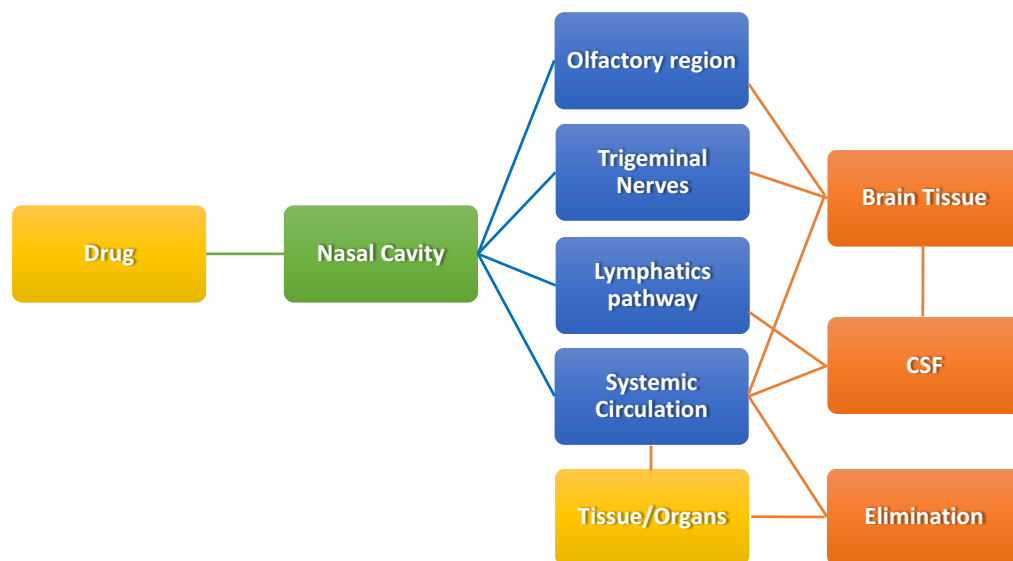


Figure. 1 Pathways for brain targeting after intranasal administration of drugs.

Following nasal administration, the therapeutic agent is absorbed from the nasal cavity through the mucus. This process is easier for small and uncharged drugs compared to large and charged molecules. In particular, the mucin is able to bind solutes and avoid their diffusion. The drugs absorption across the nasal epithelium could be obstacle by clearance mechanisms or by the limited residence time in the nasal cavity. [12]

The therapeutic agent can reach the brain through the absorption in the olfactory region, where three different pathways are involved for the transport of drug to CNS:

- **Olfactory nerve:** transports the drug from the olfactory epithelium to the CSF or several brain regions, including amygdala, piriform cortex and hypothalamus. [10]

The internalization mechanisms across the olfactory epithelium are:

1. Transcellular, by receptor mediated endocytosis or passive diffusion. This way is used for the transport of small lipophilic drugs.

2. Paracellular, by diffusion through aqueous pores. It is particularly suitable for hydrophilic and small drugs with a molecular weight around 1000 Da or 6000 Da with absorption enhancer.
 3. The olfactory nerve pathway, where the drug permeation is obtained by endocytosis or pinocytosis mechanisms and transported through the intracellular axonal transport to the olfactory bulb. [13]
- **Trigeminal nerve**, or the fifth cranial nerve, is the largest nerve of the all cranial nerves and innervates the respiratory and olfactory epithelium. Its function is the communication of sensory information from the nasal cavity, oral cavity, eyelids and cornea to the CNS. In particular, the trigeminal nerve can reach the brain from the nasal epithelium through the anterior lacerated foramen and the cribriform plate near olfactory bulb.
 - The subarachnoid space containing **CSF** and the **nasal lymphatics** are alternative routes for brain delivery. The neurotherapeutics are directly delivered to the CSF from the nasal cavity, without entering the blood to a significant amount. The fate of this drugs depends of their lipophilicity, molecular weight and degree of ionization. [14] In particular, several studies highlight a connection between the increase of the lipophilicity or partition coefficient of the drug administrated and the increase of drug concentration into the CSF. [15]

An amount of drug intranasally administrated could be cleared by mucociliary clearance system, according to its characteristics like lipophilicity and molecular weight, and absorbed by bloodstream. After, the drug could be able to reach the brain and in part eliminate by cerebrospinal fluid (CSF).

4. Strategy to enhance nose to brain delivery

One of the major problems associated with nasal administration is the rapid removal of drugs or drug delivery system from the deposition site due to the mucociliary clearance. [16]

Surface engineering of the nanocarrier may be a promising approach to manage the drug delivery properties of vesicles with a surface coating with a mucoadhesive agents. This strategy can potentially prolong the residence time and the contact between membranes and drug carriers at the absorption sites.

This strategy mainly offers two advantages: the increase of the residence time of the drug carriers in the nasal cavity and the slowing down of the mucociliary drainage. [17]

The mucoadhesion process could be defined as the attachment of the nanocarrier to the mucus and involves several mechanisms, like attractive electrostatic forces, diffusion and adsorption.

Several polymers adhere to the nasal mucosa such as sodium carboxymethylcellulose and other cellulose-derivates, carbopol[®], sodium alginate, chitosan, gelatin, pectin.

4.1. Chitosan

Chitosan (CH) is natural cationic polysaccharide composed by β -(1-4)-linked D-glucosamine and N-acetyl-D-glucosamine.

This polymer is intensively used for pharmaceutical, cosmetic, biomedical and agricultural applications. [18]

It is extracted from the exoskeleton of crustacean treated with an alkaline solution and produced by the deacetylation of the chitin. (Figure. 2)

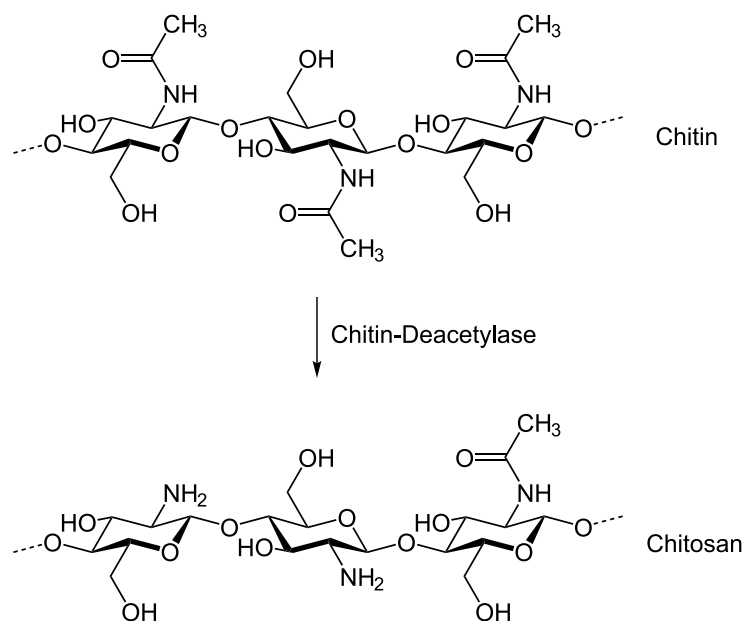


Figure. 2 Chitosan synthesis from chitin to chitosan by enzymatic deacetylation.

The molecular weight (M.W.) and the degree of acetylation can affect the chitosan interaction with the nasal mucosa. (Table. 2)

Type of CH	% Deacetylation	M.W. (kDa)
Low	75-85	50-190
Medium	75-85	250
High	>75	310-375

Table. 2 Different types of chitosan.

Chitosan mucoadhesive properties are due to the interaction between its protonated amino groups and the sialic acid residues of the mucus layers. [19]

Furthermore, chitosan is also able to transiently open the tight junctions increasing the permeability via receptor-mediated signaling, enhancing the trans-epithelial transport through intercellular pathway. This mechanism is still unknown, but probably the chitosan is able to translocate the junctional proteins, claudins and ZO-1, from the cellular membrane to the cytosol. [20]

An interesting therapeutic strategy could be a combination between chitosan induced mucoadhesion and nanocarrier characteristics.

In a study has been shown the effect of chitosan-coated nanoparticles over porcine olfactory epithelium. *In vitro* studies demonstrate that the engineered vesicles were more retained in the mucus compared to unmodified equivalents.

Furthermore, increasing the cationic charge on the coated vesicles, an increase of the interaction between particles and mucus was observed.

References

- [1]. Zhu J, Jiang Y, Xu G, Liu X. Intranasal administration: a potential solution for cross-BBB delivering neurotrophic factors. *Histol Histopathol*, 27, 537–548, 2012.
- [2]. Jiang Y, Zhu J, Xu G, Liu X. Intranasal delivery of stem cells to the brain. *Expert Opin Drug Deliv*, 8 (5), 623–632, 2011.
- [3]. Lochhead JJ, Thorne RG. Intranasal delivery of biologics to the central nervous system. *Adv Drug Deliv Rev*, 64 (7), 614–628, 2012.
- [4]. Marianecchi C, Rinaldi F, Hanieh PN, Paolino D, Di Marzio L, Carafa M. Nose to brain delivery: new trends in amphiphile-based “soft” nanocarriers. *Curr Pharm Des*, 21 (36), 5225–5232, 2015.
- [5]. Draghia R, Caillaud C, Manicom R, Pavirani A, Kahn A, Poenaru L. Gene delivery into the central nervous system by nasal instillation in rats. *Gene Ther*, 2 (6), 418-23, 1995.
- [6]. Dorman DC, Brenneman KA, McElveen AM, Lynch SE, Roberts KC, Wong BA. Olfactory transport: a direct route of delivery of inhaled manganese phosphate to the rat brain. *J Toxicol Environ Health A*. 2002 Oct 25;65(20):1493-511.
- [7]. Ménache MG, Hanna LM, Gross EA, Lou SR, Zinreich SJ, Leopold DA, Jarabek AM, Miller FJ. Upper respiratory tract surface areas and volumes of laboratory animals and humans: considerations for dosimetry models. *J Toxicol Environ Health*, 50 (5), 475-506, 1997.
- [8]. Kaliner M, Marom Z, Patow C, Shelhamer J. Human respiratory mucus. *J Allergy Clin Immunol*, 73 (3), 318-23, 1984.
- [9]. Mistry A, Stolnik S, Illum L. Nanoparticles for direct nose-to-brain delivery of drugs. *Int J Pharm*, 379 (1),146-57, 2009.
- [10]. Lledo PM, Gheusi G, Vincent JD. Information processing in the mammalian olfactory system. *Physiol Rev*, 85 (1), 281-317, 2005.
- [11]. Chen M, Wu B, Ye X, Zhou Z, Yue X, Wang Q, Wang W, Jiang Y, Lian X, Chen Z, Xu G, Liu X. Association between plasma homocysteine levels and obstructive sleep apnoea in patients with ischaemic stroke. *J Clin Neurosci*, 18 (11), 1454–1457, 2011.
- [12]. Khanvilkar K, Donovan MD, Flanagan DR. Drug transfer through mucus. *Adv Drug Deliv Res*, 48, 173-93, 2001.
- [13]. Talegaonkar S, Mishra PR. Intranasal delivery: An approach to bypass the blood brain barrier. *Indian J Pharmacol*, 36 (3), 140-147, 2004.

- [14]. Born J, Lange T, Kern W, McGregor GP, Bickel U, Fehm HL. Sniffing neuropeptides: a transnasal approach to the human brain. *Nat Neurosci*, 5 (6), 514-6, 2002.
- [15]. Sakane T, Akizuki M, Yamashita S, Nadai T, Hashida M, Sezaki H. The transport of a drug to the cerebrospinal fluid directly from the nasal cavity: the relation to the lipophilicity of the drug. *Chem Pharm Bull*, 39, 2456-8, 1991.
- [16]. Schipper NG, Verhoef JC, Merkus FW. The nasal mucociliary clearance: relevance to nasal drug delivery. *Pharm Res*, 8 (7), 807-14, 1991.
- [17]. Costantino HR, Illum L, Brandt G, Johnson PH, Quay SC. Intranasal delivery: physicochemical and therapeutic aspects. *Int J Pharm*, 337 (1-2), 1-24, 2007.
- [18]. Gupta KC, Ravikumar MNV. An Overview on Chitin and Chitosan Applications with an Emphasis on Controlled Drug Release Formulations. *J Macromol Chem Phys C* 40 (4), 273-308, 2000.
- [19]. Harris R, Acosta N, Heras A. Chitosan and inhalers: a bioadhesive polymer for pulmonary drug delivery. Doi: 10.1533/9780857098696.2.77, 2013.
- [20]. Smith JM, Dornish M, Wood EJ. Involvement of protein kinase C in chitosan glutamate-mediated tight junction disruption. *Biomaterials*, 26, 3269–3276, 2005.

Hybrid niosomes

Aims

The aim of this part of my PhD project has been mainly focused on the formulation and characterization of carrier suitable for nose to brain delivery.

In particular, the goals of this project can be summarized in the following points:

- ✓ formulation and physico-chemical characterization of hybrid niosomes in order to obtain a mucoadhesive formulation by chitosan coating.

All collected data and experimental setup are shown in the **paper:**

DLS Characterization of Non-Ionic Surfactant Vesicles.

- ✓ Preparation and physico-chemical characterization of pentamidine-loaded niosomes. *In vivo* studies have been performed to evaluate the effect of pentamidine in a sub-acute MPTP mouse model of Parkinson's disease (PD) after intranasal administration of pentamidine-loaded niosomes.

All collected data and experimental setup are shown in the **paper (submitted): Pentasomes for delivery of pentamidine to CNS by intranasal route.**

1. Niosomes

Non-ionic surfactants, namely niosomes, are widely studied as an alternative tool to liposomes. In the 1970, niosomes were first reported as suitable ingredients for cosmetic application. [1]

The main components of these vesicles are nonionic surfactants and cholesterol. Both components are self-assembled into an aqueous medium obtaining a closed bilayer structures, due to the high interfacial tension between water and hydrophobic tail of the surfactant.

The main non-ionic surfactant classes used to obtain niosomes are alkyl ethers, alkyl esters (such as Span[®] and Tween[®]), alkyl amides and fatty acids.

The cholesterol, a steroidal compound, forms hydrogen bonds with the hydrophilic head of the amphiphile, influencing bilayer fluidity and permeability and increasing the niosomal blood stability. (Figure. 1)

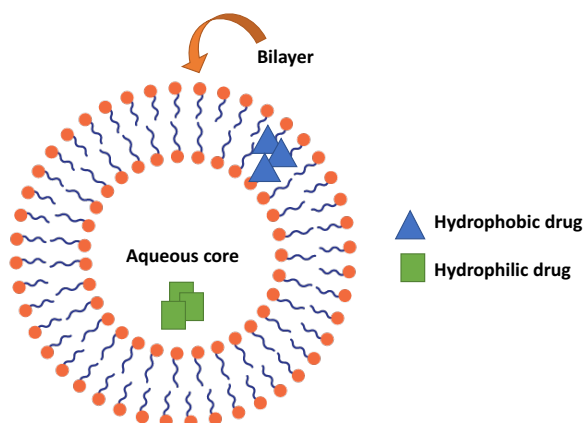


Figure. 1 Structure of niosomes.

Niosomes, as liposomes, are able to entrap hydrophobic drugs in the bilayer and hydrophilic drugs in the aqueous core. Their surface may be functionalized in order to acquire a specific targeting or to increase the biological or physical stability.

The main factors playing a critical role in the surfactant self-assembling are:

- The Hydrophilic-Lipophilic Balance (HLB): this value represents the hydrophilic/hydrophobic part ratio in the surfactant molecule. Its value ranges from 0 to 20 on an arbitrary scale: values between 0-10 are characteristic for more hydrophobic substances, while values between 10-20 are of hydrophilic substances.

- The critical packing parameter (CPP) modifying this parameter nanostructures with several shapes will be obtained: [2]

$$CPP = V / (a_0 \times l_c)$$

where V and l_c represent the volume and length of the hydrophobic group, and a_0 is the area of the hydrophilic heads.

According with CPP value, the nanostructure shape could evolve in: spherical micelles ($CPP \leq 1/3$), cylindrical micelles ($1/3 \leq CPP \leq 1/2$), bilayers ($1/2 \leq CPP \leq 1$) and inverse micelles ($CPP > 1$).

In order to increase the structural stability of the niosomes, charged molecules such as dicetyl phosphate DCP (negatively charged) and stearylamine (positively charged). are used. They enhance the surface charge density preventing the niosomes aggregation. Generally, these molecules are added to the niosomal formulation in an amount of 2.5-5 mol%, because a higher concentration could prevent the niosomal formation. [3]

The niosomes can be prepared with several methods such as thin film hydration (TFH), the organic solvent injection method, the reverse phase evaporation method and the bubble method.

Generally, for niosomes characterization the following parameters are evaluated: [4]

- ❖ **Size and Morphology**: cumulative information about the average particles and the particle size distribution can be obtained by dynamic light scattering (DLS) measurements.
The microscopic techniques (scanning electron microscopy (SEM), transmission electron microscopy (TEM), cryotransmission electron microscopy (cryo-TEM) and atomic force microscopy (AFM) are used to characterize the nanocarrier in terms of morphology, structure and geometry.
- ❖ **ζ-potential**: the surface charge of nanocarriers play a fundamental role in the *in vivo* behavior, formulation stability and drug/vesicle interaction. A ζ-potential value more positive than +30mV or more negative than -30mV prevent the aggregation phenomena.
- ❖ **Bilayer characterization**: according to sizes and number of *lamellae*, niosomes can be classified in: (1) small unilamellar vesicles (SUV) of 10-100nm; (2) large unilamellar vesicles (LUV) of 100-1000nm and multilamellar vesicles (MLV) with two or more bilayers. [5]
The number of lamellae can be evaluated by small angle X-ray scattering (SAXS) or AFM techniques. [6] Membrane fluidity of niosomes is determined through the mobility of a fluorescent probe (1,6 diphenyl-1,3,5-hexatriene, DPH) added to the niosomal formulation. By fluorescence polarization measurement, the microviscosity of vesicles is evaluated to evaluate the packing structure of the niosomal membrane. [7]

❖ **Stability**: it is evaluated by DLS in terms of mean vesicles size, ζ -potential, size distribution over time at different temperatures.

Furthermore, the stability in the biological fluids can be evaluated in function of time and temperature.

❖ **Entrapment efficiency (EE)**: the amount of drug loaded into the niosomes is generally expressed as: $EE = (\text{entrapped amount} / \text{total amount}) \times 100$, where the total amount is the loading drug amount and the entrapped amount is the drug entrapped in the niosomes. It is generally evaluated by UV/VIS spectrophotometry or high-performance liquid chromatography (HPLC).

2. Formulation and physico-chemical characterization of hybrid niosomes

An interesting therapeutic strategy for nose to brain delivery could be a combination between chitosan mucoadhesion and nanovesicles characteristics.

In particular, niosomes are non-ionic surfactant vesicles capable to entrap both hydrophilic and lipophilic drugs, minimizing drug degradation and inactivation after administration, and increasing drug bioavailability and targeting to the pathological area. [8]

In the first part this work has been focused on the complexation between negatively charged niosomal vesicles and chitosan, a cationic mucoadhesive polysaccharide.

Three different formulations of unilamellar niosomal vesicles composed by a mixture of Tween 20 or Tween 21 or Span 20 with cholesterol and dicetyl phosphate (DCP) have been prepared and characterized.

The study of the aggregation behavior between the charged vesicles and chitosan has been carried out in terms of size and ζ -potential variation and stability over time of the selected samples. These experiments have been performed by dynamic light scattering (DLS) and Laser Doppler Electrophoresis measurements. The effect of chitosan charge ratio is investigated and discussed within the framework of the re-entrant condensation and charge inversion behavior. [9]

DLS analyses were carried out to evaluate dimensions and ζ -potential characteristics in order to select the most appropriate formulations to be coated with chitosan.

Span20 niosomes were characterized by a highly negative charge able to form electrostatic interactions with the positively charged polysaccharide. DCP was added to Tween 20 and Tween 21 niosomes in order to support the chitosan coating.

The aggregation of negatively charged niosomal vesicles in the presence of different amount of chitosan was further investigated.

For all samples, the addition of chitosan led to a progressive diameter increase of the complexes, starting from a value close to the Z-Average of uncoated niosomes, when only few polycation molecules adsorb on the vesicle surface, and growing to larger and larger sizes due to the aggregation of chitosan-coated vesicles. At the same time, the ζ -potential value of the hybrid niosomes increases adding the polyelectrolyte, approaching less negative values until the point of charge inversion (isoelectric point) is reached. This behavior was connected to the progressive charge neutralization of the complexes, promoted by the adsorption of positive charges of the chitosan onto the negative charges at the vesicle surface.

Further addition of chitosan promotes the reversal of ζ -potential toward positive values and the decrease of the Z-Average of the hybrid niosomes toward lower values. In particular, at this higher polyelectrolyte concentration, the hybrid niosomes reach a size similar to the one measured at low chitosan concentrations.

This peculiar behavior is known in the colloid literature as re-entrant condensation and is associated to the charge inversion of the chitosan coated vesicles. [10]

The aggregation mechanism and the formation of stable structures are the results of the balance between electrostatic repulsion and short-range effective attraction interactions due to the non-uniform charge distribution at the particle surface (charge patch attraction). [11]

In order to check the integrity of the hybrid niosomes during the whole aggregation process, the leakage of calcein entrapped in the core of the hybrid niosomal vesicles were monitored.

The vesicular membranes of all analyzed samples are undamaged while chitosan coating occurs.

The stability studies were carried out to investigate if significant changes of the size and ζ -potential of surfactant vesicle dispersion occur during storage. The uncoated and coated systems are characterized by no significant variations of dimension and ζ -potential during the storage period, especially if they are maintained at 4°C.

The selected formulations are able to obtain a positively charged hybrid vesicle suspension, stable during polymer coating process and during the analyses period.

The obtained results suggest the potential application of hybrid niosomes to mucosal delivery.

References

- [1]. Handjani-Vila RM, Ribier A, Rondot B, Vanlerberghie G. Dispersions of lamellar phases of non-ionic lipids in cosmetic products. *Int J Cosmet Sci*, 1 (5), 303-14, 1979.
- [2]. Israelachvili JN, Mitchell DJ, Ninham BW. Theory of self-assembly of lipid bilayers and vesicles. *Biochim Biophys Acta*, 470 (2), 185-201, 1977.
- [3]. Junyaprasert VB, Teeranachaideekul V, Supaperm T. Effect of charged and non-ionic membrane additives on physicochemical properties and stability of niosomes. *AAPS Pharm Sci Tech*, 9 (3), 851–859, 2008.
- [4]. Marianecci C, Di Marzio L, Rinaldi F, Celia C, Paolino D, Alhaique F, Esposito S, Carafa M. Niosomes from 80s to present: the state of the art. *Adv Colloid Interface Sci*, 205, 187-206, 2014.
- [5]. Seleci DA, Seleci M, Walter J, Stahl F, Scheper T. Niosomes as Nanoparticulate Drug Carriers: Fundamentals and Recent Applications. *J Nanomaterials*, doi.org/10.1155/2016/7372306
- [6]. Liu T, Guo R, Hua W, Qiu J. Structure behaviors of hemoglobin in PEG6000/Tween 80/Span 80/H2O niosome system. *Col Surf A Phys Eng Asp*, 293 (1–3), 255–261, 2007.
- [7]. Manosroi A, Jantrawut P, Manosroi J. Anti-inflammatory activity of gel containing novel elastic niosomes entrapped with diclofenac diethylammonium. *Int J Pharm*, 360 (1-2), 156-63, 2008.
- [8]. Marianecci C, Rinaldi F, Mastriota M, Pieretti S, Trapasso E, Paolino D, Carafa M. Antiinflammatory activity of novel ammonium glycyrrhizinate/niosomes delivery system: Human and murine models. *J Control Release*, 164, 17–25, 2012.
- [9]. Sennato S, Bordi F, Cametti C, Marianecci C, Carafa M, Cametti M. Hybrid niosome complexation in the presence of oppositely charged polyions. *J Phys Chem B*, 112, 3720–3727, 2008.
- [10]. Grosberg Y, Nguyen TT, Shklovskii BI. Colloquium: The physics of charge inversion in chemical and biological systems. *Rev Mod Phys*, 74, 329-345, 2002.
- [11]. Nguyen TT, Shklovskii BI. Complexation of DNA with positive spheres: Phase diagram of charge inversion and reentrant condensation. *J Chem Phys*, 115, 7298-7308, 2001.

Paper:

**DLS Characterization of Non-Ionic
Surfactant Vesicles for
Potential Nose to Brain Application**

DLS Characterization of Non-Ionic Surfactant Vesicles for Potential Nose to Brain Application

Federica Rinaldi¹, Patrizia N. Hanieh², Carlotta Marianecchi^{2,*}, Maria Carafa²

¹Center for Life Nano Science@Sapienza, Fondazione Istituto Italiano di Tecnologia, Rome, Italy

²Department of Drug Chemistry and Technology, University of Rome "Sapienza", Rome, Italy

Email address:

federica.rinaldi@iit.it (F. Rinaldi), patrizianadia.hanieh@uniroma1.it (P. N. Hanieh), maria.carafa@uniroma1.it (M. Carafa), carlotta.marianecchi@uniroma1.it (C. Marianecchi)

To cite this article:

Federica Rinaldi, Patrizia N. Hanieh, Carlotta Marianecchi, Maria Carafa. DLS Characterization of Non-Ionic Surfactant Vesicles for Potential Nose to Brain Application. *Nanoscience and Nanometrology*. Vol. 1, No. 1, 2015, pp. 8-13. doi: 10.11648/j.nsnm.20150101.12

Abstract: The aim of this paper is the preparation and characterization of drug delivery systems for a potential brain delivery by intranasal administration. It is possible to reach the central nervous system with alternative routes through which therapeutic agents can bypass the blood brain barrier: that is the nasal administration. Intranasal drug administration is non-invasive and it could be a promising drug delivery method for patients who suffer from chronic and crippling Central Nervous System diseases. Among the formulation strategies for enhanced nose to brain drug delivery, the use of colloidal carriers has become a revolutionary approach. The success of a therapeutic strategy by using nanocarriers depends on their ability to entrap drugs, to penetrate through anatomical barriers, to efficiently release the incorporated drugs, to show a good stability in nanometric size range and good biocompatibility. The use of vesicular systems (niosomes), in nose to brain delivery is here presented. One of the major problems associated with nasal administration is the rapid removal of drugs or drug delivery systems, from the deposition site through mucociliary clearance. This effect is responsible of reduction of contact time between drug or drug delivery systems and nasal epithelium. This problem could be solved by coating nanocarriers with a mucoadhesive agent: chitosan. In this paper the preparation and characterization of hybrid niosomes by Tween 20 and Tween 21 together with dicetyl phosphate or Span 20 and the cationic polyelectrolyte chitosan are described in order to obtain intranasal drug delivery systems. In particular through dynamic light scattering, laser Doppler electrophoresis and fluorescence measurements the aggregation behavior between vesicles and polyelectrolyte can be monitored. Overall phenomenology is well described in terms of the re-entrant condensation and charge inversion behavior, observed in different colloidal systems. The physical stability of hybrid niosomes obtained by the three different surfactants was also evaluated.

Keywords: Niosomes, Chitosan, Dynamic Light Scattering, Laser Doppler Electrophoresis, Fluorescence

1. Introduction

The blood brain barrier (BBB) represents the major obstacle to a direct access to the Central Nervous System (CNS) if a conventional pharmaceutical approach is used. The tight junctions between the BBB cells are responsible of the inability to enter into the brain tissue for most compounds, in effect the penetration is possible only for the 2% of small polar molecules. [1]

Actually the difficult BBB crossing has limited the use of a lot of therapeutic agents in Alzheimer's disease, stroke, brain tumor, head injury, depression, anxiety and other CNS disorders treating. It's possible to reach brain with alternative routes through which therapeutic agents can bypass the BBB: intracerebroventricular, intraparenchymal, or intrathecal

administrations, but these routes of administration are invasive, risky, and expensive techniques requiring surgical expertise especially for multiple dosage regimens. [2]

Up to a short time ago, the nasal route has been employed for therapeutic agents delivery in the treatment of local diseases: nasal allergy, sinusitis, nasal infections and nasal congestion; actually the interest of many researchers is now focused on the nasal administration route in the therapy of neurologic diseases in mice, rats, primates and humans. By this administration route drugs in fact is possible to reach the brain through the olfactory region and respiratory epithelium because the olfactory nerve cells and trigeminal nerves are in direct contact with both the environment and the CNS. Moreover intranasal (IN) route is non invasive, resulting in better patient compliance, it doesn't require sterility

requirements or any drug modifications and it has the advantage to achieve liver degradation escape (avoidance of the first passage effect). Through nasal administration the drug come into contact with nasal epithelium where the enzymatic degradation of drugs is lower if compared to that of gastrointestinal tract and liver. Anyway, the drug degradation is possible, so to enhance the stability of the IN administered drugs, one of the possible strategies is the entrapment (especially in case of peptide or protein) in drug delivery systems able to protect the therapeutic agent administration. The use of conventional and new drug delivery systems (DDS) allows to face the major issues in drug release: (1) unfavorable pharmacokinetics and biodistribution which lead to unwanted side effects (e.g. chemotherapy), (2) early drug degradation in the bloodstream by reticulo-endothelial system (RES), and (3) inefficient uptake at target sites that leads to low drug efficacy. In this sense, nanocarriers offer an innovative approach to drug delivery, providing a range of features including cargo protection and increased dose delivery to target sites. Actually, the complexity of human diseases may lead to ineffective in vivo drug treatments, consequently the development of biologically functional nanocarriers that incorporate drugs to selectively bind and target specific cells becomes crucial. [3]

The success of a therapeutic strategy by using nanocarriers depends on their ability to entrap drugs, penetrate through anatomical barriers, release the incorporated drugs, and to show a good stability in nanometric size range. Many of the conventional DDS (e.g. liposomes, niosomes, micelles, and polymer based nanodevices) have reached the late stages of development, and some of them were approved. [3, 4]

In particular, vesicular systems may increase nose-to-brain drug delivery enhancing drug chemical and biological stability. In fact the presence of a hydrophilic core is responsible of poorly water-soluble drug entrapment while the hydrophobic shell protect the system and, entrap lipophilic drugs enhancing brain uptake after intranasal administration. Numerous amphiphilic components together with different preparation techniques, lead to the formation of many vesicular systems: liposomes, niosomes, transfersomes, ethosomes, vesosomes, colloidosomes, and pharmacosomes. [5] Vesicles have spherical structure with a hydrophobic bilayer, and an aqueous core, they are prepared by phospholipids or surfactants that must be biodegradable, biocompatible and with a possible application in neuromedicine. Different studies have also demonstrated that surfactants can be used to prepare stable colloidal supramolecular devices showing a certain degree of selectivity for brain delivery. Surfactant nanocarriers, in particular niosomes, have the capability of entrap both lipophilic and hydrophilic drugs, in the apolar membrane and in the aqueous core, respectively.

They can be functionalized on their surface to obtain different type of targeting or to enhance their biological and/or physical stability. These systems have been widely used in IN delivery but one of the major problems associated with nasal administration, is the rapid removal of drugs or DDS, from the deposition site through mucociliary clearance. This effect is responsible of reduction of contact time between drug

or DDS and nasal epithelium. This problem could be solved by coating nanocarriers with a mucoadhesive agent. In particular the DDS can be coated by Chitosan, a cationic, mucoadhesive polysaccharide, able to form electrostatic interactions with the negatively charged epithelial cells reducing the mucociliary clearance. Chitosan is also able to open reversibly tight junctions enhancing the extracellular pathways through olfactory and trigeminal nerve. [6]

Chitosan originates from chitin and in particular is produced by its deacetylation (Figure 1).

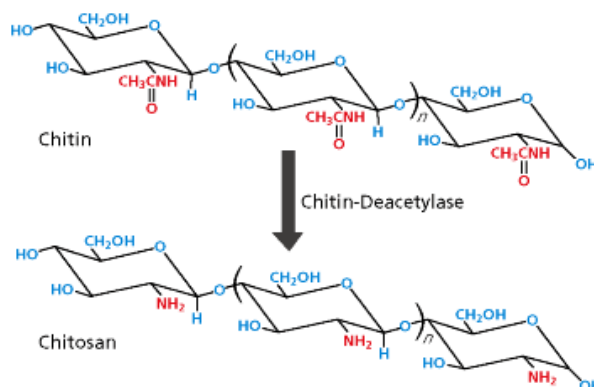


Figure 1. Chitin to chitosan conversion.

The aim of the present study is the evaluation of vesicular systems and chitosan interaction in order to obtain chitosan coated vesicles able to reach the brain by a IN administration avoiding the effect of the mucociliary clearance. Among vesicular systems, non-ionic surfactant ones or niosomes (NSVs) were chosen. Niosomes are similar, in terms of structure and physical properties, to liposomes. [7] They are prepared following the same procedures and under the same variety of conditions to produce unilamellar or multilamellar vesicles. The research interest in niosomal formulations is recently widening because niosomes are able to overcome some disadvantages associated with liposomes: surfactants are easily derivatized, more stable and give a higher versatility to the vesicular structure and moreover they have lower costs than phospholipids. [3]

To this aim, the complexation between negatively charged niosomal vesicles and a cationic, mucoadhesive polysaccharide: the chitosan has been investigated. In this work, three different formulation of unilamellar niosomal vesicles composed by a mixture of polysorbate 20 (Tween 20) or polysorbate 21 (Tween 21) or sorbitan monolaurate (Span 20) with cholesterol have been prepared and characterized.

Tween 20 and Tween 21 vesicles show a quite negative ζ -potential value, not sufficient to perform a stable complexation with chitosan, so a more negative ζ -potential value is obtained adding to the formulation a ionic surfactant, dicetyl phosphate (DCP), at an appropriate concentration.

On the other hand vesicles made of Span 20 do not need addition of DCP because they are characterized by a highly negative ζ -potential value that guarantees the right interaction with the chitosan.

The study of the aggregation behavior between charged vesicles with the oppositely charged macromolecule has been carried out in terms of evaluation of complexes physical properties such as size, size stability and ζ -potential in view of a possible application of such aggregates in brain delivery through nasal administration. These experiments have been performed by dynamic light scattering (DLS) and laser Doppler electrophoretic measurements.

The effect of chitosan/ DCP charge ratio is investigated and discussed within the framework of the re-entrant condensation and charge inversion behavior [8]

2. Materials and Methods

2.1. Materials

Polysorbate 20 (Tween 20), polysorbate 21 (Tween 21), sorbitanmonolaurate (Span 20), Dicapryl phosphate (DCP), Cholesterol (Chol), Hepes salt {N-(2-idroxyethyl) piperazine-N'-(2-ethanesulfonic acid)}, Sephadex G75, Calcein and Chitosan (low molecular weight) were purchased from Sigma-Aldrich. All other products and reagents were of analytical grade.

2.2. Vesicles Preparation and Purification

The thin layer evaporation method was used to prepare non-ionic surfactant vesicles from Tween 20, Tween 21 or Span 20. In each vesicle formulation, Chol and DCP were added at different molar ratios (Table 1). [9, 10]

Table 1. Sample composition.

Sample	Tween20	Tween21	Span20	DCP	Chol
NioTw20	15mM				15mM
NioTw20+DCP	7,5mM			7,5mM	15mM
NioTw21	15mM				15mM
NioTw21+DCP		17,6mM		7,5mM	15mM
NioSpan20			15mM		15mM

All the vesicle constituents were firstly dissolved in an organic mixture (CH₃OH/CHCl₃ 3/1 v/v), then solvent were removed under vacuum at different temperatures depending on the surfactant used, as reported in the Table 2. The obtained "film" was hydrated with 5 mL of Hepes buffer (0.01M pH 7.4). The suspension was vortexed for about 5 minutes and then sonicated (5 minutes and different amplitudes and temperatures) (Table 2) using a microprobe operating at 20 kHz (VibraCell-VCX 400-Sonics, Taunton, MA, USA).

Table 2. Sonication conditions.

Sample	Temperature (°C)	Amplitude
Nio Tw20+DCP	25	16
NioTw21+DCP	25	16
NioSpan20	60	18

The vesicle suspension was purified by gel permeation chromatography using SephadexG75 (glass column of 50 x 1.2 cm) using Hepes buffer as the eluent. The obtained

purified vesicle suspension was then extruded using cellulose filters with appropriate pore diameters.

2.3. Chitosan Solution Preparation

The low molecular weight chitosan solution is obtained in acetate buffer (0.2 M, pH 4.4) after stirring overnight.

2.4. Preparation of Hybrid Niosomes

The chitosan-coated niosomes (hybrid niosomes) formation was promoted by adding 1ml of chitosan solution (at an appropriate concentration) to an equal volume of uncoated niosomes. The obtained suspension was stirred for 3 h in a thermostated water bath at 10 °C.

2.5. Dynamic Light Scattering Measurements

Vesicles mean diameter (Z-Average) and size distribution (polydispersity index, PDI) were measured at the temperature of 25 °C by means of the dynamic light scattering (DLS) technique, using a Malvern ZetaSizerNano 90S, equipped with a 5 mW HeNe laser (wavelength $\lambda= 632.8$ nm) and a digital logarithmic correlator. The normalized intensity autocorrelation functions were detected at a 90° angle and analyzed by using the Contin algorithm [11] in order to obtain the decay time of the electric field autocorrelation functions. The decay time is used to obtain the distribution of the diffusion coefficient D of the particles, which can be converted into an effective hydrodynamic radius R_H using the Stokes-Einstein relationship $R_H=K_B T/6\pi\eta D$, where $K_B T$ is the thermal energy and η the solvent viscosity. The values of the radii reported here correspond to the intensity weighted average. [12]

2.6. ζ -Potential Measurements

The electrophoretic mobility measurements were carried out by means of the laser Doppler electrophoresis technique using the Malvern ZetaSizerNano 90S apparatus equipped with a 5mW HeNe laser. The mobility u was converted into the ζ -potential using the Smoluchowski relation $\zeta = u\eta/\epsilon$, where η and ϵ are the viscosity and the permittivity of the solvent phase, respectively. [8]

2.7. Spectrofluorometric Analysis

Niosomal integrity during the chitosan coating process was evaluated by means of fluorescence analyses (Perkin-Elmer LS50B spectrofluorometer).

Calcein loaded vesicles were prepared hydrating the surfactant thin film with a calcein solution (0.01 M of calcein in Hepes buffer 0.01 M pH 7.4). Free calcein was eliminated by extensive dialysis (cellulose dialysis bag membrane 8000 MWCO-Spectrum, The Netherlands). The calcein concentration inside vesicles was approximately 10^{-2} M. At this concentration, the dye is self-quenched and is responsible of a low fluorescence signal, while if the probe is released, the quenching process produce a remarkable increase in fluorescence values due to the dilution of the probe in the

external aqueous medium. [13]

3. Results and Discussion

In this study, niosomal vesicles were prepared and characterized in order to obtain a delivery systems for a potential nose to brain application. For this purpose, formulations with different compositions were prepared (Table 1). DLS analyses were carried out to evaluate dimensions and ζ -potential characteristics in order to verify their suitability to be coated with chitosan. It can be noticed that, as shown in table 3, Span niosomes were characterized by a sufficient negative charge able to form electrostatic interactions with the positively charged polyelectrolyte.

Table 3. Light scattering analysis of vesicular systems in absence and in presence of DCP.

Sample	Z-Average (nm) ±DS	ζ -Potential (mV) ± DS	PDI ± DS
NioSpan20	202,91 ± 5,31	-48,34 ± 0,23	0,31 ± 0,01
NioTw20	152,53 ± 1,52	-26,42 ± 4,52	0,12 ± 0,02
NioTw20+DCP	157,34 ± 1,24	-44,22 ± 1,61	0,31 ± 0,01
NioTw21	159,32 ± 3,93	-34,23 ± 4,24	0,52 ± 0,01
NioTw21+DCP	136,52 ± 5,21	-51,72 ± 0,62	0,34 ± 0,02

DCP addition to Tween formulations is needed to achieve a suitable negative ζ -potential value useful for the interaction with chitosan. Therefore, the presence of DCP plays a fundamental role in decreasing ζ -potential values, and this effect is not associated to a size variation of vesicles. On the other hand, the addition of DCP leads to opposite effects on PDI values. In particular it produces a PDI increase in the case of Tween 20 vesicles, while it causes a decrease in the case of Tween 21 ones. This phenomenon can be explained looking at the molar ratio between Tweens and DCP (Table 1). The addition of DCP produces a quite monodisperse vesicular population in both samples, but it can be noticed that it could be better to not use an equimolar amount of DCP.

As previously described, the hybrid niosomes were obtained by adding a proper amount of chitosan to niosomal suspension. In particular, the aggregation behavior of negatively charged niosomal vesicles in the presence of different amount of chitosan was investigated. In figure 2 the behavior of the Z-Average (panels A, C, E) and the corresponding ζ -potential values (panels B, D, F) of different niosomal suspensions in the presence of different concentrations of chitosan solution are reported.

For all the samples, the addition of chitosan promotes the progressive increase of the diameter of the complexes, starting from a value close to the Z-Average of uncoated niosomes when only few polycation molecules adsorb on the vesicle surface, and growing to larger and larger sizes due to the subsequent aggregation of chitosan coated vesicles. Also the value of ζ -potential of the hybrid niosomes increases adding

the polyelectrolyte approaching less negative values until the point of charge inversion (isoelectric point) is reached. This behavior is connected to the progressive charge neutralization of the complexes, promoted by the adsorption of positive charges of the chitosan onto the negative charges at the vesicle surface.

Further addition of chitosan promotes the reversal of ζ -potential toward positive values and the decrease of the Z-Average of the hybrid niosomes toward lower values. In particular at this higher polyelectrolyte concentration, the hybrid niosomes reach a size similar to the one measured at low chitosan concentrations. This peculiar behavior is known in the colloid literature [14] as re-entrant condensation and is associated to the charge inversion of the chitosan coated vesicles.

The aggregation mechanism and the formation of stable structures are the results of the balance between electrostatic repulsion and short-range effective attraction interactions due to the non uniform charge distribution at the particle surface (charge patch attraction). [15]

This behavior was observed for all samples studied. The aggregation mechanism and the formation of stable structures were justified in light of a balance between electrostatic repulsion and short-range effective attraction interactions due to the non uniform charge distribution at the particle surface (charge patch attraction). [16]

It is interesting to highlight that the chitosan concentration responsible of charge inversion is similar for Tween vesicles and is higher in comparison with the one necessary to obtain charge inversion of Span 20 vesicular suspension. Probably this is due to the presence of PEG chains on Tween vesicle surfaces. PEG can act as a kind of shield to an initial chitosan surface deposition and interaction.

In order to check the integrity of the hybrid niosomes during the whole aggregation process, the leakage of calcein entrapped in the core of the hybrid niosomal vesicles was monitored. The release of calcein induced by the coatings with the polyelectrolyte was studied as a function of chitosan concentration at a temperature of 25 °C. The percent of dye leakage from the aggregates (I_F) was calculated as:

$I_F = (I - I_N) / (I_E - I_N)$, where I is the fluorescence intensity of the hybrid niosomal suspension, I_N is the one of the uncoated niosomes, and I_E the value corresponding to the complete rupture of the vesicles caused by adding, for example, ethanol to the suspension.

In the hybrid niosomes aggregates, calcein is present at a self-quenched concentration inside of the single vesicle aqueous core. To eliminate the calcein from the external medium, an exhaustive dialysis was carried out, but a residual fluorescence was observed. This fluorescence is probably due to some amount of calcein that remain entrapped in the external polyethylene hydrophilic layer on the surface of niosomes alone and of hybrid niosome aggregates.

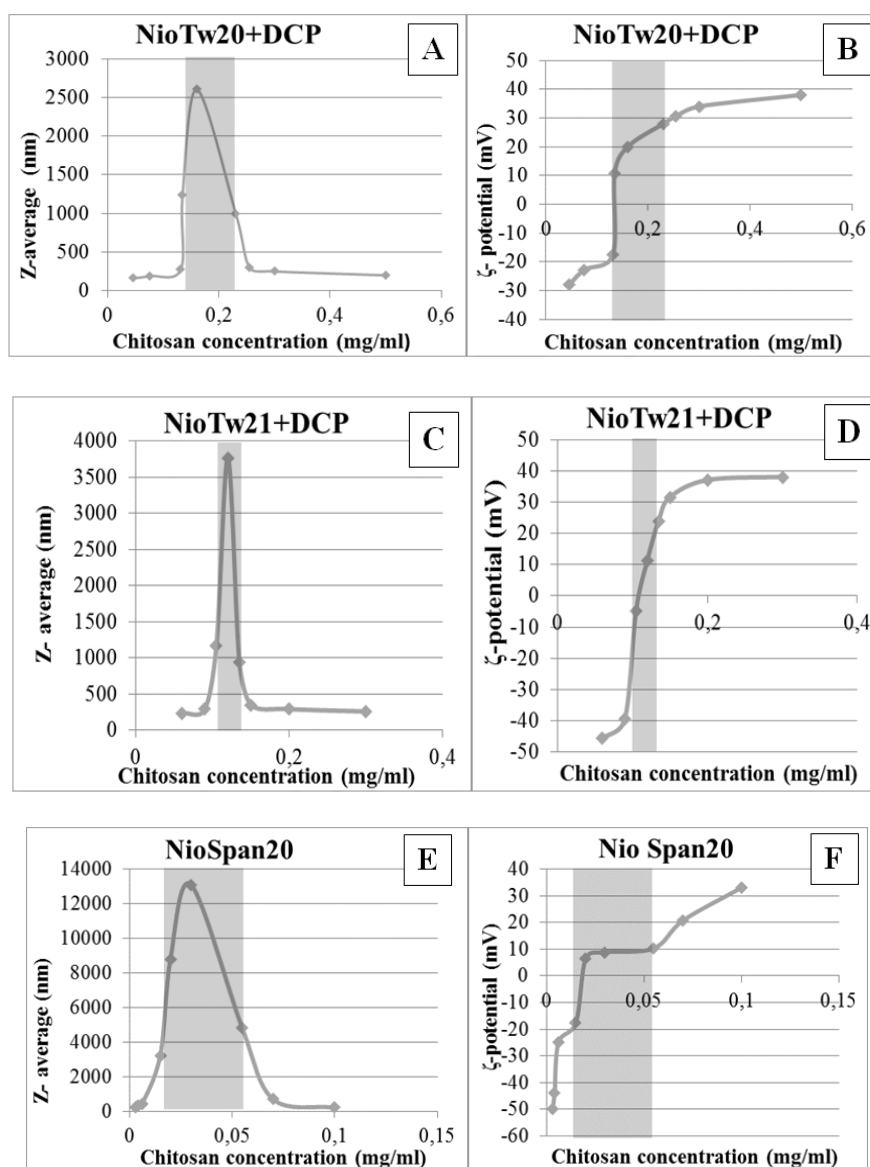


Figure 2. Z-Average (panel A, C, E) and the corresponding ζ -potential values (panel B, D, F) of different niosomal suspensions in the presence of different concentrations of chitosan solution are reported. The shaded area represents the region of instability.

The evaluation of increase of calcein fluorescence in the hybrid niosomal suspension, due to probe dequenching and dilution following complete rupture of the vesicles is useful to follow the resistance of the vesicles during polymer coating.

In tables 4, 5 and 6 are reported the fluorescence of the samples formed by the three different surfactants, prepared with different amount of chitosan.

Table 4. Fluorescence of NioTw20+DCP+Calcein in presence of different concentrations of chitosan solution.

Chitosan concentration (mg/ml)	Fluorescence (AU)
Uncoated	88,49
0,045	70,69
0,060	67,74
0,131	52,41
0,135	35,60

0,150	32,16
0,255	38,50
0,300	38,26
0,500	37,56

Table 5. Fluorescence of NioTw21+DCP+Calcein in presence of different concentrations of chitosan solution.

Chitosan concentration (mg/ml)	Fluorescence (AU)
Uncoated	74,10
0,060	68,26
0,090	61,41
0,105	60,29
0,120	56,30
0,135	47,84
0,150	46,33
0,200	40,633
0,300	38,937

Table 6. Fluorescence of NioSpan20+Calcein in presence of different concentrations of chitosan solution.

Chitosan concentration (mg/ml)	Fluorescence (AU)
Uncoated	78,92
0,003	75,26
0,004	72,94
0,006	70,81
0,015	69,36
0,020	58,14
0,030	57,27
0,055	47,86
0,070	40,71
0,100	37,11

Obtained data show that hybrid niosomal fluorescence never exceeds the one of uncoated niosomes (at the same dilution) confirming that no calcein release following vesicular degradation occurs. These results indicate that vesicular membranes of all analyzed samples are undamaged while chitosan coating occurs. For all the formulation, a fluorescence decrease with the increase of the chitosan concentration can be observed. Probably chitosan coating on vesicular surface, act as a fluorescence-screen for calcein molecules that are present on the hybrid niosome surface. The

vesicles integrity was also confirmed by DLS measurements (data not shown).

Vesicle integrity after chitosan coating, was evaluated during a time interval of 24 hours. In particular no variations of fluorescence and size were detected (data not shown), so it can be concluded that samples are not damaged by the chitosan coating.

Vesicular formulations were stored at 4 °C and 25 °C for a period of 90 days to evaluate their physical stability. Samples from each batch were withdrawn at definite time intervals (1 day, 30 days, 60 days and 90 days) to measure ζ -potential and the mean hydrodynamic diameter. These kind of measurements were carried out on a limited number of samples in particular those characterized by similar size to uncoated sample and by a positive ζ -potential. Apart from providing the hydrodynamic diameter and ζ -potential value, DLS provides also valuable information on the homogeneity of the suspension. A single sharp peak in the DLS profile implies the existence of a single population of scattering particles that correspond to low PDI value. In particular all samples are characterized by PDI value that is always lower than 0.4, and vesicular suspensions can be considered as monodisperse systems.

Table 7. Mean hydrodynamic diameter (Z-Average) and ζ -Potential values of uncoated vesicles and of selected chitosan coated vesicles.

Sample	Z-Average (nm) \pm DS	ζ -Potential (mV) \pm DS	PDI \pm DS
NioTw20+DCP	157,34 \pm 1,24	-44,22 \pm 1,61	0,31 \pm 0,01
NioTw20+DCP+Chitosan (0,3mg/ml)	252,91 \pm 4,42	37,73 \pm 0,72	0,31 \pm 0,02
NioTw21+DCP	136,52 \pm 5,21	-51,72 \pm 0,62	0,34 \pm 0,02
NioTw21+DCP+Chitosan (0,2mg/ml)	262,12 \pm 2,41	33,92 \pm 0,71	0,21 \pm 0,01
NioSpan20	202,91 \pm 5,31	-48,34 \pm 0,23	0,31 \pm 0,01
NioSpan20+Chitosan (0,1mg/ml)	292,73 \pm 6,81	43,43 \pm 0,52	0,21 \pm 0,01

In table 8 physical stability data of the three different uncoated and coated formulations are reported. These studies were carried out to investigate if significant changes of the size and ζ -potential of surfactant vesicle dispersion occur during storage. The measurements carried out by DLS indicate that all selected surfactants form vesicular structures with no significantly different sizes and ζ -potential. The uncoated and coated systems are characterized by no

significant variations of dimension and ζ -potential during the storage period, especially if they are maintained at 4°C. The high negative or positive ζ -potential values are important in preventing aggregation phenomena. In fact, it has been reported that to prevent aggregation due to electrostatic interactions, a nanovesicle should have a ζ -potential value of at least -30 mV or greater + 30 mV. [17]

Table 8. Physical stability in terms of dimensions and ζ -potential variations of uncoated (panel A) and coated (panel B) vesicles. Data were collected at days 1 and 90 and are the mean of three experiments \pm SD.

	NioTw20+DCP		NioTw20+DCP+Chitosan (0,3mg/ml)					
	25 °C	4°C	25 °C		4°C			
	Z-Average (nm)	ζ -Potential (mV)	Z-Average (nm)	ζ -Potential (mV)	Z-Average (nm)	ζ -Potential (mV)	Z-Average (nm)	ζ -Potential (mV)
t=0	157,34 \pm 1,24	-44,22 \pm 1,61	157,34 \pm 1,24	-44,22 \pm 1,61	252,91 \pm 4,42	37,73 \pm 0,72	252,91 \pm 4,42	37,73 \pm 0,72
t=90	153,91 \pm 1,43	-41,01 \pm 2,23	166,12 \pm 7,32	-42,84 \pm 1,11	241,94 \pm 4,43	33,82 \pm 1,43	337,01 \pm 4,82	38,22 \pm 0,73

Table 8. continue.

	NioTw21+DCP		NioTw21+DCP+Chitosan (0,2mg/ml)					
	25 °C	4°C	25 °C		4°C			
	Z-Average (nm)	ζ -Potential (mV)	Z-Average (nm)	ζ -Potential (mV)	Z-Average (nm)	ζ -Potential (mV)	Z-Average (nm)	ζ -Potential (mV)
t=0	136,52 \pm 5,21	-51,72 \pm 0,62	136,52 \pm 5,21	-51,72 \pm 0,62	262,12 \pm 2,41	33,92 \pm 0,71	262,12 \pm 2,41	33,92 \pm 0,71
t=90	121,12 \pm 3,43	-31,11 \pm 1,02	113,01 \pm 3,64	-53,11 \pm 2,02	197,01 \pm 3,92	31,62 \pm 1,01	253,82 \pm 2,31	36,22 \pm 1,72

Table 8. *continue.*

	NioSpan20		NioSpan20+Chitosan (0,1mg/ml)					
	25 °C	4°C	25 °C		4°C			
	Z-Average (nm)	ζ-Potential (mV)	Z-Average (nm)	ζ-Potential (mV)	Z-Average (nm)	ζ-Potential (mV)	Z-Average (nm)	ζ-Potential (mV)
t=0	202,91±5,31	-48,34±0,23	202,91±5,31	-48,34±0,23	292,73±6,81	43,43±0,52	292,73±6,81	43,43±0,52
t=90	258,11±7,83	-32,22±1,52	224,82±7,91	-48,51±1,52	275,82±6,72	25,72±1,22	272,92±7,62	36,22±1,71

4. Conclusions

In this work, the complexation process between negatively charged vesicles built up by three different surfactants (Tween 20, Tween 21 and Span 20) and chitosan, a cationic polyelectrolyte, with mucoadhesive properties, is described.

The aggregation behavior can be deeply investigated by size, ζ-potential and fluorescence evaluations, in order to select the most appropriate samples to perform intranasal administration. From the obtained results the selected Tw20, Tw21 and Span vesicles coated with a chitosan concentration able to obtain a positively charged hybrid vesicle, are: a) homogenous and monodisperse vesicular population; b) characterized by dimensions compatible with the proposed route of administration; c) stable in terms of dimension and ζ average variation, if stored at 4°C.

These kind of measurements can be useful to perform an initial screening and needs to be confirmed by a complete preclinical evaluation.

References

- [1] J. P. Blumling 3rd and G. A. Silva, "Targeting the brain: advances in drug delivery", *Curr. Pharm. Biotechnol.*, vol. 13, pp. 2417-2426, 2012.
- [2] X. Yi, D. S. Manickam, A. Brynskikh and A. V. Kabanov, "Agile delivery of protein therapeutics to CNS", *J. Controlled Release*, vol. 190, pp. 637–663, 2014.
- [3] C. Marianecchi, L. Di Marzio, F. Rinaldi, C. Celia, D. Paolino, F. Alhaique, S. Esposito and M. Carafa, "Niosomes from 80s to present: The state of the art", *Adv. Colloid Interface Sci.*, vol. 205, pp. 187–206, 2014.
- [4] M. Estanqueiro, M. H. Amaral, J. Conceição and J. M. Sousa Lobo, "Nanotechnological carriers for cancer chemotherapy: The state of the art", *Coll. Surf. B Biointerfaces*, vol. 126, pp. 631-648, 2015.
- [5] K. K. Jain, "Drug Delivery to the Central Nervous System", Berlin and Heidelberg:Springer, 2010.
- [6] S. V. Dhuria, L. R. Hanson and W. H. Frey 2nd, "Intranasal Delivery to the Central Nervous System: Mechanisms and Experimental Considerations", *J. Pharm. Sci.*, vol. 99, pp. 1654-1673, 2010.
- [7] F. Uchegbu and A. T. Florence, "Non-ionic surfactant vesicles (niosomes): Physical and pharmaceutical chemistry", *Adv. Colloid Interface Sci.*, vol. 58, pp. 1-55, 1995.
- [8] S. Sennato, F. Bordi, C. Cametti, C. Marianecchi, M. Carafa and M. Cametti, "Hybrid Niosome Complexation in the Presence of Oppositely Charged Polyions", *J. Phys. Chem. B*, vol. 112, pp. 3720-3727, 2008.
- [9] M. Carafa, C. Marianecchi, G. Lucania, E. Marchei and E. Santucci, "New vesicular ampicillin-loaded delivery systems for topical application: characterization, in vitro permeation experiments and antimicrobial activity", *J. Controlled Release*, vol. 95, pp. 67–74, 2004.
- [10] C. Marianecchi, D. Paolino, C. Celia, M. Fresta, M. Carafa and F. Alhaique, "Non-ionic surfactant vesicles in pulmonary glucocorticoid delivery: characterization and interaction with human lung fibroblasts", *J. Controlled Release*, vol. 147, pp. 127–135, 2010.
- [11] S. W. Provencher, "Contin: a general purpose constrained regularization program for inverting noisy linear algebraic and integral equations", *Comput. Phys. Commun.*, vol. 27, pp. 213-242, 1982.
- [12] C. De Vos, L. Deriemaeker and R. Finsy, "Quantitative assessment of the conditioning of the inversion of quasi-elastic and static light scattering data for particle size distributions", *Langmuir*, vol. 12, pp. 2630-2636, 1996.
- [13] B. Maherani, E. Arab-Tehrany, A. Kheirloom, D. Geny and M. Linder, "Calcein release behavior from liposomal bilayer: influence of physicochemical/mechanical/structural properties of lipids", *Biochimie*, vol. 95, pp. 2018-2033, 2013.
- [14] Y. Grosberg, T. T. Nguyen and B. I. Shklovskii, "Colloquium: The physics of charge inversion in chemical and biological systems", *Rev. Mod. Phys.*, vol. 74, pp. 329-345, 2002.
- [15] T. T. Nguyen and B. I. Shklovskii, "Complexation of DNA with positive spheres: Phase diagram of charge inversion and reentrant condensation", *J. Chem. Phys.*, vol. 115, pp. 7298-7308, 2001.
- [16] F. Bordi, C. Cametti, M. Diociaiuti and S. Sennato, "Large equilibrium clusters in low-density aqueous suspensions of polyelectrolyte-liposome complexes: A phenomenological model", *Phys. Rev. E*, vol. 71, pp. 050401/1-0504014, 2005.
- [17] C. Marianecchi, F. Rinaldi, M. Mastriota, S. Pieretti, E. Trapasso, D. Paolino and M. Carafa, "Anti-inflammatory activity of novel ammonium glycyrrhizinate/niosomes delivery system: human and murine models", *J. Controlled Release*, vol. 164, pp. 17-25, 2012.

Paper:

**Pentosomes for delivery of pentamidine
to CNS by intranasal route**

(Submitted)

Pentosomes for delivery of pentamidine to CNS by intranasal route

Hanieh P.N.¹, Marianecchi M.¹, Rinaldi F.², Gigli S.³, Seguella L.³, Esposito G.³, Carafa M.¹

¹ Department of Drug Chemistry and Technology, University of Rome “Sapienza”, Rome, Italy.

² Center for Life Nano Science@Sapienza, Fondazione Istituto Italiano di Tecnologia, Rome, Italy.

³ Department of Physiology and Pharmacology ‘Vittorio Ersamer’, La Sapienza University of Rome, Rome, Italy.

1. Introduction

Parkinson’s disease (PD) is a progressive neurodegenerative disorder that involve the movement control and balance of the body.

Symptoms consist mainly in the rigidity, resting tremor and bradykinesia with the progressive loss of dopaminergic neurons localized in the substantia nigra of the brain. [1]

Currently, the therapy is only symptomatic and do not arrested or slow down the neurodegeneration.

The protein S100 calcium-binding B (S100B) is a small protein necessary for neurodevelopment and plasticity of the astrocytes but it is overexpressed in several neurodegenerative diseases, including PD and Alzheimer’s disease.

Its mechanism of action is the inhibition of the tumor suppressor protein p53 and the stimulation of the protein kinase B and the nuclear dbf2-related kinase. [2, 3]

Furthermore, it promotes numerous pathological process such as neuroinflammation, cell growth and apoptosis. [4]

Pentamidine isethionate (P) is an antiprotozoal drug generally employed for the treatment of *Pneumocystis carinii* pneumonia in the United States. Many researches have demonstrated the ability of this molecule to block the interaction between S100B and p53 *in vitro* resulting a promising agent for the treatment of Parkinson’s disease. [5]

However, its systemic administration causes toxicity, in particular renal [6] and also the pharmacokinetic profile of P is characterized by low blood brain barrier crossing. [7]

The present work focuses on the development of an intranasal formulation for the pentamidine delivery with the aim of achieving directly the brain, decreasing drug levels within tissues vulnerable to toxicity, and increased accumulation at the target site.

For this purpose, pentamidine loaded niosomes, namely Pentasome, have been formulated and characterized of suitable for nose to brain delivery. Moreover, in order to improve the residence time of this vesicles in the nasal mucosa, chitosan coating was employed.

2. Materials and Methods

2.1. Materials

Polysorbate 20 (Tween 20), Dicapryl phosphate (DCP), Cholesterol (Chol), Pentamidine isethionate (Pent), Hepes salt {N-(2-idroxyethyl) piperazine-N'-(2-ethanesulfonic acid)}, Sephadex G75, Chitosan (Chit) (low molecular weight) were purchased from Sigma-Aldrich.

All other products and reagents were of analytical grade.

2.2. Pentasomes preparation and purification

The vesicles were obtained by thin layer evaporation method as previously reported [8], according to the compositions shown in the table 1.

All the vesicle hydrophobic constituents were firstly dissolved in CH₃OH/CHCl₃ (3:1 v/v) mixture. After the solvent evaporation, the film obtained was hydrated with a solution of pentamidine (5 mg/ml) in hepes buffer.

The multilamellar vesicular suspension was vortexed for about 5 minutes and then sonicated (5 minutes, 16% amplitude, at 60°C) using a microprobe operating at 20 kHz (VibraCell-VCX 400-Sonics, Taunton, MA, USA).

The unilamellar vesicle suspension was purified by gel permeation chromatography using SephadexG75 (glass column of 50 x 1.2 cm) with hepes buffer as the eluent.

2.3. Preparation of Chitosan-coated Pentasomes

The chitosan-coated pentasomes (C-pentasomes) formation was prepared by adding 1 ml of chitosan solution (DLS paper) to an equal volume of pentasomes.

The obtained suspension was stirred for 3 h in a thermostated water bath at 10 °C.

2.4. Entrapment efficiency (E.E.%)

Pentamidine entrapment efficiency in Pentasomes was determined using UV spectrophotometer. Spectrophotometric analyses were carried out at 270 nm, by means of a spectrophotometer (Perkin-Elmer, lambda 3a, UV-Vis spectrometer) equipped by 1.0 cm path-length quartz cells and drug EE % was calculated as follows:

$$EE\% = [(Concentration\ of\ drug\ determined) / (Total\ concentration\ of\ drug\ loading)] \times 100$$

Results are the average of three different batches \pm standard deviation.

2.5. Dynamic light scattering and Electron transfer studies

Pentasomes and C-pentosome mean diameters (Z-Average), size distributions (polydispersity index, PDI) and ζ -potential were measured at the temperature of 25 °C by means a Malvern ZetaSizerNano 90S.

2.6. Pentasomes bilayer fluidity determination

The fluidity of Pentasomes bilayer was determined by fluorescence anisotropy studies using DPH as fluorescence probe.

DPH was added to vesicle composition at the final concentration of 2×10^{-3} M and to obtain DPH-labeled Pentasomes, DPH solution was added to the constituents and the fluorescent probe loaded vesicles were obtained by film technique as reported above.

To avoid any experimental artifact, i.e. to allow the fluorescent probe disposition in the vesicle bilayer, samples were stored 3 h at room temperature before the fluorescence anisotropy experiments.

2.7. Pentasomes stability studies

For colloidal stability at different temperatures, the formulations were stored at 4 and 25°C for a period of 90 days.

Samples from each batch were withdrawn at definite time intervals (1, 30, 60 and 90 days) and the ζ -potential, the mean of hydrodynamic diameter of Pentasomes and pentamidine EE were determined.

In order to study the stability of pentasome in the biological fluids, human serum (HS) or artificial cerebrospinal fluid (aCSF) was added to vesicle suspensions until reached at 90% [9] or 45% respectively.

2.8. *In vitro* release studies

In vitro release of pentamidine from niosomes was evaluated by dialysis (8,000 MW cutoff; Spectrum).

Briefly, an aliquot of the pentasomes and HS (45%) or aCSF (90%) was placed in dialysis tubing and immersed in buffer, gently magnetically stirred at 37°C.

The medium was regularly sampled over a 24 h period at appropriate time intervals and reinserted back in the medium after the measurements, in order to maintain the volume of the medium constant.

Released pentamidine was detected at 270 nm, by means of a spectrophotometer (Perkin-Elmer, lambda 3a, UV-Vis spectrometer) equipped by 1.0 cm path-length quartz cells.

All aliquots were analyzed immediately after sampling. All release experiments were carried out in triplicate.

The values reported in the present paper represent the mean values and lay within 10% of the mean.

2.9. *In vivo* studies

Animal experiments were performed in C57Bl/6J mice (eight-weeks old male, weight range around 30 g).

Parkinson disease was induced by daily injection of 1-methyl-4-phenyl-1,2,3,6-tetrahydropyridine (MPTP), a neurotoxin which causes symptoms of PD, 25 mg/kg 25 mg/kg) for four consecutive days starting from day 1.

Mice were randomly divided into five groups: (1) vehicle; (2) MPTP group; (3 and 4) MPTP group receiving daily C-Pentasomes at increasing doses (0.005-0.05 μ M); (5) MPTP receiving empty Pentasomes, as internal group.

C-Pentosome was intranasally administrated from day 0 until day 5, once at day.

Three days after last MPTP administration, rotarod test and pole test were assessed to determine the functional outcomes on PD.

After behavioral tasks, animal was euthanized and brains were isolated in order to perform biochemical assays and immunohistological staining.

All the experiments were carried out in accordance with the National Institutes of Health Guidelines for the Care and Use of Laboratory Animals (Institute of Laboratory Animal Resources, 1996) and those of the Italian Ministry of Health (D.L. 116/92).

The study was approved by the Institutional Local Animal Care and Use Committees.

3. Results

3.1. Characterization of Pentasomes

Pentasomes characterization is summarized in Table 1.

DLS analysis showed that the size of Pentasomes is around 172.0 nm and after the addition of chitosan (C-Pentasomes) an increase of dimension is observed.

The change of ζ -potential from negative surface charging to positive confirms that the vesicular surface is covered by chitosan. Generally, vesicles form a stable dispersion when the absolute value of ζ -potential is around ± 30 mV, since it guarantees the electric repulsion between particles. [10]

The PDI of both formulations showed values of 0.2, indicating homogenous populations of vesicles. In addition, EE studies show that Pentasomes encapsulate the 24% of loaded pentamidine.

Sample	Tw20 (mM)	DCP (mM)	Chol (mM)	P (mg/ml)	C (mg/ml)	Hydrodynamic diameter (nm) \pm SD	ζ -Potential (mV) \pm SD	PDI \pm SD	EE%
Pentasomes	15.0	7.5	15.0	5	-	172.0 \pm 3.9	-35.0 \pm 0.8	0.2 \pm 0.0	24%
C-Pentasomes					0.18	350.7 \pm 17.2	+39.0 \pm 1.1	0.2 \pm 0.0	

Table.1

3.2. Pentasomes bilayer characterization

Anisotropy is related to the fluidity of the bilayer: it is inversely proportional to the membrane fluidity and the high value of anisotropy indicates a high structural order and/or a low membrane fluidity.

As shown in the table 2, the fluorescence anisotropy value is similar for all samples and the bilayer is mildly rigid, also after chitosan addition at the formulation.

Therefore, chitosan is only absorbed onto the vesicle surface without intercalation in the bilayer.

Sample	Fluidity (A.U.)
Pentosomes	0.27
C-Pentosomes	0.28

Table. 2

3.3. Pentosomes stability studies

The stability studies of Pentosomes are shown in the figure 1 and they suggest a high colloidal stability. No show significant variations of size and ζ -potential are recorded at two different storage temperatures over 90 days.

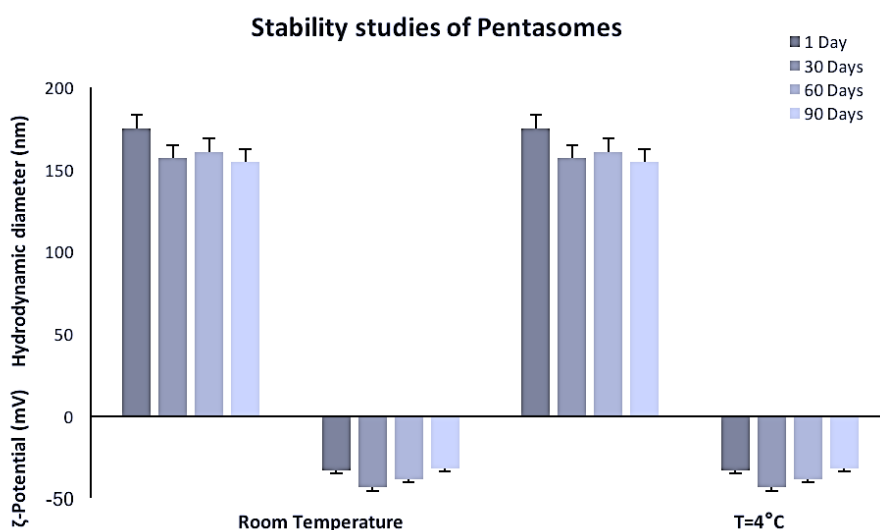


Figure. 1

Moreover, the concentration of pentamidine entrapped in Pentosomes during the storage period was evaluated.

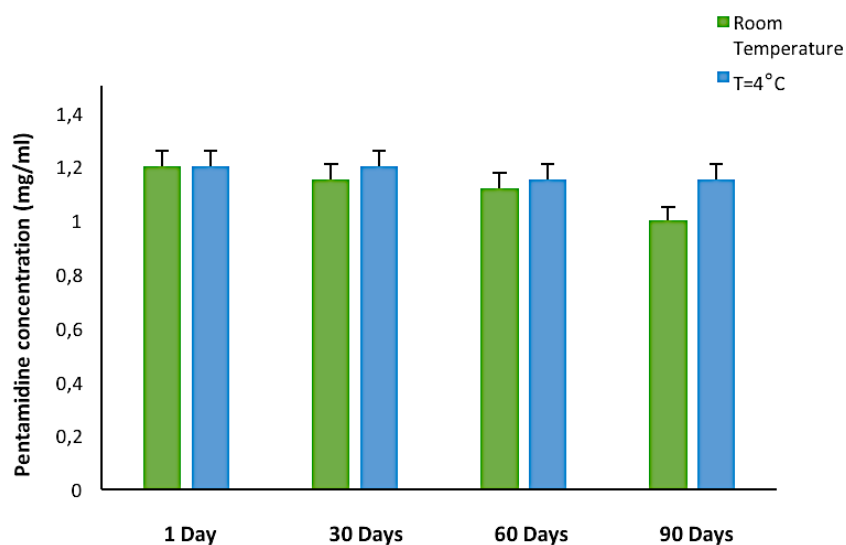


Figure. 2

As shown in the figure 2, the pentamidine concentration is constant at both storage temperatures. The effect of biological fluids (HS and aCSF) on the stability of Pentasomes was evaluated. The experiments were performed observing size and ζ -potential variation at definite time intervals up to 3 hours at 37°C.

Stability studies in vitro of Pentasomes in the biological fluids

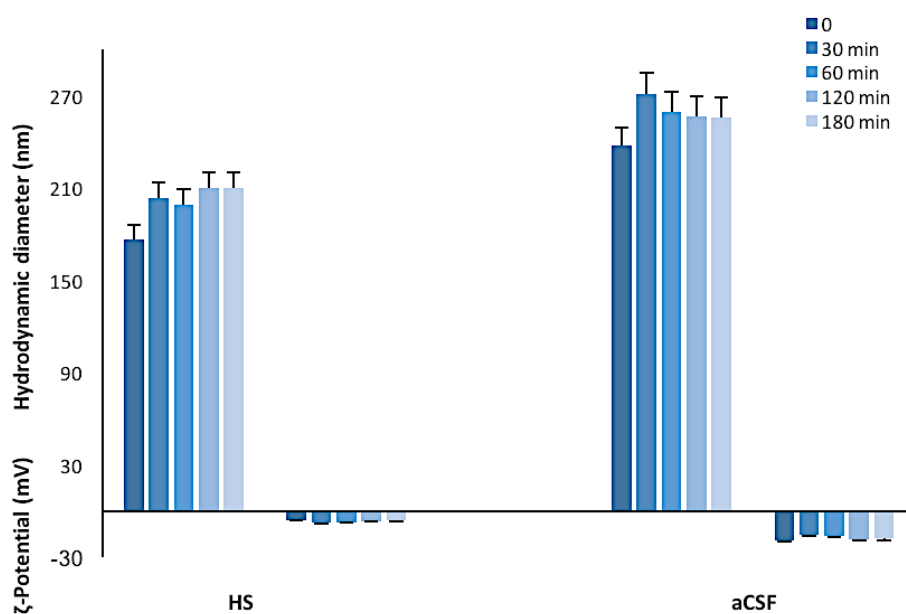


Figure. 3

During the analyzed time interval, in both fluids an increase of dimension and a decrease of ζ -potential values of Pentasomes is observed.

This phenomenon is not associate at vesicular breaking, since the size increase is observed immediately after the contact between Pentasomes and HS or aCSF and it is maintained constant up to 3 h.

In particular, in HS this increase is probably due to human proteins absorption on vesicular surface.

3.4. *In vitro* drug release studies

In vitro release profiles of pentamidine are obtained by contacting Pentasome and HS or aCSF up to 24 hours.

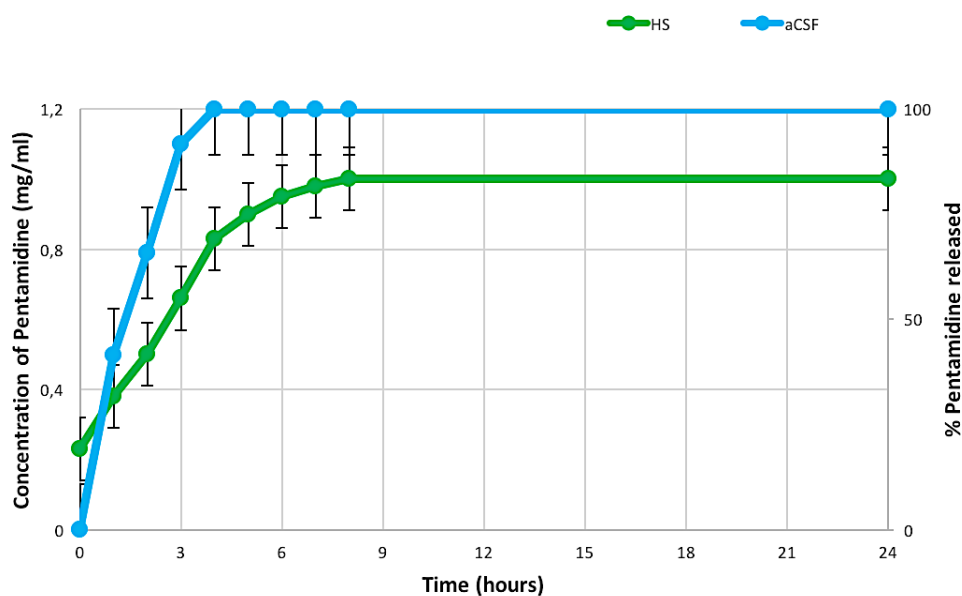


Figure. 4

After 24h, Pentasomes release 80% and 100% of their pentamidine cargo, in HS and aCSF respectively. (Figure. 4)

In particular, in presence of aCSF Pentasomes a 100% pentamidine release after 4 hours was observed.

3.5. In vivo studies

The rotarod test is used to investigate the motor coordination and behavior of mice when they are placed into a center of the square arena.

Instead, in the pole test is assessed the agility of animals and their bradykinesia. The mice are placed on top of a pole and the T_{turn} and total locomotor activity (T_L) were measured. The T_{turn} is the time used to proceed to downward and the T_L is the time until the mice arrive on the floor.

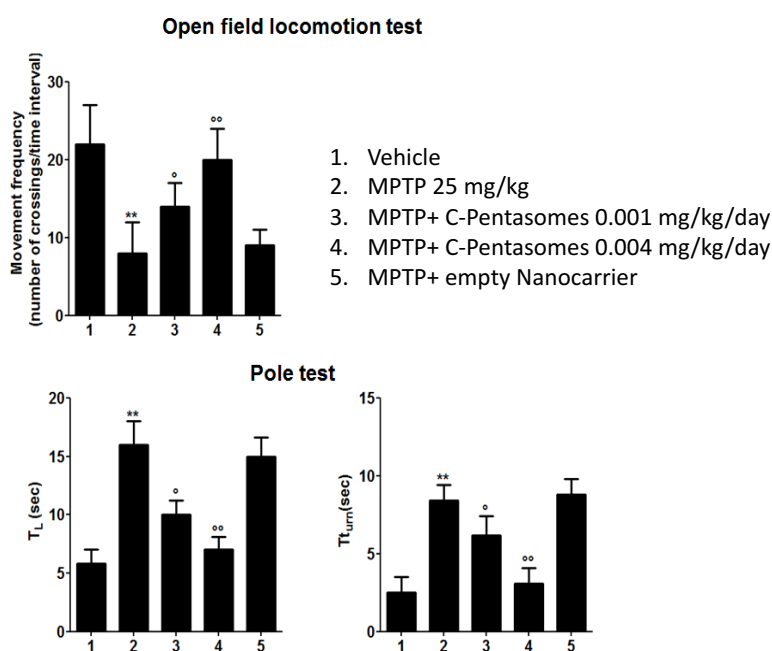


Figure. 5

In the figure 5, MPTP treatment caused a significant decrease of movement frequency in intoxicated mice versus vehicle group (-63%).

This effect was reverted by C-Pentosomes treatment in a dose-dependent manner: for the mice treated with 0.001 mg/kg was assessed an increase of 60% and with 0.004 mg/kg of 137% compared to MPTP group.

After administration of niosomes without drug (empty nanocarrier) a mild improvement of the mice movement was observed

These results confirm that the Pentasomes are able to reach the brain after intranasal administration. In the same experimental conditions, during the pole test both T_L and T_{turn} were significantly higher in MPTP-intoxicated mice compared to respective vehicle groups (T_L : +181%; T_{turn} : +220%).

Conversely, C-Pentosomes was able to revert such effect, decreasing both T_L , 37% (for mice treated with 0.001 mg/kg of C-Pentosomes) and 56% (0.004 mg/kg), and T_{turn} , 23% (0.001 mg/kg) and 58% (0.004 mg/kg), compared to MPTP group.

Also in this study, an enhance of coordination performance is observed after C-Pentosomes administration in a dose-dependent manner.

In parallel with motor impairments, MPTP neurotoxin induces in the mice a neuronal dopaminergic loss localized into striatum and substantia nigra.

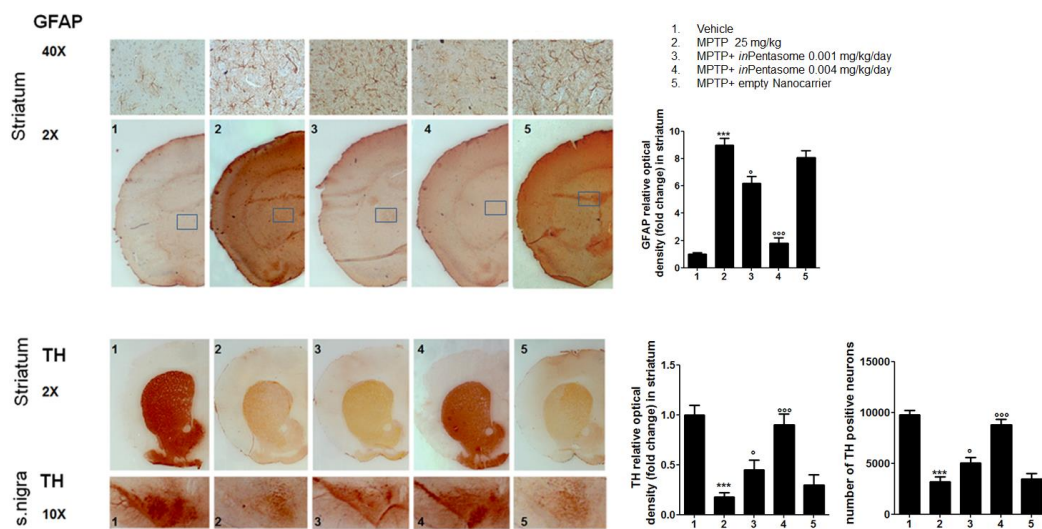


Figure. 6

In the figure 6, immunohistochemistry staining highlighted a significant reduction of TH^+ positive cells in MPTP-treated mice of 82% in the striatum and 68% in the substantia nigra compared to vehicle group.

Pentamidine released from Pentosomes was able to rescue the dopaminergic cellular density in a dose-dependent fashion.

In the group 3, the cells increase of 150% in the striatum and 58% in the substantia nigra compared to MPTP group, whereas in the group 4 is observed a cellular increase of 405% and 174% respectively.

Conversely, the empty vector did not show any significant improvement in TH^+ protein level of nigrostriatal axis MPTP-induced.

Finally, in order to test whether pentamidine effects were due to its ability to reduce neuroinflammation severity, astrogliosis and proinflammatory cytokines expression were evaluated. Immunohistochemistry staining for GFAP showed a marked astrogliosis in the striatum of MPTP-treated mice versus vehicle group (+800%). (Figure. 7)

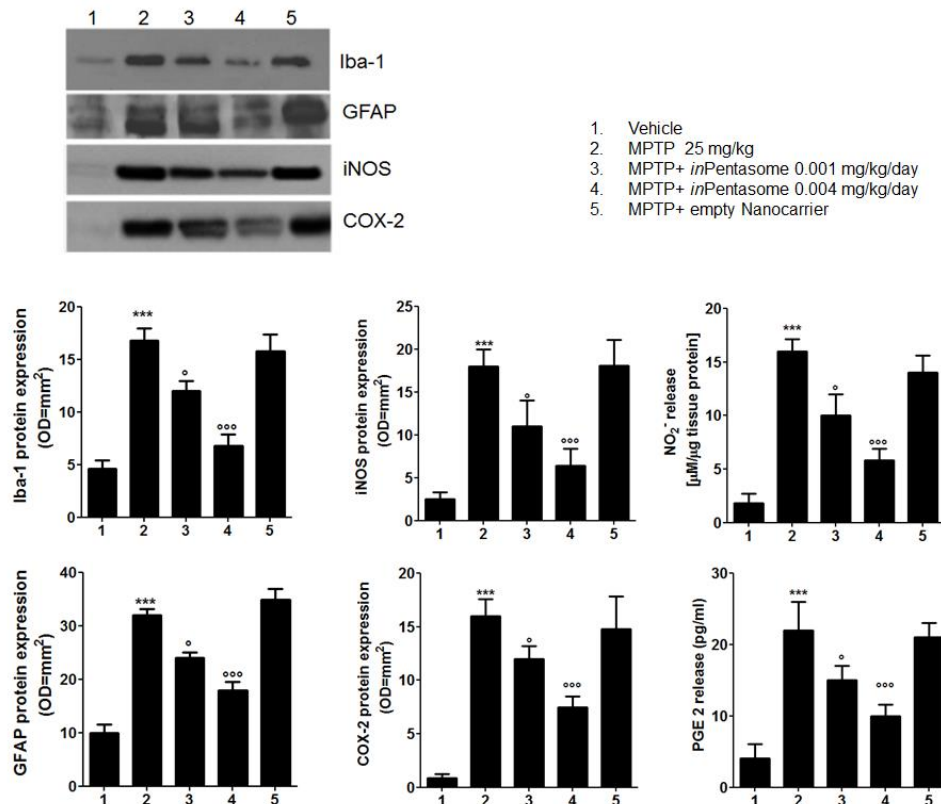


Figure. 7

Once again, increasing doses of pentamidine reduced significantly the number of striatal GFAP+ positive cells of 32% (0.001 mg/kg) and 80% (0.004 mg/kg) compared to MPTP group.

Whereas the empty nanocarrier did not affect the neuroinflammatory process MPTP-mediated.

Along this line, following MPTP treatment an increased GFAP (+230%), COX-2 (+1450%), iNOS (+510%) and Iba-2 (+265%) protein expression was observed by immunoblot analysis, as well as nitrite (+855%) and PGE2 (+430%) release.

Proinflammatory cytokines level was markedly reduced when 0.001 mg/kg of C-Pentosomes was administrated (GFAP: -27%; COX-2: -25%; iNOS: -40%; Iba-2: -24%; NO: -38%; PGE2: -29% compared to MPTP group) and 0.004 mg/kg (GFAP: -51%; COX-2: -55%; iNOS: -66%; Iba-2: -59%; NO: -60%; PGE2: -52%; versus MPTP group).

Instead, no effects were observed after empty nanocarrier administration.

4. Conclusions

In these studies, Pentasomes have shown to be able to entrap the necessary concentration of pentamidine in order to observe *in vivo* therapeutic effects.

The nanocarrier formulated are stable over time at both storage temperatures and biological fluids.

The results obtained from the *in vivo* studies suggest that the encapsulation of pentamidine in C-Pentasomes improves the nose to brain delivery of the drug after intranasal administration.

Furthermore, the neuroprotective and neurorestorative effect of Pentasomes in a mice model of PD are demonstrated.

Therefore, it can be concluded that C-Pentasomes administered by a non-invasive route such as the intranasal route could be a promising tool for the treatment of PD.

References

- [1]. Magrinelli F, Picelli A, Tocco P, Federico A, Roncari L, Smania N, Zanette G, Tamburin S. Pathophysiology of Motor Dysfunction in Parkinson's Disease as the Rationale for Drug Treatment and Rehabilitation. *Parkinsons Dis*, doi: 10.1155/2016/9832839, 2016.
- [2]. Arcuri C, Bianchi R, Brozzi F, Donato R. S100B increases proliferation in PC12 neuronal cells and reduces their responsiveness to nerve growth factor via Akt activation. *J Biol Chem*, 280, 4402–4414, 2005.
- [3]. Millward TA, Heizmann CW, Schäfer BW, Hemmings BA. Calcium regulation of Ndr protein kinase mediated by S100 calcium-binding proteins. *EMBO J*, 17, 5913–5922, 1998.
- [4]. Donato R, Sorci G, Riuzzi F, Arcuri C, Bianchi R, Brozzi F, Tubaro C, Giambanco I. S100B's double life: intracellular regulator and extracellular signal. *Biochim Biophys Acta*, 1793, 1008–1022, 2009.
- [5]. Capoccia E, Cirillo C, Marchetto A, Tiberi S, Sawikr Y, Pesce M, D'Alessandro A, Scuderi C, Sarnelli, Cuomo, R, Steardo L, Esposito G. S100B-p53 disengagement by pentamidine promotes apoptosis and inhibits cellular migration via aquaporin-4 and metalloproteinase-2 inhibition in C6 glioma cells. *Oncol Lett*, 9 (6), 2864–2870, 2015.
- [6]. Smith J, Stewart BJ, Glaysher S, Peregrin K, Knight LA, Weber DJ, Cree IA. The effect of pentamidine on melanoma. *Anticancer Drugs*, 21 (2), 181–185, 2010.
- [7]. Sanderson L, Dogruel M, Rodgers J, De Koning HP, Thomas SA. Pentamidine Movement across the Murine Blood-Brain and Blood-Cerebrospinal Fluid Barriers: Effect of Trypanosome Infection, Combination Therapy, P-Glycoprotein, and Multidrug Resistance-Associated Protein. *J Pharmacol Exp Ther*, 329 (3), 967–977, 2009.
- [8]. Marianecchi C, Rinaldi F, Esposito S, Di Marzio L, Carafa M. Niosomes encapsulating Ibuprofen-cyclodextrin complexes: preparation and characterization. *Curr Drug Targets*, 14 (9), 1070-8, 2013.
- [9]. Stanwick JC, Baumann MD, Shoichet MS. Enhanced neurotrophin-3 bioactivity and release from a nanoparticle-loaded composite hydrogel. *J Control Release*, 160 (3), 666-75, 2012.
- [10]. Marianecchi C, Rinaldi F, Mastriota M, Pieretti S, Trapasso E, Paolino D, Carafa M. Anti-inflammatory activity of novel ammonium glycyrrhizinate/niosomes delivery system: human and murine models. *J Controlled Release*, 164, 17-25, 2012.

Nanoemulsios

This project was developed in the last period of my PhD and deals with the preliminary development of nanoemulsion formulations suitable for a potential application in brain delivery.

1. Nanoemulsions

Emulsions are heterogeneous dispersions of two immiscible liquids, in which one is dispersed as fine droplets (internal phase) in the other liquid (external phase).

Emulsions can be classified according to the droplet size in macroemulsion (ME) and nanoemulsion (NE), and according to the external phase in oil-in-water (o/w) or water-in-oil (w/o).

These systems are extensively used in cosmetic, food and pharmaceutical field and they may be formulated as sprays, creams, liquids and ointments.

Both types of emulsions are used as drug delivery system to increase the oral and parenteral bioavailability of therapeutic agents, in particular the peptides, but NEs are preferred for the treatment of brain disorders [1] because they show:

- an average droplet size between 20 and 500 nm;
- a high surface area per unit volume;
- appear transparent, due to their inability to scatter the light [2];
- the ability to entrap poorly aqueous soluble drugs;
- a long-term stability, the NEs are kinetically stable against sedimentation and creaming phenomena, due to their very small droplet size;

Nanoemulsions are typically composed by oil, water and emulsifier, such as surfactants, protein or lipid. [3, 4] (Figure. 1)

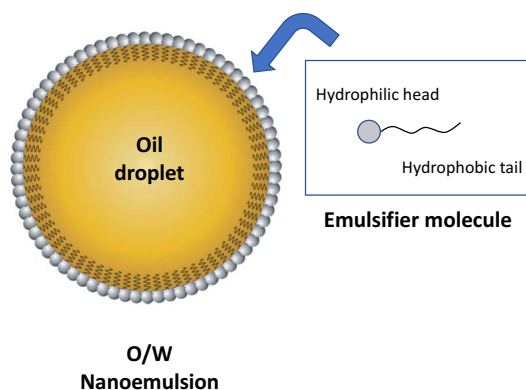


Figure. 1 Oil droplet structure in NEs.

The emulsifying agent is necessary to obtain a homogeneous mixture between the two phases, and it stabilized the NEs through steric impediment and repulsive interactions. [5]

Moreover, surfactants in the NEs could contribute to increase the brain uptake as stealth agents [6], Pgp inhibitors [7], permeation enhancers [8].

In particular, poloxamer and polysorbate (Tween 80/20) surfactants have been widely evaluated for brain delivery as promote receptor mediated uptake via the lipoprotein receptor. Both surfactants promote the adsorption of apolipoprotein E on the surface of the carrier. The affinity of apolipoprotein E for LDL receptor localized in the BBB allows the carrier uptake by receptor mediated endocytosis (RME). [9, 10, 11]

Also the oil in the NEs can be utilized as absorption enhancer. [12] For example, the oils rich of polyunsaturated fatty acids, such as docosahexaenoic acid (DHA) plays an important role for the brain healthy. They are constituents of human brain and retina and reach the brain due to the presence of specific transporters, DHA transporter or specific fatty acid binding lipoprotein carriers, localized on BBB. [13, 14]

Therefore, O/W NEs containing oils rich in DHA could promote enhanced brain uptake by RME mechanism. [15]

Some oils can show a bioactive effect and therefore a synergic effect with the drug loaded in NEs. In particular, the essential oils show a wide-spectrum biological activities, including antioxidant, antibacterial, antiviral, antifungal, anti-inflammatory and anticancer ones. [16, 17]

NE can be prepared by means of two methods: (1) the high-energy methods are used in the laboratory and industrial scale and include the high-pressure homogenization method, in which the mixture is exposed to high pressure to obtain a finally-dispersed emulsion with a very small droplet size. [18]

Similarly, in the microfluidization method, the emulsion ingredients are exposed to high pressure and then are forced at very high speed across a small orifice. [19]

(2) The low energy methods include (i) the phase inversion technique, which use the increase of temperature to obtain the NEs, and (ii) the spontaneous emulsification method, where the O/W emulsion is spontaneously obtained by using a hydrophobic oil and a water-miscible solvent. [20]

NEs are prepared by using biocompatible compound and for this reason they are generally considered safe and non-toxic.

2. Nanoemulsions for brain delivery

By virtue of their lipophilic nature and low globule size, NEs exhibit an excellent potential for brain delivery. [21]

Several studies demonstrate the improvement of brain delivery of neurotherapeutic agents loaded in NEs.

Kumara et al. [22], have evaluated the biodistribution of risperidone in the blood and brain of rats following intranasal and intravenous administration of the nanoemulsions containing risperidone. They obtained a higher drug amount in the brain of the rats after NE administration compared to other formulations. Furthermore, NEs seemed to be more effective after nasal administration rather than intravenous route.

In a similar study, Jain et al. [23] have formulated amiloride mucoadhesive NEs for intranasal delivery. Histopathological assessment and nasal irritation study of the nasal mucosa have shown that the granular cellular structure and the surface of the nasal epithelium was totally intact. Therefore, they have demonstrated that the NEs formulation was nontoxic and non-irritant for the nasal mucosa.

In another study, NEs are used to deliver the saquinavir mesylate, a protease inhibitor with poor water-solubility, to the brain. [24] *In vivo* biodistribution studies demonstrated a higher concentration of drug in the brain for the NEs intranasal administered compared to the formulations administered intravenously.

Therefore, the use of NEs as intranasal drug delivery system is set to bring about significant results in targeting drugs to the brain in the treatment of CNS diseases.

3. Aim

The aim of this part of my PhD project has been mainly focused on the formulation and physical-chemical characterization of nanoemulsions obtained by neem oil.

All collected data and experimental setup are shown in the **paper: Neem oil nanoemulsions: characterisation and antioxidant activity**.

References

- [1]. Shinde RL, Jindal AB, Devarajan PV. Microemulsions and Nanoemulsions for Targeted Drug Delivery to the Brain. *Curr Nanoscience*, 7 (1), 119-133, 2001.
- [2]. McClements DJ. Theoretical prediction of emulsion color. *Adv Colloid Interface Sci*, 97 (1-3), 63-89, 2002.
- [3]. Gehrman S, Bunjes H. Preparation of lipid nanoemulsions by premix membrane emulsification with disposable materials. *Int J Pharm.*, 511 (2), 741-4, 2016.
- [4]. Rajendran SRCK, Udenigwe CC, Yada RY. Nanochemistry of Protein-Based Delivery Agents. *Front Chem*, 4 (31), 2016.
- [5]. Mason TG, Wilking JN, Meleson K, Chang CB, Graves SM. Nanoemulsions: formation, structure, and physical properties. *J Phys Condens Matter*, 18, R635-R666, 2006.
- [6]. Oyewumi MO, Yokel RA, Jay M, Coakley T, Mumper RJ. Comparison of cell uptake, biodistribution and tumor retention of folate coated and PEG coated gadolinium nanoparticles in tumor bearing mice. *J Control Release*, 95 (3), 613-626, 2004.
- [7]. Cornaire G, Woodley J, Hermann P, Cloarec A, Arellano C, Houin G. Impact of excipients on the absorption of P-glycoprotein substrates in vitro and in vivo. *Int J Pharm*, 278, 119-131, 2004.
- [8]. Varma MV, Panchagnula R. Enhanced oral paclitaxel absorption with vitamin E-TPGS: effect on solubility and permeability in vitro, in situ and in vivo. *Eur J Pharm Sci*, 25, 445-453, 2005.
- [9]. Barchet TM, Amiji MM. Challenges and opportunities in CNS delivery of therapeutics for neurodegenerative diseases. *Expert Opin Drug Deliv*, 6 (3), 211-225, 2009.
- [10]. Koo Y L, Reddy GR, Bhojani M, Schneider R, Philbert MA, Rehemtulla A, Ross BD, Kopelman R. Brain cancer diagnosis and therapy with nanoplatforms. *Adv Drug Deliv Rev*, 58, 1556-1577, 2006.
- [11]. Garcia E, Andrieux K, Gil S, Couvreur P. Colloidal carriers and blood brain barrier (BBB) translocation: A way to deliver drug to the brain? *Int J Pharm*, 298, 274-292, 2005.
- [12]. Sztrihai L, Betz AL. Oleic acid reversibly opens the blood-brain barrier. *Brain Res*, 550, 257-262, 1991.
- [13]. Neuringer M, Connor WE. The essentiality of n-3 fatty acids for the development and function of retina and brain. *Ann Rev Nutr*, 8, 517-541, 1988.

- [14]. Lukiw WJ, Bazan NG. Docosahexaenoic acid and the aging brain. *J Nutr*, 138, 2510-2514, 2008.
- [15]. Chen CT, Liu Z, Ouellet Calon, F, Bazinet RP. Rapid-oxidation of ecosapentaenoic acid in mouse brain: An in situ study. *Prostaglandins Leukot Essent Fatty Acids*, 80 (2-3), 157-163, 2009.
- [16]. Seow YX, Yeo CR, Chung HL, Yuk HG. Plant essential oils as active antimicrobial agents. *Crit Rev Food Sci Nutr*, 54 (5), 625-44, 2014.
- [17]. Burt S. Essential oils: their antibacterial properties and potential applications in foods--a review. *Int J Food Microbiol*, 94 (3), 223-53, 2004.
- [18]. Shah P, Bhalodia D, and Shelat P. Nanoemulsion: a pharmaceutical review. *Systematic Reviews in Pharmacy*, 1 (1), 24-32, 2010.
- [19]. Jafari SM, He Y, Bhandari B. Nano-Emulsion Production by Sonication and Microfluidization—A Comparison. *Int J Food Prop*, 9 (3), 475-485, 2007.
- [20]. Theissen O, Gompper G. Lattice-Boltzmann study of spontaneous emulsification. *Eur Phys J B*, 11, 91-100, 1999.
- [21]. Vyas TK, Shahiwala A, Amiji MM. Improved oral bioavailability and brain transport of Saquinavir upon administration in novel nanoemulsion formulations. *Int J Pharm*, 347 (1-2), 93-101, 2008.
- [22]. Kumar M, Misra A, Babbar AK, Mishra AK, Mishra P, Pathak K. Intranasal nanoemulsion based brain targeting drug delivery system of risperidone. *Int J Pharm*, 358 (1-2), 285-91, 2008.
- [23]. Jain N, Akhter S, Jain GK, Khan ZI, Khar RK, Ahmad FJ. Antiepileptic Intranasal Amiloride Loaded Mucoadhesive Nanoemulsion: Development and Safety Assessment. *J Biomed Nanotechnol*, 7 (1), 142-3, 2011.
- [24]. Mahajan HS, Mahajan MS, Nerkar PP, Agrawal A. Nanoemulsion-based intranasal drug delivery system of saquinavir mesylate for brain targeting. *Drug Deliv*, 21 (2), 148-54 2014.

Paper:

**Neem oil nanoemulsions: characterisation
and antioxidant activity**

Neem oil nanoemulsions: characterisation and antioxidant activity

Federica Rinaldi^a, Patrizia Nadia Hanieh^b, Catia Longhi^c, Simone Carradori^d, Daniela Secci^b, Gokhan Zengin^e, Maria Grazia Ammendolia^f, Elena Mattia^c, Elena Del Favero^g, Carlotta Marianecchi^b and Maria Carafa^b

^aFondazione Istituto Italiano di Tecnologia, Center for Life Nano Science@Sapienza, Rome, Italy; ^bDipartimento di Chimica e Tecnologie del Farmaco, “Sapienza” University of Rome, Rome, Italy; ^cDipartimento di Sanità pubblica e Malattie infettive, “Sapienza” University of Rome, Rome, Italy; ^dDipartimento di Farmacia, “G. d’Annunzio” University of Chieti-Pescara, Chieti, Italy; ^eDepartment of Biology, Selçuk Üniversitesi Alaeddin Keykubat Yerleşkesi, Konya, Turkey; ^fCentro nazionale per le tecnologie innovative in sanità pubblica, Istituto Superiore di Sanità, Rome, Italy; ^gDipartimento di Biotecnologie Mediche e Medicina Traslazionale, University of Milan, Segrate, Italy

ABSTRACT

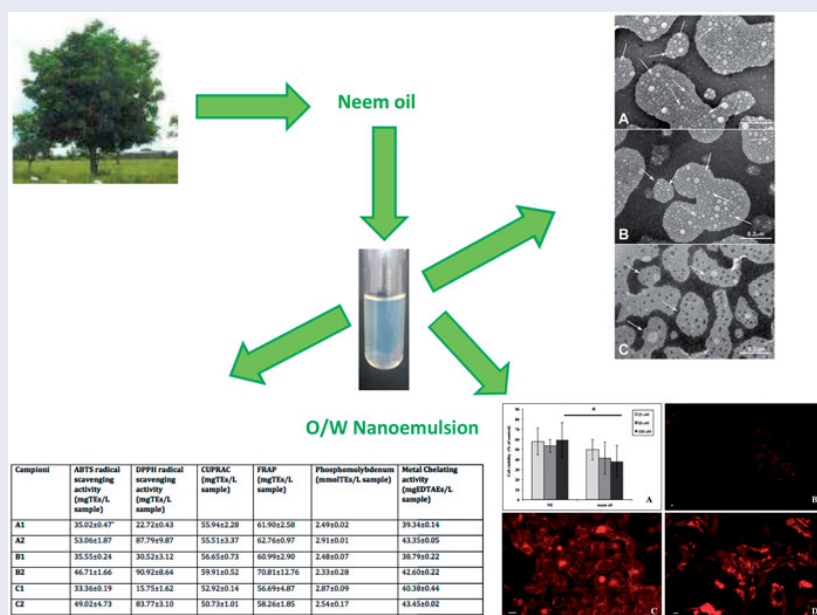
The aim of the present work is to develop nanoemulsions (NEs), nanosized emulsions, manufactured for improving the delivery of active pharmaceutical ingredients. In particular, nanoemulsions composed of Neem seed oil, contain rich bioactive components, and Tween 20 as nonionic surfactant were prepared. A mean droplet size ranging from 10 to 100 nm was obtained by modulating the oil/surfactant ratio. Physicochemical characterisation was carried out evaluating size, ζ -potential, microviscosity, polarity and turbidity of the external shell and morphology, along with stability in simulated cerebrospinal fluid (CSF), activity of Neem oil alone and in NEs, HEp-2 cell interaction and cytotoxicity studies. This study confirms the formation of NEs by Tween 20 and Neem oil at different weight ratios with small and homogenous dimensions. The antioxidant activity of Neem oil alone and in NEs was comparable, whereas its cytotoxicity was strongly reduced when loaded in NEs after interaction with HEp-2 cells.

ARTICLE HISTORY

Received 27 July 2017
 Revised 7 September 2017
 Accepted 7 September 2017

KEYWORDS



Neem oil; nanoemulsions; physicochemical characterisation; antioxidant activity; cell interaction studies



Introduction

According to the European Commission definition, nanotechnology is a branch of engineering devoted to designing, producing and using structures and devices having one or more dimensions

of about 100 nanometres or less. Nanoscience and nanotechnology are the study and application of extremely small things and can be used across all the other science fields, such as chemistry, biology, physics, materials science, engineering and in

CONTACT Carlotta Marianecchi  carlotta.marianecchi@uniroma1.it  Department of Drug Chemistry and Technology, University of Rome “Sapienza”, Piazzale A. Moro 5, 00185 Roma, Italy

© 2017 The Author(s). Published by Informa UK Limited, trading as Taylor & Francis Group. This is an Open Access article distributed under the terms of the Creative Commons Attribution License (<http://creativecommons.org/licenses/by/4.0/>), which permits unrestricted use, distribution, and reproduction in any medium, provided the original work is properly cited.

pharmaceutical sector. New or extensively used drugs can be better formulated if loaded in specific nanocarriers in order to overcome problems such as low solubility, large biodistribution, low bioavailability, adverse effects, high costs and so on. Along the diverse nanocarriers that are widely used in pharmaceuticals, nanoemulsions have attracted great attention in drug delivery and pharmacotherapy. In particular, nanoemulsions act as an excellent and versatile vehicle for poorly aqueous soluble drugs, which are otherwise difficult to formulate in conventional dosage forms. Nanoemulsions are submicron emulsions composed of generally recognized as safe (GRAS) grade excipients approved by the United States Food and Drug Administration (FDA) and with the possibility to use different oils that can modulate the drug activity. Nanoemulsions are easily produced in large quantities by high shear stress or mechanical extrusion process and can be engineered with specific attributes such as size, surface charge, prolonged blood circulation and targeting properties. Nanoemulsions can be prepared in order to tune their physicochemical properties to be applied in therapy, diagnostics or theranostics.

The size of the droplets varies depending on the drug particles, mechanical energy, composition and relative amount of the surfactants¹. Nanoemulsions are also known as miniemulsions, fine-dispersed emulsions, submicron emulsions, etc., which can be either oil in water (O/W) or water in oil (W/O) emulsion. The amount of oil in O/W nanoemulsions may vary but generally is within 5–20% w/w. Sometimes a mixture of oils may be used to improve drug solubilisation in the oil phase. A co-surfactant or a co-solvent may be used in addition to the surfactant to facilitate the stabilisation process^{2,3}. The significant property that differentiates the nanoemulsions from other emulsion systems is that a nanoemulsion shows a different pattern in physical and rheological properties with decreasing droplet size. Nanoemulsion is much more stable than other emulsion systems and is more translucent compared to microemulsions⁴. Few nanoemulsions have been manufactured commercially in oral, topical, ophthalmic and even in intravenous (IV) drug delivery system. IV administration of nanoemulsions requires biodegradable surfactants. Numerous researches are presently being carried out in order to manufacture nanoemulsions from different classes of drugs for a variety of purposes. The use of nanoemulsions spreads from antibiotic therapy, atherosclerosis treatment, transdermal drug delivery and ophthalmic application to as far as cancer therapy, vaccine delivery, etc^{5–7}.

One of the most appealing challenges in nanotechnology is to find an opportune strategy to bypass blood–brain barrier (BBB) and to reach the central nervous system (CNS). Among the numerous approaches proposed, the direct nose-to-brain drug delivery is a potential strategy to overcome the obstacles presented by the BBB. Intranasal delivery bypasses the BBB to target CNS, reducing systemic exposure of drug, thereby reducing the systemic side effects. It is an attractive option of drug delivery due to its noninvasiveness^{8–10}.

Moreover, several researches suggest that the “nose-to-brain” route is one of the most important developments of

pharmaceutical research in brain treatment, including the following: (i) the potential to avoid gastrointestinal (GI) and hepatic first-pass metabolism; (ii) the possibility of delivering drugs not suitable for oral administration, such as peptides and proteins; and (iii) most importantly, the transport of exogenous material directly from the nasal cavity to the brain, thus bypassing the BBB¹¹.

It is still unknown whether the drug is being released from the carrier system in the nasal cavity and transported to CNS, or the carrier system is transported along olfactory and/or trigeminal nerve pathways into the CNS where the drug is released. Thus, more basic research is required to determine the possible transport pathway of therapeutic carrier to the CNS and their further fate into the biological system⁸.

In addition to the vesicular systems, widely used in nasal administration, other carriers are able to encapsulate drug and to perform intranasal delivery to CNS, such as cyclodextrins, micro- and nanoemulsions and nanoparticles¹¹.

Nanoemulsions, by virtue of their lipophilic nature and low globule size, are widely explored as a delivery system to enhance uptake across the nasal mucosa. The possibility of using mucoadhesive agents such as polyelectrolyte polymers can prolong the nasal mucosa interaction, providing an extended delivery of the drug to the olfactory region and henceforth to the brain⁸.

The aim of this research study was to prepare and characterise a functional O/W nanoemulsion by using Neem oil. Neem oil is a deep yellow extract from *Azadirachta indica* A. Juss. (Meliaceae) seeds widely used in India and in other South-East countries as versatile medicinal product for several diseases, as pesticide/insecticide, and in cosmetics due to its low toxicity in *in vivo* studies¹². These pharmaceutical properties are correlated with the content of limonoids (e.g. azadirachtin) as the most bioactive metabolites¹³. In this study, we made an effort to prepare nanoemulsions from Neem seed oil. We used Tween 20 as a nonionic surfactant because nonionic surfactants are known to be less affected by pH^{14,15}. The aim was to prepare NEs with the possibility of combining, in a future study, the pharmacological properties of Neem oil and those of the therapeutic agent targeted by nanoemulsion.

Materials and methods

Materials

Neem oil was purchased by Neem Italia (Moniga del Garda (BS), Italy) and is characterised by an ECOCERT certificate (Biocert Italia IT013BC041 – ICEA 264BC001). Tween 20 (Tw20), Hepes salt {*N*-(2-hydroxyethyl) piperazine-*N*-(2-ethanesulphonic acid)} and pyrene were Sigma-Aldrich products (Sigma-Aldrich, Milan, Italy). Distilled water (Ecological Product System s.r.l., Rome, Italy) was used for all experiments. All other products and reagents were of analytical grade.

Nanoemulsion preparation

Nanoemulsions (NEs) were prepared using different amounts of Tw20 and Neem oil (Table 1) in different weight ratios. Tw20

Table 1. Sample compositions, size, ζ -potential, PDI values and lipophilic shell features (polarity and microviscosity) of NEs.

Samples	Medium	Noil (%w/w)	Tw20 (%w/w)	HD (nm) \pm SD	ζ -Pot (mV) \pm SD	PDI \pm SD	Polarity (AU) \pm SD	MicroV (AU) \pm SD
A1	Water	33.3	66.6	30.98 \pm 0.49	-7.29 \pm 1.54	0.20 \pm 0.01	0.97 \pm 0.01	1.18 \pm 0.02
A2	Hepes			30.47 \pm 0.28	-16.80 \pm 1.22	0.23 \pm 0.01	0.94 \pm 0.02	1.19 \pm 0.01
B1	Water	20.0	80.0	21.73 \pm 0.30	-6.35 \pm 1.87	0.22 \pm 0.01	0.97 \pm 0.01	1.22 \pm 0.03
B2	Hepes			22.62 \pm 0.23	-13.80 \pm 1.40	0.24 \pm 0.01	0.97 \pm 0.01	1.22 \pm 0.01
C1	Water	12.4	83.6	15.42 \pm 0.11	-5.45 \pm 0.21	0.18 \pm 0.01	0.97 \pm 0.01	1.21 \pm 0.02
C2	Hepes			16.76 \pm 0.27	-15.00 \pm 1.79	0.22 \pm 0.01	0.96 \pm 0.01	1.21 \pm 0.01

NE samples were prepared using two different aqueous media: water and Hepes buffer (10^{-2} M pH 7.4). Noil: Neem oil; Tw20: Tween 20; HD: hydrodynamic diameter; ζ -Pot: ζ -potential; MicroV: microviscosity. Results are expressed as means \pm SD ($n = 3$).

concentration in the samples was always remarkably above CMC (0.048 mM in water, at 20 °C).

Where indicated, the fluorescent probe pyrene (4 mM) was added to the surfactant/oil mixture before NE preparation. The NEs were obtained by a simple preparation method, as previously reported¹⁶. Neem oil, Tw20 and distilled water, or Hepes buffer (10⁻² M, pH 7.4) where indicated, were used in the preparation of water-based (O/W) emulsion. The emulsions contained Neem oil and surfactant with ratios of 1:2, 1:4 and 1:7, respectively. To form the emulsion, the two phases were vortexed for about 5 min. Each emulsion with microscale droplets was sonicated for 20 min at 50 °C using a tapered microtip operating at 20 kHz at an amplitude of 18% (Vibracell-VX 400, Sonics, Taunton, MA) to obtain NEs.

Dynamic light scattering measurements

Dynamic light scattering (DLS) on a Malvern Zetasizer Nano ZS90 (Malvern Instruments Ltd., Worcestershire, United Kingdom) was used to measure the size and the ζ -potential of the NEs allowing to determine the mass distribution of particle size as well as the dispersed particle electrophoretic mobility. Obtained data represent means of the measurements of ζ -potential (mV) and of the hydrodynamic diameter (nm) for the NE droplets. It is important to notice that size distribution results are expressed as % of intensity of the colloidal dispersion. The polydispersity index (PDI) value was also determined as an evaluation of the breadth of the size distribution: a PDI value lower than 0.3 indicates a homogenous and monodisperse population.

Lipophilic shell characterisation

The fluorescence experiments on NEs incorporating pyrene were carried out to evaluate the micropolarity of the lipophilic shell surrounding the oil droplet by a Perkin-Elmer LS55 spectrofluorometer. Using the pyrene probe, which is entrapped mainly in the lipophilic shell, it is possible to investigate the lateral distribution and the dynamics of membrane compounds. Pyrene is a spatially sensitive probe, displaying a peculiar band around 460 nm when two molecules are spatially proximal (excimer); it is worthy to notice that when the excimer fluorescence decreases, there is an increase in monomer fluorescence. The monomer and the excimer possess different fluorescent signals and by evaluating the ratio of the fluorescence intensities it is possible to understand the probe distribution in the lipid network. The pyrene monomer fluorescent spectrum consists of five peaks. It is well established that the ratio I1/I3 between the intensities of the first (I1) and third (I3) vibration bands of the pyrene fluorescence spectrum (corresponding to 372 nm and 382 nm, respectively) is related to the polarity of the pyrene environment. Low values of the I1/I3 ratio correspond to a nonpolar environment. This ratio increases as the polarity of the medium rises¹⁷. Since pyrene is solubilised inside the hydrocarbon chain of the NE shell, the information obtained from fluorescence of pyrene in our systems refers to the lipophilic shell of NE pigeonhole¹⁸. The presence of pyrene intramolecular excimers depends on the rate of conformational change of the molecule, which is sensitive to the viscosity of the probe microenvironment¹⁹. Hence, the IE/IM ratio, where IM and IE stand for the intensity of the monomer and the excimer fluorescence, respectively, is used to estimate the microviscosity. Because of its high hydrophobicity, the solubilisation zone of pyrene occurs in the lipidic shell, as was established in the case of polymeric micellar solutions²⁰. The pyrene probe may also evidence (only qualitatively) the micropolarity variation in the solubilisation region, by the

change in the ratio of monomer vibronic band intensities measured at 377 nm and 397 nm²¹.

Physicochemical stability

Specific studies on physical stability of NEs, composed of Tw20 and Neem oil at different ratios, were carried out to investigate whether significant size and ζ -potential changes in NE dispersion occur during storage at the two selected temperatures, using water or Hepes buffer as aqueous phase. The NEs were stored at 4 and 25 °C for a period of 90 days. Samples were analysed at definite time intervals (1, 30, 60 and 90 days) and the ζ -potential and the mean of hydrodynamic diameter of vesicles were measured as previously described.

Biological studies were carried out in the presence of simulated cerebrospinal fluid (CSF), pH 7.3, to evaluate the stability of NE if administered nasally. The CSF was prepared as described by McNay et al.²². NEs were diluted in CSF to obtain a final CSF concentration of 45% in Hepes buffer (pH 7.4, 10 mM). The average size, polydispersity index and ζ -potential were evaluated at different time points (30, 60, 120 and 180 min) at 37 °C.

Small angle X-ray scattering (SAXS)

Small angle X-ray scattering (SAXS) experiments were carried out at the European Synchrotron Radiation Facility (ESRF, Grenoble, France). Measurements were acquired at the high-brilliance beamline ID02, with two sample-detector distances, in the region of momentum transfer $0.017 \text{ nm}^{-1} \leq q \leq 5 \text{ nm}^{-1}$ ($q = (4\pi/\lambda) \sin(\theta/2)$, where θ is the scattering angle). Samples were inserted in 2 mm capillaries (KI-beam, ENKI, Concesio, Italy) and placed horizontally onto a thermostatted sample holder ($T = 25 \pm 0.1$ °C). Very short frames were collected (exposure time 0.1 s) and checked for effects induced by radiation damage before be averaged. After radial integration and background subtraction, the SAXS profiles report the scattered radiation intensity as a function of momentum transfer, q . The intensity decay behaviour can give information on the structure of the particles in solution on the nanometre length scale. Synchrotron small-angle X-ray scattering (SAXS) techniques can give information on the internal structure of formulations for drug delivery^{23,24}.

Transmission electron microscopy (TEM)

Ten microlitres of diluted samples was adsorbed for 1 min onto Formvar-coated copper grids, then negatively stained with 2% filtered aqueous sodium phosphotungstate adjusted to pH 7.0. Negatively stained preparations were observed by a Philips 208 S transmission electron microscope (Philips Electron Optics, Eindhoven, The Netherlands) at 80 kV.

Radical scavenging activity

Free radical scavenging activity (DPPH)

Test solution (1 ml) was added to DPPH solution (4 ml, 0.004% methanolic solution). The sample absorbance was noted at 517 nm after 30-min incubation at room temperature in the darkness. Results were expressed as milligrams of Trolox equivalents per sample amount (mg TE)²⁵.

ABTS (2,2 azino-bis (3-ethylbenzothiazoline-6-sulphonic acid)) radical cation scavenging activity

ABTS⁺ radical cation was produced directly by reacting 7 mM ABTS solution with 2.45 mM potassium persulphate and allowing

the mixture to stand for 12–16 h in the darkness at the room temperature. Firstly, ABTS solution was diluted with methanol to an absorbance of 0.70 ± 0.02 at 734 nm. Test solution (1 ml) was mixed with ABTS solution (2 ml) and mixed. The sample absorbance was noted at 734 nm after 30-min incubation at room temperature. Results were expressed as milligrams of Trolox equivalents per sample amount (mg TEs)²⁶.

Evaluation of total antioxidant capacity by phosphomolybdenum assay

Test solution (0.3 ml) was mixed with 3 ml of reagent solution (0.6 M sulphuric acid, 28 mM sodium phosphate and 4 mM ammonium molybdate). The sample absorbance was read at 695 nm after 90-min incubation at 95 °C. Results were expressed as millimoles of Trolox equivalents per sample amount (mmol TEs)²⁷.

Reducing power assays

Cupric ion reducing (CUPRAC) method

Test solution (0.5 ml) was added to reaction mixture containing CuCl_2 (1 ml, 10 mM), neocuproine (1 ml, 7.5 mM) and NH_4Ac buffer (1 ml, 1 M, pH 7.0). Similarly, a blank was prepared for each sample (sample solution (0.5 ml) and reaction mixture (3 ml) without CuCl_2). Absorbance at 450 nm was read after 30-min incubation at room temperature. Results were expressed as milligrams of Trolox equivalents per sample amount (mg TEs)²⁸.

Ferric reducing antioxidant power (FRAP) method

Sample solution (0.1 ml) was added to FRAP reagent (2 ml) containing acetate buffer (0.3 M, pH 3.6), 2,4,6-Tris(2-pyridyl)-s-triazine (TPTZ) (10 mM) in 40 mM HCl and ferric chloride (20 mM) in a ratio of 10:1:1 (v/v/v). Then, the absorbance was read at 593 nm after 30-min incubation at room temperature. Results were expressed as milligrams of Trolox equivalents per sample amount (mg TEs)²⁹.

Metal chelating activity on ferrous ions

Test solution (2 ml) was added to FeCl_2 solution (0.05 ml, 2 mM). The reaction was initiated by the addition of 5 mM ferrozine (0.2 ml). Similarly, a blank was prepared for each sample (sample solution (2 ml), FeCl_2 solution (0.05 ml, 2 mM) and water (0.2 ml)). Then, the absorbance of sample and blank was noted at 562 nm after 10-min incubation at room temperature. Results were expressed as milligrams of EDTA equivalents per sample amount (EDTAEs)³⁰.

Cell culture conditions and treatments of cells with NEs

HEp-2 laryngeal cancer cells were grown in MEM medium (Sigma), supplemented with 1% penicillin–streptomycin and 10% foetal calf serum (FCS) in a 5% CO_2 atmosphere. Proliferation was evaluated by 3-(4,5-dimethylthiazol-2-yl)-2,5-diphenyltetrazolium bromide (MTT) assay as described²⁷. Briefly, 96-well plates were seeded with 5×10^3 cells/well and different amounts of Neem oil were added to the cells, either as NEs (A2 sample) or as free oil. After 24-h exposure of the cells to the different preparations, 20 μl of a 5 mg/ml MTT solution in PBS was added to each well, and the plates incubated for 3 h. After the formazan crystals were dissolved by the addition 100 μl of dimethyl sulphoxide, optical density (OD) at 570 nm was determined with a spectrophotometer/fluorimeter microplate reader (PerkinElmer, Hopkinton, MA)³¹ and the values

measured for treated cells, compared to those of untreated controls.

To visualise the uptake of NEs by HEp-2 cells, NEs loaded with Nile red dye (NE-NR) were prepared. HEp-2 cells seeded on cover slips into a 12-well plate were exposed to either NE-NR (10 μl of sample A1 NE-NR in 1 ml of the cell culture medium) or to free NR prepared as 1 mg/mL stock solution in acetone and used at a final concentration of 100 ng/mL. After 7- or 24-h incubation, cells were washed with phosphate-buffered saline solution (PBS) and fixed in methanol/acetone (1:1) for 5 min at -20°C . After three washes, coverslips were mounted on slides with 0.1% (w/v) p-phenylenediamine in 10% (v/v) PBS, 90% (v/v) glycerol, pH 8.0 and the specimens observed by fluorescence microscopy using a Leica DM4000 fluorescence microscope equipped with an FX 340 digital camera.

Statistical methods

Statistical significance of differences was evaluated by one-way ANOVA with repeated measures followed by *post hoc* paired Student's *t*-test.

Results and discussion

The Neem oil nanoemulsions, prepared by adding the amphiphilic substance (Tw20) at different weight ratio, were obtained by the method previously described. The role of the surfactant in NE formation is to facilitate the stabilisation process^{2,3}. Typical examples of aqueous soluble surfactants are nonionic surfactants (e.g. Tw20) which are preferred because they are usually less irritating than the ionic ones³².

The major feature of nanoemulsions is their great stability of droplet suspension. Stability of an emulsion is hampered in two ways: flocculation by coalescence and Ostwald ripening. In nanoemulsion systems, flocculation is naturally prevented by steric stabilisation, essentially due to the submicrometric droplet size. The second one is the reduction of the configurational entropy which occurs when interdroplet distance becomes lower than the adsorbed layer thickness. In case of the second problem, stability is dependent on the droplet radius r , the Hamaker constant A and the adsorbed layer thickness δ . The stability is very high if the δ/r value is high. In case of nanoemulsion droplets, δ/r becomes extremely high in comparison with macroemulsions, which completely prevents their capability to coagulate².

The results reported in Table 1 for all NEs were part of the general factorial design to establish the combination of variables and their interactions yielding nanoemulsions with desirable properties for nose-to-brain targeting. For each dependent variable (hydrodynamic diameter, PDI and ζ -potential), the effects corresponding to the investigated factors (emulsifier amount and aqueous phase type) and interactions were taken into account.

To stabilise the NE droplets and prevent the formation of aggregates, NEs need to show an appropriate ζ -potential value able to avoid droplet coalescence or fusion by repulsive, steric or electrostatic effects³³.

DLS measurements indicate that different surfactant ratios form NEs with different but comparable sizes (Table 1), but in general, it can be pointed out that increasing surfactant content, the dimensions decrease. The dimensions of NEs in water or Hepes buffer are the same for the same sample. Furthermore, all samples show negative ζ -potential values (Table 1), indicative of the absence of droplet aggregation. There is a significant difference in ζ -potential values, if NEs have water or Hepes buffer as external phase. This is probably due to the presence of salt and to the

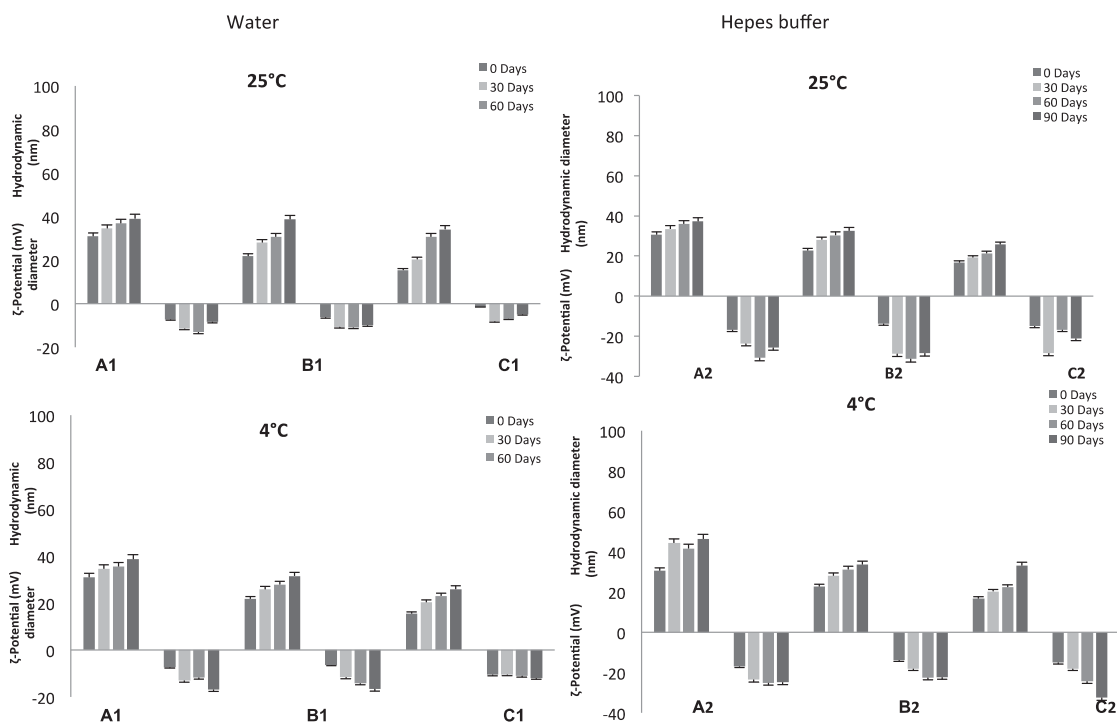


Figure 1. Shelf-life stability of evaluated NEs. Hydrodynamic diameter and ζ -potential values of different NEs (A–C) prepared using water¹ or Hepes buffer² as aqueous phase up to 90 days stored at 25 and 4 °C temperatures. Results are expressed as means \pm SD ($n = 3$).

ion content. This content is greater in buffer solution, so in this solution, ions will be able to adsorb on NE droplet surface and so to increase ζ -potential absolute values.

As reported by Đorđević et al.³⁴, at a given concentration of surfactants in the formulation, more surfactant molecules are expected to be adsorbed per unit area in case of larger droplets leading to greater negative charge and, hence, more negative ζ -potential values. It is obvious that all nanoemulsions prepared with different aqueous phase types show different ζ -potential values.

Apart from providing the hydrodynamic diameter and ζ -potential value, DLS provides also valuable information on the homogeneity of the suspension. A single sharp peak in the DLS profile implies the existence of a single population of scattering particles. The polydispersity index (PDI) values of NEs are reported in Table 1: it is clear that all samples are homogenous and possess NE population with limited dispersity ($PDI < 0.3$) and reduced dimensions useful to carry out a nose-to-brain administration. For the emerged reasons, only data related to samples with Hepes buffer (10^{-2} M pH 7.4) as external phase will be presented and discussed, although every experiment has been performed for all the samples reported in Table 1.

In order to characterise the nature of the lipophilic shell, microviscosity and polarity have been evaluated. Pyrene-loaded NEs were prepared following the procedure described previously and the fluorescence spectrum allowed calculating the values of polarity and microviscosity reported in Table 1. Polarity and microviscosity values are quite similar for all NEs; this is probably due to the formation of the same shell and in particular of the same inner structure independently from the surfactant amount used in the preparation of NEs.

NEs stability is a complex issue and involves chemical, physical and biological stability, which are all interrelated. The evaluation of these parameters is fundamental to determine the potential *in*

vitro/in vivo applications in nanomedicine. The physical stability studies of NEs are shown in Figure 1. From the analysis of reported results, it is clear that all NE samples, stored at the two different temperatures and prepared with the two different aqueous solutions, show high colloidal stability. In 90 days, dimension and ζ -potential variations of all NE samples at the two different temperatures show a similar trend, with no significant changes in physical characteristics of the formulation. Stability studies performed at 25 and 4 °C show that all analysed samples are stable for at least three months.

The effect of CSF on the stability of the NEs is another important aspect to take into account in order to evaluate and to understand the behaviour of the vesicles when they are in contact with fluids different from Hepes buffer. Experiments were performed at 37 °C checking the size and ζ -potential of the droplets by DLS analysis up to 3 h. During the time interval analysed, the same trend is observed for all NEs. NEs in 45% CSF maintained their size and ζ -potential values.

It can be concluded that in the presence of CSF, the selected samples show a good stability, with no significant changes in dimensions and ζ -potential values (Figure 2). X-ray scattering experiments have been performed to characterise the structure of nanoemulsions on the nanometre length scale. Figure 3 reports the SAXS intensity spectrum for A2. Structural features are identifiable in different regions of the spectrum; at low q ($q < 0.1 \text{ nm}^{-1}$, large lengths), the intensity profile shows that aggregates have a globular shape of finite size, of the order of 30 nm. At higher q values, in the region $0.18 < q < 0.75 \text{ nm}^{-1}$, the intensity as a function of q , $I(q)$, is proportional to $q^{-1.66}$. This decay behaviour, evidenced as a line of slope -1.66 in the log-log scale of Figure 3, is characteristic of connected substructures or sponge phases, on distances between 8 and 30 nm. Results show that the internal structure of the aggregates is not a classical core-shell structure with well-defined interfaces

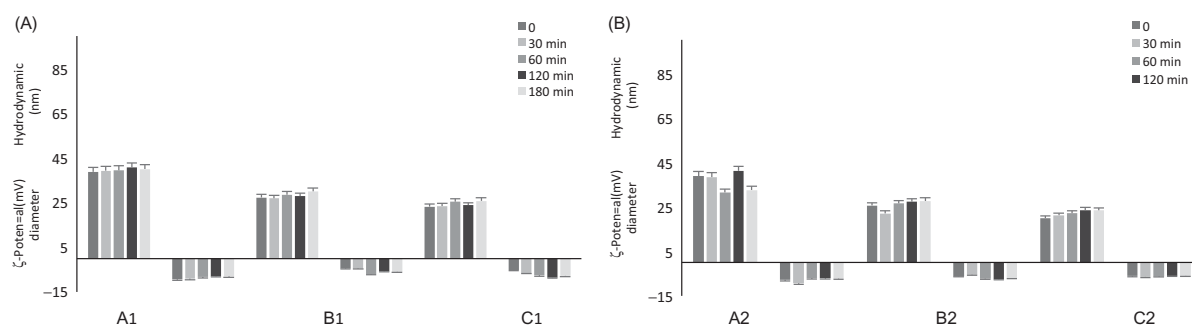


Figure 2. Stability in CSF. Size and ζ -potential measurements by DLS of different NEs (A–C) prepared using water (A) and Hepes buffer 10^{-2} M, pH 7.4 (B) at 37°C up to 3 h.

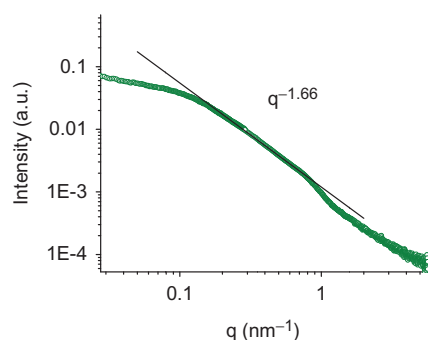


Figure 3. SAXS intensity spectrum. Scattered radiation intensity as a function of momentum transfer q of A2 sample at room temperature. The flattening of the intensity for $q < 0.1 \text{ nm}^{-1}$ shows that aggregates have a globular shape of finite size, of the order of 30 nm. At higher q ($0.18 < q < 0.75 \text{ nm}^{-1}$), the intensity $I(q)/q^{-1.66}$. This decay behaviour is characteristic for an internal core composed by connected substructures or sponge phases.

between the oil region, the surfactant region and the water. The oil phase is finely dispersed in nanosubstructures condensed by Tween molecules in a 30 nm aggregate.

At lower oil content, the overall dimensions are quite smaller, but with very similar internal structure (samples are less monodisperse). Similar oil substructures are confined in a smaller nanosized aggregate stabilised by a higher fraction of surfactant.

In order to investigate the morphology of the NEs, the three Hepes samples (A2, B2 and C2) were investigated by TEM. **Figure 4** reveals that all nanoemulsion samples were almost spherical in shape, similar to other nanoemulsions prepared with different types of oil³⁵. The TEM analyses confirm the presence of lipid emulsion droplets with an internal structure characterised by the presence of core with sponge-like features.

Starting from the promising biological activities of Neem oil, we firstly analysed the effect of this natural product in terms of antioxidant, reducing power and chelating properties. Pure Neem oil was characterised by a high antioxidant effect as demonstrated by a large number of assays with respect to reference compounds such as Trolox and EDTA (**Table 2**). These results also suggest that standardised Neem oil might be beneficial for the preparation of nanoemulsion with putative pharmacological effects.

Moreover, the prepared nanoemulsions were subjected to the same biological evaluation as regards their antioxidant, reducing power and chelating properties. As shown in **Table 3**, antioxidant activity (ABTS and DPPH tests) was strongly influenced by the aqueous component, being Hepes buffer better than water. In the other assays (CUPRAC, FRAP, phosphomolybdenum and chelating tests), the activities were quite comparable without any

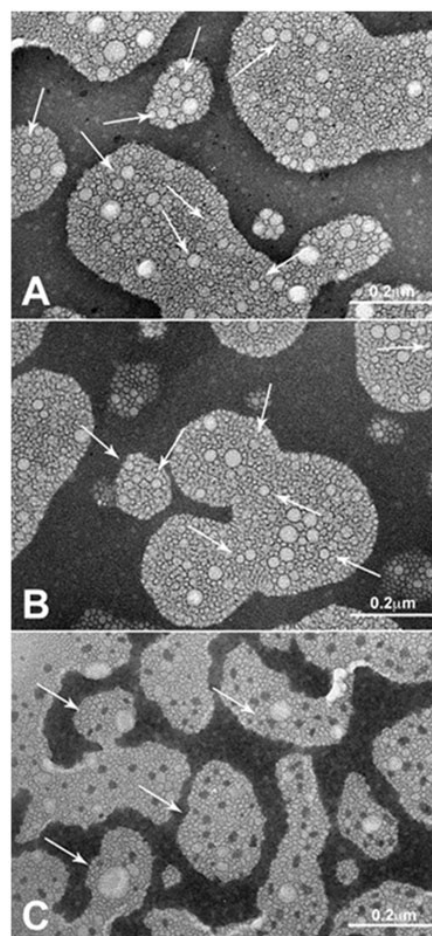


Figure 4. Transmission electron photomicrographs of the Hepes nanoemulsion samples. Panel A: A2; Panel B: B2; Panel C: C2. Arrows indicate NE sizes corresponding to DLS measures.

Table 2. Antioxidant and chelating properties of pure Neem oil.

Assay	Results ^a
DPPH scavenging activity (mg TEs/g oil)	7.59 ± 0.07
ABTS scavenging activity (mg TEs/g oil)	14.78 ± 2.33
CUPRAC assay (mg TEs/g oil)	76.14 ± 5.57
FRAP assay (mg TEs/g oil)	51.13 ± 1.42
Phosphomolybdenum assay (mmol TEs/g oil)	0.77 ± 0.06
Metal chelating activity (mg EDTAEs/g oil)	19.26 ± 0.56

^aValues expressed are means \pm SD of three parallel measurements. TE: Trolox equivalent; EDTAE: EDTA equivalent.

Table 3. Antioxidant and chelating properties of prepared Neem oil-loaded NEs.

Samples	ABTS radical scavenging activity (mg TE/L sample)	DPPH radical scavenging activity (mg TE/L sample)	CUPRAC (mg TE/L sample)	FRAP (mg TE/L sample)	Phosphomolybdenum (mmol TE/L sample)	Metal chelating activity (mg TE/L sample)
A1	35.02 ± 0.47*	22.72 ± 0.43	55.94 ± 2.28	61.90 ± 0.02	2.49 ± 0.02	39.34 ± 0.14
A2	53.06 ± 1.87	87.79 ± 9.87	55.51 ± 3.37	62.76 ± 0.97	2.91 ± 0.01	43.35 ± 0.05
B1	35.55 ± 0.24	30.52 ± 3.12	56.65 ± 0.73	60.99 ± 2.90	2.48 ± 0.07	38.49 ± 0.22
B2	46.71 ± 1.66	90.92 ± 8.64	59.91 ± 0.52	70.81 ± 12.76	2.33 ± 0.28	42.60 ± 0.22
C1	33.36 ± 0.19	15.75 ± 1.62	52.92 ± 0.14	56.69 ± 4.87	2.87 ± 0.09	40.38 ± 0.44
C2	49.02 ± 4.73	83.77 ± 3.10	50.73 ± 3.10	58.26 ± 1.85	5.54 ± 1.85	43.45 ± 0.02

*Values expressed are means ± SD of three parallel measurements.

TE: Trolox equivalents; EDTAE: EDTA equivalents; Na: not active.

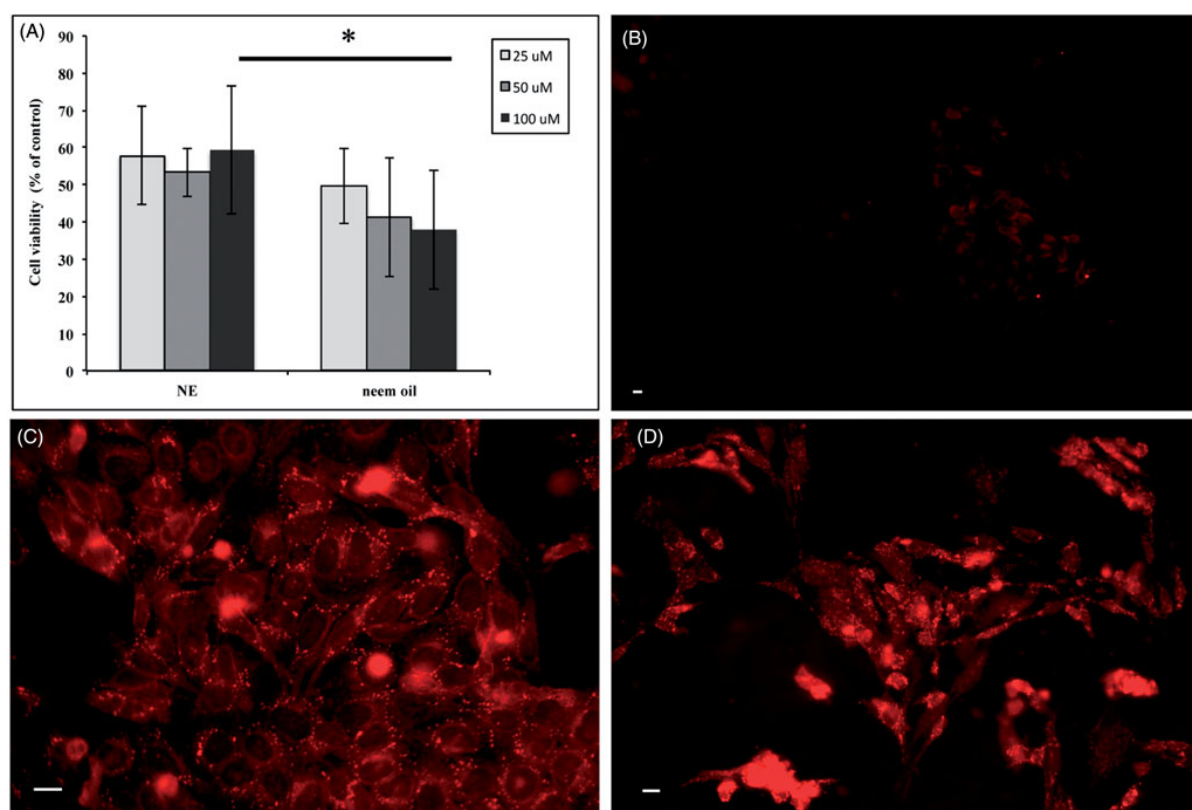


Figure 5. Exposure of HEp-2 cells to Neem oil-based NEs. HEp-2 cells were treated with NEs or free Neem oil as described (see Methods). The OD values obtained by MTT assay for treated cells were converted into numbers of cells on a standard curve and expressed as percentages of untreated controls. Bars represent the mean of three independent experiments ± SD. * $p < .05$ (Panel A). Fluorescence microscopy images of HEp-2 control cells exposed to free Nile red (Panel B) and HEp-2 cells exposed to Nile red-loaded NEs for 7 (Panel C) and 24 h (Panel D) obtained by fluorescence microscopy as described (see Methods). Scale bar: 10 μ m.

significant difference between HEPES buffer and water. These biological results, in terms of Trolox or EDTA equivalents, were also not modified by the decreasing content of loaded Neem oil amount (from 9.2 mg/mL for A/A1 to 2.6 mg/mL for C/C1). Collectively, these results could suggest not only a structural role, but also a protective effect of Neem oil as a pivotal component for the stability, conservation and microbial resistance of these nanoemulsions.

It has been reported that bioactive compounds extracted from Neem oil could affect multiple cellular pathways leading to apoptotic cell death³⁶. Moreover, in different tumour cell lines, Neem oil has shown to exert anticancer activity via caspase-dependent and independent apoptosis as well as autophagy-mediated cell death³⁷.

In order to use NEs as carriers of pharmacological active compounds, we tested the effects of Neem-based NEs on the proliferation of tumour cell lines of different origin. Figure 5 illustrates the results obtained from HEp-2 human laryngeal carcinoma cells, treated for 24 h with increasing amounts of NEs. The bar graph (Panel A) shows that the proliferation of cells exposed to 100 μ M Neem oil complexed into NEs is significantly higher than that detected in the samples treated with the same amount of free oil, indicating that the toxic effect of this agent is reduced in our oil/surfactant NE preparation.

To further evaluate the NEs as potential carriers of bioactive substances, we assessed their cellular uptake by fluorescence microscopy analysis of HEp-2 cells exposed for either 7 or 24 h to Nile red-loaded NEs or Nile red dye alone. No signal could be

detected in HEp-2 control cells exposed to free Nile red for 7 h and similar results were obtained after 24 h (Panel B). In contrast, a strong fluorescent intracellular signal, as a punctuated pattern increasing with the time of incubation, could be visualised in the cytoplasm of cells exposed to the NEs (Panel C: 7 h and Panel D: 24 h). Altogether, these data strongly suggest that our preparations might represent suitable systems to deliver bioactive compounds into the cells.

Conclusion

This study confirms the possibility of preparing NEs by Tween 20 and Neem oil at different weight ratios. Among the different formulation tested, the three (both in water and in Hepes buffer) prepared and characterised in the present research paper show the smallest hydrodynamic size and a homogenous sample size distribution. The evaluation of the antioxidant activity of Neem oil alone or as NEs confirms that the structured oil in NEs does not lose its activity and is less cytotoxic than the free oil after interaction with HEp-2 cells. A future step will be to load a drug inside NEs to enhance Neem oil antioxidant activity or to offer a double therapeutic effect in the same formulation. This type of system could be successfully applied in nose-to-brain delivery.

Disclosure statement

The authors report no conflicts of interest. The authors alone are responsible for the content and writing of this article.

Funding

EDF thanks BIOMETRA Dept., University of Milan, for financial support (Piano sostegno ricerca – Linea B 2016).

References

- Divsalar A, Saboury AA, Nabiuni M, et al. Characterization and side effect analysis of a newly designed nanoemulsion targeting human serum albumin for drug delivery. *Colloids Surf B Biointerfaces* 2012;98:80–4.
- Anton N, Benoit JP, Saulnier P. Design and production of nanoparticles formulated from nano-emulsion templates – a review. *J Control Release* 2008;128:186–96.
- Sharma N, Bansal M, Visht S, et al. Nanoemulsion: a new concept of delivery system. *Chron Young Sci* 2010;1:2–4.
- Devarajan V, Ravichandran V. Nanoemulsions: as modified drug delivery tool. *Int J Compr Pharm* 2011;2:1–5.
- Leite GM, Domingues RJ, Silva J, et al. Antimicrobial effects of a microemulsion and a nanoemulsion on enteric and other pathogens and biofilms. *Int J Food Microbiol* 2007;118:15–9.
- Ganta S, Talekar M, Singh A, et al. Nanoemulsions in translational research – opportunities and challenges in targeted cancer therapy. *AAPS PharmSciTech* 2014;15:694–708.
- Sutradhar KB, Amin ML. Nanoemulsions: increasing possibilities in drug delivery. *Eur J Nanomed* 2013;5:97–110.
- Singh K, Ahmad Z, Shakya P, et al. Nano formulation: a novel approach for nose to brain drug delivery. *J Chem Pharm Res* 2016;8:208–15.
- Clementino A, Batger M, Garrastazu G, et al. The nasal delivery of nanoencapsulated statins – an approach for brain delivery. *Int J Nanomed* 2016;11:6575–90.
- Sennato S, Bordi F, Cametti C, et al. Hybrid niosome complexation in the presence of oppositely charged polyions. *J Phys Chem B* 2008;112:3720–7.
- Marianecchi C, Rinaldi F, Hanieh PN, et al. Nose to brain delivery: new trends in amphiphile-based “Soft” Nanocarriers. *Curr Pharm Des* 2015;21:5225–32.
- Subaprija R, Nagini S. Medicinal properties of neem leaves: a review. *Curr Med Chem Anticancer Agents* 2005;5:149–56.
- Carradori S, Mannina L, De Cosmi F, et al. Optimization of the microwave-assisted extraction of *Azadirachta indica* (Neem) leaves using NMR-based metabolic fingerprinting. *Curr Bioactive Compd* 2015;11:142–5.
- Mason TG, Wilking JN, Meleson K, et al. Nanoemulsions: formation, structure, and physical properties. *J Phys Condens Matter* 2006;18:635–66.
- Rajasekaran C, Meignanam E, Vijayakumar V, et al. Investigations on antibacterial activity of leaf extracts of *Azadirachta indica* A. Juss (Meliaceae): a traditional medicinal plant of India. *Ethnobot Leaflets* 2008;12:1213–7.
- Ghotbi RS, Khatibzadeh M, Kordbacheh S. Preparation of neem seed oil nanoemulsion. *Proceedings of the 5th International Conference on Nanotechnology: Fundamentals and Applications*; 2014;11-13:Paper N. 150; Prague, Czech Republic.
- Kalyanasundaram K, Thomas JK. Environmental effects on vibronic band intensities in pyrene monomer fluorescence and their application in studies of micellar systems. *J Am Chem Soc* 1977;99:2039–44.
- Vanderkooi JM, Callis JB. Pyrene. A probe of lateral diffusion in the hydrophobic region of membranes. *Biochemistry* 1974;13:4000–6.
- Zachariasse KA. Intramolecular excimer formation with diarylalkanes as a microfluidity probe for sodium dodecyl sulfate micelles. *Chem Phys Lett* 1978;57:429–32.
- Vasilescu M, Angelescu DG, Bandula R, Staikos G. Microstructure of polyelectrolyte nanoaggregates studied by fluorescence probe method. *J Fluoresc* 2011;21:2085–91.
- Vasilescu M, Bandula R, Lemmetyinen H. Micropolarity and microviscosity of Pluronic L62 and L64 core-shell aggregates in water at various concentrations and additives examined by absorption and fluorescence probes. *Colloids Polym Sci* 2010;288:1173–84.
- McNay EC, Sherwin RS. From artificial cerebro-spinal fluid (aCSF) to artificial extracellular fluid (aECF): microdialysis perfusate composition effects on *in vivo* brain ECF glucose measurements. *J Neurosci Methods* 2004;132:35–43.
- Marianecchi C, Di Marzio L, Del Favero E, et al. Niosomes as drug nanovectors: multiscale pH-dependent structural response. *Langmuir* 2016;32:1241–9.
- Sandri G, Motta S, Bonferoni MC, et al. Chitosan-coupled solid lipid nanoparticles: tuning nanostructure and mucoadhesion. *Eur J Pharm Biopharm* 2017;110:13–18.
- Locatelli M, Zengin G, Uysal A, et al. Multicomponent pattern and biological activities of seven *Asphodeline* taxa: potential sources of natural-functional ingredients for bioactive formulations. *J Enzyme Inhib Med Chem* 2017;32:60–7.
- Zengin G, Locatelli M, Carradori S, et al. Total phenolics, flavonoids, condensed tannins content of eight *Centaurea* species and their broad inhibitory activities against cholinesterase, tyrosinase, α -amylase and α -glucosidase. *Not Bot Horti Agrobo* 2016;44:195–200.
- Zengin G, Menghini L, Malatesta L, et al. Comparative study of biological activities and multicomponent pattern of two

- wild Turkish species: *Asphodeline anatolica* and *Potentilla speciosa*. *J Enzyme Inhib Med Chem* 2016;31:203–8.
28. Zengin G, Locatelli M, Ceylan R, Aktumsek A. Anthraquinone profile, antioxidant and enzyme inhibitory effect of root extracts of eight *Asphodeline* taxa from Turkey: can *Asphodeline* roots be considered as a new source of natural compounds? *J Enzyme Inhib Med Chem* 2016;31:754–9.
 29. Zengin G, Ceylan R, Guler GO, et al. Enzyme inhibitory effect and antioxidant properties of *Astragalus lagurus*. *Curr Enzym Inhib* 2016;12:177–82.
 30. Secci D, Carradori S, Bizzarri B, et al. Novel 1,3-thiazolidin-4-one derivatives as promising anti-*Candida* agents endowed with anti-oxidant and chelating properties. *Eur J Med Chem* 2016;117:144–56.
 31. Ammendolia MG, Iosi F, Maranghi F, et al. Short-term oral exposure to low doses of nano-sized TiO₂ and potential modulatory effects on intestinal cells. *Food Chem Toxicol* 2017;102:63–75.
 32. Mangale MR, Pathak SS, Mene HR, More BA. Nanoemulsion: a pharmaceutical overview. *Int J Pharm Sci Rev Res* 2015;33:244–52.
 33. Mc Clements DJ. Edible nanoemulsions: fabrication, properties, and functional performance. *Soft Matter* 2011;7:2297–316.
 34. Đorđević SM, Čekić ND, Savić MM, et al. Parenteral nanoemulsions as promising carriers for brain delivery of risperidone: design, characterization and *in vivo* pharmacokinetic evaluation. *Int J Pharm* 2015;493:40–54.
 35. Klang V, Matsko NB, Valenta C, Hofer F. Electron microscopy of nanoemulsions: an essential tool for characterization and stability assessment. *Micron* 2012;43:85–103.
 36. Kikuchi T, Ishii K, Noto T, et al. Cytotoxic and apoptosis-inducing activities of limonoids from the seeds of *Azadirachta indica* (neem). *J Nat Prod* 2011;74:866–70.
 37. Srivastava P, Yadav N, Lella R, et al. Neem oil limonoids induces p53-independent apoptosis and autophagy. *Carcinogenesis* 2012;33:2199–207.

Conclusions

Nanocarrier development for the treatment of CNS disorders has opened a new opportunity for many researchers to enhance the delivery of therapeutic agents to the brain.

Nanocarriers also provide additional advantages such as increased drug protection against degradation, enhanced drug bioavailability and drug targeting.

In this thesis, several drug delivery systems have been specifically designed to reach the brain by different routes.

The obtained results have shown that both proposed structures, Bubblesomes[®] and C-Pentasomes, are able to deliver probes/drugs to the CNS after intravenous administration, combined with FUS application, and intranasal administration, respectively.

In future studies, *in vivo* behavior of NBs[®] loaded with different drugs should be investigated in terms of drug release into the brain after FUS application in order to confirm the findings obtained with fluorescent probe loaded NBs[®].

Neem oil nanoemulsions (NEs), by virtue of their lipophilic nature, low globule size and stability over time, are a promising tool as a drug delivery system.

NEs will be loaded by active substances in order to enhance Neem oil antioxidant activity or to offer a double therapeutic effect within the same formulation.

To enhance their uptake across the nasal mucosa, NEs could be covered by a mucoadhesive agent, such as polyelectrolyte polymers, in order to prolong their nasal mucosa interaction and to provide an extended delivery of the drug to the olfactory region and henceforth to the brain.

The improvement of innovative neuro-nanomedicine will provide a concrete opportunity to obtain therapeutic benefits.

Appendix 1:

**Patent Number
WO 2017/178954 A1**

(12) INTERNATIONAL APPLICATION PUBLISHED UNDER THE PATENT COOPERATION TREATY (PCT)

(19) World Intellectual Property
Organization
International Bureau



(43) International Publication Date
19 October 2017 (19.10.2017)

(10) International Publication Number
WO 2017/178954 A1

- (51) International Patent Classification:
A61K 49/22 (2006.01) *A61K 47/69* (2017.01)
- (21) International Application Number:
PCT/IB2017/052060
- (22) International Filing Date:
10 April 2017 (10.04.2017)
- (25) Filing Language: Italian
- (26) Publication Language: English
- (30) Priority Data:
102016000037062 11 April 2016 (11.04.2016) IT
- (71) Applicant: UNIVERSITÀ DEGLI STUDI DI ROMA "LA SAPIENZA" [IT/IT]; Piazzale Aldo Moro, 5, 00185 Rome (IT).
- (72) Inventors: CARAFA, Maria; c/o Università degli Studi di Roma "La Sapienza", Piazzale Aldo Moro, 5, 00185 Rome (IT). BETTUCCI, Andrea; c/o Università degli Studi di Roma "La Sapienza", Piazzale Aldo Moro, 5, 00185 Rome (IT). MARIANECCI, Carlotta; c/o Università degli Studi di Roma "La Sapienza", Piazzale Aldo Moro, 5, 00185 Rome (IT). RINALDI, Federica; c/o Università degli Studi di Roma "La Sapienza", Piazzale Aldo Moro, 5, 00185 Rome (IT). BIAGIONI, Angelo; c/o Università degli Studi di Roma "La Sapienza", Piazzale Aldo Moro, 5, 00185 Rome (IT).
- (74) Agent: PRIMICERI, Maria Vittoria; c/o Studio Associato Cavattoni-Raimondi, viale Parioli, 160, 00196 Rome (IT).
- (81) Designated States (unless otherwise indicated, for every kind of regional protection available): AE, AG, AL, AM, AO, AT, AU, AZ, BA, BB, BG, BH, BN, BR, BW, BY, BZ, CA, CH, CL, CN, CO, CR, CU, CZ, DE, DJ, DK, DM, DO, DZ, EC, EE, EG, ES, FI, GB, GD, GE, GH, GM, GT, HN, HR, HU, ID, IL, IN, IR, IS, JP, KE, KG, KH, KN, KP, KR, KW, KZ, LA, LC, LK, LR, LS, LU, LY, MA, MD, ME, MG, MK, MN, MW, MX, MY, MZ, NA, NG, NI, NO, NZ, OM, PA, PE, PG, PH, PL, PT, QA, RO, RS, RU, RW, SA, SC, SD, SE, SG, SK, SL, SM, ST, SV, SY, TH, TJ, TM, TN, TR, TT, TZ, UA, UG, US, UZ, VC, VN, ZA, ZM, ZW.
- (84) Designated States (unless otherwise indicated, for every kind of regional protection available): ARIPO (BW, GH, GM, KE, LR, LS, MW, MZ, NA, RW, SD, SL, ST, SZ, TZ, UG, ZM, ZW), Eurasian (AM, AZ, BY, KG, KZ, RU, TJ, TM), European (AL, AT, BE, BG, CH, CY, CZ, DE, DK, EE, ES, FI, FR, GB, GR, HR, HU, IE, IS, IT, LT, LU, LV, MC, MK, MT, NL, NO, PL, PT, RO, RS, SE, SI, SK, SM, TR), OAPI (BF, BJ, CF, CG, CI, CM, GA, GN, GQ, GW, KM, ML, MR, NE, SN, TD, TG).
- Published:
— with international search report (Art. 21(3))

(54) Title: NANOBUBBLES AND USES THEREOF

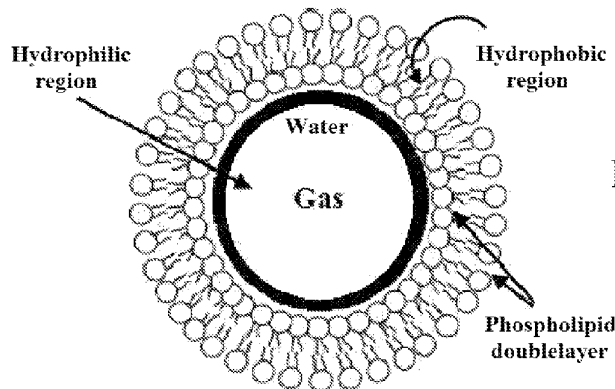


Figure 1

(57) Abstract: Nanobubbles characterised by a double lipophilic layer surrounding a central gaseous portion, with an aqueous layer placed between the said central portion and the said lipophilic double layer, are the subject of the invention. The lipophilic double layer may contain within it compounds of a lipophilic nature. The aqueous layer located between the lipophilic double layer and the central gaseous portion may contain compounds of a hydrophilic nature within it. The nanobubbles may also further comprise target-molecules associated with the lipophilic double layer, preferably polypeptides, polynucleotides, antibodies or antibody fragments.

WO 2017/178954 A1

NANOBUBBLES AND USES THEREOF

* * * * *

Technical field of the invention

The invention relates to nanobubbles and uses thereof; the invention also relates to the process of producing said nanobubbles.

In particular the invention relates to stabilised nanoparticle systems of a polymer nature capable of acting as vehicles for agents suitable for use in the diagnostic, therapeutic and theranostic fields.

Known art

Sonography is an imaging technique that has an essential role in the diagnosis of many types of diseases and is a clinical research method based on the detection of ultrasound waves reflected by the various tissues making up a biological system. In general, in all ultrasound techniques, reconstruction of the images of various parts of the body is based on the detection of ultrasound waves reflected at tissue discontinuities present within them. This technology is non-invasive and convenient, but has some limitations - for example it is impossible to reach and therefore display blood vessels having a diameter of less than 200-300 microns.

The possibility of obtaining good quality ultrasound images, even for those parts of the human body which because of their anatomy and physiology are otherwise difficult to study, is thus not only the result of the high technological level achieved in the construction of present-day ultrasound machines, but also the development of a class of agents capable of improving the quality, that is the contrast, of ultrasound images, with a consequent increase in the diagnostic power of this investigation technique; these agents are known as Ultrasound Contrast Agents (UCAs).

These agents, which comprise gas microbubbles coated with a "shell" of variable composition, injected intravenously, make it possible to improve the qualitative display of various parts of the body in direct contact with tissues having similar acoustic characteristics and zones

characterised by microvascularisation, which is a characteristic of some organs such as for example the heart, or some diseases, for example prostate diseases.

The dispersion of gas-containing microbubbles in blood gives rise to a specific acoustic impedance discontinuity between the bubbles and the blood, this acoustic impedance being the physical quantity parameterising the resistance offered by a medium to the propagation of a wave. This is defined as the ratio between the acoustic pressure at a point and the consequent velocity of movement - around the equilibrium position - of the particles of the medium in which the wave is being propagated; this quantity is equal to the product of the density of the medium in which the elastic wave propagates and the wave propagation velocity; it is measured in rayls (Ry): $1 \text{ Ry} = 1 \text{ kg}/(\text{m}^2 \text{ s})$.

The specific acoustic impedance discontinuity between gas microbubbles and blood, which can exceed values of 10^3 Ry, causes great diffusion of the elastic energy generated by the ultrasound probe that is incident on the microbubble-blood system, and there is therefore an increase in the intensity of the reflected echo; this in turn is translated into an increase in the contrast of the ultrasound image of the blood vessel affected by the elastic wave in comparison with that found when bubbles are absent.

There are different types of bubbles currently in use in diagnosis; they are however rather unstable and only allow an improvement in the ultrasound image to be obtained for a short period of time.

A further limitation is associated with the micrometre size of such agents, which are unable to improve the ultrasound image of vessels having dimensions smaller than a few microns.

The problem associated with microembolisms or risks associated with administering particles having dimensions similar to those of capillaries (1-10 μm) into the circulating flow, which might cause occlusions within them, should also not be underestimated.

Commercially available preparations comprise microbubbles covered with a single layer of molecules of an amphiphilic nature, purely for the purpose of rendering the contrast agent more stable

(1 - 6).

These structures however offer little stability in terms of gas retention and must therefore be reconstituted at the time of use (7 - 8).

Publications relating to the production of bubbles nanometre-sized bubbles (or nanobubbles) from liposomes that are capable of acting as a vehicle for a gas relate to structures of dimensions varying between 400 and 800 nm, produced using very complex formulations (9 - 11).

Work by Schroedera et al. in 2009 proposed the combination of liposomes and ultrasound, but the liposomes are suggested as an external stimulus to modulate the release of medicinal compounds (12).

A recent patent application relating to nanometre-sized bubbles relates to structures coated with a single layer of molecules of an amphiphilic nature (13).

The nanobubbles described therein comprise a single layer and therefore demonstrate little or inadequate stability. They are also characterised by a compartment of an apolar nature of insufficient size to include any lipophilic medicinal compounds. The bubbles prepared in this way in the aforementioned application also show too wide a size distribution and therefore reduced applicability in vivo because it is difficult for them to reach the microcirculation, they may give rise to the risk of causing microembolisms, and also they do not show that water is present in the internal compartment and they are therefore unable to act as a vehicle for polar medicinal compounds.

This invention is therefore provided to resolve the problems in the known art.

Summary of the invention

The invention relates to nanobubbles characterised by a double lipophilic layer containing an aqueous layer and a central gaseous portion as illustrated in Figure 1.

Another object of the invention is compositions and formulations containing the abovementioned nanobubbles.

Another object of the invention is the process for producing nanobubbles.

Yet another object of the invention is the use of nanobubbles in the diagnostic, therapeutic and theranostic fields.

Other objects will be obvious from the following detailed description.

Brief description of the figures

Figure 1 - Diagrammatical illustration of the structure of the nanobubbles in which an internal gaseous compartment surrounded by a layer of water (suitable for acting as a vehicle for medicinal compounds or a diagnostic agent of a hydrophilic nature), both enclosed by a double lipophilic layer (capable of acting as a vehicle for a medicinal compounds or diagnostic agent of a lipophilic nature).

Figure 2 - Experiment on the stability of nanobubbles analysed by SAXS (Small Angle X-ray Scattering) after thirty days' storage at a temperature of 4°C; Graph A: Span 20 nanobubbles. Graph B: DMPC nanobubbles.

“q” is the transferred vector momentum as a function of the intensity of the beam; the intensity of “q” on a logarithmic scale is proportional to q^{-n} where “n” is the gradient of the straight line providing information on the nature of the object being examined.

Figure 3 - Experiment on the stability of Span 20 nanobubbles examined by pulse-echo after ninety days' storage at a temperature of 4°C; the nanobubbles retain the same acoustic efficiency if examined after a period of approximately three months following their preparation.

Figure 4 - Experiment on the stability of DMPC nanobubbles carried out over a period of three months at different storage temperatures, by DLS (dynamic light scattering) analysis.

Figure 5 - Frequency response of the photoacoustic cell for a disperse suspension of SonoVue® over time, compared with the case where the cell is filled with water alone. Two resonance peaks for the photoacoustic cell are present (inherent vibration modes) in the band between 200-300 Hz and 400-600 Hz.

Figure 6 - Stability experiment on SonoVue® microbubbles analysed by pulse-echo at a temperature of 37°C; the medicinal product rapidly loses acoustic efficiency over time.

Figure 7 - Frequency response of the photoacoustic cell corresponding to two different solutions present within it: Graph A, dispersed suspension of SonoVue®; Graph B, dispersed solution of nanobubbles. Two resonance peaks of the photoacoustic cell (inherent vibration modes) are present in the band between 200-300 Hz and 400-600 Hz.

Figure 8 – Attenuation of ultrasound intensity at 14 MHz as a function of temperature for a sample of nanobubbles having a Hepes concentration of 37%.

Figure 9 - Attenuation (expressed in dB/cm) measured at the frequency of 14 MHz for Span 20 nanobubbles at various concentrations in Hepes buffer solution.

Figure 10 - Attenuation frequency spectrum of the ultrasound signal of Span 20 nanobubbles measured using the pulse technique.

Figure 11 - Diagram comparing the acoustic efficiency of a sample of Span 20 nanobubbles with only gas or with probes: at the top SPAN 20 + CHOL + PFC; in the middle SPAN 20 + CHOL + PFC + NILE RED; at the bottom SPAN 20 + CHOL + PFC + calcein.

Figure 12 - Experiment on stability of DMPC nanobubbles performed over a period of three hours, 180 minutes, at a temperature of 37°C in the presence of 45% (v/v) human and bovine serum, using DLS (dynamic light scattering) analysis.

Figure 13: Transport of calcein through the BBB after administration to mice, using lipid and surfactant nanobubbles. A) Fluorescence microscope images showing the location of the calcein in thin coronal sections of the brain. B) Quantification of calcein in the brain in terms of detected fluorescence.

Detailed description of the invention

The invention relates to nanobubbles characterised by a double lipophilic layer surrounding a central gaseous portion, with a layer of water being located between the said central portion and the said lipophilic double layer (Figure 1). The lipophilic double layer may contain compounds of a lipophilic nature within it. The aqueous layer located between the lipophilic double layer and the central gaseous

portion may contain compounds of a hydrophilic nature within it.

The nanobubbles may also further contain targeting molecules located on the surface of the lipophilic double layer, preferably polypeptides, polynucleotides, antibodies or antibody fragments, which can be prepared using techniques known to those skilled in the art.

The invention is based on having selected components which make it possible to obtain nanobubbles with a lipophilic double layer using the process according to the invention; these components stabilise the structure of the nanobubbles making it possible to prevent escape of the gas contained within them, thus imparting stability over very long periods. This is confirmed by the stability tests illustrated in Figures 2A, 2B, 3, 4 and 10.

Using the process according to the invention and with the said components it is not only possible to prepare nanobubbles of nanometre size but also to obtain maximum dimensional uniformity in the preparation, as indicated by the polydispersity index shown in Table 2, which is always below 0.25, and preferably 0.2 or less.

The components are selected from the following phospholipids: 1,2-dimyristoyl-*sn*-glycero-3-phosphocholine (DMPC), dipalmitoylphosphatidylcholine (DPPC), distearoylphosphatidylcholine (DSPC), dicetyl phosphate (DCP), in combination with cholesterol.

Nanobubbles produced using any one selected from the following surfactants - Span 20 and 60 and Tween 85, 81, 80, 65, 61, 60, 21, 20 - are similarly stable.

For the purposes of this description by Tween 85 is meant polyoxyethylene glycol sorbitan trioleate; by Tween 81 is meant polyoxyethylene (polyoxyethylene units = 4) glycol sorbitan monooleate; by Tween 80 is meant polyoxyethylene (polyoxyethylene units = 20) glycol sorbitan monooleate; by Tween 65 is meant polyoxyethylene glycol sorbitan tristearate; by Tween 61 is meant: polyoxyethylene (polyoxyethylene units = 4) glycol sorbitan monostearate; by Tween 60 is means polyoxyethylene (polyoxyethylene units = 20) glycol sorbitan monostearate; by Tween 21 is meant polyoxyethylene (polyoxyethylene units = 4) glycol sorbitan monolaurate; by Tween 20 is meant polyoxyethylene (polyoxyethylene

units = 20) glycol sorbitan monolaurate.

For the purposes of this invention by Span 20 is meant [2-[(2R,3R,4S)-3,4-dihydroxyoxolane-2-yl]-2-hydroxyethyl] dodecanoate; by Span 60 is meant sorbitan monostearate.

The gas inserted within the nanobubbles belongs to the class of perfluorocarbons, preferably tetradecafluorohexane is used.

The method for preparing the nanobubbles according to the invention comprises the following essential steps:

- (a) Preparing a film by dissolving an aliquot of cholesterol and one or more cationic phospholipid surfactants in an organic solvent and subsequent evaporation, this preparation step being characteristic of preparation using film and being known to those skilled in the art and described in (15);
- (b) Hydrating the film obtained in stage (a) with water, the water may be replaced by an aqueous solution obtaining a water-soluble therapeutic and/or diagnostic agent such as a diagnostic probe (for example a fluorescent, radioactive, or luminescent probe or other known therapeutic or diagnostic agents);
- (c) Placing the mixture obtained in stage (b) in a sealed container or reactor, then adding an aliquot of a straight, branched or cyclic C₃-C₇, preferably C₆ chain perfluorocarbon PFC, liquid in equilibrium with its gas phase, at atmospheric pressure;
- (d) Subjecting the suspension obtained in the previous stage to sonication at ambient temperature, for example using an ultrasound sonicator provided with a microprobe and operating at a frequency of 20 kHz and an amplitude of 16% (Vibracell-VCX 400-Sonics, USA) to obtain unilamellar structures; this stage may possibly be replaced by processes having the same effects, for example extrusion with repeated filtration passes through a membrane with a cut-off from 1.5 μm to 0.1 μm, or any other technique known to those skilled in the art;
- (e) The suspension obtained in the previous stage is then cooled, avoiding freezing, preferably to a temperature of not less than 4°C.

The suspension obtained in paragraph (e) can undergo a further purification step to select a population of nanobubbles of uniform dimensions; for example nanobubbles can be selected by centrifuging

the suspension, preferably at 600 rpm for 20 minutes at 25°C and then removing the supernatant; alternatively, if the process in paragraph (d) provides for extrusion, the centrifuging stage may be omitted.

Where not otherwise specified the steps in the process are preferably carried out at ambient temperature.

The nanobubbles so obtained are characterised by measurements of dimensions and ζ potential, SAXS and acoustic measurements.

Therapeutic and/or diagnostic agents of a lipophilic nature are added by adding suitable aliquots in stage (a).

Using the procedure described the inventors have surprisingly found that the nanobubbles prepared are characterised by the fact that they have a central core holding gas surrounded by an aqueous layer, all enclosed by a double layer (as discovered experimentally by Small Angle X-Ray Scattering, SAXS, investigations, Figures 2A and 2B).

Figure 2 (Graphs A and B) shows spectra having characteristic peaks corresponding to an internal distance within the particles, which provides indications about their local structure. A change in intensity such as q^4 indicates the presence of a sharp interface between two media. It is therefore reasonably possible to state that the particle comprises a double layer in the presence of a sharp interface between two media (double layer/gas). The formation of nanobubbles containing gas, which are still stable after 30 days, in that the local structure is the same, is therefore proven.

The nanobubbles according to the invention are capable of overcoming the limitation of existing contrast media in that they are more stable over time and extremely uniform in shape and dimensions in comparison with those in the known art; in particular these characteristics allow them also to be used when applied to paediatric and veterinary diagnostics, in particular small animals, avoiding the risk of the formation of microembolisms which might occur following the use of preparations of micrometre-sized or nanobubble preparations which do not have uniform dimensions.

The possibility of adding both water-soluble and liposoluble therapeutic and/or diagnostic agents to the nanobubbles according to

the invention makes it possible to produce vectors for use in diagnostic, therapeutic and theranostic applications.

In therapy, in particular, nanobubbles can behave like cavitation nuclei capable of being activated by exposure to low frequency power ultrasound (US). The cavitation induced by the US which results in the destruction of the gas bubbles is capable of opening cell membrane pores of approximately 300 nm in diameter.

This phenomenon, known as “sonoporation”, may be functional in increasing cell uptake or the passage of medicinal compounds and genetic material across biological membranes; in some cases it is very difficult to overcome the aforesaid membranes; for example the blood-brain barrier (BBB) is a barrier which is difficult to overcome using strategies currently available. We have surprisingly found that using the nanobubbles according to the invention sonoporation of the BBB is achieved in an effective, transient and reversible manner.

The composition of the proposed systems has the advantage that it can be easily applied industrially, making use of phospholipids or surfactants added to variable fractions of cholesterol.

As shown in Figure 1, the nanometre-sized nanobubbles according to the invention are characterised by an apolar double layer or bilayer membrane comprising phospholipids and/or surfactants in combination with cholesterol.

The inventors have carried out different tests in order to select the type and quantity of phospholipid or surfactant capable of providing a double layer in the presence of cholesterol making it possible to obtain the structure shown in Figure 1 and the corresponding innovative characteristics illustrated below.

Numerous components mixed together in the presence of cholesterol in various molar ratios were tested in order to obtain the nanobubbles. The following phospholipids and surfactants were tested: 1,2-dipalmitoyl-*sn*-glycero-3-phosphocholine (DPPC), 1,2-dipalmitoyl-*sn*-glycero-3-phosphoethanolamine (DPPE), 1,2-dimyristoyl-*sn*-glycero-3-phosphocholine (DMPC), dicetyl phosphate (DCP), 1,2-dipalmitoyl-*sn*-glycero-3-phosphate (DPPA), phosphatidylcholine (PC), 1,2-distearoyl-*sn*-glycero-3-phospho-(1'-*rac*-glycerol) (PG), 1,2-

dioctadecanoyl-*sn*-glycero-3-phospho-(1'-rac-glycerol) (DSPG), 1,2-dioleoyl-*sn*-glycero-3-phosphocholine (DOPC), 1,2-dihexanoyl-*sn*-glycero-3-phosphocholine (DHPC), 1,2-dilauroyl-*sn*-glycero-3-phosphocholine (DLPC), 1,2-dioctadecanoyl-*sn*-glycero-3-phosphate (DSPA), 1,2-distearoyl-*sn*-glycero-3-phosphoethanolamine (DSPE), 1,2-diarachidoyl-*sn*-glycero-3-phosphocholine (DAPC), 1,2-dipalmitoyl-*sn*-glycero-3-phosphate (DPPA), polyoxyethylene glycol sorbitan monopalmitate (Tween 40), polyoxyethylene cetyether (Brij 35), polyoxyethylene monostearate (MYRJ 52), sorbitan monolaurate (Span 20), sorbitan monooleate (Span 80), sorbitan trioleate (Span 85).

The combinations yielding the best results are reported in Table 1.

From the experiments performed it emerged that of the components tested the combinations of DMPC+cholesterol, DMPC+DCP+cholesterol, DPPC+cholesterol and Span20+cholesterol in particular are capable of giving rise to the nanobubbles according to this invention when present in particular molar ratios (Table 1).

Table 1

Components	Ratio %
DMPC-Chol	40-60 : 20-40
DMPC-DCP-Chol	50-70 : 50-30
DPPC-Chol	60-90 : 40-10
Span20+Chol	30-50 : 70-50

Nanobubble structure and dimensions

The dimensions of the nanobubbles according to Dynamic Light Scattering (DLS) measurements are approximately 150 nm (130-260 nm) and the surface charge expressed as the ζ potential value is from weakly to markedly negative (-4 / -71 mV). (Table 2).

Table 2.

Nanobubble sample	Dimensions (nm) ± SD	ζ potential (mV) ± SD	Polydispersity index (pdi)
DMPC	151.90 ± 3.55	-4.35 ± 0.15	0.20
DMPC+DCP	130.10 ± 2.20	-70.90 ± 1.60	0.20
DPPC	166.00 ± 1.88	-15.70 ± 0.57	0.10
Span 20	243.30 ± 3.70	-41.90 ± 1.82	0.12

The polydispersity index (pdi) associated with the measurements of dimensions is always below 0.25, preferably 0.2 or less. This index is important in that it provides an idea of the range of dimensions in the nanobubble population. In particular it is important to have a vesicular suspension with a monodisperse population so that it will behave uniformly both during storage and after administration in vivo in the distribution and cell internalisation stages. The vesicular structure so produced is characterised by a double layer of a lipophilic nature including an internal compartment in which an aqueous layer and the gas coexist (Figure 1), these structural characteristics being confirmed, as previously mentioned, by studies carried out using Small Angle X-ray Scattering (SAXS) (Figure 2).

Stability

Stability tests surprisingly proved that the structures produced are extremely stable.

As established by the DLS analysis, Figure 4, pulse echo analysis, Figure 3, and SAXS analysis, Figure 2, the stability of the nanobubbles in suspension during storage is in fact extremely high, at least 3 months at a storage temperature of 4°C. Figure 2 shows that the SAXS spectra for nanobubbles stored for 1 month are the same as those prepared 1 day before. Figure 3 clearly shows that the nanobubbles maintain the same attenuation after 90 days.

Figure 4 shows that dimensions and zeta potential do not significantly change after 90 days' storage.

They are also stable for at least 180 minutes at temperatures simulating in vivo conditions (37°C and 40°C) (Figure 8) and for 180 min in the presence of 45% (v/v) (fig.12) human and bovine serum.

These are very much better data than those reported in US2014/0147390 and WO2014/054026.

Acoustic efficiency and interaction with ultrasound

The system has been tested in terms of acoustic efficiency and it has surprisingly been found that the nanobubbles are stable, in terms of maintaining dimensions and zeta potential, persistence of acoustic signal, and gas retention that is very much better than that of known products. The experiment with ultrasound illustrated in Figure 3, using the pulse echo technique, points out that the attenuation measured at 14 MHz does not undergo any changes after 90 days for any of the concentrations tested, and in comparison with Figure 6 for SonoVue[®], diluted according to the manufacturer's specifications and measured using the same technique, it is found that the latter's stability is reduced after approximately 100 hours. Figure 5 shows that using a technique of the photoacoustic type the stability of SonoVue[®] is reduced after 100 hours, confirming what was obtained using the previous technique.

Efficiency of the nanobubbles from the point of view of interaction with ultrasound was evaluated using an investigation technique widely used to characterise the products currently on the market in the same class as those described in this description. This is based on the transmission and reception of short ultrasound pulses caused to propagate through a solution of nanobubbles (this technique is also known as the pass-echo technique) (16).

Analyses of the differences in information content between the emitted signal and the received signal provide the acoustic characterisation of the nanobubbles: the parameters describing the efficiency of nanobubbles are the attenuation experienced by the acoustic signal passing through the therapeutic and/or diagnostic agent (greater attenuation is reflected in greater ultrasound image contrast), and the corresponding frequency band at which this is obtained.

The efficiency of trapping gas within the nanobubbles was instead evaluated using a photoacoustic technique (17): this choice was due to the fact that the photoacoustic signal generated by a liquid

periodically heated by a coherent (laser) light is extremely sensitive to the quantity of gas present in a liquid solution. The results found were compared with those for a clinically approved ultrasound contrast agent comprising a liquid suspension of micrometre-sized bubbles of SF₆ gas coated with a single layer of phospholipids (SonoVue® - Bracco Imaging, Milan, Italy) (Figure 7 Graphs A and B). It will be seen from the figure that the two resonance peaks for the photoacoustic cell (around approximately 300 and 600 Hz) shown by the cell when filled with only distilled water (Figure 7 Graph A, open circles) or with a solution of Hepes ([N-(2-hydroxyethyl) piperazine-N-(2-ethanesulfonic acid)], 10 mM, pH 7.4) (Figure 7 Graph B, open circles), experience attenuation (indicated by ΔA_1 and ΔA_2 in both Figure 7A and Figure 7B) when the cell is filled with SonoVue® (Figure 7 Graph A, solid circles) or a solution of nanobubbles (Figure 7 Graph B, solid circles).

Because the attenuation of the resonance peaks is proportional to the quantity of gas present in the liquid (17), both that provided by the SonoVue® microbubbles (Figure 7 Graph A, solid circles) or the nanobubbles according to the invention (Figure 7 Graph B, solid circles), comparison shows that there is a greater capacity for trapping gas within the shells of the nanobubbles according to the invention in comparison with SonoVue®.

The measurements made have provided precise indications regarding both the objective acoustic properties of the vesicular nanobubbles and the improvements which this new formulation introduces into the scope of medical diagnosis through imaging. In the latest generation ultrasound instruments the operating frequency band in fact has an upper limit of a frequency of 20-25 MHz, well above the frequency bands of existing ultrasound contrast agents within the range 2-6 MHz corresponding to diameters of the order of 3-6 μm (SonoVue®). From the measurements performed the vesicular nanobubbles according to the invention instead have dimensions at least twenty times smaller (diameters of approximately 100 nm), provided an operating frequency band in the range 15-30 MHz; this frequency is not only more compatible with present day ultrasound machines, but is also capable of ensuring operation at maximum

efficiency with ultrasound machines which will achieve even higher frequency bands in the future, up to 40 MHz.

The nanobubbles according to the invention guarantee operation between 5 and 40 MHz, better if at 20 MHz. These small dimensions make it possible to use nanobubbles diagnostically in paediatric and veterinary contexts, where the dimensions of the peripheral blood vessels are small (20).

In addition to the frequency band characteristics, the results obtained show a considerable increase in the diagnostic power of the nanobubbles according to the invention in comparison with that demonstrated by micrometre-sized contrast agents. In fact measurement of attenuation of the ultrasound signal passing through the DMPC nanobubbles sample provides values of around 18 dB/cm (attenuation of the acoustic signal for every centimetre thickness of the layer of sample passed through), which, for the same quantity of micro- and nanobubbles in suspension should be compared with the value of approximately 5-6 dB/cm provided by SonoVue[®], measured using the same experimental technique. Nanobubbles comprising DMPC or DPPC or Span 20 on the other hand provide attenuation values of 18 dB/cm for those phospholipids and 6-8 dB/cm for surfactants.

Finally, when the acoustic efficiency of the nanobubbles according to the invention were measured as a function of time it was found that they are capable of maintaining their acoustic properties unchanged for times which are wholly compatible with their diagnostic and therapeutic applications, demonstrating that they remain efficient for times of several hours.

Figure 10 shows that the nanobubbles, in this example of Span 20, have unchanged attenuation when the frequency of the ultrasound is varied and the dilution is increased.

Acting as a vehicle for medicinal compounds and/or probes

Thanks to their structure (Figure 1) the nanobubbles according to this invention are capable of acting as vehicles for both medicinal compounds of a hydrophilic nature in the aqueous layer within the bilayer, and lipophilic medicinal compounds in the double layer, at the same time as a gaseous compound, and are therefore capable of being

used in the therapeutic, diagnostic and theranostic fields. The nanobubbles may for example contain perfluorocarbons and medicinal compounds of a lipophilic and hydrophilic nature at the same time.

Molecules of the fluorescent type of a hydrophilic and lipophilic nature have also been included in the proposed structures, in addition to the gas, to assess whether physical chemical properties and/or stability remained unchanged.

In order to demonstrate this capability, model hydrophilic and lipophilic molecules, calcein and Nile red, were included within the nanobubbles together with the gas. The nanobubbles charged with the fluorescent probes were characterised in terms of acoustic efficiency, comparing it with that of the nanobubbles as such (Figure 11).

The experiment shown in Figure 11 has shown that the joint transport of probes does not have an adverse effect on the acoustic efficiency of the nanobubbles and does not interfere with the structure of the gaseous compartment in that the probes, depending upon their characteristics, are located selectively in the aqueous or lipophilic compartment.

In addition to this, the materials used for preparation of the nanobubbles and the gas are not toxic.

It can be concluded that the nanobubbles proposed have the following advantages:

- (a) They have nanometre-sized dimensions and comprise a double layer of a lipophilic nature made up of amphiphilic molecules;
- (b) The formulations proposed, prepared using the process according to the invention, are capable of providing nanobubbles with a stable double layer, in comparison with those known to the inventors. They are in fact highly stable in aqueous solution at a storage temperature of 4°C (at least 3 months) and at temperatures simulating in vivo conditions (37 and 40°C) up to 180 min (Figure 8); and also in the presence of human and bovine serum for 180 minutes at a temperature of 37°C (Figure 12). The nanobubbles according to the invention are stable without the need to make use of preservative and reconstitution techniques such as lyophilisation and subsequent dehydration and the addition of gas.

(c) In comparison with known formulations and in particular those described in patent applications US2014/0147390 and WO2014/054026, the nanobubbles according to the invention are produced with highly uniform dimensions (Table 2), a property which allows them to be used in the veterinary and paediatric fields, avoiding the risk of microembolisms.

(d) They show no changes in physical-chemical properties and stability after the inclusion of model molecules of a hydrophilic and lipophilic nature;

(e) Their dimensions do not change during photoacoustic experiments;

(f) Use of the nanobubbles according to the invention makes it possible to achieve sonoporation of the blood-brain barrier in an effective, transient and reversible manner;

(g) They are capable of trapping a larger quantity of gas, for example more than 30% in comparison with SonoVue[®], despite their smaller dimensions (Figure 7).

The latter point was assessed using a photoacoustic technique measuring the decreasing amplitude of the resonance peaks corresponding to the intrinsic frequencies of an acoustic resonator used as a photoacoustic cell as the concentration of nanobubbles in the cell was varied. The photoacoustic cell, of brass, was an acoustically resonant structure of cylindrical shape having an internal volume of $V = 7.68 \text{ cm}^3$, within which was located the liquid solution which has to be characterised photoacoustically; an argon ion laser (wavelength 4880 Å units), periodically modulated in amplitude at a variable frequency between 50 and 2000 Hz, struck the liquid through a transparent window of the cell. The periodic heating of the liquid caused periodic variations in its volume which were reflected in displacements of a small polyvinyl membrane in contact with the liquid; these displacements were measured with a laser vibration meter. The measurement relating to gas content within the nanobubbles was based on the fact that the more gas is present in the micro/nanobubbles dispersed in the liquid, the greater will be the decrease in amplitude of the oscillation of the polyvinyl membrane at

the resonant frequencies of the photoacoustic cell (17-19).

In the measurements made, 1.4 ml of SonoVue® solution were diluted in 7.68 ml of distilled water causing relative variations in vibration amplitude for the first and second resonance frequencies of the photoacoustic cell equal to $(\Delta A_1 / A_1)_{SV} \approx 0.77$ and $(\Delta A_2 / A_2)_{SV} \approx 0.48$ respectively (Figure 7a). As far as the nanobubbles are concerned, 0.7 ml of nanobubbles solution in 7.68 ml of Hepes generated a relative variation in vibration amplitudes at the two resonance frequencies of $(\Delta A_1 / A_1)_{NB} \approx 0.54$ and $(\Delta A_2 / A_2)_{NB} \approx 0.33$ respectively, (Figure 7b).

Because the measured values for the nanobubbles were approximately 30% lower than those obtained with SonoVue®, the greater capacity for trapping gas within the nanobubbles must therefore be estimated to be 30% greater than that of SonoVue® for the same volume of micro/nanobubbles dispersed in the liquid.

The following examples will be provided as an illustration of the invention and are not to be regarded as limiting its scope.

Examples

Sample preparation

The nanobubbles in Table 1 (DMPC, DPPC, Span and Chol) were prepared using the “film” technique as described in the literature (14, 15). In particular the components of a lipophilic nature, that is phospholipids or surfactants and cholesterol in the ratios described in Table 1, and therapeutic and/or diagnostic agents of a lipophilic nature were dissolved in a mixture of organic solvents (3/1 v/v chloroform/methanol), subsequently evaporated in a rotavapor to give rise to the formation of a uniform thin layer of the components, called a film, on the walls of the preparation container. The film obtained was hydrated by adding an aqueous phase (10 mM Hepes buffer pH 7.4, or aqueous solutions of therapeutic and/or diagnostic agents of a hydrophilic nature) when required in order to obtain the nanobubbles.

Liquid PHF (tetradecafluorohexane) in equilibrium with its gas was added to the film to obtain different nanobubble formulations. In one particular mode this technique provides for the insertion of liquid and gaseous PHF at the same time through drawing PHF in the liquid phase into a syringe, where a saturated environment is created within

it with an equilibrium between liquid and gaseous PHF. The PHF present in the body of the syringe (gas and a suitable quantity of liquid PHF) was introduced into the suspension vesicles. The dispersion was then stirred mechanically and sonicated for 15 minutes at a temperature of 25°C using an ultrasound sonicator provided with a microprobe operating at a frequency of 20 kHz and an amplitude of 16% (Vibracell-VCX 400-Sonics, USA). The nanobubbles obtained were then subjected to cooling by means of a thermal shock in a bath with water and ice, for a period of 2 minutes. The nanobubbles were then purified from the excess material by centrifuging using an MPW-260R centrifuge (MPW Med. Instruments) at 600 rpm for 20 minutes at 25°C.

Experiment to establish dimensions and structure

Dimensioning using DLS and structural analysis using SAXS.

Dynamic light scattering is used to study the structure of colloidal suspensions and more generally aggregates having dimensions which can vary from a few nm to a few micrometres.

From a study of the fluctuations in such a signal information is obtained on the shape, dimensions and state of aggregation of the particles included in the sample.

DLS measurements were carried out on samples having the compositions shown in Table 1 prepared according to the method previously described and then purified. These are measurements which were performed on both empty samples and those charged with fluorescent agents and gas. The analyses were performed at 25°C; each analysis relates to at least 3 measurements from which the software derives a mean value representative of the diameter of the vesicles.

The distribution curve for nanobubble dimensions is characterised by a polydispersity index (PDI), which should not be greater than 0.25 for monodispersed populations.

These measurements have been useful for initial characterisation of the vesicles prepared, and to carry out stability studies over time and at different temperatures. The change in the dimensions of the sample, which will be smaller the more stable the sample, in that it will not experience changes in dimensions over time

caused by phenomena of a degradative type, is detected in these studies.

DETERMINATION OF ζ POTENTIAL

The presence of charged particles in a suspension is of great importance for the stability of the dispersion itself, as the particles will tend to repel each other.

An important consequence of the presence of electrical charges on the surface of the particles is that they will demonstrate effects, known as “kinetic effects”, under the influence of an applied electric field.

Measurement of the **ζ potential** provides information on the physical-chemical characteristics of the particles in suspension and is extensively used to predict the stability of systems in relation to aggregation phenomena.

The stability of suspensions is strongly influenced by the surface charge; the greater the charge present on the surface of the vesicles the greater will be their tendency to remain separated because of the repulsion effect occurring between particles having the same charge.

If all the particles in suspension have very high negative or positive ζ potentials they will tend to repel each other and there will be no coalescence or flocculation.

A suspension is generally considered stable when the ζ potential values are less than -30 mV or greater than +30 mV.

MEASUREMENT EQUIPMENT

Measurements were performed using the same computerised inspection system (Malvern Zetasizer Nano ZS 90, Malvern, UK) used for DLS.

ζ potential measurements were made at the temperature of 25°C on samples stored at 25°C and 4°C, or 37°C in the case of the stability studies at body temperature, after dimensioning using the DLS technique. These measurements were performed during the characterisation and stability studies.

Because each element has its own internal structure, which can be determined by making use of radiation of a wavelength comparable to the measurements of interest, Small Angle X Ray Scattering (SAXS)

experiments, a technique which can be used to gain access to a distance range of the order of nm, were carried out in order to investigate the structural and morphological characteristics of the samples containing gases.

The ERSF (European Synchrotron Radiation Facility, Grenoble, France) ID02 facility was used for the experiments in this work.

The ESRF synchrotron is capable of producing extremely bright X-rays, that is a thin and very intense beam.

In the study the SAXS measurements were obtained by keeping the position of the sample fixed and automatically moving the detector in a vacuum tube from 0.75 m and 10 m from the sample, so as to be able to gain access to a wide range of scattering wave vectors: $0.1 \text{ nm}^{-1} < q < 3 \text{ nm}^{-1}$, where $q = (4\pi/\lambda) \sin(\theta/2)$, with λ being wavelength ($\sim 0.1 \text{ nm}$) and θ the scattering angle. The samples were placed in plastics capillaries (KI sheet, ENKI srl, Concesio, Italy) of internal diameter of 2 mm, thickness 0.05 mm and with 98% X-ray transmission, sealed with polyethylene caps.

The capillaries were then mounted horizontally in a 6-station sample holder and were filled after they had been installed. In this configuration it is possible to guarantee almost simultaneous measurements of empty and solvent samples under the same conditions; this is very important in order to be able to subtract backgrounds in an optimum way and compare the results obtained.

In order to be able to carry out precise temperature measurements an ad hoc built thermostat suitable for fitting to the ID02 line was used; the temperature stabilisation error within the capillaries was less than 0.05°C .

The measurements were made at 25°C with a very short exposure time, 0.1 s, to minimise any damage due to the use of radiation.

The SAXS profiles obtained show the diffracted radiation intensity as a function of momentum transfer, q . Some spectra for empty and solvent cells were also obtained, carefully compared and subtracted from the spectra of each sample.

The analyses performed made it possible to obtain information on the dimensions, uniformity and shape of the gas-containing samples in suspension.

Results of stability analyses

Stability analyses in terms of changes in dimensions over time at two different storage temperatures were carried out using DLS (Figure 4), while confirmation that the initial gas concentration within the nanobubbles was maintained after storage for three months was obtained from acoustic attenuation experiments (Figure 3). The vesicular of samples prepared, both empty and containing gas, were subjected to dimensioning and ζ potential analyses after purification.

Study of the dimensions and surface charge of the vesicular systems was extended over time and the abovementioned parameters were assessed over a time interval of approximately 3 months at two different temperatures in order to study the stability of the samples.

This study was performed holding identical aliquots of the samples in test tubes held at ambient temperature on a laboratory bench and in a refrigerator at 4°C.

Initially dimensioning and ζ potential measurements were made every day for the first week of storage and then at a frequency of once per week.

Through this study the stability of the samples in terms of any changes in the parameters which we were investigating probably caused by the occurrence of degradation phenomena, or aggregation and coalescence, was followed over time.

Changes in dimensions and zeta potential were also studied to assess the stability of the nanobubbles in the presence of both human and bovine sera at a concentration of 45% (v/v) over a time period of 3 hours at a temperature of 37°C (Figure 12).

This study enabled us to follow the stability of the samples in terms of any changes over time in the parameters which were investigating, probably as a result of the occurrence of adsorption and degradation phenomena following interaction between the nanobubbles and plasma proteins. From the data shown in Figure 12 it is clearly apparent that the nanobubbles are stable if placed in contact with

human and bovine serum over the time interval investigated.

Acoustic characterisation results and interaction with ultrasound

Because nanobubbles full of gas dispersed in a liquid act as diffusion (scattering) centres for an elastic wave propagating in the liquid and incident upon them, the efficiency of gas trapping within the nanobubbles was also evaluated using a previously described high frequency ultrasound pulse technique (7). This technique, which makes use of the same physical principle (measurement of the intensity of the reflected echo) as is also used for the formation of ultrasound images can be used to evaluate the efficiency of the nanobubbles as a contrast medium in medical ultrasound imaging; in fact the increased attenuation of the ultrasound signal transmitted by the solution containing nanobubbles is associated with the increased efficiency with which the incident elastic energy is scattered into space, consequently increasing the ultrasound reflection capacity (increased echogenicity) to the source of the waves themselves, which in the clinical situation will be the sensor connected to the ultrasound unit used for medical investigation. The two-way correspondence between the increased attenuation of the acoustic signal measured by the pulse-echo technique and the increase in the scattering capacity of the nanobubbles also makes it possible to use the ultrasound pulse technique to measure the frequency spectrum of the nanobubbles' scattering efficiency, or to determine the ultrasound frequency at which the elastic energy is most diffused by the nanobubbles into space.

An ultrasound transducer (PanametricsU8423040 V319) having a central frequency of 14 MHz and a pass band of between 11 and 17 MHz at -6 dB was used for the measurements. The transducer, which was fed from an ultrasound pulse generator/receiver (Panametrics500 PR), acts as both an emitter and receiver of elastic waves. During the emission stage this generates short ultrasound pulses (lasting a few microseconds) which propagate in the dispersed liquid solution of nanobubbles present in a small hollow cell - of cylindrical shape - made in a Plexiglas tube. One of the base surfaces of the cell comprises the

transducer surface; the other being of Plexiglas reflects the ultrasound pulses incident upon it which then return to the transducer, again passing through the solution. The transducer, acting as an elastic wave receiver at this stage, is used to detect the reflected elastic wave, the physical characteristics of which (amplitude, phase, frequency spectrum) are obtained by analysing the electrical signal produced by the pass receiver.

The experimental procedure used first provides for filling the cylindrical cell with a buffer solution of Hepes (10 mM, pH 7.4) to obtain the reference acoustic signal; subsequently solutions of nanobubbles at different temperatures in the same Hepes buffer solution are placed in the cell to measure the attenuation of the echo of the reflected signal.

Figure 9 shows the change in attenuation (expressed as dB/cm) measured at the frequency of 14 MHz for the nanobubbles described here, as their concentration varies in Hepes buffer solution. A linear variation with increasing nanobubble concentration was found; the maximum attenuation value (approximately 6 dB/cm at a nanobubble concentration in Hepes of a little less than 40%) is comparable with that measured using the same technique in SonoVue® which, as mentioned, is a commercially available ultrasound contrast agent formed of lipid microshells containing SF₆.

The frequency spectrum of the ultrasound signal attenuation measured using the pulse technique, Figure 10, shows that the ultrasound frequencies at which elastic energy is most scattered by the nanobubbles in space increases with frequency for the same nanobubble concentration in Hepes, reaching maximum values in the frequency range between 22 and 24 MHz.

Sonoporation experiment results

Nanobubbles of Span 20/Chol and DMPC/Chol containing the fluorescent probe calcein prepared using the method according to the invention were used to carry out in vivo experiments to open up the blood-brain barrier (BBB) following exposure to focused ultrasound (FUS).

The experimental conditions under which the investigations into passage across the BBB were carried out were developed using a series of prior experiments in which nanobubbles and Sonovue® were sonoporated in order to cross the BBB using a probe which normally does not cross it - Evans blue dye.

Each rat (totalling 5 per experiment) was anaesthetised with isoflurane and placed in a stereotaxic system. The focused ultrasound transducer was placed above the shaved head of the mouse, on which ultrasound gel was placed.

A suspension containing nanobubbles (0.13 $\mu\text{l/g}$ for the experiment using DMPC/Chol nanobubbles and 0.08 $\mu\text{l/g}$ for the experiment using Span 20/Chol nanobubbles, in concentrations of 2.14×10^{-8} and 1.28×10^8 nanobubbles/ml) with gas and calcein within and the Evans blue probe present in the solution outside the nanobubble respectively was injected into the caudal vein of the rats (mean weight 30 g). FUS was then applied through a transducer with a frequency of 3.5 MHz, which was in turn connected to an ultrasound generator. FUS was applied for 55 seconds in a pulsed manner, with a 5 second pause, three times, in order to dissipate the heat produced by the ultrasound and to avoid overheating of the part.

The animals were sacrificed after 48 hours and ultrathin cryosections were made of the brains of every rat to observe the presence of fluorescence due to the presence of calcein carried into the brain via the nanobubbles, using fluorescence microscopy; the calcein itself was quantified using appropriate software (Image J software - <https://imagej.nih.gov/ij/>). The Evans blue probe, which is unable to cross the intact BBB in the absence of pores caused by Sonoporation, also passed into the brain following exposure to FUS.

Figure 13 shows quantification of the fluorescence in the brain following transport by DMPC/Chol and Span20/Chol nanobubbles. From the graph it is obvious that both the samples are efficiently capable of cavitating, thus releasing the calcein which will spread into the brain through the transient pores just created by the sonoporation. In this experiment, in which the quantity of calcein within the brain was not normalised with respect to the quantity transported by the

nanobubbles, it was found that surfactant nanobubbles were more efficient at transporting calcein into the brain (Figure 13). The fact that both samples are in any event capable of carrying calcein across the BBB by sonoporation represents a finding of extreme interest in that it demonstrates the effectiveness of nanobubbles in the process of cavitation and sonoporation and joint transport of a hydrophilic and a gas molecule. This result demonstrates the applicability of such systems as targeting systems in the therapeutic field through the application of FUS externally to the site where the material trapped in the nanobubbles, diagnostic materials such as ultrasound and/or theranostic probes, have to be released.

References

- (1) E Stride and N Saffari "Microbubble ultrasound contrast agents: a review" *Proc. Instn Mech. Engrs* 2003 217:429-447
- (2) Unnikrishnan S, Klibanov AL. "Microbubbles as ultrasound contrast agents for molecular imaging: preparation and application" *Am J Roentgenol.* 2012 199:292-9.
- (3) J.M. Gorce, M. Arditi, M. Schneider "Influence of Bubble Size Distribution on the Echogenicity of Ultrasound Contrast Agents: A Study of SonoVue®" *Invest. Radiol.* 2000 35:661-671.
- (4) D Cosgrove "Ultrasound contrast agents: an overview." *Eur J Radiol.* 2006 60:324-30.
- (5) V Zarnitsyn, CA Rostad, MR Prausnitz "Modeling transmembrane transport through cell membrane wounds created by acoustic cavitation" *Biophys. J. Biophys J* 2008 95:4124-38.
- (6) EC Unger, E Hersh, M Vannan et al. "Local medicinal compounds and gene delivery through microbubbles" *ProgCardiovasc Dis* 2001 44:45-54.
- (7) L Hoff "Acoustic properties of ultrasonic contrast agents" *Ultrasonics*, 1996 34: 591-593.
- (8) PJA Frinking, N de Jong "Acoustic modeling of shell-encapsulated gas bubbles" *Ultrasound Med. Biol.* 24, 523-533, 1998.

- (9) Y Endo-Takahashi, Y Negishi, A Nakamura et al. "pDNA-loaded Bubble liposomes as potential ultrasound imaging and gene delivery agents" *Biomaterials* 2013 34:2807-2813
- (10) Y Endo-Takahashi, Y Negishi, A Nakamura et al. "Systemic delivery of miR-126 by miRNA-loaded Bubble liposomes for the treatment of hind limb ischemia" *SCIENTIFIC REPORTS* 2014 4:3883 DOI: 10.1038/srep03883.
- (11) N Hamano, Y Negishi, D Omata et al. "Bubble Liposomes and Ultrasound Enhance the Antitumor Effects of AG73 Liposomes Encapsulating Antitumor Agents" *Mol. Pharmaceutics* 10 (2013) 774–779
- (12) ZA Schroedera, J Kost, Y Barenholz, "Ultrasound, liposomes, and medicinal compounds delivery: principles for using ultrasound to control the release of medicinal compounds from liposomes" *Chemistry and Physics of Lipids* 2009 162:1–16
- (13) A Exner T Krupka L Solorio, "Stabilized nanobubbles for diagnostic and therapeutic applications" Patent application number: US2014/0147390 - Publication date: 2014-05-29
- (14) E. Santucci, M. Carafa, T. Coviello, E. Murtas, F.M. Riccieri, F. Alhaique, A. Modesti, A. Modica, Vesicles from polysorbate 20 and cholesterol. A simple preparation and characterization, *STP Pharma. Sci.* 6 (1996) 29–32.
- (15) M. Carafa, E. Santucci, F. Alhaique, T. Coviello, E. Murtas, F.M. Riccieri, G. Lucania, M.R. Torrisi, Preparation and properties of new unilamellar non-ionic/ionic surfactant vesicles, *Int. J. Pharm.* 160 (1998) 51–59).
- (16) L. Hoff "Acoustic Characterization of Contrast Agents for Medical Ultrasound Imaging" first ed., Kluwer Academic Publishers, Dordrecht, The Netherlands, 2001
- (17)A. Rosencwaig, 1980, Photoacoustics and Photoacoustic Spectroscopy, John Wiley & Sons.
- (18) A. C. Tam 1986, Applications of photoacoustics sensing techniques, «*Rev. Mod. Phys.*», 58, pp. 381-431.

- (19) Alippi A., Bettucci A., Biagioni A., et al., Photoacoustic cell for ultrasound con-trast agent characterization, Rev. Sci. Instrum., 81, (2010), pp. 1-7
- (20) PereraReshani H., Hernandez Christopher, Zhou Haoyan, Kota Pavan, Burke Alan, Exner Agata A. Ultrasound imaging beyond the vasculature with new generation contrast agents. WIREs Nanomed Nanobiotechnol 2015, 7: 593-608.
- (21) University Of The Witwatersrand, Johannesburg "Liposomal medicinal compounds delivery system" Patent application number WO 2014/054026 publication date:10 April 2014

CLAIMS

1. Nanobubbles comprising an external lipophilic double layer containing within it an aqueous layer located around a central gaseous portion.
2. Nanobubbles according to claim 1 in which the lipophilic double layer contains cholesterol in combination with at least one of phospholipids and surfactants selected from 1,2-dipalmitoyl-*sn*-glycero-3-phosphocholine (DPPC), Span 20, 1,2-dimyristoyl-*sn*-glycero-3-phosphocholine (DMPC), dipalmitoylphosphatidylcholine (DPPC) and distearoylphosphatidylcholine (DSPC), dicetyl phosphate (DCP), Span 60 and Tween 85, 81, 80, 65, 61, 60, 21, 20.
3. Nanobubbles according to either of claims 1 or 2 having a diameter of between 120 and 380 nm, preferably between 130 and 300 nm.
4. Nanobubbles according to any one of claims 1 to 3 having a stability in aqueous solution of at least 180 minutes at a temperature of between 37°C and 40°C.
5. Nanobubbles according to any one of claims 1 to 4 having a stability in aqueous solution of at least 3 months at a temperature of 4°C.
6. Nanobubbles according to any one of claims 1 to 5 in which the gas present in the central gaseous portion is selected from linear, branched or cyclic C₃-C₇ perfluorocarbons, preferably tetradecafluorohexane.
7. Nanobubbles according to any one of claims 1 to 6, further comprising at least one agent selected from therapeutic and diagnostic agents of a lipophilic and hydrophilic nature and combinations thereof.

8. Nanobubbles according to claim 7 in which the agents of a hydrophilic nature are within the aqueous layer and the agents of a lipophilic nature are within the lipophilic double layer.
9. Nanobubbles according to any one of claims 1 to 8, further comprising at least one targeting molecule linked to the lipophilic double layer, preferably selected from polypeptides, polynucleotides, antibodies and antibody fragments.
10. Nanobubbles according to any one of claims 1 to 9 for use in the human, paediatric and animal medical, theranostic, diagnostic field, in particular ultrasound imaging.
11. Nanobubbles according to any one of claims 1 to 9 for use in treatments providing for a step of sonoporation of the blood-brain barrier.
12. Pharmaceutical compositions comprising nanobubbles according to any one of claims 1 to 9, and a pharmaceutically acceptable vehicle.
13. Pharmaceutical compositions according to claim 12 further comprising at least one agent selected from therapeutic and diagnostic agents of a lipophilic nature and hydrophilic nature and combinations thereof.
14. Composition according to either of claims 12 or 13 in which the polydispersity index of the dimension distribution curve for the nanobubbles in the composition is less than 0.25, preferably less than 0.20.
15. Composition according to any one of claims 12 to 14 for use in the human, paediatric and animal medical, theranostic, diagnostic field, in particular ultrasound imaging.

16. Composition according to any one of claims 12 to 14 for use in treatments providing for a step of sonoporation of the blood-brain barrier.

17. Method for the preparation of nanobubbles according to any one of claims from 1 to 9 comprising the following essential steps:

- (a) preparing a film by dissolving an aliquot of cholesterol in combination with one or more of cationic phospholipids and surfactants in an organic solvent and subsequent evaporation of the said solvent;
- (b) hydrating the film obtained in stage (a) with water;
- (c) placing the mixture obtained in stage (b) in a sealed reactor, then adding an aliquot of a liquid perfluorocarbon in equilibrium with its gas phase;
- (d) sonicating or extruding the suspension obtained in the previous stage at ambient temperature;
- (e) cooling the suspension obtained in the previous stage without reaching the freezing point, preferably to a temperature of not less than 4°C.

18. Method according to claim 17 comprising a further step of purification of the suspension, preferably by centrifuging.

19. Method according to claim 18 in which centrifuging is performed at 600 rpm for 25 minutes at a temperature of 25° centigrade.

20. Method according to any one of claims 17-19 in which the perfluorocarbon has a linear, branched or cyclic C₃-C₇, preferably C₆, chain.

21. Method according to any one of claims 17-20 in which in step (a) an aliquot of an agent selected from lipophilic therapeutic and diagnostic agents and mixtures thereof is added to the organic solvent.

22. Method according to any one of claims 17-21 in which in step (b) water is completely or partially replaced by an aqueous solution

containing an agent selected from hydrophilic therapeutic and diagnostic agents and mixtures thereof.

23. Method according to either of claims 21 or 22 in which the agent is selected from fluorescent, radioactive and luminescent probes.

24. Nanobubbles directly obtained with the process according to claims 17-23.

25. Nanobubbles directly obtained with the process according to claims 17-23 for use in the human, paediatric and animal diagnostic, and in particular ultrasound imaging and theranostic, medical fields.

Nanobubbles directly obtained with the process according to claims 17-23, for use in treatments providing for a step of sonoporation of the blood-brain barrier

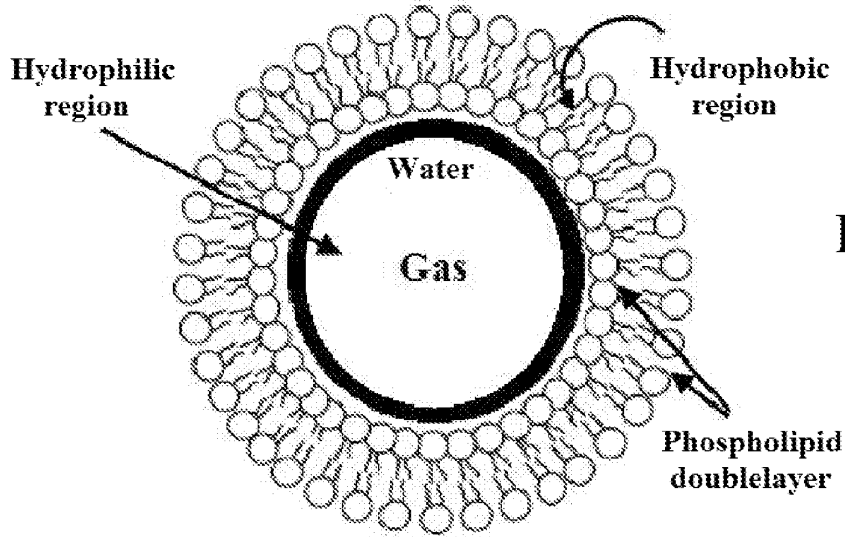


Figure 1

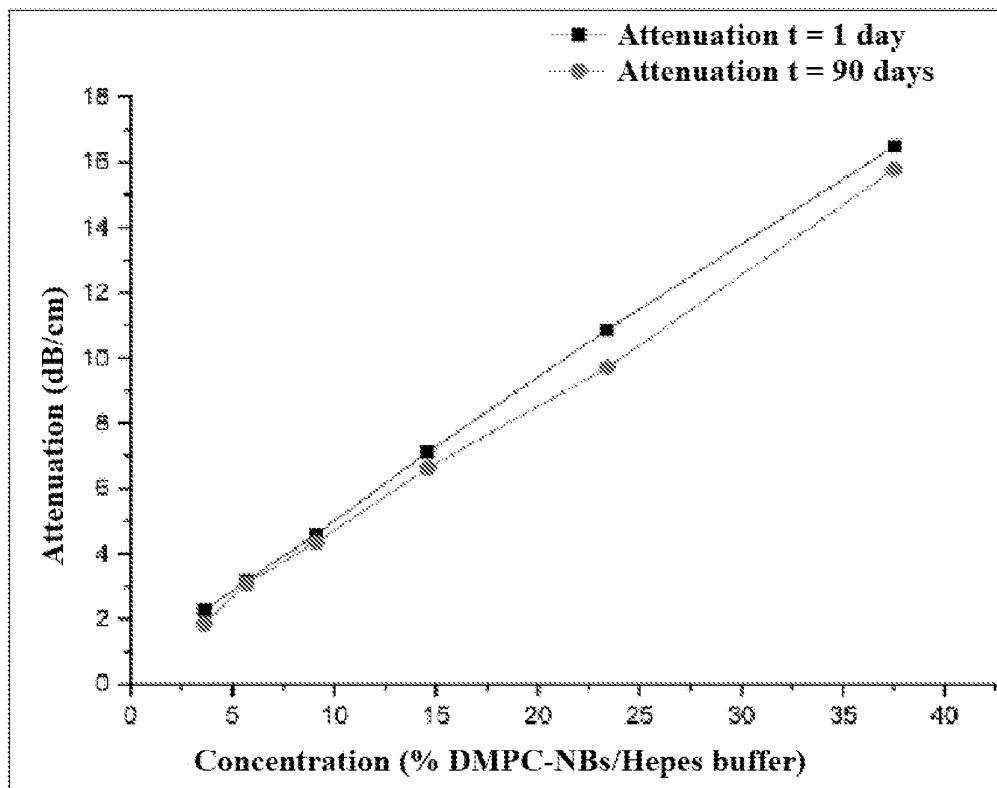


Figure 3

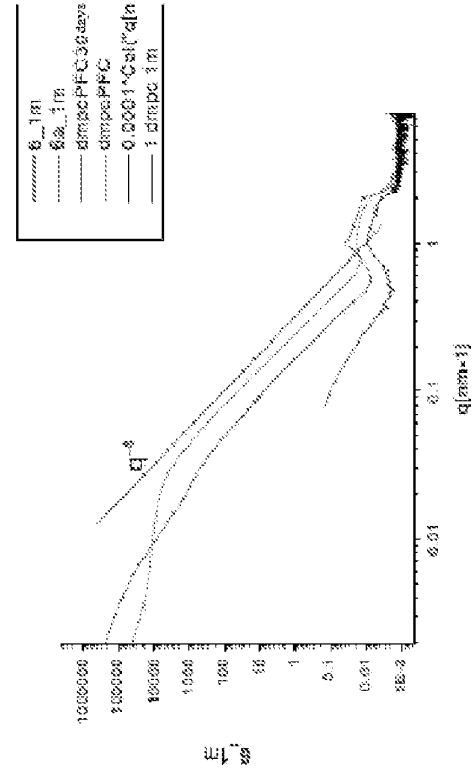


Figure 2A

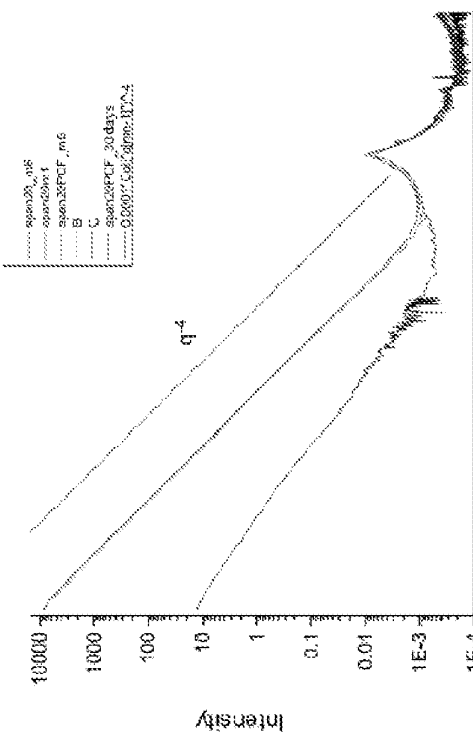


Figure 2B

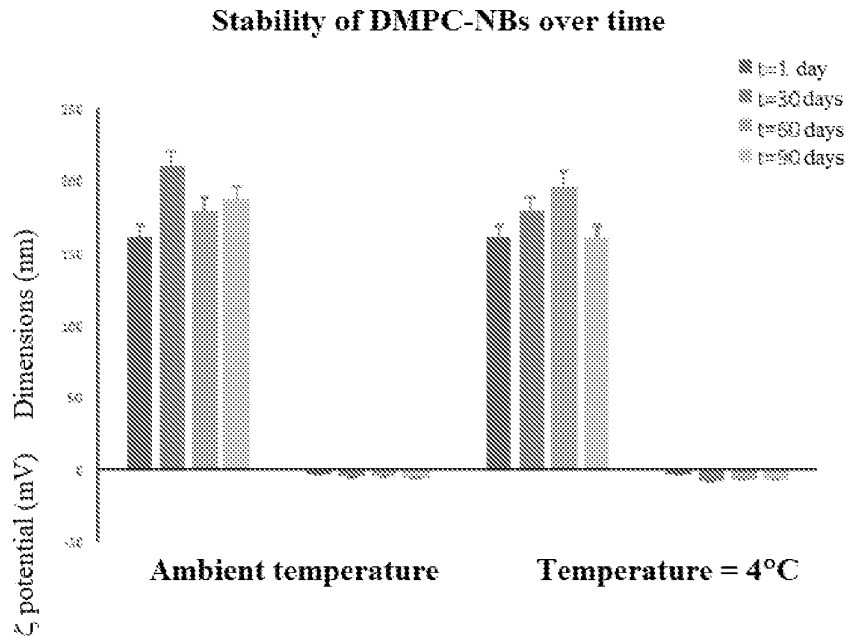


Figure 4

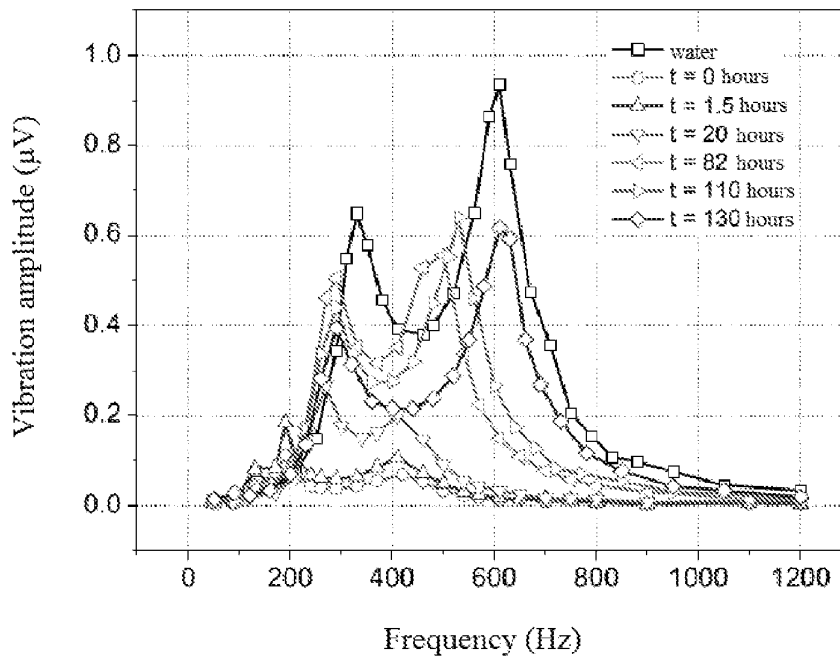


Figure 5

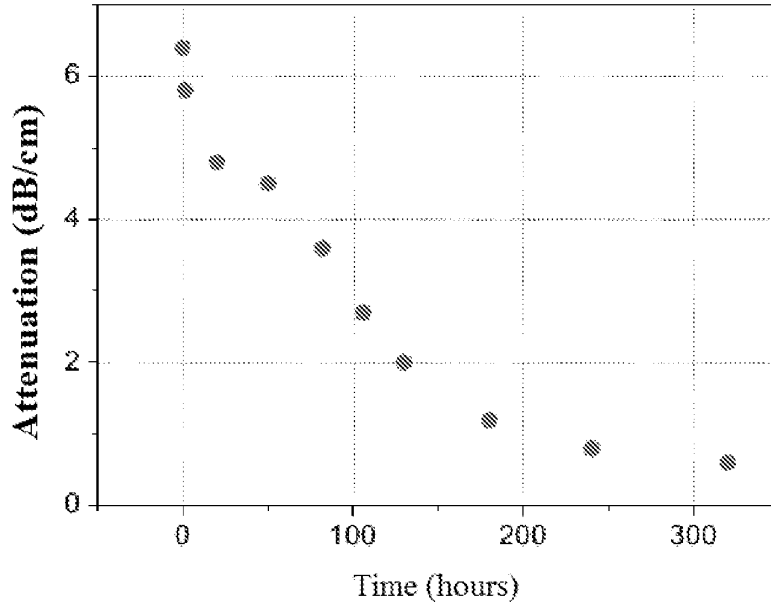


Figure 6

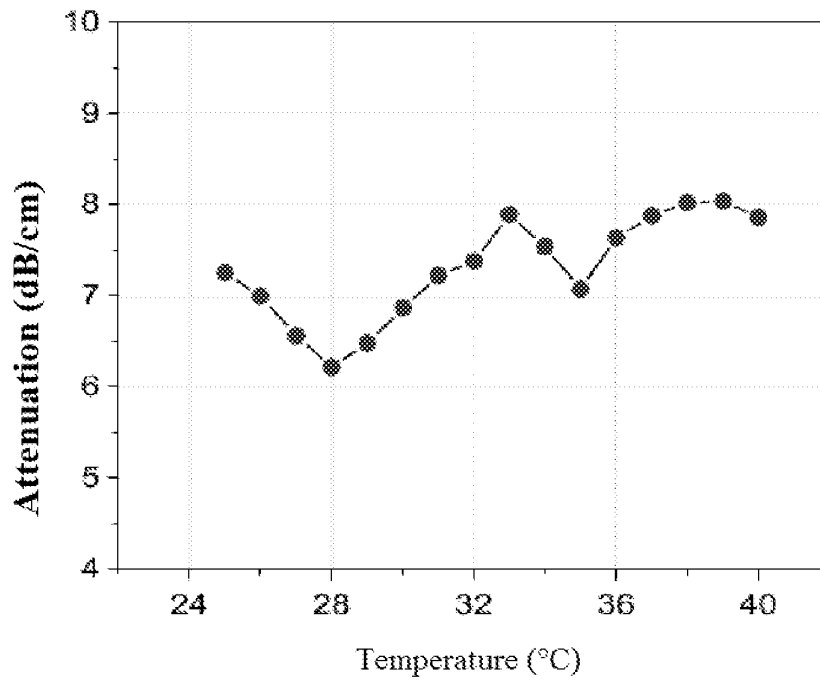


Figure 8

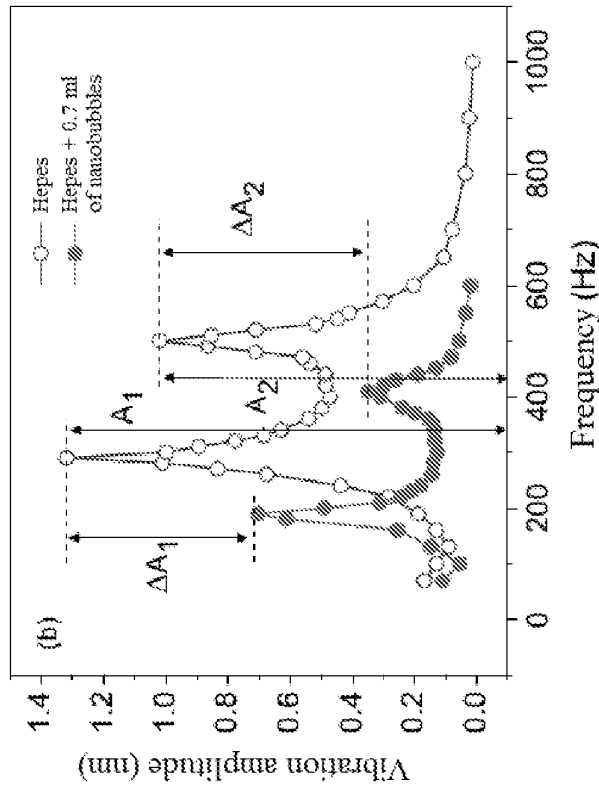


Figure 7B

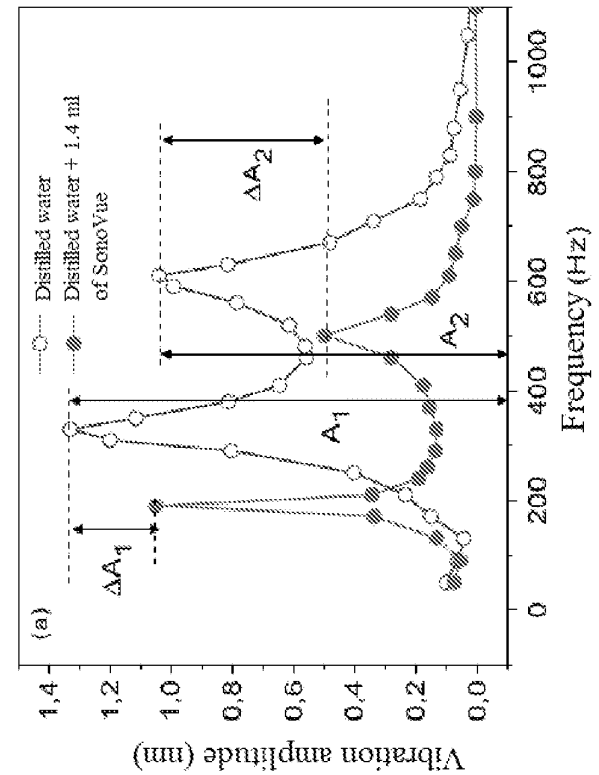


Figure 7A

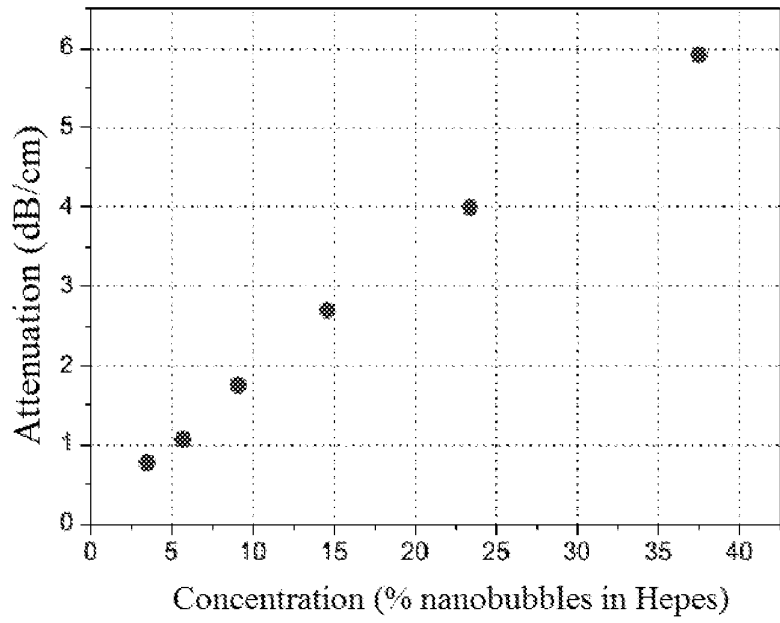


Figure 9

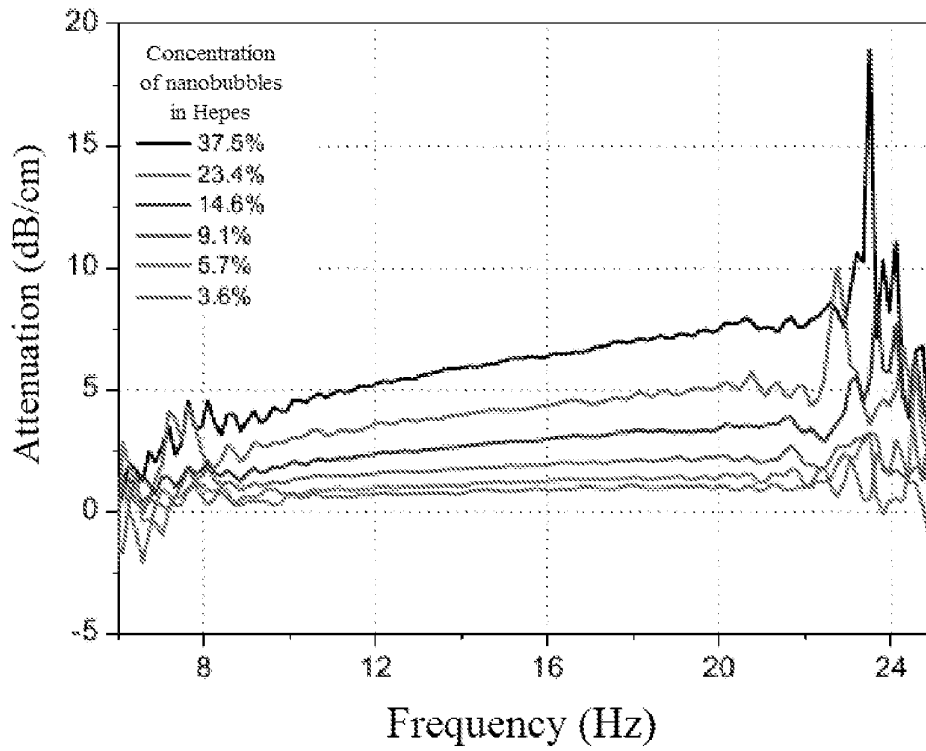


Figure 10

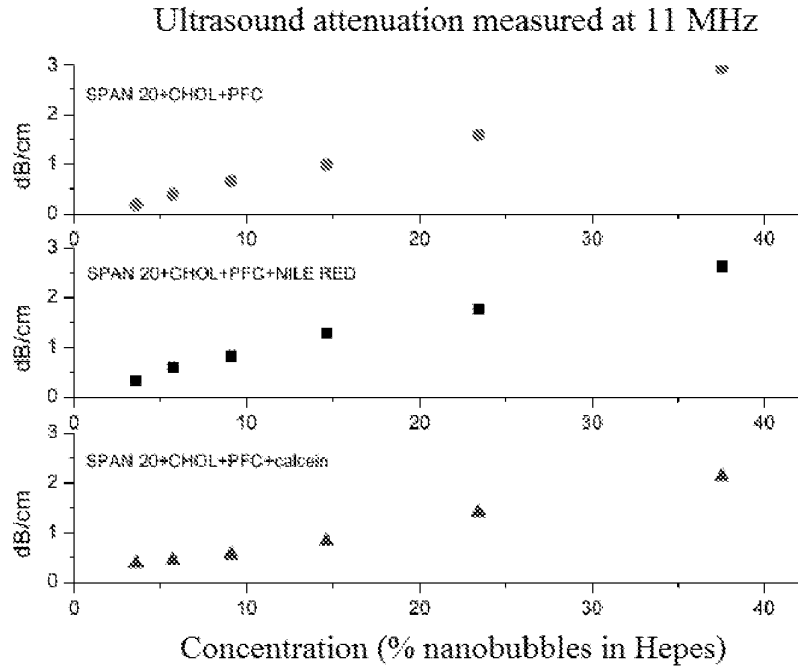


Figure 11

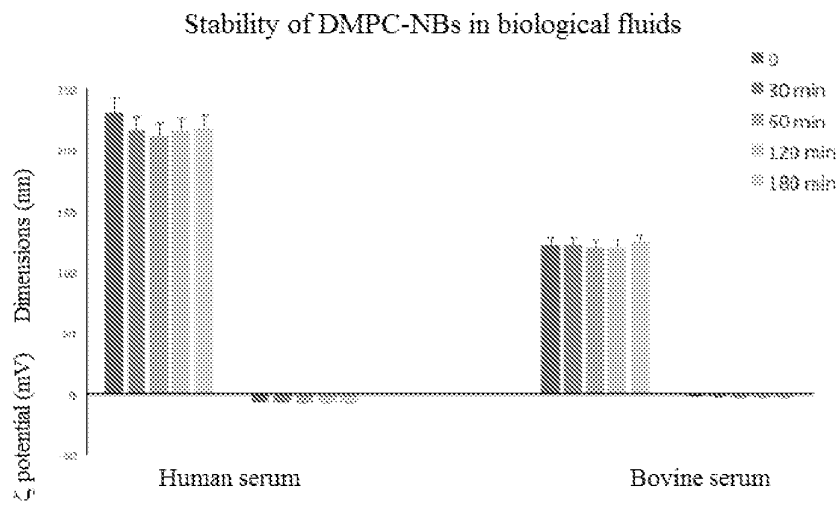


Figure 12

Quantity of calcein found in the brain

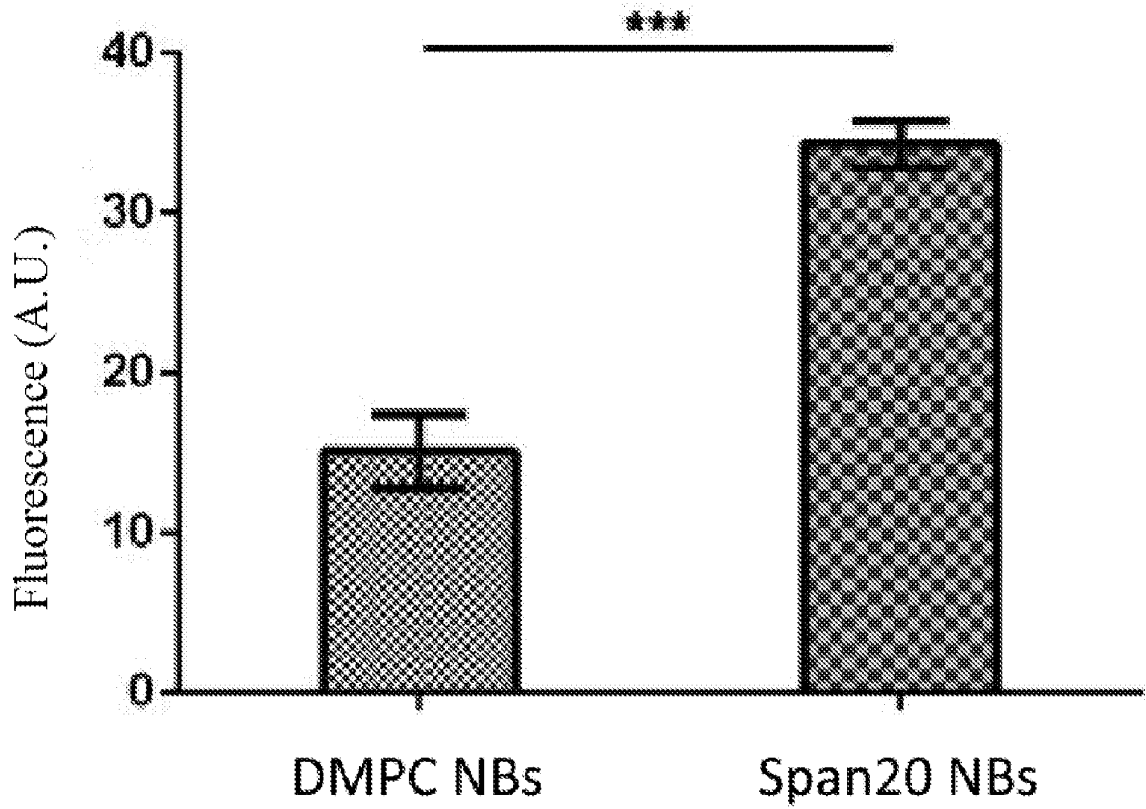


Figure 13

Appendix 2:

Nose to brain delivery: new trends in amphiphile-based “soft” nanocarriers

Nose to Brain Delivery: New Trends in Amphiphile-Based “Soft” Nanocarriers

Carlotta Marianecchi^{a#}, Federica Rinaldi^{b#}, Patrizia N. Hanieh^a, Donatella Paolino^{c,d}, Luisa Di Marzio^e and Maria Carafa^{a*}

^aDepartment of Drug Chemistry and Technology, University of Rome “Sapienza”, Rome, Italy; ^bCenter for Life Nano Science@Sapienza, Fondazione Istituto Italiano di Tecnologia, Rome, Italy; ^cDepartment of Health Sciences, University of Catanzaro “Magna Græcia”, Catanzaro, Italy; ^dIRC FSH-Interregional Research Center for Food Safety & Health, University of Catanzaro “Magna Græcia”, Catanzaro, Italy; ^eDepartment of Pharmacy, University of Chieti - Pescara “G d’Annunzio”, Chieti - Pescara, Italy



Maria Carafa

Abstract: The aim of the present paper is to highlight the potential of nasal mucosa as an administration route for targeting the central nervous system, in particular, the brain. Among the formulation strategies for enhance nose to brain drug delivery, the use of colloidal carriers has become a revolutionary approach. These systems should be able to entrap drugs in the desired amount, to penetrate through anatomical barriers, to efficiently release the loaded drugs in the site of action and moreover to show a good physicochemical, biological stability and good biocompatibility. The use of vesicular systems (liposomes and niosomes) together with the use of micelles, in nose to brain delivery are here presented. Vesicle structure is characterized by the presence of a hydrophobic bilayer and an aqueous core that is absent in micelles. Amphiphilic molecules are responsible for soft nanocarriers formation, in particular: liposomes are formed by phospholipids, while niosomes by non-ionic surfactant and micelles by amphiphilic polymers.

Keywords: Intranasal delivery, nose-to-brain, central nervous system, liposomes, niosomes, micelles, polymersomes.

1. INTRODUCTION

The possibility to reach the central nervous system (CNS) is specifically regulated by three barriers: the arachnoid epithelium (AE), the choroid plexus epithelium (CPE) and the blood-brain barrier (BBB). The blood and cerebrospinal fluid (CSF) are separated from AE and CPE, whereas brain's cells and blood from BBB.

The selectivity of these barriers is fundamental to the protection and to the physiology of CNS, but it represents also a big hindrance for the treatment of CNS diseases with traditional systemic pharmaceutical delivery. The BBB can be the major obstacle for a conventional approach, because it represents the only direct access to cell's brain. The tight junctions between the BBB cells prevent most compounds from entering brain tissue and the penetration of molecules in the brain is possible only for the 2% of small polar molecules [1]. In fact the 100% of large-molecule drugs and the 98% of small-molecule drugs are not able to cross BBB and to perform passive diffusion the molecule drugs must have lipophilic nature and ≈ 400 DA in mass [1,2]. So, even if drugs could be administered easily through systematic administration (e.g., by intravenous injection) the BBB would limit the access of drugs to the brain. So for many years, the BBB has inhibited the use of a lot of therapeutic agents for treating Alzheimer's disease, stroke, brain tumor, head injury, depression, anxiety and other CNS disorders [3].

It's possible to reach brain with alternative routes through which therapeutic agents can bypass the BBB: intracerebroventricular, intraparenchymal, or intrathecal administrations, but these routes of administration are invasive, risky, and expensive techniques requiring surgical expertise especially for multiple dosing regimens [4]. Until a short time ago, the nasal route has been employed for delivery of therapeutic agents for the treatment of local diseases: nasal allergy, sinusitis, nasal infections and nasal congestion; today the interest of many researchers for the nasal route is

high; it can be employed in the therapy of neurologic diseases in mice, rats, primates and humans.

By this administration route drugs can reach the brain through the olfactory region and respiratory epithelium because the olfactory nerve cells and trigeminal nerves are in direct contact with both the environment and the CNS.

The interest for nasal route is related to [5]:

- High vascularization of the epithelium of nasal mucosa
- Presence of porous endothelial membrane
- Ease of accessibility
- Broad surface area for rapid and greater drug adsorption
- Fast pharmacological activity onset
- Lower enzymatic degradation respect to gastrointestinal and liver degradation
- High total blood flow per cm^3 .

Until now the mechanisms of CNS delivery through nasal route administration are not entirely understood, but recent data demonstrate involvement of vasculature, cerebrospinal fluid, and lymphatic system pathway seems to be involved in the transport of drugs through nasal route. Also the fate *in vivo* of the therapeutic agent depends on the properties of drug, the formulation characteristics and the delivery device employed [6].

In Fig. (1) the different fate of a drug administered by nasal route is represented. In particular the drug will be cleared by mucociliary clearance system. An amount of therapeutic agent, according to typical characteristics like lipophilicity and molecular weight, could be absorbed by bloodstream and at a later stage eliminated by clearance mechanism. The drug present in the blood could be able to reach the brain, but later it could be also eliminated from CSF.

The alternative route, through which the therapeutic agent can reach the brain, is represented by the absorption by the olfactory region. This is a route very interesting for research as to the drug can arrive in CSF and subsequently in the brain. Three different pathways are involved in the passage by olfactory epithelium and drugs can cross this epithelium through one or a combination of pathways in particular: transcellular uptake, paracellular uptake and

*Address correspondence to this author at the Department of Drug Chemistry and Technologies, Sapienza University of Rome, Piazzale A. Moro, 5 - 00185 Rome, Italy; Tel: +390649913603; Fax: +390649913133; E-mail: maria.carafa@uniroma1.it

[#]These authors equally contributed to this paper.

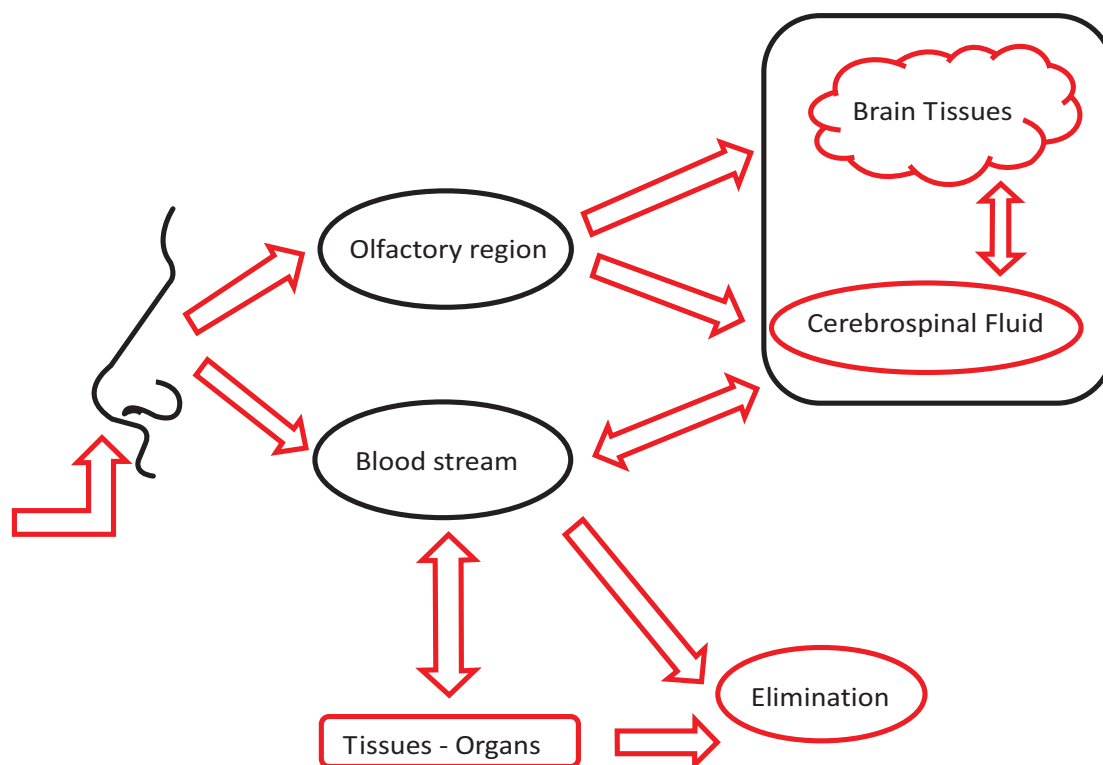


Fig. (1). Possible routes of transport to the CNS after nasal administration of drugs.

via olfactory nerve. In the olfactory region, olfactory receptor neurons are interspersed among supporting cells and basal cells to form the olfactory epithelium. Drugs can be transported through the nasal mucosa to the CNS by entering perivascular channels in the *lamina propria* or via extracellular or intracellular mechanisms involving olfactory and trigeminal nerves [6]. In the transcellular uptake three different internalization mechanisms are implicated: receptor mediated endocytosis, fluid phase endocytosis or passive diffusion, while in the second pathway the drug permeation by olfactory epithelium occurs through tight junction between the cells or by clefts opening in the membrane. The transport from the olfactory epithelium to CSF by paracellular route is particularly suitable for small and hydrophilic molecules. In the case of the uptake through olfactory nerve, the drug permeation can occur extracellularly or by intracellular axonal transport to olfactory bulb [7]. This pathway can be the principal route for brain delivery of some therapeutic agents following nasal administration.

Also branches of the trigeminal nerve innervate the respiratory and olfactory epithelia of the nasal cavity, so the trigeminal pathway, often not considered by researchers, can represent a significant way for drugs to reach the brain. Therefore very important is the relationship between the trigeminal and olfactory routes for the brain drug delivery, because of the unique neural connection that the olfactory and the trigeminal nerves provide between the nose and CSF [8].

Equally, intranasal route (IN) is non invasive resulting in better patient compliance, it doesn't require sterility requirements or any drug modifications, and it has the big advantage to escape liver degradation (first passage effect).

Even if nasal administration is characterized by lower enzymatic degradation respect to gastrointestinal and liver, the degradation of drug is possible, so the entrapment of therapeutic agents

(especially of peptide or protein) in carriers can be useful and advantageous [9].

Therefore nanocarriers offer an innovative approach to drug delivery, providing a range of features including cargo protection, increased dose delivery to target sites, enhanced drug transport through various biological membranes or prolonging and controlling drug release. Actually, the complexity of human body overall may lead to ineffective drug treatments. The healthy protective mechanisms in the body frequently may lead to ineffective *in vivo* drug treatments. Consequently, the development of biologically functional nanocarriers that incorporate drugs to selectively bind and target specific cells becomes crucial. There have been many attempts to functionalize and design nanocarriers so as to increase their efficacy; nevertheless, although the criteria for a successful nanocarrier are quite numerous, only few nanocarriers have actually shown significant clinical potential. Due to the rapid growth of nanotechnology, it can be asserted that the study of drug delivery and disease treatment has been revolutionized [10, 11].

In particular, vesicular systems may increase nose-to-brain drug delivery enhancing drug chemical and biological stability. Numerous amphiphilic components together with different preparation techniques lead to the formation of many vesicular systems: liposomes, niosomes, transfersomes, ethosomes, vesosomes, colloidosomes, and pharmacosomes [9-11].

In addition to vesicular systems, other carriers are able to encapsulate drug and to perform intranasal delivery to CNS: cyclodextrins, microemulsions and nanoparticles.

In all the proposed systems, the presence of a hydrophilic core is responsible for water-soluble drug entrapment while the hydrophobic shell protect the system and entrap lipophilic drugs enhancing brain uptake after intranasal administration. Furthermore the carrier can reach specifically the brain region.

Several approaches have been used to improve the efficacy of nanocarriers and in particular they concern modifications on carrier surface. An example is the incorporation of CPPs (cell-penetrating peptides), useful as bio-enhancers. They are able to increase the absorption by nasal mucosa and consequently the brain uptake, because of this many researchers use these peptides as functional moieties in nanocarrier formulation.

There are different types of CPP that have different origin, size and sequence, but all CPPs are characterized by positive charge at physiological pH, being this a fundamental characteristic to interact with a lipid membrane. [12, 13] Some examples are represented by: the transcription-activating factor (Tat), penetratin and the SynB vectors (family of vectors derived from the antimicrobial peptide protegrin 1) [14].

One of the major problems associated with nasal administration is the rapid removal of drugs or drug delivery system (DDS), from the deposition site through mucociliary clearance. This effect is responsible for the reduction of contact time between drug or DDS and nasal epithelium. This problem could be solved by coating nanocarriers with mucoadhesive agent. In particular the DDS can be prepared with Chitosan, that is a cationic, a mucoadhesive polysaccharide, able to form electrostatic interactions with the negatively charged epithelial cells reducing the mucociliary clearance. Chitosan is also able to open reversibly tight junctions enhancing the extracellular pathways through olfactory and trigeminal nerve [6]. Chitosan originates from chitin and in particular is produced by its deacetylation (Fig. 2). It can be produced with different molecular weight (M.W.) and in particular for the nasal delivery is employed a glutamate salt of chitosan (M.W. around 250 kDa) soluble in water (up 6.5 pH) and characterized by a deacetylation degree around 80% [7].

Others mucoadhesive agents are acrylic acid derivatives, lectin and low methylated pectin. They are able to form a viscous gel when they enter in contact with the nasal epithelium with consequent reduction of mucociliary clearance.

The clearance can be reduced also through preparation of DDS with particular ligands able to bind receptor presents on the olfactory and respiratory epithelia, such as lectin, ulex europeus agglutinin I (UEA I). Another way to DDS surface modification can be the addition of efflux transporter inhibitors or vasoconstrictors.

Through these improvements clearance reduction, increase of residence time of the DDS at delivery site and consequent improvement of transport to CNS can be obtained [6].

Despite of the great interest in nose-to-brain delivery, very little information is available about factors such as surface characteristics and size that may affect the transport of nanocarriers from the nasal cavity to the CNS. A very recent study [15] evaluates the influence

of nanovectors characteristics on their potential transport across the olfactory epithelium. Model systems - 20, 100 and 200 nm sized fluorescent polystyrene (PS) nanoparticles, non-modified or surface modified with polysorbate 80 (P80-PS) or chitosan (C-PS) - were assessed for transport across excised porcine olfactory epithelium. This *in vitro* study confirms the importance of tailoring nanovector properties to influence *in vivo* fate. Chitosan modified nanoparticles resulted in the highest tissue association amongst the tested systems, with the associated nanoparticles primarily located in the mucus, while the polysorbate 80 modified nanoparticles showed some penetration into the epithelial cell layer. Interesting data on nanocarrier safety were collected: C-PS nanoparticles produced damaging effect on the epithelial cell layer in a size dependent manner with 20 nm sized nanoparticles causing substantial tissue damage, relative to the 100 and 200 nm ones. Regarding the transport across the excised olfactory tissue, none of the nanoparticle systems tested, irrespective of particle size or surface modification, seemed to be transported across the epithelium.

The design of the right formulation is fundamental for the nose to brain delivery and the choice of the device (sprays, nose droppers or needle-less syringes) is fundamental because different devices can address the entrapped and untrapped drug to different regions of the nasal cavity. A longer residence time is obtained by using nasal spray deposits in the forepart of the nose, with consequent better brain delivery.

The OptiMist™ and the ViaNase™ are able to reach olfactory region or respiratory epithelia and to escape the deposition in the lungs or esophagus, so these devices have the possibility to transport into the CNS, along olfactory nerves, the drug or the DDS. The nasal administration through sprays devices is very useful, because prevents the nasal drop deposition into nasal cavity and the consequent rapid mucociliary clearance.

The volume of the administered dose is an important factor to consider because it has effect on the deposition within the nasal cavity. Furthermore, the position of the head of the patient, when the formulation is administered, is very important and represents a factor that can influence the delivery to CNS. For example the position "head down and forward" is the most promising to obtain targeting to olfactory region but maybe this position is not ideal in terms of patient compliance [6].

So in order to obtain the better formulation to brain delivery a lot of factors must be taken into account and probably a compromise between them it must be achieved.

In this review an up-to-date overview on vesicular system (liposome and niosomes) applied to nose to brain delivery will be presented. The use of micelles will be also discussed (Fig. 3).

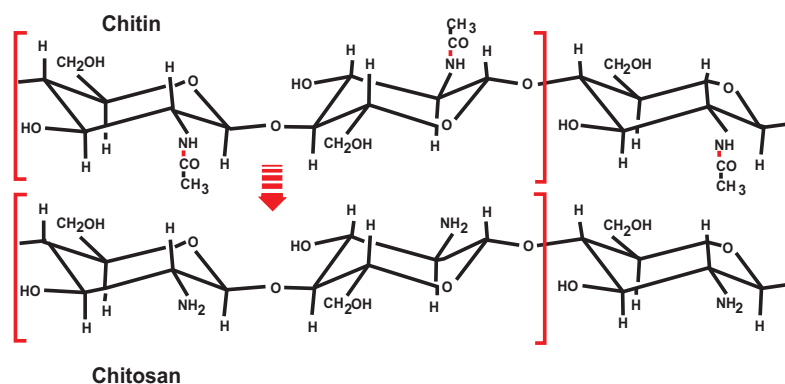


Fig. (2). Chitosan structure.

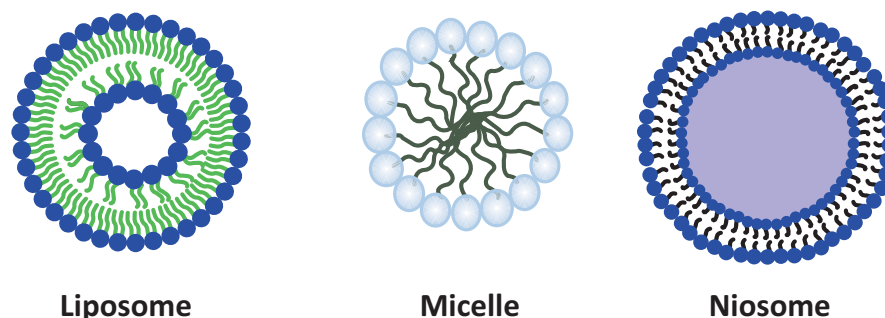


Fig. (3). Drug delivery systems based on amphiphilic compounds.

2. AMPHIPHILE-BASED “SOFT” NANOCARRIERS

The aim of the present paper highlights the potential of nasal mucosa as an administration route for targeting the CNS, in particular, the brain.

Among the formulation strategies for enhanced nose to brain drug delivery, the use of colloidal carriers has become a revolutionary approach.

The success of a therapeutic strategy by using nanocarriers depends on their ability to entrap drugs, to penetrate through anatomical barriers, to release the incorporated drugs, and to show a good stability in nanometric size range [16].

The use of vesicular systems (liposomes and niosomes), in nose to brain delivery is here presented.

Amphiphilic molecules are responsible for colloidal vesicles formation. Vesicles have spherical structures with a hydrophobic bilayer, and an aqueous core. Liposomes are formed by phospholipids, while niosomes, by non-ionic surfactant, present liposome-like features [17].

Lipid and surfactant nanocarriers made up of biodegradable and biocompatible materials show promise for application in neuromedicine due to their capability of passing intact across the BBB. Different investigations have also demonstrated that surfactants can be used to prepare stable colloidal supramolecular devices showing a certain degree of selectivity for brain delivery.

In this section, the use of liposomes, niosomes and micelles is described, with particular attention to the correlation between the modifications that can be made on the vesicular nanocarriers and their therapeutic applications in nose to brain delivery.

2.1. Liposomes and Niosomes

Liposomes were firstly highlighted by Alec D Bangham in the 1960s at the University of Cambridge. They are characterized by single or multiple concentric lipid bilayers encapsulating an aqueous compartment (Fig. 3) [18, 19].

The first formulations were prepared solely by natural lipids, while nowadays they can include natural and/or synthetic lipids and surfactants. They have the capability of entrap both lipophilic and hydrophilic drugs, in the lipid membrane and in the aqueous core, respectively. They can be functionalized on their surface to obtain different type of targeting or to enhance their biological and/or physical stability.

The size of these nearly spherical lipid vesicles can range from a few nanometers to several micrometers. However, liposomes applied to medical use range between 50 and 450 nm [20, 21].

The success of liposomes as drug carriers has been reflected in a number of liposome-based formulations, which are commercially available [22, 23].

Intranasal drug absorption is highly dependent on physicochemical properties of drugs. However, there is a lack of knowledge about correlations between the efficiency of direct nose to brain transport and the physicochemical properties of administered drugs. Although many different drug types (small molecules, biomacromolecules, and specialized drug delivery systems) have been shown to enter the brain via direct nose-to-brain transport, and performed studies on the influence of *M.W.*, partition coefficient and distribution coefficient were unable to identify the correlations with the extent of direct nose-to-brain transport [24].

Numerous drugs have been delivered by liposomes, but all of them have low molecular weight.

Zhen-Zhen Yang *et al.* have prepared rivastigmine liposomes (Lp) and cell penetrating peptide (CPP) modified liposomes (CPP-Lp) to improve rivastigmine distribution in brain for Alzheimer disease (AD) therapy and proceed to enhance pharmacodynamics by intranasal administration and to minimize side effects. Liposomes were prepared using: Egg Phosphatidylcholine (EPC):Cholesterol (Chol) (1:1, molar ratio) and EPC, Chol, 1,2-distearoyl-sn-glycero-3-phosphoethanolamine-N-[amino(polyethyleneglycol)]-CPP (DSPE-PEG-CPP) (1:1:0.06, molar ratio) by extrusion technique. BBB model with BMVEC cells (Brain microvascular endothelial cells) was used, and transport efficiency was evaluated. Lp and CPP-Lp at a rivastigmine concentration of 5 mg/mL were used for IN administration to rats. The results revealed that Lp and especially the CPP-Lp formulation could enhance the permeability across the BBB by murine brain microvascular endothelial cells model *in vitro*. IN administration of rivastigmine solution and rivastigmine liposomes demonstrated the capacity to improve rivastigmine distribution and adequate retention in CNS regions especially in hippocampus and cortex, which were the regions most affected by AD, than that of intravenous administration. In addition, there was very mild nasal toxicity of liposomal formulations. The data suggest that rivastigmine CPP-Lp improve the brain delivery and enhance pharmacodynamics with respect to BBB penetration and nasal olfactory pathway into brain after IN administration and simultaneously decrease the hepatic first pass metabolism and gastrointestinal adverse effects of the drug [25].

As a potential strategy for AD treatment quercetin loaded liposomes were also used.

Phachonpai *et al.*, due to recent findings that demonstrated the crucial role of oxidative stress on the pathophysiology of the disease, decided to use the potent antioxidant quercetin by a nasal administration of quercetin liposomes in order to obtain a protection against neurodegeneration in AD. Quercetin dehydrate (98%), high-purity egg L- α -Phosphatidylcholine and cholesterol were used to prepare quercetin encapsulated liposomes (QL). All animals were treated by QL, containing 0.5 mg of quercetin in 20 μ L, or liposomes without quercetin. After 1 week of treatment, they were sacrificed and removed the brains to determine the density of neu-

rons and cholinergic neurons in hippocampus using histochemical and immunohistochemical techniques.

QL attenuated the degeneration of neurons and cholinergic neurons in hippocampus. Therefore, the neuroprotective effect of QL occurred partly via the reduction of oxidative stress [26].

The main proposed pathway of quercetin delivery via nasal administration was through the olfactory epithelium and found in the CSF later, because the liposomes behaved as semilipophilic particles. Therefore, QL could be rapidly absorbed into the CSF [26].

Terdthai Tong-un together with the authors of the previous study, analyzed the effects of quercetin liposomes via nasal route on improving cognitive behavior and reducing biochemical markers of oxidative stress such as Superoxide Dismutase (SOD), catalase, glutathione and Malondialdehyde (MDA) in the hippocampus in animal model of AD induced by ethylcholine mustard azirinium ion (AF64A). To this aim, male Wistar rats were pretreated with QL, containing the same dose of quercetin of the previous study (0.5 mg of quercetin in 20 μ L), via IN route once daily continually for 2 weeks before and 1 week after AF64A administration. Learning and memory were evaluated using the Morris water maze test, 7 days after the AF64A administration and then the rats were sacrificed for determining the content of MDA and the activities of SOD, catalase and glutathione in the hippocampus. QL via nasal administration significantly improved memory impairment by inhibiting the oxidative damage in hippocampus. The possible underlying mechanisms might be partly associated with a decrease in the level of MDA whereas the activity of SOD, catalase and glutathione increase [27].

The same research group determined the effect of QL administered IN on the anti-anxiety, anti-depression like activity and cognitive enhancing effect [28].

Male Wistar rats were administered QL, containing the same dose of the previous study via IN route once daily continually for 4 weeks. The anxiolytic activity, anti-depression like activity and cognitive enhancing effect were determined after single administration, 1-4 week of treatment using elevated plus maze test, forced swimming test and Morris water maze test respectively. QL encapsulation via nasal route possessed anxiolytic, anti-depression like activity and cognitive enhancing effect at all treatment duration [28].

Salama *et al.* prepared a new system: phospholipid based colloidal nanocubic vesicles encapsulating olanzapine, an atypical antipsychotic drug that suffers from low brain permeability due to efflux by P-glycoproteins and hepatic first-pass metabolism, for its brain targeting via the nasal route.

The nanocubic vesicles were prepared by incorporating non-ionic copolymers, poloxamer 188 or 407, in the lipid bilayer. The effect of phospholipid:poloxamer molar ratio on the physicochemical properties of the nanocubic vesicles was investigated. The *in vivo* behavior and brain targeting of these vesicles were evaluated in rats. TEM photographs showed that the vesicles looked spherical before adding poloxamer. However, after poloxamer incorporation, the vesicles showed a predominant cubic shape, except those containing phospholipid:poloxamer in the molar ratio 5:1 which were spherical. Differential Scanning Calorimetry (DSC) studies confirmed perturbation of the packing characteristics as well as fluidization of the lipid bilayer by the polymer with consequent formation of the nanocubic structure. The mean diameter of the vesicles was in the range of 363-645 nm. All vesicles were elastic and the elasticity was found to depend on both poloxamer type and concentration. The IN nanocubic vesicles were significantly more efficient in targeting olanzapine to the brain compared to the liposomal vesicles with drug targeting efficiency values of 100% and 80%, respectively, and absolute bioavailability of 37.9% and 14.9%, respectively [29].

The same research group investigated the presence of a possible direct correlation between vesicle elasticity and the amount of drug reaching the brain intranasally [30]. Transfersomes by phosphatidylcholine (PC) as the lipid matrix and sodium deoxycholate (SDC), Span[®] 60, Cremophor[®] EL, Brij[®] 58, and Brij[®] 72 as surfactants were prepared and the influence of the type of surfactant and PC-to-surfactant ratio on vesicle morphology, size, membrane elasticity, drug entrapment, and *in vitro* drug release was studied. The prepared transfersomes were mainly spherical in shape, with diameters ranging from 310 to 885 nm. Transfersomes containing SDC and Span[®] 60 with optimum lipid-to-surfactant molar ratio showed suitable diameters (410 and 380 nm, respectively) and deformability indices (17.68 and 20.76 mL/sec, respectively). Values for absolute drug bioavailability in rat plasma for transfersomes containing SDC and those containing Span[®] 60 were 24.75 and 51.35%, whereas AUC (0-360 min) values in rat brain were 22,334.6 and 36,486.3 ng/mL/min, respectively. This interesting study revealed that the deformability index, in addition to size and surface modifications [15], is a parameter having a direct relation with the amount of the drug delivered to the brain by the nasal route.

Li *et al.* investigated the effects of IN administration of Galanthamine Hydrobromide (GH) loaded flexible liposomes on the efficiency of acetylcholinesterase inhibition, as well as the pharmacokinetic behavior of GH in rat brain. The GH loaded flexible liposomes were deeply characterized for shape, entrapment capacity, size distribution and zeta potential by transmission electron microscopy (TEM), ultracentrifugation and dynamic light scattering (DLS), respectively. The inhibition of acetylcholinesterase was investigated using rat brain homogenates and microdialysis was used to determine the pharmacokinetic behavior of GH in rat's brain. Cytotoxicity studies were also performed on rat pheochromocytoma PC-12 cell line. The results revealed that GH intranasally administered increases acetylcholinesterase inhibition compared with oral administration and that GH loaded in flexible liposomes is the most efficient formulation with C_{max} and AUC values 3.52 and 3.36 times higher than those of orally administered GH, moreover, the T_{max} was greatly shortened from 1.5 h for oral administration to 0.75 h for intranasal administration of GH loaded flexible liposomes. Cell viability studies showed that the flexible liposome carrier is not toxic to the cultured cells and the cytotoxicity of GH to cells was clearly decreased by loading in flexible liposomes. These results indicate that intranasal administration of GH loaded flexible liposomes could readily transport GH into brain tissues, suggesting some promise for this approach in successful brain-drug targeting in AD treatment [31].

Migliore *et al.* evaluated the efficiency of cationic liposomes for the delivery of proteins to the brain by employing the nasal route of administration. They loaded the liposomes with ovalbumin and 50 μ g was intranasally administered to rat, it was observed that after 6 hours ovalbumin was widely distributed throughout the brain of the rat [32].

Niosomes were first reported in the 1970s as suitable ingredients for cosmetic application. They are formed by the self-assembly of non-ionic amphiphiles in aqueous media and provide a concentric bilayer showing architecture similar to that of liposomes, although lacking their bilayer arrangement. Different papers in literature report the use of niosomes for nose to brain administration [17].

In particular, Nagaraju *et al.* studied the possibility of deliver folic acid in niosomes (FANs), because of the low blood level of folates is the primary cause of depression in Alzheimer's disease. Folic acid is a water-soluble vitamin showing difficulty in crossing the blood-brain barrier and thus was formulated as niosomal nasal drug delivery systems to target the brain. FANs were prepared using different non-ionic surfactants i.e., Span[®] 20, Span[®] 60, Span[®] 80, Tween 20, Tween 80 and cholesterol by using lipid layer hydra-

tion technique. These structures were characterized in terms of their physicochemical properties. The prepared niosomes were in the size range of 3.05-5.625 μm . Niosomes prepared with Span[®] 60 and cholesterol in the ratio of 1:1 shown higher entrapment efficiency of 69.42% and better *in vitro* drug release of 64.2% at the end of 12 hrs and therefore considered as optimized formulation. Niosomes showed good stability over the period of storage. *Ex-vivo* perfusion studies performed using rat model, showed that about 48.15% of drug is absorbed through nasal cavity at the end of 6 hrs [33].

2.2. Micelles

A key property of amphiphilic molecules is their capability to form micelles by self-assembly in a particular solvent [34].

Micelles are spherical aggregates of highly concentrated amphiphilic molecules which, in aqueous media, self-assemble pointing hydrophilic head groups on their surfaces hydrophobic chains into internal, compact matrixes. The amphiphilic molecules form a dynamic equilibrium between the molecules solubilized in the aqueous medium and the micelles present with a continuous and constant exchange of components. Polymeric vesicles, the so-called polymersomes, are self-assembled polymeric shells which form from copolymer amphiphile blocks, such as polyethylene glycol-poly(lactic acid) (PEG-PLA) and PEG-polycaprolactone (PEG-PCL). These biomaterials boast amphiphilic properties like the phospholipids, but they are formed by polymers covalently conjugated into linear or branched structures. Polymersomes are different from polymeric nanoparticles due to their mechanical properties and compositions and form a polymeric bilayer surrounding an internal aqueous core, which can load hydrophobic or hydrophilic drugs.

The nano-sized micelles have been extensively studied as core-shell-type colloidal carriers for delivery of drugs and genes [35, 36].

The use of these carriers could increase the availability of drugs to the CNS, since their small diameter would potentially allow the nanoparticles to be transported transcellularly along the neurons to the brain through various endocytic pathways of sustentacular or neuronal cells present in the nasal membrane [37].

Micellar nanocarriers were proposed to treat different pathologies, such as migraine, psychosis and brain tumors.

Methoxypolyethylene glycol (MPEG)-polycaprolactone (PCL) (MPEG-PCL) were prepared and loaded with coumarin. The efficiency of brain delivery following intravenous and intranasal routes of administration of MPEG-PCL nanomicelles was compared and the amount of coumarin measured in brain tissue after intranasal administration was significantly higher than that observed after intravenous administration, providing further evidence that the intranasal route is an effective method for brain-targeted drug delivery [38].

The obtained results prompted to conjugate MPEG-PCL copolymers with Tat peptide (MPEG-PCL-Tat) and MPEG-PCL-Tat micelles were loaded with coumarin. The presence of Tat, a cell penetrating peptide, led to a coumarin concentration in brain tissue of rats significantly higher than in rats administered coumarin-loaded MPEG-PCL micelles [38].

The same nanocarriers were proposed as delivery systems of the anti-cancer drug camptothecin (CPT) and the drug activity with intranasal delivery appears to be superior to the results obtained with the administration of simple CPT solution, which reportedly results in high drug levels in the systemic circulation [39].

Small interfering RNA (siRNA) has great potential as a therapeutic agent against different CNS diseases [40] and the development of effective strategies that would enhance siRNA delivery to the brain is of great clinical interest. In order to improve the efficiency of brain siRNA delivery systems, an approach that combines

siRNA nose-to-brain delivery with Tat- modified micelles was developed [41, 42].

The results reported in this studies suggest that the proposed system of delivery of nucleic acid to the brain by intranasal administration using MPEG-PCL-Tat relies primarily on an increase in the transfer of nucleic acid to the brain via the olfactory nerve and trigeminal nerve pathways.

It can be underlined that to improve drug delivery to the brain the above reported approaches could be applied and that drug-loaded surface-loaded polymer micelles could be useful against intractable neuropsychiatric disorders, brain tumors, and cerebral infarction [43]. Nose to brain delivery of micellar carriers was also proposed as a novel approach to migraine therapy; in particular, two different triptans were loaded in micelles: Zolmitriptan [44] and Sumatriptan [45].

Various GRAS (generally regarded as safe) approved surfactants, such as Transcutol P[®] and Pluronic[®] F127, were employed for formulating micellar nanocarriers after mixing with Polyethylene glycol-400 (PEG-400), benzyl alcohol and Vitamin E-TPGS (TPGS, d- α -Tocopheryl polyethylene glycol 1,000 succinate).

In both studies, toxicity evaluation indicated the safety of the developed micellar nanocarrier for administration in the nasal cavity. *In vivo* biodistribution studies in rats, conducted with the radio-labeled drug-loaded formulations, indicated the superiority of the developed nanocarrier for brain targeting when compared with intravenous and nasal administration of drug solutions.

The encouraging results obtained in lower animals provided an excellent lead to further evaluate micellar formulations in higher animals and finally in clinical settings.

Nanomicellar carriers, as well as phospholipid based colloidal nanocubic vesicles [29], were also proposed for brain delivery of olanzapine (OZ).

OZ-loaded micellar nanocarriers were prepared, using a mixture of Pluronic[®] L121 (L121) as a hydrophobic block copolymer (EO₅-PO₆₈-EO₅) and Pluronic[®] P123 (P123) as a more hydrophilic block copolymer (EO₂₀-PO₆₉-EO₂₀), adopting thin-film hydration method and their nose-to-brain targeting potential was investigated. NMR studies confirmed the formation of core-shell type micelles and the incorporation of OZ into the micelle core. Optimizing the drug: Pluronic[®] L121: Pluronic[®] P123 ratio would encourage the development of stable micelles having high drug loads as well as an efficient sustained drug-release [46].

The presence of a mucus layer and quick clearance can limit the use of nose-to-brain drug delivery route. Amphiphilic methacrylic copolymer-functionalized poly(ϵ -caprolactone) nanocapsules were proposed as a mucoadhesive system to deliver olanzapine after intranasal administration leading to an enhanced amount of drug in the brain of rats (1.5-fold higher compared to the drug solution) with no effect on the nasal mucosa integrity after repeated doses [47].

In an interesting study by Zhuang *et al.* [48], "natural" vesicles, mouse lymphoma cell line (EL-4) derived exosomes (Exo), were used to encapsulate curcumin (Exo-cur) or a signal transducer and activator of transcription 3 inhibitor (Exo-JSI124) were delivered noninvasively to microglia cells via an intranasal route.

Exosomes are cell-derived vesicles and are present in many biological fluids, with a diameter between 30 and 100 nm.

Exo-cur and Exo-JSI124 were prepared by simply mixing active substances with EL-4 exosomes in appropriate buffer. After centrifugation, samples were subsequently collected, washed and resuspended in PBS. Exo-cur or Exo-JSI124 was administered intranasally as drops with a small pipette. Intranasal administration of Exo-cur or Exo-JSI124 allowed a rapid delivery of encapsulated drugs to the brain that were selectively taken up by microglial cells, inducing apoptosis [48].

Table 1. "Soft" nanocarriers in nose to brain delivery.

Carrier	Drug	Action	Refs.
Liposomes and CPP-modified liposomes	Rivastigmine	Alzheimer Disease	[25]
Liposomes	Quercetin	Alzheimer Disease; anxiety and depression	[26-28]
Liposomes	Galanthamine Hydrobromide	Alzheimer Disease	[31]
Liposomes	Ovalbumin	Model chemical	[32]
Niosomes	Folic Acid	Depression in Alzheimer Disease	[33]
Polymeric micelles	Coumarin	Model chemical	[37]
Tat-modified polymeric micelles	Coumarin	Model chemical	[37]
Tat-modified polymeric micelles	Camptothecin	Brain tumor	[38]
Tat-modified polymeric micelles	siRNA	Transfer of nucleic acid to the brain	[41, 42]
Surfactant micelles	Zolmitriptan	Migraine	[44]
Surfactant micelles	Sumatriptan	Migraine	[45]
Nanocubic vesicles	Olanzapine	Phycosis	[29]
Transfersomes	Olanzapine	Phycosis	[30]
Polymeric micelles	Olanzapine	Phycosis	[46]
Mucoadhesive polymeric micelles	Olanzapine	Phycosis	[47]
EL-4 exosomes	Curcumin	Anti-inflammatory	[48]
EL-4 exosomes	Activator of transcription 3 inhibitor (JSI124)	Anti-inflammatory	[48]

These results should prompt further investigations on the effects of exosomes released from resident cells located in intranasal cavity on brain cells, in particular, brain immune cells [49].

It is conceivable that exosomes or other vesicular carriers showing the same feature of these "natural" vesicles, delivered to the nasal cavity, could play a role in brain immune tolerance.

Analyzing literature related to intranasal delivery, interesting approaches using particular amphiphilic based soft nanocarriers can be found. In particular systems as virosomes and lyophilized gels containing unsaturated fatty acid liposomes (ufasomes) [50, 51] have been proposed as innovative carriers for intranasal delivery. The study of their potential use in nose to brain delivery could be the object of future researches.

CONCLUSION

A feasible approach to CNS delivery is the nasal route of administration of vesicular carriers (Table 1), which bypasses the blood-brain barrier and delivers active substances inducing considerably less, if any, peripheral uptake than other administration modes. Intranasal drug administration is non-invasive and it could be a promising drug delivery method for patients who suffer from chronic and crippling CNS diseases. According to this evidence, it can be looked forward to many more efforts in developing vesicular carriers able to reach CNS by the nasal route, according to the evidence that, despite the many stimulating studies there is still a long road ahead to becoming a clinical reality.

It has been shown that the application of drug loaded amphiphile-based nanocarriers to the nasal cavity can increase the amount of bioactive substances that reaches the CNS directly from the nasal cavity. However, the factors that govern the transport of the drug and/or nanocarriers are still unclear.

In sum, and considering that data on long term therapeutic and side effects of nasal administration of drugs in humans are still sparse, much more work is needed to fully characterize the potential of nose to brain delivery in patients.

CONFLICT OF INTEREST

The authors confirm that this article content has no conflict of interest.

ACKNOWLEDGEMENTS

Declared none.

REFERENCES

- Blumling III JP, Silva GA. Targeting the brain: advances in drug delivery. *Curr Pharm Biotechnol* 2012; 13: 2417-26.
- Chen H, Chen CC, Acosta C, Wu SY, Sun T, Konofagou EE. A new brain drug delivery strategy: focused ultrasound-enhanced intranasal drug delivery. *PLoS One* 2014; 9: e108880.
- Kulkarni K, Bhambere T, Chaudhary G, Talele S, Moghal R. Brain targeting through intranasal route. *Int J PharmTech Res* 2013; 4: 1441-50.
- Yi X, Manickam DS, Brynskikh A, Kabanov AV. Agile delivery of protein therapeutics to CNS. *J Control Release* 2014; 190: 637-63.
- Pardeschi CV, Belgamwar VS. Direct nose to brain drug delivery via integrated nerve pathways bypassing the blood-brain barrier: an excellent platform for brain targeting. *Expert Opin Drug Deliv* 2013; 10: 957-72.
- Shyeilla V D, Hanson LR, FREY II W. Intranasal delivery to the central nervous system: mechanisms and experimental considerations. *J Pharm Sci* 2010; 99: 1654-73.
- Illum L. Nasal drug delivery possibilities, problems and solutions. *J Control Release* 2003; 87: 187-98.
- Kozlovskaya L, Abou-Kaoud M, Stepensky D. Quantitative analysis of drug delivery to the brain via nasal route. *J Control Release* 2014; 189: 133-40.
- Kewal KJ. *Drug Delivery to the Central Nervous System*. Berlin and Heidelberg; Springer 2010; pp. 175-85.
- Marianecci C, Di Marzio L, Rinaldi F, *et al*. Niosomes from 80s to present: The state of the art. *Adv Colloid Interface Sci* 2014; 205: 187-206.
- Estanqueiro M, Amaral MH, Conceição J, Sousa Lobo JM. Nanotechnological carriers for cancer chemotherapy: the state of the art. *Colloids Surf B-Biointerfaces* 2015; 126: 631-48.

- [12] Morris MC, Deshayes S, Heitz F, Divita G. Cell penetrating peptides: from molecular mechanisms to therapeutics. *Biol Cell* 2008; 100: 201-17.
- [13] Eiriksdottira E, Konateb K, Langel U, Divita G, Deshayes S. Secondary structure of cell-penetrating peptides controls membrane interaction and insertion. *Biochim Biophys Acta Biomembr* 2010; 1798: 1119-28.
- [14] Lalatsa A, Schatzlein AG, Uchegbu IF. Strategies to deliver peptide drugs to the brain. *Mol Pharm* 2014; 11: 1081-93.
- [15] Illum L, Mistry A, Stolnik S. Nose-to-brain delivery: Investigation Into Transport of nanoparticles with different surface characteristics and size in excised porcine olfactory epithelium. *Mol Pharm* 2015; 12: 2755-66
- [16] Patel Z, Patel B, Patel S, Pardeshi C. Nose to brain targeted drug delivery bypassing the blood-brain barrier: An overview. *Drug Inv Today* 2012; 4: 610-15.
- [17] Cosco D, Di Marzio L, Marianecchi C, *et al.* Colloidal supramolecular aggregates for therapeutic application in neuromedicine. *Curr Med Chem* 2014; 21: 4132-53.
- [18] Bangham AD, Horne RW. Negative staining of phospholipids and their structural modification by surface-active agents as observed in the electron microscope. *J Mol Biol* 1964; 8: 660-8.
- [19] Bangham AD, Hill MW, Miller NG. Preparation and use of liposomes as models of biological membranes. In: Korn ED, Ed. *Methods in membrane biology*. Vol 1. New York: Plenum 1974: pp. 1-68.
- [20] Etheridge ML, Campbell SA, Erdman AG, Haynes CL, Wolf SM, McCullough J. The big picture on nanomedicine: the state of investigational and approved nanomedicine products. *Nanomedicine* 2013; 9: 1-14.
- [21] Bozzuto G, Molinari A. Liposomes as nanomedical devices. *Int J Nanomed* 2015; 10: 975-99.
- [22] Fanciullino R, Ciccolini J. Liposome-encapsulated anticancer drugs: still waiting for the magic bullet?. *Curr Med Chem* 2009; 16: 4361-73.
- [23] Dhuria SV, Hanson LR, Frey WH. Intranasal delivery to the central nervous system: mechanisms and experimental considerations. *J Pharm Sci* 2010; 99: 1654-73.
- [24] Lee KR, Maeng HJ, Chae JB, *et al.* Lack of a primary physicochemical determinant in the direct transport of drugs to the brain after nasal administration in rats: potential involvement of transporters in the pathway. *Drug Metab Pharmacokinet* 2010; 25: 430-41.
- [25] Yang ZZ, Zhang YQ, Wang ZZ, Wu K, Lou JN, Qi XR. Enhanced brain distribution and pharmacodynamics of rivastigmine by liposomes following intranasal administration. *Int J Pharm* 2013; 452: 344-54.
- [26] Phachonpai W, Wattanathorn J, Muchimapura S, Tong-Un T, Preechagoon D. Neuroprotective effect of quercetin encapsulated liposomes: a novel therapeutic strategy against Alzheimer's disease. *Am J Appl Sci* 2010; 7: 480-5.
- [27] Tong-Un T, Wannanon P, Wattanathorn J, Phachonpai W. Cognitive-enhancing and antioxidant activities of quercetin liposomes in animal model of Alzheimer's disease. *OnLine J Biol Sci* 2010; 10: 84-91.
- [28] Tong-Un T, Wannanon P, Wattanathorn J, Phachonpai W. Quercetin liposomes via nasal administration reduce anxiety and depression-like behaviors and enhance cognitive performances in rats. *Am J Pharmacol Toxicol* 2010; 5: 80-8.
- [29] Salama HA, Mahmoud AA, Kamel AO, Hady MA, Awad GAS. Phospholipid based colloidal poloxamer-nanocubic vesicles for brain targeting via the nasal route. *Colloid Surf B-Biointerf* 2012; 100: 146-54.
- [30] Salama HA, Mahmoud AA, Kamel AO, Abdel Hady M, Awad GA. Brain delivery of olanzapine by intranasal administration of transferrin vesicles. *J Liposome Res* 2012; 22: 336-45.
- [31] Li W, Zhou Y, Zhao N, Hao B, Wang X, Kong P. Pharmacokinetic behavior and efficiency of acetylcholinesterase inhibition in rat brain after intranasal administration of galanthamine hydrobromide loaded flexible liposomes. *Pharmacology* 2012; 34: 272-9.
- [32] Migliore MM, Vyas TK, Campbell RB, Amiji MM, Waszczak BL. Brain delivery of proteins by the intranasal route of administration: a comparison of cationic liposomes versus aqueous solution formulations. *J Pharm Sci* 2010; 99: 1745-61.
- [33] Nagaraju R, Pallavi K, Deepthy K, Haritha M. Formulation and Evaluation of Niosomal Nasal Drug Delivery System of Folic Acid for Brain Targeting. *Curr Drug Disc Technol* 2013; 10: 270-82.
- [34] Otsuka H, Nagasaki Y, Kataoka K. PEGylated nanoparticles for biological and pharmaceutical applications. *Adv Drug Deliv Rev* 2003; 55: 403-19.
- [35] Kakizawa Y, Kataoka K. Block copolymer micelles for delivery of gene and related compounds. *Adv Drug Deliv Rev* 2002; 54: 203-22.
- [36] Truong NP, Whittaker MR, Mak CW, Davis TP. The importance of nanoparticle shape in cancer drug delivery. *Expert Opin Drug Deliv* 2015; 12: 129-42.
- [37] Lochhead JJ, Thorne RG. Intranasal delivery of biologics to the central nervous system. *Adv Drug Deliv Rev* 2011; 64: 614-28.
- [38] Kanazawa T, Taki H, Tanaka K, Takashima Y, Okada H. Cell-penetrating peptide-modified block copolymer micelles promote direct brain delivery via intranasal administration. *Pharm Res* 2011; 28: 2130-9.
- [39] Taki H, Kanazawa T, Akiyama F, Takashima Y, Okada H. Intranasal delivery of camptothecin-loaded Tat-modified nanomicelles for treatment of intracranial brain tumors. *Pharmaceuticals* 2012; 5: 1092-102.
- [40] Pappas TC, Bader AG, Andruss BF, Brown D, Ford LP. Applying small RNA molecules to the directed treatment of human diseases: realizing the potential. *Expert Opin Ther Targets* 2008; 12: 115-27.
- [41] Kanazawa T, Akiyama F, Kakizaki S, Takashima Y, Seta Y. Delivery of siRNA to the brain using a combination of nose-to-brain delivery and cell-penetrating peptide-modified nano-micelles. *Biomaterials* 2013; 34: 9220-6.
- [42] Kanazawa T, Morisaki K, Suzuki S, Takashima Y. Prolongation of life in rats with malignant glioma by intranasal siRNA/drug code-livery to the brain with cell-penetrating peptide-modified micelles. *Mol Pharm* 2014; 11: 1471-8.
- [43] Kanazawa T. Brain delivery of small interfering ribonucleic acid and drugs through intranasal administration with nano-sized polymer micelles. *Med Devices Auckl* 2015; 8: 57-64.
- [44] Jain R, Nabar S, Dandekar P, Patravale V. Micellar nanocarriers: potential nose-to-brain delivery of zolmitriptan as novel migraine therapy. *Pharm Res* 2010; 27: 655-64.
- [45] Jain R, Nabar S, Dandekar P, *et al.* Formulation and evaluation of novel micellar nanocarrier for nasal delivery of sumatriptan. *Nanomedicine* 2010; 5: 575-87.
- [46] Abdelbary GA, Tadros MI. Brain targeting of olanzapine via intranasal delivery of core-shell difunctional block copolymer mixed nanomicellar carriers: *in vitro* characterization, *ex vivo* estimation of nasal toxicity and *in vivo* biodistribution studies. *Int J Pharm* 2013; 452: 300-10.
- [47] Fonseca FN, Betti AH, Carvalho FC, *et al.* Mucoadhesive amphiphilic methacrylic copolymer-functionalized poly(ϵ -caprolactone) nanocapsules for nose-to-brain delivery of olanzapine. *J Biomed Nanotechnol* 2015; 11: 1472-81.
- [48] Zhuang X, Xiang X, Grizzle W, *et al.* Treatment of Brain Inflammatory Diseases by Delivering Exosome Encapsulated Anti-inflammatory Drugs From the Nasal Region to the Brain. *Mol Therapy* 2011; 19: 1769-79.
- [49] Haney MJ, Klyachko NL, Zhao Y, *et al.* Exosomes as drug delivery vehicles for Parkinson's disease therapy. *J Control Release* 2015; 207:18-30.
- [50] Romero EL, Morilla MJ. Topical and mucosal liposomes for vaccine delivery. *Wiley Interdiscip Rev Nanomed Nanobiotechnol* 2011; 3: 356-75.
- [51] Salama AH, Aburahma MH. Ufasomes nano-vesicles-based lyophilized platforms for intranasal delivery of cinnarizine: preparation, optimization, *ex-vivo* histopathological safety assessment and mucosal confocal imaging. *Pharm Dev Technol* 2015; 21: 1-10.

Appendix 3:

Drug delivery in overcoming the blood–brain barrier: role of nasal mucosal grafting

Drug delivery in overcoming the blood–brain barrier: role of nasal mucosal grafting

Carlotta Marianecchi¹
Federica Rinaldi²
Patrizia Nadia Hanieh¹
Luisa Di Marzio³
Donatella Paolino^{4,5}
Maria Carafa¹

¹Department of Drug Chemistry and Technology, University of Rome “Sapienza”, Rome, Italy;

²Center for Life Nano Science@Sapienza, Fondazione Istituto Italiano di Tecnologia, Rome, Italy;

³Department of Pharmacy, University “G. d’Annunzio”, Chieti, Italy; ⁴IRC FSH-Interregional Research Center for Food Safety & Health, Campus Universitario “S. Venuta”, University of Catanzaro “Magna Græcia”, Catanzaro, Italy; ⁵Department of Health Sciences, Campus Universitario “S. Venuta”, University of Catanzaro “Magna Græcia”, Catanzaro, Italy

Abstract: The blood–brain barrier (BBB) plays a fundamental role in protecting and maintaining the homeostasis of the brain. For this reason, drug delivery to the brain is much more difficult than that to other compartments of the body. In order to bypass or cross the BBB, many strategies have been developed: invasive techniques, such as temporary disruption of the BBB or direct intraventricular and intracerebral administration of the drug, as well as noninvasive techniques. Preliminary results, reported in the large number of studies on the potential strategies for brain delivery, are encouraging, but it is far too early to draw any conclusion about the actual use of these therapeutic approaches. Among the most recent, but still pioneering, approaches related to the nasal mucosa properties, the permeabilization of the BBB via nasal mucosal engrafting can offer new potential opportunities. It should be emphasized that this surgical procedure is quite invasive, but the implication for patient outcome needs to be compared to the gold standard of direct intracranial injection, and evaluated whilst keeping in mind that central nervous system diseases and lysosomal storage diseases are chronic and severely debilitating and that up to now no therapy seems to be completely successful.

Keywords: CNS, BBB, nasal mucosa, grafting, lysosomal storage diseases, enzyme replacement therapies

Introduction

There are more than 1,000 agents which are active on central nervous system (CNS) pathologies that have shown promising perspectives in preclinical studies but failed to show good results in the later phases of the development process (at Phase III or even after registration).^{1–5}

For this reason, disorders of the CNS represent one of the largest areas of unsatisfied medical needs, with about 2 billion people affected worldwide and many pharma companies moving away from such fields of innovative research because of the high risk of failure associated with CNS medicines, together with the ever increasing approval time.^{6,7}

One of the major reasons for the poor translation of neuroscience research into medicines is the high degree of complexity of the human CNS, and effective noninvasive treatment of neurological diseases is often limited by the very limited access of therapeutic agents into the CNS owing to the presence of two anatomical and biochemical dynamic barriers: the blood–brain barrier (BBB) and the blood–cerebrospinal fluid barrier (BCSFB).⁸

It is already well known that BBB is formed by endothelial cells (ECs), which line up in capillaries of the brain and spinal cord by a variety of pericytes, vascular smooth muscle cells, astrocytes, and microglia.⁹ The BBB, composed of densely packed cells

Correspondence: Maria Carafa
Department of Drug Chemistry and Technology, University of Rome “Sapienza”, Piazzale Aldo Moro 5, 00185 Rome, Italy
Tel +39 06 4991 3603
Fax +39 06 4991 3133
Email maria.carafa@uniroma1.it

submit your manuscript | www.dovepress.com

<http://dx.doi.org/10.2147/DDDT.S100075>

Drug Design, Development and Therapy 2017:11 325–335

325

 © 2017 Marianecchi et al. This work is published and licensed by Dove Medical Press Limited. The full terms of this license are available at <https://www.dovepress.com/terms.php> and incorporate the Creative Commons Attribution – Non Commercial (unported, v3.0) License (<http://creativecommons.org/licenses/by-nc/3.0/>). By accessing the work you hereby accept the Terms. Non-commercial uses of the work are permitted without any further permission from Dove Medical Press Limited, provided the work is properly attributed. For permission for commercial use of this work, please see paragraphs 4.2 and 5 of our Terms (<https://www.dovepress.com/terms.php>).

with copious intercellular tight junctions (TJs), active efflux pumps, and a trilamellar basement membrane, regulates the synaptic signaling function. Furthermore, BBB protects the CNS from neurotoxic substances, ensures brain nutrition, and prevents the entry of unwanted cells into the brain as well as the absorption of polar or high molecular weight (HMW) molecules larger than 500 Da; in other words, more than 98% of therapeutic drugs.¹⁰⁻¹²

The BBB also displays immunological and transportation features. The immune barrier is composed of microglia, perivascular mast cells, and macrophages. The transport barrier includes para- and transcellular routes. In addition, the brain is extremely rich in vascularity, with each neuron in contact with a capillary.¹³⁻¹⁵

The BCSFB is formed by the TJs of choroid plexus cells surrounding the microvascular endothelium with intracellular

gap and fenestration. Owing to their structural difference, BBB and BCSFB have different main functions, but they both participate in controlling the transfer of molecules between the blood and the brain parenchyma or cerebrospinal fluid (CSF).

Under certain physiological conditions, circulating molecules can only gain access to the brain or CSF via a transcellular route through the capillary endothelial cells or choroid plexus cells, by either passive or active transport, or both.

Furthermore, if molecules overcome the BBB, they are not able to do so in high amounts, and they are exposed to degradation and/or rapid efflux from the CNS.¹⁶

Different transporters suitable for targeting molecules and delivering endogenous and exogenous compounds across the BBB are located on the BBB (Figure 1).

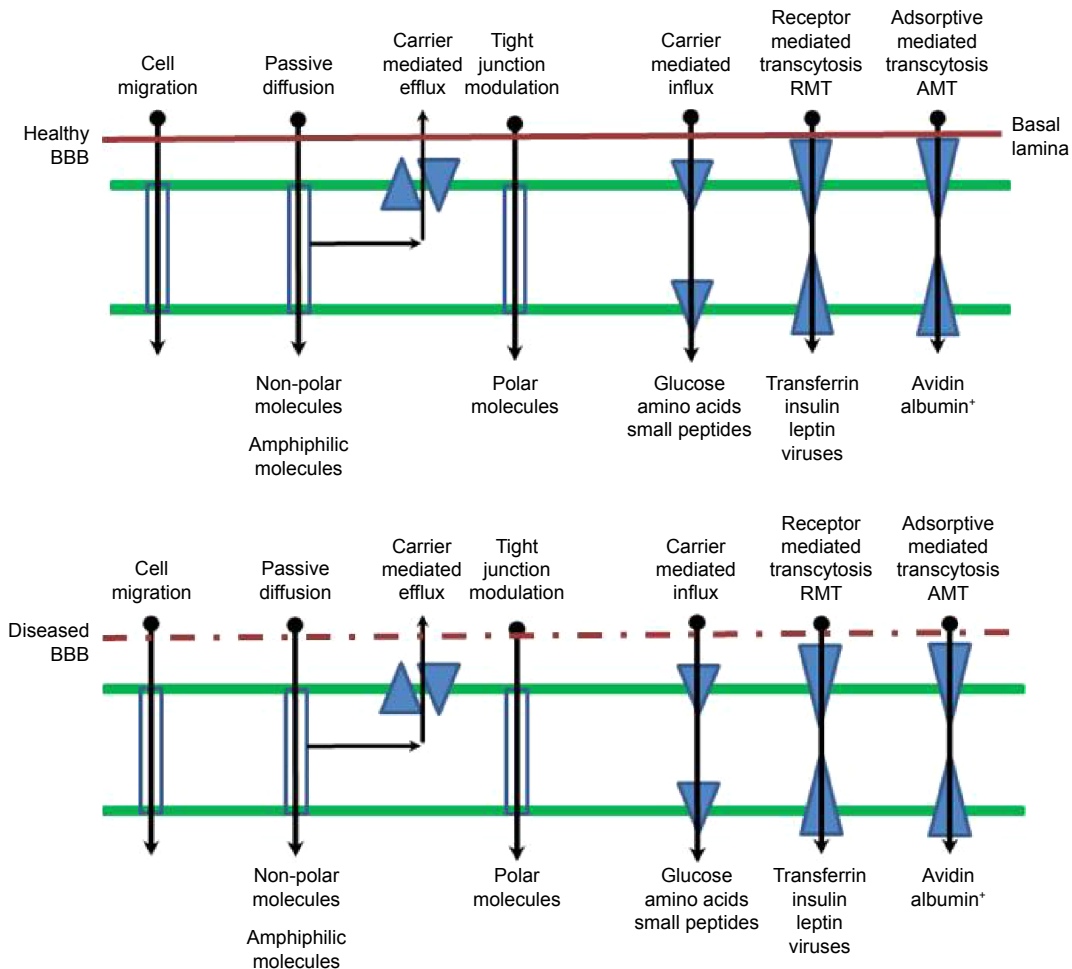


Figure 1 Transport routes across the blood-brain barrier.

Note: Green lines indicate tight junctions; blue boxes indicate no carrier or receptor mediated transport.

Abbreviations: BBB, blood-brain barrier; RMT, receptor-mediated transcytosis; AMT, adsorptive-mediated transcytosis.

All these highly regulated and efficient features supply BBB with multiple functions as a physical barrier (TJ), a transport barrier (P-gp), a metabolic or enzymatic barrier, and an immunological barrier.^{17,18}

Functions and organization of the BBB can be altered under pathological conditions, such as multiple sclerosis, epilepsy, acquired immune deficiency syndrome (AIDS), dementia, stroke, and brain cancer.^{19,20}

It should also be pointed out that alterations in the barrier, as in the blood–brain tumor barrier (BBTB), often form an increased obstacle in CNS therapy by preventing the delivery of potentially effective therapeutic agents.²¹

Molecular and physiological mechanisms involved in the transport of compounds through the BBB can be used to design drug and drug carriers for brain delivery.

Ligands such as peptides, monoclonal antibodies (mAbs), modified proteins, peptidomimetic antibodies, and penetrating peptides can be conjugated to bioactive compounds or to colloidal supramolecular aggregates and potentially used to cross the BBB and accumulate inside the CNS.²²

The paradox is that more than 99% of the global CNS drug development effort is devoted to CNS drug discovery, while less than 1% is devoted to CNS drug delivery.²³

Fortunately, scientists realized how important is the pathway from the systemic circulation to the CNS, and a few years ago, the Stroke Therapy Academic Industry Roundtable Preclinical Recommendations group highly recommended that future neurological disease research should consider also the method of drug delivery when developing novel drugs.²⁴

Current methodologies for drug delivery across the BBB

In order to bypass or cross the BBB, many strategies have been developed: invasive techniques, such as temporary disruption of the BBB or intraventricular and intracerebral direct administration of the drug, and noninvasive techniques. The invasive strategies, however, compromise the integrity and the functions of the BBB, allowing the potential accumulation of neurotoxic xenobiotics and exogenous agents; a state that is moderately to severely neurotoxic.^{25,26}

Noninvasive chemical approaches involve the “manipulation” of active substances to be administered with the aim of increasing physiological stability and degree of penetration into the brain by passive diffusion or by active targeting. For this purpose, several methods have been proposed, such as the lipidization via addition of lipid-like molecules to the structure; the addition of molecules able to use specific

endogenous transporters (eg, nutrients and other essential compounds), and the synthesis of prodrugs. Chemical modifications can be considered a safe, noninvasive approach, but they need chemical or enzymatic *in vivo* transformations that sometimes may lead to the loss of therapeutic activity or the activation of the physiological defense mechanisms of the membrane pumping out exogenous compounds.

Along with chemical modifications, there is an increase in multidisciplinary investigations, intended to facilitate the crossing of BBB, that combine biological, nanotechnological, and even biophysical expertise. In this sense, the most recent approaches concern TJ opening (eg, through the utilization of compounds like bradykinin via second messengers), receptor-mediated, adsorptive-mediated transportation (some potentially useful technologies based on receptor-mediated transcytosis are currently under clinical evaluation for brain tumor therapy – [Clinicaltrials.gov](https://clinicaltrials.gov): NCT01967810, NCT02048059, NCT01480583, NCT01386580, NCT01818713), and efflux pump inhibition by specific inhibitors that appears to be a strategy capable of delivering the drug to the brain without affecting the integrity of the endothelial layer and TJ that might cause toxicities. Also, energy-based physical methods, such as ultrasound, microwave, or electromagnetic fields, are under evaluation.

Another approach for the improvement of brain targeting is represented by the combination of the drug with the living cells, acting as Trojan horses that can cross the BBB.^{27–29}

In recent times, much attention has been given to nanotechnology in many areas because of its significant potential for the successful treatment of severe diseases such as cancer and neurological diseases.

A promising noninvasive approach to brain delivery involves nanomedicine, which takes advantage of the possible assembly of several biomaterials that can provide a delivery platform, at nanoscale size, capable of raising brain levels of drug substances otherwise unable to cross the BBB.^{23,30}

The success of a therapeutic strategy by means of nanocarriers depends on their ability to entrap drugs, to penetrate through anatomical barriers, and to release the incorporated drugs, accompanied by a good stability in the nanometric size range.²⁶

One possible strategy is the drug encapsulation into brain-targeted nanocarriers such as polymeric nanoparticles, dendrimers, vesicular carriers, metal, and silicon. These nanocarriers can have an organic or inorganic core and a surface coating with organic moieties able to interact

with the biological system at a molecular level for crossing the BBB.³¹

Modification of nanocarrier surface by adsorption or covalent linking of hydrophilic polymers, such as PEG, polysorbate 80, or polysaccharides, leads to an increase in nanocarrier circulation in the blood, whereas the surface derivatization with molecules that recognize cellular receptors facilitates the penetration of nanoparticles through the BBB.³²

The strategy often termed active targeting involves two types of transports: adsorptive-mediated transcytosis (AMT) and receptor-mediated transcytosis (RMT). The AMT has gained considerable attention because several studies assess that this strategy has the possibility to enhance the transport of nanocarriers across the BBB, using cationic proteins or cell-penetrating peptides.³³ However, as AMT is a nonspecific process, conjugation of such cationic proteins will also increase the adsorptive uptake process of nanocarriers in other parts of the body, which may possibly create toxic and immunogenic concerns. Transport of nanocarriers to the brain using the RMT process is more specific than AMT. The RMT involves addition of endogenous molecules on the nanocarrier surface, which are substrates for specific receptors expressed on the BBB. Addition of proteins (eg, transferrin, lactoferrin, Apolipoprotein E [ApoE]); peptides (eg, glutathione); or antitransferrin receptor antibody OX26 on the surface of liposomes, polymeric nanoparticles, and lipidic nanoparticles significantly increased the BBB penetrations of such nanocarriers.³⁴

Size of the nanocarrier along with surface charge, surface hydration, and targeting strategy are important characteristics for development of a successful brain-targeted nanocolloid drug delivery system for glioblastoma multiforme (GBM) treatment. Among various possible nanocarriers, liposomes, polymeric nanoparticles, and lipid nanocarriers are the most widely studied, and will be discussed in detail in the following sections.

Preliminary results reported in the large number of studies on the potential strategies to overcome and/or cross the BBB are encouraging, but it is far too early to draw any conclusion about the actual practical applications of these therapeutic approaches.

Challenge in nasal delivery to CNS

Nasal delivery has conventionally been restricted to topically/locally acting therapeutic agents for the treatment of nasal problems (eg, cold and nasal hypersensitivity). Recently, nasal route received increased attention as a substitute for oral and parenteral routes for several systemic therapeutic agents. The highly vascularized and immunogenic nasal

mucosa allows fast onset of action, enhanced bioavailability and patient compliance.^{35–37}

The pioneering method of intranasal delivery for drug delivery into the CNS was first described in 1991 by Dr William H Frey, and nowadays, it has proven to be a safe and efficient way to deliver exogenous molecules to the CNS.^{38–42} After nasal administration for CNS delivery, four physiological steps are possible, and they include the olfactory nerve pathway, trigeminal nerve pathway, vascular pathway, and the lymphatic pathway.⁴³

During the last two decades, four areas, including intranasal delivery validation, pathway elucidation, intranasal delivery of various therapeutics for the treatment of neurological diseases, and enhancement of the efficiency of intranasal delivery, have been explored.^{44,45}

Nasal cavity delivery and nasal absorption are promising approaches but are still uncertain. Direct intranasal transport is not always well established, and controversial results were obtained when similar substances were administered, and sometimes, even opposite results have been reported after nasal delivery to the CSF.^{46,47}

A few years ago, Merkus and van den Berg,⁴⁸ reviewing more than 100 papers, reported that no significant pharmacokinetic evidence was yet capable of establishing that, in humans, the intranasal route of administration actually provides enhanced targeting to the CNS, compared to the systemic route.

The real potential of the nasal route for drug delivery purposes clearly needs to be explored, developing new approaches and amending theories.³⁷

Nasal mucosal properties (ie, permeability to very large and polar molecules), are used in recent but still pioneering approaches, and among the various techniques, the permeabilization of the BBB via nasal mucosal engrafting could offer new important opportunities.

Nasal mucosal grafting: potential for drug delivery and implications for enzyme replacement therapies

Nasal mucosal grafting

Over the last few decades, the management of anterior skull base defects, CSF leaks, and encephaloceles by endoscopic, minimally invasive approaches is improving. Whether the etiology of these defects is spontaneous, traumatic, or surgical (eg, removal of brain tumors through the nose without facial incisions), the large majority of such defects can be repaired by means of free mucosal grafts that can be applied as a single layer reconstruction for small leaks or as a multilayer reconstruction for larger defects.⁴⁹

Middle turbinate, inferior turbinate, and nasal septum can be used as donor sites for free mucosal grafts for endoscopic endonasal reconstruction of the skull base. In this sense, the harvest of a nasal floor free mucosal graft was recently proposed as a rapid, potentially less morbid method.⁵⁰ Accessibility, ease of placement, and high take rate make free mucosal grafts suitable candidates for reconstruction of many skull base defects.⁵¹

The repairs by mucosal grafts are permanent, watertight, and immunocompetent, and they can also be used to replace large regions of the BCSFB within the arachnoid with relatively permeable mucosa.^{52,53} In principle, the engrafted mucosa can be dosed with therapeutic agents applied topically. Given the lack of underlying arachnoid membrane, these mucosal grafts, using purely autologous tissues, could be proposed to solve problems related to the BBB crossing by HMW or polar agents and a direct delivery to the brain and to the subarachnoid space (Figure 2).

This approach was tested for the first time by Bleier et al⁵⁴ in a proof-of-concept extracranial graft model in mice. The applied mucosal grafting method was adapted by a surgical technique that is currently used in the field of endoscopic skull base surgery defects.⁵⁵ The ability of septal mucosal grafts to allow diffusion of HMW markers into the CNS was investigated. A murine model, mimicking the human skull base, was developed and validated. A polypropylene reservoir, allowing topical dosing of the graft with different fluorescent markers (20–500 kDa), was surgically implanted over the mucosal graft. The whole mucosal implant was well tolerated, and no evidence of subcutaneous infection or distress related to the surgical site was observed. Furthermore, the delivery via the

mucosal graft was compared to the intranasal delivery, and a minimal delivery, similar to that of the negative control (dura membrane kept intact), was obtained. The direct exposure of the brain to the marker solution was used as positive control (no intervening dura or nasal mucosa). This study showed that the mucosal grafts allowed good permeability to HMW molecules and that the transport rate seemed to be molecular weight dependent. By extending the exposure duration, this effect was partially overcome. By developing different drug eluting polymers, the release rate can be modulated over time, and this could be a great challenge in combining innovative surgical and technological approaches.⁵⁴

The interesting findings of this study are limited by the possibility of comparing an animal model to a clinical setting owing to regional differences in convection throughout the murine and human brain. First of all, in humans, the ratio between mucosal graft area and brain volume ratio is much higher. In addition, in the clinical application, diffusion to more distal regions of the brain can be possible via CSF circulation, while it should be quite impossible in the murine model because of the occlusion of the smaller subarachnoid space after craniotomy.

Despite the aforementioned limitations of nasal mucosal grafting, the delivery of glial-derived neurotrophic factor (GDNF) was investigated in a mouse model for the treatment of Parkinson disease (PD).⁵⁶ In this study, a murine 6-hydroxydopamine PD model was applied. A parietal craniotomy and arachnoid defect was repaired with a heterotopic donor mucosal graft. Given the permeability of these mucosal grafts to HMW molecules, as previously reported, the possibility, by means of this approach, to

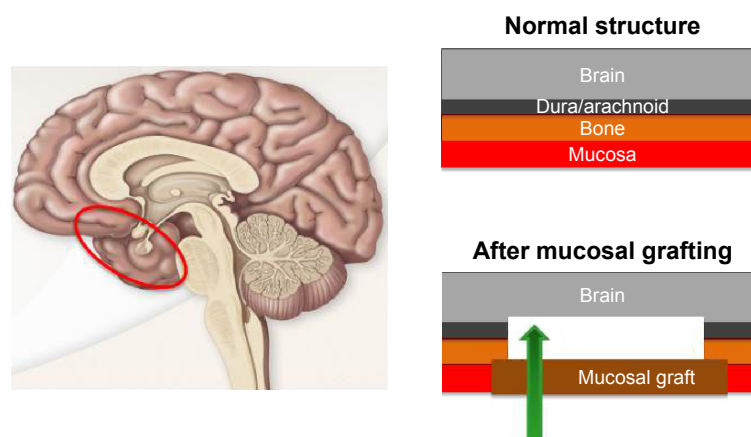


Figure 2 Graphic description of nasal mucosa graft.

Notes: The area circled in red indicates the nasal mucosal grafting area; the green arrow indicates absorption direction; and the white boxed area indicates removed bone and dura/arachnoid.

bypass the BBB and to deliver HMW neuroactive substances, engrafted over an arachnoid defect, directly to the CNS was evaluated.⁵⁴

GDNF was released by a polypropylene reservoir placed over the mucosal graft. Cyanoacrylate adhesive was used to attach the reservoir to the skull, and dental cement was applied to the skull. To maintain structural integrity, two bone screws were implanted into the skull before cement application.

GDNF was delivered through the mucosal graft, and the therapeutic efficacy was evaluated and compared with direct intrastriatal GDNF injection using behavioral assays (rotarod and apomorphine rotation). To compare the preservation of substantia nigra cell bodies, an immunohistological analysis was also used. Both behavioral and histological results demonstrated the therapeutic efficacy of transmucosal GDNF delivery. No significant difference was reported in neuronal survival between the transmucosal and injected GDNF mice, suggesting that the transmucosal pathway could be as effective as direct intraparenchymal injection in GDNF delivering to the end-target structures deep within the brain. Furthermore, the proposed mucosal grafting method could show advantages over the simple intranasal drug delivery while avoiding the concerns over the limitations of olfactory uptake in humans. In principle, the graft may be placed adjacent to the sphenoid sinus, which creates an intrinsic reservoir capable of retaining a greater volume of any intranasally applied solution. This reservoir can also help to enhance mucosal residence time by limiting the immediate clearance of the drug from the nose because of the mucociliary clearance.⁵⁷

This surgical procedure can be an efficient method to assure drug localization in the CNS, especially in the case of HMW drugs, such as enzymes that are widely used in the treatment of lysosomal storage diseases.

The local effect of this surgical procedure is the replacement of BBB and BCSFB, while the effect on the remaining part of BBB and BCSFB has not been evaluated and is not easily predictable by the results reported in the three cited research papers. Furthermore, the long-term effects of grafting nasal mucosa have not yet been evaluated because this technique has only been reported in a few very recent experimental studies on mice.^{54–56}

Lysosomal storage diseases

Lysosomal storage diseases (LSDs) include more than 50 inherited metabolic disorders characterized by the intralysosomal accumulation of undegraded substrates. Chemical properties of the accumulated substrate allow

classification of the different types of LSDs. Individually, these disorders are rare, but their cumulative prevalence is relatively high when compared with other groups of rare diseases, and they reach an incidence of one over 8,000 newborns.⁵⁸

LSDs are responsible for various clinical consequences on multiple organs and systems with visceral, ocular, hematological, skeletal, and neurological manifestations, and there is partial phenotypic overlap among different disorders. Symptoms may emerge in utero, during the newborn period, or in late adulthood. About 75% of LSD patients present a neurological impairment.

LSDs are often responsible for physical and neurological disabilities, and they can interfere with patients' health and life expectancy. Therefore, the LSD therapy requires a multidisciplinary collaboration.

LSDs are caused by mutations in genes encoding soluble acidic hydrolases, integral membrane proteins, activator proteins, transporter proteins, or nonlysosomal proteins that are necessary for the lysosomal functions. These deficiencies are responsible for intralysosomal accumulation of undegraded substrates in multiple tissues and organs.

Perturbation of lysosomal function may also lead to less obvious consequences, such as PD, which is the prevalent neurodegenerative disorder. Histopathologically, PD is characterized by the accumulation of insoluble aggregates of the presynaptic protein α -synuclein in typical intraneuronal inclusions (Lewy bodies), by the selective loss of dopaminergic neurons in the substantia nigra, and clinically by movement and postural defects. Although the mechanisms underlying this connection have not been fully elucidated, dysfunctions in several lysosomal proteins (and lysosomal gene mutations) have been involved in the pathogenesis of PD.

Mutations in gene encodings, essential components of the endolysosomal–autophagic pathway, have also been described in other neurodegenerative diseases, including Alzheimer disease, Huntington disease, frontotemporal dementia, and Charcot-Marie-Tooth type 2B.

In the past 25 years, much effort has been directed at developing specific therapies to correct the metabolic defects of these disorders by means of different strategies that were intended to target a specific event in the pathogenetic cascade, increasing the activity of the defective enzyme or protein by different ways.

The normal enzyme, obtained by recombinant technology or its precursor secreted in the circulation by engineered cells, may be administered through the endocytic pathway, by

intravenous administration. It is also possible to correct the gene mutation by delivering a wild-type copy of the mutated gene or to protect from degradation the mutant enzyme by increasing its residual activity.

Other strategies, aimed at restoring the equilibrium between the synthesis of substrates and their degradation by lysosomal enzymes, have been studied. They include reduction of substrate synthesis, enhancement of the clearance of substrates from cells and tissues, and manipulation of specific cellular pathways, involved in vesicle trafficking (Figure 3).⁵⁹

Moreover, alterations in the BBB are likely involved in LSDs as well as in all neurodegenerative diseases.⁶⁰ Actually, neuroinflammatory changes present in neurodegeneration commonly affect the BBB or its function by altering transport systems, affecting the integrity of TJ, enhancing immune cell entry, or influencing the BBB's role as a signaling interface.⁶¹ In addition, ion balance, disruption of transport systems, and altered function of BBB constitutive enzymes^{61,62} are also induced by BBB dysfunction. The BBB impairment influences drug therapy, in particular the process regulating the entry of drugs normally excluded from the brain.^{61,63}

Enzyme replacement therapy

Enzyme replacement therapy (ERT) is one of the approaches for several LSD treatments. In the early 1990s the efficacy of ERT in Gaucher disease was demonstrated, and this approach has been used to treat other LSDs, including Fabry disease, Pompe disease, and Mucopolysaccharidosis I, II, and VI.^{64–71}

After the conclusion of the first phase of ERT development, advantages and limitations of this approach have emerged. Important limitations include the reduced bioavailability of intravenously injected recombinant enzymes, and, therefore, strategies to improve ERT efficacy need to be identified. Recombinant enzymes are HMW molecules that are unlikely diffuse across membranes and are unable to reach therapeutic concentrations in some target tissues, particularly the brain. An additional major goal in future years should be the discovery of a BBB crossing enzyme because two-thirds of LSDs are involved in neurological symptoms and progressive neurodegeneration.

Strategies to improve the delivery of enzymes to the CNS are currently undergoing preclinical and clinical evaluation. For example, β -glucuronidase, which is deficient in Mucopolysaccharidosis VII, has been chemically modified to

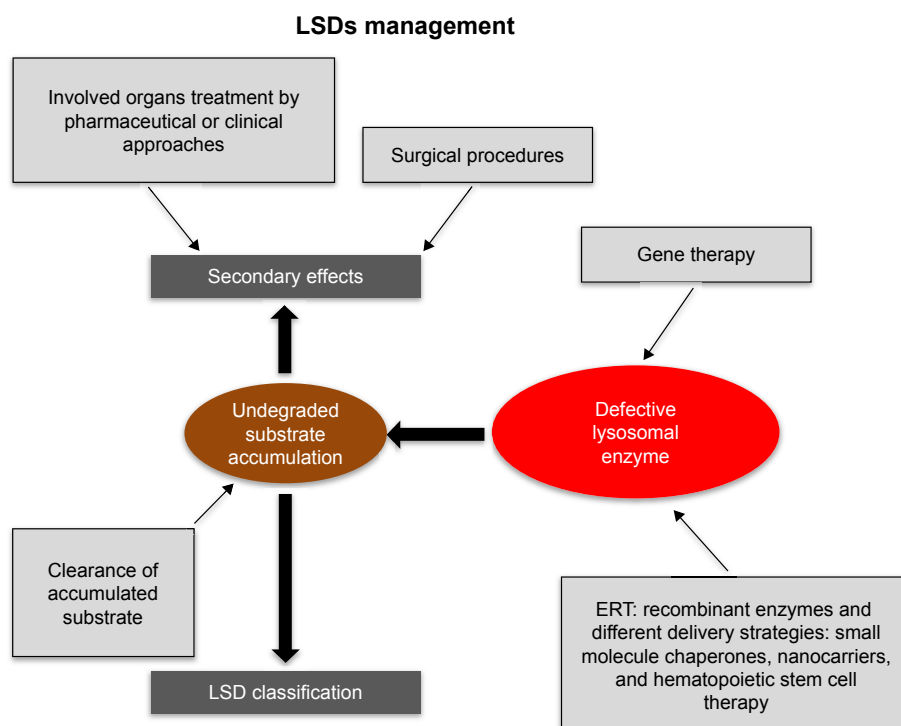


Figure 3 Schematic representation of therapeutic approaches to LSDs.
Abbreviations: LSDs, lysosomal storage diseases; ERT, enzyme replacement therapy.

increase its plasma half-life and facilitate its traffic through the BBB.^{72,73} Other approaches consider the use of so-called Trojan horses, made of chimeric enzymes conjugated with peptides that can allow penetration through the BBB leading to brain delivery by specific pathways such as the apolipoprotein and receptor pathways. These approaches have been evaluated in preclinical studies for α -iduronidase, iduronate-2-sulfatase, arylsulfatase A, and tripeptidyl peptidase I.^{74–78}

In addition to these approaches, preclinical studies are evaluating the use of invasive procedures to deliver recombinant enzymes directly into the CSF for the treatment of several lysosomal disorders. Intrathecal and lumbar or cisterna magna punctures have been studied for the administration of various types of mucopolysaccharidoses in animal models.^{79–82} Intrathecal ERT has been translated into human therapy for mucopolysaccharidoses types I and VI. Devices for continuous intrathecal infusion have been developed and tested in preclinical studies. Some clinical trials of intrathecal administration of ERT are ongoing, and others have been completed. Invasive techniques for BBB crossing were based on neurosurgery or on a temporary chemical/physical disruption of the barrier, produced by biochemical and immunological changes or by an osmotic shift.^{83–85} However, both these approaches entail several drawbacks such as the invasiveness and the high costs of neurosurgery, the physiological stress, or the transient increase in the intracranial pressure, along with high risk of infections and damages from toxins, due to the BBB temporary opening. Therefore, to improve drug delivery to the brain, noninvasive techniques have been explored, and among them the nanotechnology-based approach surely represents one of the most encouraging procedures.

To obtain a selective targeting to receptors highly expressed on the BBB, several possible ligands have been identified including transferrin, lactoferrin, insulin and leptin, and the LDL-receptor related protein LRP1.¹¹ The proposed nanocarriers include a wide variety of drug-delivery vehicles, including dendrimers, micelles, liposomes, nanoscale ceramics, and polymer nanoparticles.^{86–88} Different carriers offer different approaches to enzyme delivery. Liposomes are the first generation of nanoparticulate drug-delivery systems that reached the market, and they consist of one or more phospholipid bilayers delimiting an internal aqueous compartment. They are able to deliver hydrophobic, hydrophilic, and amphiphilic molecules. It has been reported that β -galactosidase loaded liposomes injected by rat tail vein can penetrate the BBB and reach the lysosomes in the CNS more efficiently than the free enzyme.⁸⁹ Similar results

have been obtained by *ex vivo* and *in vivo* studies on saposin C-loaded liposomes that improve the neurological condition.⁹⁰ Liposomes modified with lysosomotropic octadecyl-rhodamine B (Rh) and loaded with therapeutic glucocerebrosidase α (VPRIVTM) increase lysosomal delivery of the enzyme into Gaucher cells.⁹¹ Biodegradable and biocompatible nanoparticles, composed of poly (D,L-lactide-*co*-glycolide) (PLGA), have been investigated for recombinant proteins, plasmid DNA, and low molecular weight compounds brain delivery.⁹² Recently, *in vitro* and *in vivo* animal studies demonstrated the ability of PLGA nanoparticles, modified with glycopeptides (g7-NPs), to efficiently cross the BBB and to be transported intra- and intercellularly within vesicles for a more effective treatment of neurological disorders.^{93–95} Pegylated immunoliposomes, derivatized with the 8D3 antitransferrin receptor antibody, have been used to target the luciferase and α -galactosidase genes into the rat brain and to assure their activity after intracellular delivery.

Systemic gene therapy, together with several recombinant vector systems, is under evaluation and appears to be promising.^{96,97} Finally, it was shown that hemopoietic stem cells, derived from the monocyte/macrophage lineage and genetically modified to produce replacement enzymes, are capable of crossing the BBB in rodent models and entering into the CNS.^{98,99} However, so far neither nanocarriers nor adeno-associated virus vectors nor cell-based therapies capable of crossing the BBB have reached clinical trials in LSD, for both technological and toxicological problems.

Conclusion

The BBB plays a fundamental role in protecting and maintaining the homeostasis of the brain. For this reason, drug delivery to the brain is much more difficult than to other compartments of the body. The brain capillary endothelium excludes from the brain around 100% of large-molecule and more than 98% of small-molecule drugs.

Consequently, possible therapies with charged or macromolecular drugs, which could be capable of preventing or even reversing certain neurologic diseases, are actually clinically ineffective owing to their inability to cross the BBB. This is the central and crucial problem for an effective treatment of both LSDs and the associated neuropathology.

The fact that therapeutic approaches capable of modifying the natural evolution of many LSDs in the peripheral organs have been published and/or are under development (eg, enzyme replacement therapy, nanotechnology, gene therapy, and the use of stem cells) makes LSDs the ideal

environment in which to further investigate the relationship between lysosomal dysfunction-related neurodegeneration and the development of new strategies capable of crossing the BBB and reaching the brain compartment.

A number of studies showed that, in neurodegenerative diseases and LSDs, the function and integrity of the BBB and, in particular, of TJ, might be compromised. In these conditions, an increased passive extravasation of solutes, including proteins up to at least a molecular weight of 150 kDa, into the brain can be demonstrated. In general, damage to the BBB can induce even worse CNS damages. Furthermore, the neuropathology, related to the accumulation of storage products, and the correlation between the two processes, needs to be better understood.

It must be clarified that the ERT treatment or other approaches must bypass the BBB barrier function. At present, the best way to reach the CNS crossing the BBB, whether by a clinical approach or a technological one using innovative drug delivery systems, is not clearly defined. Valid results obtained on a large-animal are still not available and the nasal mucosal grafting approach appears not yet feasible for clinical translation.

Mucosal grafting requires an endoscopic procedure, and this can seriously limit patient compliance. However, because the grafting technique is adapted from an existing endoscopic surgical procedure, its safety profile has been well established over several decades of clinical use and is associated with a lower morbidity rate than other currently accepted methods of BBB invasive penetration. It should be emphasized that this surgical procedure is quite invasive, but at present, patients are subjected to direct intracranial injection that is not always tolerated, because neurodegenerative diseases and LSDs are chronic and severely debilitating diseases, and to this day no therapy seems to be completely successful.^{100–102}

Disclosure

The authors report no conflicts of interest in this work.

References

- Pardridge WM. Why is the global CNS pharmaceutical market so under-penetrated? *Drug Discov Today*. 2002;7(1):5–7.
- Nutt D, Goodwin G. ECNP summit on the future of CNS drug research in Europe 2011: report prepared for ECNP. *Eur Neuropsychopharmacol*. 2011;21(7):495–499.
- Turner RC, Dodson SC, Rosen CL, Huber JD. The science of cerebral ischemia and the quest for neuroprotection: navigating past failure to future success. *J Neurosurg*. 2013;118(5):1072–1085.
- Garg T, Bhandari S, Rath G, Goyal AK. Current strategies for targeted delivery of bio-active drug molecules in the treatment of brain tumor. *J Drug Target*. 2015;23(10):865–887.
- Iqbal K, Liu F, Gongm C. Tau and neurodegenerative disease: the story so far. *Nat Rev Neurol*. 2016;12(1):15–27.
- Palmer AM, Alavijeh MS. Translational CNS medicines research. *Drug Discov Today*. 2012;17(19–20):1068–1078.
- Pangalos MN, Schechter LE, Hurko O. Drug development for CNS disorders: strategies for balancing risk and reducing attrition. *Nat Rev Drug Discov*. 2007;6(7):521–532.
- Gaudin A, Andrieux K, Couvreur P. Nanomedicines and stroke: toward translational research. *J Drug Deliv Sci Tec*. 2015;30(B):278–299.
- Bernacki J, Dobrowolska A, Nierwinska K, Malecki A. Physiology and pharmacological role of the blood-brain barrier. *Pharmacol Rep*. 2008;60(5):600–622.
- Cardoso FL, Brites D, Brito MA. Looking at the blood-brain barrier: molecular anatomy and possible investigation approaches. *Brain Res Rev*. 2010;64(2):328–363.
- Abbott NJ, Patabendige AA, Dolman DE, Yusof SR, Begley DJ. Structure and function of the blood–brain barrier. *Neurobiol Dis*. 2010;37(1):13–25.
- Pardridge WM. Drug transport across the blood-brain barrier. *J Cereb Blood Flow Metab*. 2012;32(11):1959–1972.
- Aguzzi A, Barres B, Bennett ML. Microglia: scapegoat, saboteur, or something else? *Science*. 2013;339(6116):156–161.
- Daneman R, Rescigno M. The gut immune barrier and the blood-brain barrier: are they so different? *Immunity*. 2009;31(5):722–735.
- Banks WA. Blood-brain barrier as a regulatory interface. *Forum Nutr*. 2010;63:102–110.
- Chen Y, Dalwadi G, Benson HA. Drug delivery across the blood-brain barrier. *Curr Drug Deliv*. 2004;1(4):361–376.
- Pardridge WM. Molecular biology of the blood–brain barrier. *Mol Biotechnol*. 2005;30(1):57–70.
- Abbott NJ, Ronnback L, Hansson E. Astrocyte-endothelial interactions at the blood–brain barrier. *Nat Rev Neurosci*. 2006;7(1):41–53.
- de Vries HE, Kooij G, Frenkel D, Georgopoulos S, Monsonego A, Janigro D. Inflammatory events at blood–brain barrier in neuroinflammatory and neurodegenerative disorders: implications for clinical disease. *Epilepsia*. 2012;53(6):45–52.
- Obermeier B, Daneman R, Ransohoff RM. Development, maintenance, and disruption of the blood–brain barrier. *Nat Med*. 2013;19(12):1584–1596.
- van Tellingend O, Yetkin-Arik B, de Gooijerd MC, Wesseling P, Wurdinger T, de Vries HE. Overcoming the blood–brain tumor barrier for effective glioblastoma treatment. *Drug Resist Updat*. 2015;19:1–12.
- Vlieghe P, Khrestchatsky M. Medicinal chemistry based approaches and nanotechnology-based systems to improve CNS drug targeting and delivery. *Med Res Rev*. 2013;33(3):457–516.
- Aparicio-Blanco J, Martín-Sabroso C, Torres-Suarez AI. In vitro screening of nanomedicines through the blood brain barrier: a critical review. *Biomaterials*. 2016;103:229–255.
- Fisher M, Feuerstein G, Howells DW, et al. Update of the stroke therapy academic industry roundtable preclinical recommendations. *Stroke*. 2009;40(6):2244–2250.
- Calias P, Banks WA, Begley D, Scarpa M, Dickson P. Intrathecal delivery of protein therapeutics to the brain: a critical reassessment. *Pharmacol Ther*. 2014;144(2):114–122.
- Celia C, Cosco D, Paolino D, Fresta M. Nanoparticulate devices for brain drug delivery. *Med Res Rev*. 2011;31(5):716–756.
- Stojanov K, Zuhorn IS, Dierckx RA, de Vries EF. Imaging of cells and nanoparticles: implications for drug delivery to the brain. *Pharm Res*. 2012;29(12):32313–32340.
- Chen Y, Liu L. Modern methods for delivery of drugs across the blood–brain barrier. *Adv Drug Deliv Rev*. 2012;64(7):640–665.
- Hersh DS, Wadajkar AS, Roberts NB, et al. Evolving drug delivery strategies to overcome the blood brain barrier. *Curr Pharm Des*. 2016;22(9):1177–1193.
- Banks WA. From blood-brain barrier to blood-brain interface: new opportunities for CNS drug delivery. *Nat Rev Drug Discov*. 2016;15(4):275–292.

31. Singh D, Kapahi H, Rashid M, Prakash A, Majeed AB, Mishra N. Recent prospective of surface engineered nanoparticles in the management of neurodegenerative disorders. *Artif Cells Nanomed Biotechnol.* 2016;44(3):780–791.
32. Ingallina C, Rinaldi F, Bogni A, et al. Niosomal approach to brain delivery: development, characterization and in vitro toxicological studies. *Int J Pharm.* 2016;511(2):969–982.
33. Herve F, Ghinea N, Scherrmann JM. CNS delivery via adsorptive transcytosis. *AAPS J.* 2008;10(3):455–472.
34. Bhaskar S, Tian F, Stoeger T, et al. Multifunctional Nanocarriers for diagnostics, drug delivery and targeted treatment across blood-brain barrier: perspectives on tracking and neuroimaging. *Part Fibre Toxicol.* 2010;7:3.
35. Illum L. Nasal drug delivery – recent developments and future prospects. *J Control Release.* 2012;161(2):254–263.
36. Hansen K, Kim G, Desai KG, et al. Feasibility investigation of cellulose polymers for mucoadhesive nasal drug delivery applications. *Mol Pharm.* 2015;12(8):2732–2741.
37. Kumar A, Pandey AN, Jain SK. Nasal nanotechnology: revolution for efficient therapeutics delivery. *Drug Deliv.* 2016;23(3):671–683.
38. Frey WH. *Neurologic Agents for Nasal Administration to the Brain.* Emeryville, CA: Chiron Corporation; 1991.
39. Zhu J, Jiang Y, Xu G, Liu X. Intranasal administration: a potential solution for cross-BBB delivering neurotrophic factors. *Histol Histopathol.* 2012;27:537–548.
40. Jiang Y, Zhu J, Xu G, Liu X. Intranasal delivery of stem cells to the brain. *Expert Opin Drug Deliv.* 2011;8(5):623–632.
41. Lochhead JJ, Thorne RG. Intranasal delivery of biologics to the central nervous system. *Adv Drug Deliv Rev.* 2012;64(7):614–628.
42. Marianecci C, Rinaldi F, Hanieh PN, Paolino D, Di Marzio L, Carafa M. Nose to brain delivery: new trends in amphiphile-based “soft” nanocarriers. *Curr Pharm Des.* 2015;21(36):5225–5232.
43. Chen M, Wu B, Ye X, et al. Association between plasma homocysteine levels and obstructive sleep apnoea in patients with ischaemic stroke. *J Clin Neurosci.* 2011;18(11):1454–1457.
44. Pires A, Fortuna A, Alves G, Falcão A. Intranasal drug delivery: how, why and what for? *J Pharm Pharm Sci.* 2009;12(3):288–311.
45. Jiang Y, Li Y, Liu X. Intranasal delivery: circumventing the iron curtain to treat neurological disorders. *Expert Opin Drug Deliv.* 2015;12(11):1717–1725.
46. Born J, Lange T, Kern W, McGregor GP, Bickel U, Fehm HL. Sniffing neuropeptides: a transnasal approach to the human brain. *Nat Neurosci.* 2002;5(6):514–516.
47. Merkus P, Guchelaar HJ, Bosch DA, Merkus FW. Direct access of drugs to the human brain after intranasal drug administration? *Neurology.* 2003;60(10):1669–1671.
48. Merkus FW, van den Berg MP. Can nasal drug delivery bypass the blood-brain barrier?: questioning the direct transport theory. *Drugs R D.* 2007;8(3):133–144.
49. Bleier BS, Wang EW, Vandergrift WA, Schlosser RJ. Mucocele rate following endoscopic skull base reconstruction using vascularized pedicled flaps. *Am J Rhinol Allergy.* 2011;25(3):186–187.
50. Suh JD, Ramakrishnan VR, DeConde AS. Nasal floor free mucosal graft for skull base reconstruction and cerebrospinal fluid leak repair. *Ann Otol Rhinol Laryngol.* 2012;121(2):91–95.
51. Ting JO, Metson R. Free graft techniques in skull base reconstruction. *Adv Otorhinolaryngol.* 2013;74(1):33–41.
52. Bernal-Sprekelsen M, Alobid I, Mullol J, Trobat F, Toma’s-Barbera’n M. Closure of cerebrospinal fluid leaks prevents ascending bacterial meningitis. *Rhinology.* 2005;43(4):277–281.
53. Miyake MM, Bleier BS. The blood-brain barrier and nasal drug delivery to the central nervous system. *Am J Rhin Allergy.* 2015;29(2):124–127.
54. Bleier BS, Kohman RE, Feldman RE, Ramanlal S, Han X. Permeabilization of the blood-brain barrier via mucosal engrafting: implications for drug delivery to the brain. *PLoS One.* 2013;8(4):e61694. 1–7.
55. Bleier BS, Palmer JN, Sparano AM, Cohen NA. Laser-assisted cerebrospinal fluid leak repair: an animal model to test feasibility. *Otolaryngol Head Neck Surg.* 2007;137:810–814.
56. Bleier BS, Kohman RE, Guerra K, et al. Heterotopic mucosal grafting enables the delivery of therapeutic neuropeptides across the blood brain barrier. *Neurosurgery.* 2016;78(3):448–457.
57. Merkus F, Verhoef J, Schipper N, Martin E. Nasal mucociliary clearance as a factor in nasal drug delivery. *Adv Drug Deliv Rev.* 1998;29(1–2):13–38.
58. Fuller M, Meikle PJ, Hopwood JJ. Epidemiology of lysosomal storage diseases: an overview. In: Mehta A, Beck M, Sunder-Plassmann G, editors. *Fabry Disease: Perspectives from 5 Years of FOS.* Oxford, UK: Oxford PharmaGenesis; 2006.
59. Parenti G, Andria G, Ballabio A. Lysosomal storage diseases: from pathophysiology to therapy. *Annu Rev Med.* 2015;66:471–486.
60. Mehta A, Winchester B. *Lysosomal Storage Disorders: A Practical Guide.* Chichester, UK: Wiley; 2012.
61. Carvey PM, Hendey B, Monahan AJ. The blood-brain barrier in neurodegenerative disease: a rhetorical perspective. *J Neurochem.* 2009;111(2):291–314.
62. Palmer AM. The role of the blood brain barrier in neurodegenerative disorders and their treatment. *J Alzheimers Dis.* 2011;24(4):643–656.
63. Cox TM. Innovative treatments for lysosomal diseases. *Best Pract Res Clin Endocrinol Metab.* 2015;29(2):275–311.
64. Barton NW, Brady RO, Dambrosia JM, et al. Replacement therapy for inherited enzyme deficiency macrophage-targeted glucocerebrosidase for Gaucher’s disease. *N Engl J Med.* 1991;324(21):1464–1470.
65. Barton NW, Furbish FS, Murray GJ, Garfield M, Brady RO. Therapeutic response to intravenous infusions of glu- cocerebrosidase in a patient with Gaucher disease. *Proc Natl Acad Sci U S A.* 1990;87(5):1913–1916.
66. Eng CM, Guffon N, Wilcox WR, et al. Safety and efficacy of recombinant human α -galactosidase A replacement therapy in Fabry’s disease. *N Engl J Med.* 2001;345(1):9–16.
67. Schiffmann R, Kopp JB, Austin HA 3rd, et al. Enzyme replacement therapy in Fabry disease: a randomized controlled trial. *JAMA.* 2001;285:2743–2749.
68. Van den Hout H, Reuser AJ, Vulto AG, Loonen MC, Cromme-Dijkhuis A, Van der Ploeg AT. Recombinant human α -glucosidase from rabbit milk in Pompe patients. *Lancet.* 2000;356(9227):397–398.
69. Kakkis ED, Muenzer J, Tiller GE, et al. Enzyme-replacement therapy in mucopolysaccharidosis I. *N Engl J Med.* 2001;344(3):182–188.
70. Muenzer J, Wraith JE, Beck M, et al. A phase II/III clinical study of enzyme replacement therapy with idursulfase in mucopolysaccharidosis II (Hunter syndrome). *Genet Med.* 2006;8(8):465–473.
71. Harmatz P, Giugliani R, Schwartz I, et al. Enzyme replacement therapy for mucopolysaccharidosis VI: a phase 3, randomized, double-blind, placebo-controlled, multinational study of recombinant human N-acetylgalactosamine 4-sulfatase (recombinant human arylsulfatase B or rhASB) and follow-on, open-label extension study. *J Pediatr.* 2006;148:533–539.
72. Grubb JH, Vogler C, Levy B, Galvin N, Tan Y, Sly WS. Chemically modified β -glucuronidase crosses blood-brain barrier and clears neuronal storage in murine mucopolysaccharidosis VII. *Proc Natl Acad Sci U S A.* 2008;105:2616–2621.
73. Huynh HT, Grubb JH, Vogler C, Sly WS. Biochemical evidence for superior correction of neuronal storage by chemically modified enzyme in murine mucopolysaccharidosis VII. *Proc Natl Acad Sci U S A.* 2012;109:17022–17027.
74. Boado RJ, Zhang Y, Zhang Y, Xia CF, Wang Y, Pardridge WM. Genetic engineering, expression, and activity of achimeric monoclonal antibody-avidin fusion protein for receptor-mediated delivery of biotinylated drugs in humans. *Bioconjug Chem.* 2012;19:731–739.
75. Osborn MJ, McElmurry RT, Peacock B, Tolar J, Blazar BR. Targeting of the CNS in MPS-IH using a nonviral transferrin- α -L-iduronidase fusion gene product. *Mol Ther.* 2008;16(8):1459–1466.

76. Zhou QH, Boado RJ, Lu JZ, Hui EK, Pardridge WM. Brain-penetrating IgG-iduronate 2-sulfatase fusion protein for the mouse. *Drug Metab Dispos.* 2012;40(2):329–335.
77. Bockenhoff A, Cramer S, Wolte P, et al. Comparison of five peptide vectors for improved brain delivery of the lysosomal enzyme arylsulfatase A. *J Neurosci.* 2014;34(9):3122–3129.
78. Meng Y, Sohar I, Sleat DE, et al. Effective intravenous therapy for neurodegenerative disease with a therapeutic enzyme and a peptide that mediates delivery to the brain. *Mol Ther.* 2014;22(3):547–553.
79. Kakkis E, McEntee M, Vogler C, et al. Intrathecal enzyme replacement therapy reduces lysosomal storage in the brain and meninges of the canine model of MPS I. *Mol Genet Metab.* 2004;83(1–2):163–174.
80. Dickson P, McEntee M, Vogler C, et al. Intrathecal enzyme replacement therapy: successful treatment of brain disease via the cerebrospinal fluid. *Mol Genet Metab.* 2007;91(1):61–68.
81. Auclair D, Finnie J, White J, et al. Repeated intrathecal injections of recombinant human 4-sulfatase remove dural storage in mature mucopolysaccharidosis VI cats primed with a short-course tolerisation regimen. *Mol Genet Metab.* 2010;99:132–141.
82. Auclair D, Finnie J, Walkley SU, et al. Intrathecal recombinant human 4-sulfatase reduces accumulation of glycosaminoglycans in dura of mucopolysaccharidosis VI cats. *Pediatr Res.* 2012;71:39–45.
83. Bobo RH, Laske DW, Akbasak A, Morrison PF, Dedrick RL, Oldfield EH. Convection-enhanced delivery of macromolecules in the brain. *Proc Natl Acad Sci U S A.* 1994;91(6):2076–2080.
84. Kroll RA, Pagel MA, Muldoon LL, Roman-Goldstein S, Neuwelt EA. Increasing volume of distribution to the brain with interstitial infusion: dose, rather than convection, might be the most important factor. *Neurosurgery.* 1996;38(4):746–752.
85. Siegal T, Rubinstein R, Bokstein F, et al. In vivo assessment of the window of barrier opening after osmotic blood-brain barrier disruption in humans. *J Neurosurg.* 2000;92(4):599–605.
86. Costantino L, Boraschi D. Is there a clinical future for polymeric nanoparticles as brain-targeting drug delivery agents? *Drug Discov Today.* 2012;17(7):367–378.
87. Spencer BJ, Verma IM. Targeted delivery of proteins across the blood-brain barrier. *Proc Natl Acad Sci U S A.* 2007;104(18):7594–7599.
88. Patel T, Zhou J, Piepmeier JM, Saltzman WM. Polymeric nanoparticles for drug delivery to the central nervous system. *Adv Drug Deliv Rev.* 2012;64(7):701–705.
89. Onodera H, Takada G, Tada K, Desnick RJ. Microautoradiographic study on the tissue localization of liposome-entrapped or unentrapped 3H-labeled beta-galactosidase injected into rats. *Tohoku J Exp Med.* 1983;140(1):1–13.
90. Chu Z, Sun Y, Kuan CY, Grabowski GA, Qi X, Saposin C. Neuronal effect and CNS delivery by liposomes. *Ann N Y Acad Sci.* 2005;1053:237–246.
91. Thekkedath R, Koshkaryev A, Torchilin VP. Lysosome-targeted octadecyl-rhodamine B-liposomes enhance lysosomal accumulation of glucocerebrosidase in Gaucher's cells in vitro. *Nanomedicine.* 2013;8(7):1055–1065.
92. Tosi G, Bortot B, Ruozi B, et al. Potential use of polymeric nanoparticles for drug delivery across the blood-brain barrier. *Curr Med Chem.* 2013;20(17):2212–2225.
93. Tosi G, Ruozi B, Belletti D, et al. Brain-targeted polymeric nanoparticles: in vivo evidence of different routes of administration in rodents. *Nanomedicine.* 2013;8(9):1373–1383.
94. Tosi G, Vilella A, Chhabra R, et al. Insight on the fate of CNS-targeted nanoparticles. Part II: intercellular neuronal cell-to-cell transport. *J Control Release.* 2014;177:96–107.
95. Vilella A, Tosi G, Grabrucker AM, et al. Insight on the fate of CNS-targeted nanoparticles. Part I: Rab5-dependent cell-specific uptake and distribution. *J Control Release.* 2014;174:195–201.
96. Pardridge WM. Drug and gene targeting to the brain with molecular Trojan horses. *Nat Rev Drug Discov.* 2002;1(2):131–139.
97. Tomanin R, Zanetti A, Zaccariotto E, D'Avanzo F, Bellettato CM, Scarpa M. Gene therapy approaches for lysosomal storage disorders, a good model for the treatment of mendelian diseases. *Acta Paediatr.* 2012;101(7):692–701.
98. Prinz M, Priller J, Sisodia SS, Ransohoff RM. Heterogeneity of CNS myeloid cells and their roles in neurodegeneration. *Nat Neurosci.* 2011;14(10):1227–1235.
99. Visigalli I, Delai S, Politi LS, et al. Gene therapy augments the efficacy of hematopoietic cell transplantation and fully corrects mucopolysaccharidosis type I phenotype in the mouse model. *Blood.* 2010;116(24):5130–5139.
100. Cassano M, Felippu A. Endoscopic treatment of cerebrospinal fluid leaks with the use of lower turbinate grafts: a retrospective review of 125 cases. *Rhinology.* 2009;47(4):362–368.
101. Kimple AJ, Leight WD, Wheless SA, Zanation AM. Reducing nasal morbidity after skull base reconstruction with the nasoseptal flap: free middle turbinate mucosal grafts. *Laryngoscope.* 2012;122(9):1920–1924.
102. Gill SS, Patel NK, Hotton GR, et al. Direct brain infusion of glial cell line-derived neurotrophic factor in Parkinson disease. *Nat Med.* 2003;9(5):589–595.

Drug Design, Development and Therapy

Publish your work in this journal

Drug Design, Development and Therapy is an international, peer-reviewed open-access journal that spans the spectrum of drug design and development through to clinical applications. Clinical outcomes, patient safety, and programs for the development and effective, safe, and sustained use of medicines are the features of the journal, which

Submit your manuscript here: <http://www.dovepress.com/drug-design-development-and-therapy-journal>

Dovepress

has also been accepted for indexing on PubMed Central. The manuscript management system is completely online and includes a very quick and fair peer-review system, which is all easy to use. Visit <http://www.dovepress.com/testimonials.php> to read real quotes from published authors.

ACKNOWLEDGEMENTS

I wish to express my sincere gratitude to Professor Maria Carafa, my supervisor, for giving me the opportunity to do research at her laboratory group, her guidance and wise advices throughout the period of my PhD.

I would also like to show gratitude to Dr. Carlotta Marianecchi for her valuable assistance and generous advices.

I express my endless gratitude to Dr. Federica Rinaldi for her continuous encouragement, kind support, shared experience, patience and for making me feel at home starting from the period of my undergraduate to the end of my PhD project.

I would like to thank all my PhD colleagues who have always supported me, in particular Paolo, for supporting me in every way possible and the enjoyable conversations over the years as a PhD student, showing a precious colleague and friend, and Martina, for her good mood, exchange ideas and help. In addition, I thank many people who have supported my PhD research: Dr. Andrea Bettucci and Dr. Angelo Biagioni (Department of Basic and Applied Sciences for Engineering, University of Rome "Sapienza") for their acoustic studies on nanobubbles; Professor Elena Del Favero (Department of Medical biotechnology, University of Milan) for their SAXS analysis on several samples; Dr. Roberto Marotta (IIT Genoa) for the wonderful Cryo-TEM pictures, Professor Giuseppe Esposito for his *in vivo* experimental studies on pentasomes,

I would also like to thank the many people from University of Edinburgh who contributed with their time, expertness, instrumentation, and advice during my visit to Edinburgh.

Special thanks to Dr. Carmel Moran for the for the opportunity to work in her research group and for receiving me so well. Thanks to PhD student Julie for her *in vivo* experimental studies, shared experience and being available for scientific and experimental discussions.

I would like to thank PhD student Adela for their friendship and support for providing me with a pleasant stay in Edinburgh.

I would like to express my heartfelt gratitude to my dear friends, who have always supported me, unwind at the end of a stressful week and never failed to give me great suggestions in both study and life.

Last but not least, I would like to extend my heartfelt gratitude to my parents, they have always been an inspiration to me and thank you for always being there for me, and my little sister Rossella, for her endless love, trust, understanding and support to follow my dreams.

LIST OF PUBLICATIONS

- [1].C. Marianecci, F. Rinaldi, C. Ingallina, **P. N. Hanieh**, M. Carafa, “Vesicular systems in dairy products: an up to date overview”, *Advances in Safety and Health*, 2014, 6 (2), 22-32.
- [2].F. Rinaldi, **P. N. Hanieh**, C. Marianecci, M. Carafa, “DLS Characterization of Non-Ionic Surfactant Vesicles for Potential Nose to Brain Application, *Nanoscience and Nanometrology*, 2015, 1(1): 8-14.
- [3].C. Marianecci, F. Rinaldi, **P. N. Hanieh**, D. Paolino, L. Di Marzio, M. Carafa, “Nose to brain delivery: new trends in amphiphilic based "soft" nanocarriers”, *Curr Pharm Des.*, 2015, Sep 22.
- [4].C. Marianecci, S. Petralito, F. Rinaldi, **P. N. Hanieh**, M. Carafa, “Some recent advances on liposomal and niosomal vesicular carriers”, *J Drug Deliv Sci Technol*, 32, 2016, 256-269.
- [5].C. Marianecci, F. Rinaldi, **P. N. Hanieh**, D. Paolino, L. Di Marzio, M. Carafa, “Drug delivery in overcoming the blood-brain barrier: role of nasal mucosal grafting”, *Drug Design, Development and Therapy*, 2017, 11, 325-335.
- [6].F. Rinaldi, **P. N. Hanieh**, C. Longhi, S. Carradori, D. Secci, G. Zengin, M.G. Amendolia, E. Mattia, E. Del Favero, C. Marianecci, M. Carafa, “Neem oil nanoemulsions: characterisation and antioxidant activity”, *J Enzyme Inhib Med Chem*, 2017, 32 (1), 1265-1273.

